UNIVERSITÉ DE NEUCHÂTEL
INSTITUT DE MICROTECHNIQUE

Contributions to the Design of IIR Digital Filters Based on Allpass Networks

THÈSE

PRÉSENTÉE À LA FACULTÉ DES SCIENCES
POUR L'OBTENTION DU GRADE DE DOCTEUR ÈS SCIENCES

PAR

Michael Ansorge

Septembre 2000

Printed by Easy Document, Montagny-près-Yverdon, Switzerland.

IMPRIMATUR POUR LA THESE

Contributions to the Design of IIR Digital Filters Based on Allpass Networks

de M. Michael Ansorge

UNIVERSITE DE NEUCHATEL

FACULTE DES SCIENCES

La Faculté des sciences de l'Université de Neuchâtel sur le rapport des membres du jury,

MM. F. Pellandini (directeur de thèse), A. Shah, M. Kunt (EPFL), A. Dabrowski (Poznan) et T. Henk (Budapest)

autorise l'impression de la présente thèse.

Neuchâtel, le 21 septembre 2000

Le doyen:

J.-P. Derendinger

To my dear wife and our sons.

Abstract

Digital allpass networks and Wave Digital Filters (WDFs) correspond to important and robust filter categories that can be flexibly adapted to satisfy general purpose or specific requirements in a large range of signal processing domains, including telecommunications, consumer electronics, multimedia, bio-medical applications, instrumentation, microsystems design, and many more.

In this report, complex and real allpass networks and Wave Digital Filters are studied, emphasizing lattice-type structures for the latter, which are composed of two parallel-connected allpass functions.

The purpose of this study is multi-fold, and comprises theoretical as well as practical aspects. Hence, regarding complex and real allpass functions, a systematic study of stability-related properties is performed, resulting in the generalization of a known stability condition, and further in several new stability conditions. Additionally, the basic features of half-band symmetric allpass filters are identified.

Moreover, an extended review of complex and real WDFs is presented, leading to several interesting results, including the provision of synoptic design tables for real lattice-type WDFs.

Specific WDF configurations are then discussed in detail, encompassing bireciprocal (i.e. half-band) WDFs, which are demonstrated to be essentially real, warped bireciprocal WDFs, various Digital Hilbert Transformers, and several filter approximation methods.

Finally, a series of examples is provided along the report, allowing in most cases to reproduce the results so as to verify the described features, or to perform comparisons.

Résumé

Les réseaux numériques passe-tout et les filtres numériques d'onde (WDFs) correspondent à d'importantes catégories de filtres robustes, que l'on peut aisément adapter pour résoudre des problèmes généraux ou spécifiques de traitement du signal dans les télécommunications, ou dans l'électronique grand-public, les multimédias, les applications bio-médicales, l'instrumentation, les microsystèmes, etc..

Ce rapport considère l'étude de filtres passe-tout et de WDFs complexes et réels, en privilégiant pour ces derniers les structures en treillis constituées de deux passe-tout branchés en parallèle.

L'objectif de cette étude est multiple et comprend des aspects théoriques et pratiques. Considérant les passe-tout complexes et réels, une étude systématique des conditions de stabilité est effectuée, résultant en la généralisation d'une condition de stabilité connue, ainsi qu'en plusieurs nouvelles conditions de stabilité. De plus, les propriétés élémentaires de filtres passe-tout demi-bande sont établies.

En outre, le passage en revue approfondi des WDFs complexes et réels conduit à plusieurs résultats intéressants, dont l'établissement d'un tableau synoptique pour la conception de WDFs réels en treillis.

Plusieurs configurations de WDFs sont ensuite discutées en détail, comprenant les WDFs demi-bande, qui s'avèrent être essentiellement réels, les WDFs demi-bande modifiés, divers transformateurs de Hilbert numériques, ainsi que quelques méthodes d'approximation.

Enfin, une suite d'exemples est fournie tout le long du rapport, permettant dans la plupart des cas de reproduire les résultats afin de vérifier les propriétés décrites, ou d'effectuer des comparaisons.

Contents

Chapter 3: Complex and Real Wave Digital Filters

Chapter 5: Design of Lattice-Type WDFs

Chapter 6: Digital Hilbert Transformers

Chapter 7: Eigenfilter Approximation of Allpass Filters and Lattice-Type WDFs

Chapter 8: Conclusion

Appendix: Terminology and Mathematical Background

Chapter 1
Introduction

1.1 Motivation and objectives

Lossless Infinite Impulse Response (IIR) digital filters, either derived from related analog reference networks, or directly designed in the digital domain, deserve a particular interest because of the numerous remarkable advantages they are offering, such as low sensitivity to filter coefficients, low round-off noise, and stability under finite-precision arithmetic conditions, more details on these issues being provided in the course of the report.

Essential representatives of lossless IIR digital filters are allpass filters, and the whole class of Wave Digital Filters (WDFs) [Fett71, Fett86], from which generic filters, but also a plenty of application specific filters, can be designed.

Wave Digital Filters are obtained following a refined methodology consisting in designing an analog lossless reference two-port suiting to the considered application. Expressing the input/output signals in terms of "wave" quantities – actually a linear combination of voltage and current quantities of the analog reference filter – in order to avoid delay-free loops in the digital domain, the lossless reference two-port is then mapped onto a digital network termed "Wave Digital Filter" using the bilinear transform [Fett71, Fett86]. Interestingly, since the lossless reference two-port is by essence featuring two complementary input/output signal pairs, WDFs provide a natural

means to realize branching filters, among other attractive filter configurations.

Moreover, the WDF design methodology is observed to inherently embrace both analog and digital filtering domains, including lumped and commensurate distributed time-continuous analog filters, analog time-discrete filters, and of course also digital filters. A natural link is thus established to the large palette of filter design methods elaborated in the frame of each of these domains, including special filter configurations, filter design charts, design tools, and approximation techniques, which fosters the valorization / reuse of the substantial accumulated amount of knowledge, and reduces design efforts of filter designers.

Simultaneously, the connection between filtering domains stimulates the elaboration of new filtering solutions, either at theoretical or at practical levels. For the latter, one notices that attractive mixed analog-digital network configurations can be established, especially in relation with the design of special purpose analog-to-digital and/or digital-to-analog converters complying with particular constraints (low power consumption, limited overall complexity, avoidance of bulky or costly discrete analog components).

An important category of filtering functions is given by *lattice-type reciprocal* functions, which are shown to rely at conceptual level, but also at implementation level if selected so, on allpass networks.

Although the majority of filtering algorithms are focusing on the process of *real* signals, there are motivations to handle *complex* signals as well, either locally in sub-units, or at larger scale according to the application. Examples are given by analytic signal processing, or phase/group delay equalization for telecommunications, among others.

The main subject of this report concerns the study of allpass and lattice-type reciprocal WDF networks of both complex and real nature, following several objectives.

The first objective aims at studying the fundamentals of complex/real allpass networks and WDFs, recalling of course known properties, and elaborating complementary ones, taking in particular care of

identifying and grouping important data that are useful for applied filter design.

Based on tbe former work, the second purpose of the report is to study particular filters subclasses, namely (multirate) half-band WDFs, and Digital Hilbert Transformers.

The third objective concerns the discussion of selected filter approximation methods, two of them being related to the design of prototype lowpass responses, whereas the last handled approximation technique deals with the so-called "eigenfilter" approach.

Finally, numerous examples are provided along tbe report to illustrate concepts and results.

1.2 Outline

The two first chapters are providing the fundamentals serving as support for the remaining chapters.

Chapter 2 discusses the elementary charecteristics of allpass networks. In addition, separating the phase response of complex allpass functions into their even and odd constituent parts, a series of properties is derived regarding the design of purely even phase response allpasses, stability conditions, and further issues. Finally, as a preparatory step for the later study of bireciprocal WDFs, the characteristics of half-band symmetric allpass networks are established.

Chapter 3 is tben systematically reviewing the field of real and complex Wave Digital Filter design, motivating the reason of recoursing to complex filtering, whereas the design of lattice-type reciprocal filters is thoroughly discussed. Also, design parameters are grouped into tables to render practical designs easier.

Chapter 4 covers the field of bireciprocal Wave Digital Filter design, discussing first the intrinsinc real nature of such networks, whereas corresponding implementation structures are next considered, noticing that two realizations are possible for antimetric-type bireciprocal WDFs.

Cbapter 5 covers then the issue of approximating prototype antimetric filters, proposing an extension to the known design framework provided in [Gazs85a]. Moreover, the approximation of warped

bireciprocal filters is also discussed, with implementation into the same framework.

Chapter 6 considers the realization of Digital Hilbert Transforms playing an important role for the process of analytic signals. A selected set of causal filter implementations are discussed, identifying in particular a WDF configuration suitable for almost linear phase response with midband symmetry, and symmetric group delay.

Chapter 7 focuses on a so-called "eigenfilter" allpass approximation technique, the purpose being to find out what is the internal symmetry of a specific matrix used in the core part of the eigenfilter method, in order to lower the computational load.

Final considerations are then drawn in Chapter 8.

1.3 Main contributions

The main contributions elaborated in this work are the following.

Chapter 2: in relationship to the study of allpass networks, several new stability assessment criteria are proposed, either based on the measure of the spanned phase range, or relying on the observation of the even and odd phase response components. Additionally, basic properties of complex half-band symmetric allpass functions are also provided.

Chapter 3: systematic review of complex and real WDFs, with proposition of specific contributions.

Chapter 4: a first contribution is given by recognizing that lattice-type reciprocal half-band WDFs featuring a so-called bireciprocal characteristic function are essentially real in nature. A second contribution concerns the implementation of real antimetric bireciprocal WDFs (and degenerate complex filters derived thereof), where two alternative structures are identified and commented.

Chapter 5: two design methods are proposed for integration into the design framework described in [Gazs85a], the first one concerning antimetric WDFs, whereas the second is covering the case of so-called "warped" bireciprocal WDFs, with provision of their fundamental equation, also applicable to non-prototype lowpass filter responses.

Chapter 6: systematic discussion of the design of Digital Hilbert Transformers.

Chapter 7: in the scope of the particular eigenfilter allpass approximation method: analysis of the internal symmetries featured by a specific matrix used in the core part of the eigenfilter method.

Appendix: general organization of the collected data and formulas.

A detailed list of contributions is provided and commented in the conclusion of each chapter.

Recommendation

It is advised to read the Appendix, introducing the terminology and mathematical background used, prior to reading the remaining part of the report.

Chapter 2

Elementary Properties of Allpass Networks

2.1 Introduction

Complex or real allpass functions are fundamental filtering networks featuring many interesting properties [Bele68, Schü94, Vaid93]. In addition to their obvious use for phase and group delay equalization, and for designing finite bandwidth fractional delays [Laak96], allpass functions appear in many other contexts, where their losslessness, their suitability to be canonically implemented in various structures, their intervention as elementary building block for the realization of lattice-type reciprocal filter functions, including the design of multirate filterbanks [Renf87a, Renf87b], are appreciated.

Furthermore, considering the close link between the phase/group delay responses of allpass networks and their pole configuration, allpasses are offering complementary stability tests, used to assess their own stability, but with obvious extension to polynomials and rational functions.

Allpass networks are therefore regularly applied, either in circuit theoretic problems as a formal support to study filter functions and related properties, or in the domain of filter approximation (polynomial phase interpolation [Henk81a], phase/group delay equalization, e.g. [Decz72, Decz73, Decz74, Dedi95, Lang92, Lang93], amplitude-

only approximation, e.g. [Lang93, Tarr95], mixed amplitude/phase approximation, e.g. [Leeb92, Föld91]), including allpass-based filter transformations [Cons70, Güll86, Iwak91], or in applications.

This chapter aims at discussing several basic properties featured by allpass networks, along the following organization. First, several definitions are recalled in Section 2.2, before handling in Section 2.3 the even/odd phase constituents of complex allpass filters, which will in particular serve to establish the explicit form of even phased allpass networks in Section 2.4. Stability related properties are next covered in detail in Section 2.5, whereas Section 2.6 is devoted to analyzing half-band symmetric allpass filters, which play an important role in (multirate) applications. Finally, Section 2.7 recalling very shortly that the identified allpass properties determined in the z-domain have their counterpart in the ψ-domain and vice-versa, the conclusions are sketched in Section 2.8.

2.2 Frequency response of complex allpass functions

2.2.1 Transfer function of complex allpass networks

It is recalled that a discrete-time function $A(z)$ is said to be allpass if [Vaid93] :

$$\left| A\left(e^{j\Omega}\right)\right| = c, \quad c>0, \quad \text{with } c \in \mathbb{R}, \quad \text{for all } \Omega, \tag{2.1}$$

i.e. when the magnitude response is constant over the complete frequency domain. $A(z)$ is further designated as a *unit-magnitude allpass* for $c = 1$, in which case the frequency response can be written as :

$$A\left(e^{j\Omega}\right) = e^{-j\beta_A(\Omega)}, \tag{2.2}$$

where $\beta_A(\Omega)$ is the phase response. In the realm of this report, allpass networks are always assumed to be of unit-magnitude type.

Transfer function

The transfer function of an Nth-order rational discrete-time allpass function is specified by [Vaid93] :

$$A(z)=\frac{z^N\cdot\tilde{D}(z)}{D(z)}=\frac{z^N\cdot\sum_{\nu=0}^{N}d_\nu^*\cdot z^{-\nu}}{\sum_{\nu=0}^{N}d_\nu\cdot z^{\nu}}, \tag{2.3a}$$

with $$d_N\neq 0. \tag{2.3b}$$

$A(z)$ can be reformulated as follows to achieve a canonic expression with respect to the number of free parameters (i.e. real and imaginary parts of the filter coefficiente) :

$$A(z)=\lambda\cdot\frac{z^N\cdot\tilde{P}(z)}{P(z)}, \tag{2.4a}$$

with $$P(z)=\sum_{\nu=0}^{N}p_\nu\cdot z^{\nu},\quad p_\nu=d_\nu/d_N,\quad p_N=1, \tag{2.4b}$$

and $$\lambda=d_N^*/d_N=e^{j\theta};\qquad \theta=\mathrm{Arg}\{\lambda\}=-2\cdot\mathrm{Arg}\{d_N\}. \tag{2.4c,d}$$

$P(z)$ is thus specified as a monic polynomial [1]. The transfer function $A(z)$ can also be rewritten in product form, cf (A.78a) :

$$A(z)=\lambda\cdot\prod_{\nu=1}^{N}\left(\frac{1-z_{\infty\nu}^*\cdot z}{z-z_{\infty\nu}}\right), \tag{2.5}$$

where $z_{\infty\nu}$, $\nu=1,\ldots,N$, correspond to the poles of the allpass function, including those located at the origin.

Poles and zeros configurations

As can be observed from equation (2.5), the poles and zeros of an allpass function occur in reciprocal conjugate pairs, each pole $z_{\infty\nu}$ being accompanied by a zero located at $1/z_{\infty\nu}^*$. This distribution includes the case where $z_{\infty\nu}=0$, the corresponding zero becoming infinite. Clearly, the poles of stable and causal allpass functions are all confined to the open unit circle; accordingly, the zeros are exclusively situated outside the unit-circle, cf Figure 2.1. Accordingly, all-

---

[1] A polynomial is said to be *monic* when its leading coefficient, associated to the highest power of the independent variable, is equal to +1 [Bele68, p. 406].

pass functions are by essence featuring a maximum phase response, cf Subsection A.8.1.

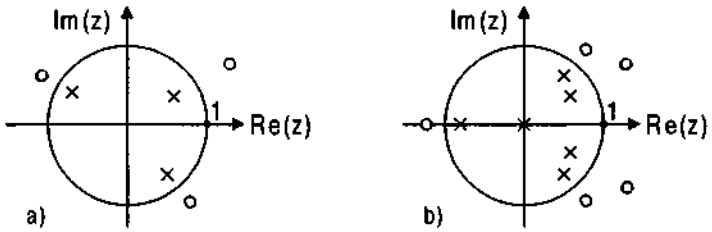

Figure 2.1: Distribution of poles and zeros of stable and non-patbological [2] allpass functions : a) complex case; b) real case.

Allpass type	Symmetry of phase response	Parity of N	List of real and independent parameters	Nb of canonic parms
Real	Odd symmetry (except possible $\theta = \pm\pi$)	Any	$p_{R0},\ldots,p_{R(N-1)}$; $p_{Iv}=0,\forall v$; with either $\lambda=\pm1$, or $\theta=0,\pm\pi$.	$N+1$
Complex with even $\beta_A(\Omega)$	Even symmetry	Even	$p'_{R0},\ldots,p'_{R(N/2-1)}$; $p'_{I0},\ldots,p'_{I(N/2-1)}$; together with θ. *(Refer to Section 2.4 for details)*	$N+1$
General complex	No symmetry	Any	$p_{R0},\ldots,p_{R(N-1)}$; $p_{I0},\ldots,p_{I(N-1)}$; together with θ.	$2N+1$

Table 2.1: Canonic number of real parameters requested to fully specify an allpass function.

2.2.2 Canonic number of parameters

Equations (2.4a) and (2.5) show that an Nth-order *complex* allpass is fully characterized by $(2N+1)$ real and independent parameters, namely :

- the real and imaginary components of the filter coefficients $p_0,\ldots,p_{N-1}$, together with θ;

[2] Cf Subsection 2.2.6.

or any linear combination thereof, including the corresponding poles $z_{\infty 1},\ldots,z_{\infty N}$. Clearly, the number of free parameters drops down to $(N+1)$ for *real* allpass networks, with $p_\nu \in \mathbb{R}$, $\forall \nu \in [0,1,\ldots,N-1]$, and $\lambda = \pm 1$ or $\theta = 0, \pm\pi$. A summary is provided in Table 2.1, including the case of complex allpass networks featuring an even phase response, that will be covered in detail in Section 2.4.

2.2.3 Phase response

Based on (2.4a), the phase response of $A(z)$, is defined as :

$$\beta_A(\Omega) = -\mathrm{Arg}\left\{ A\left(e^{j\cdot\Omega}\right)\right\} = -\left[\theta + N\Omega + 2\beta_P(\Omega)\right], \tag{2.6}$$

where $\beta_P(\Omega)$ corresponds to the phase response of polynomial $P(z)$. Decomposing the coefficients p_ν in (2.4b) into their real and imaginary constituents :

$$p_\nu = p_{R\nu} + j \cdot p_{I\nu}, \tag{2.7}$$

$\beta_P(\Omega)$ can in turn be specified as :

$$\beta_P(\Omega) = -\arctan\left(\frac{\sum_{\nu=0}^{N} p_{R\nu}\cdot\sin(\nu\Omega) + p_{I\nu}\cdot\cos(\nu\Omega)}{\sum_{\nu=0}^{N} p_{R\nu}\cdot\cos(\nu\Omega) - p_{I\nu}\cdot\sin(\nu\Omega)} \right) \tag{2.8}$$

with $\qquad p_N = 1, \quad \text{i.e. } p_{RN} = 1, \; p_{IN} = 0.$

Except for a possible phase shift of $\theta = \pm\pi$, *real* allpass functions are clearly featuring an odd phase response with $p_{I\nu} = 0, \forall \nu \in [0,1,\ldots,N]$.

Unwrapped phase response

According to Subsection A.5.2, phase responses are considered either using their *Principal Value* $\beta_{A\,\mathrm{PV}}(\Omega)$, or their *unwrapped* form $\beta_A(\Omega)$, where both expressions are connected by the pbase unwrapping factor $k_A(\Omega)$, cf (A.69). In this report, unwrapped phase responses are evaluated with respect to the reference point :

$$\beta_A(\Omega = 0) = \beta_{A\,\mathrm{PV}}(\Omega = 0) = -\left[\theta + 2\beta_P(\Omega = 0)\right], \tag{2.9a}$$

with $\qquad \beta_P(\Omega = 0) = -\arctan\left(\sum_{\nu=0}^{N} p_{I\nu} \Big/ \sum_{\nu=0}^{N} p_{R\nu}\right). \tag{2.9b}$

thus implying $k_A(\Omega = 0) = 0$.

Example

An example of a 3rd-order complex and stable allpass is presented in Figure 2.2 and Table 2.2, including the corresponding phase response in Principal Valued and unwrapped form, the related phase unwrapping factor $k_A(\Omega)$, group delay $\tau_A(\Omega)$, and poles configuration.

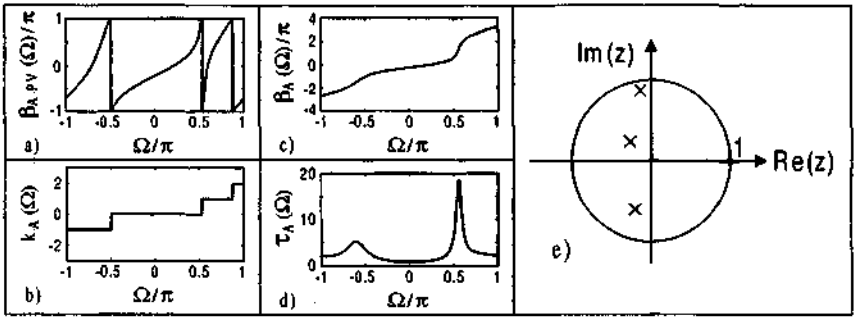

Figure 2.2: Characteristics of a 3rd-order complex allpass:
a) PV of the phase response; c) Unwrapped phase response;
b) Phase unwrapping factor; d) Group delay;
e) Poles configuration.

	ν	θ/π, $\mathrm{Re}\{z_{\infty\nu}\}$	$\mathrm{Im}\{z_{\infty\nu}\}$
θ/π	—	0	—
$z_{\infty\nu}$	1	−0.20068185138151	−0.60886993992255
	2	−0.15354945297270	0.87488889993960
	3	−0.26422833019066	0.22649405639718

Table 2.2: Parameters specifying the allpass illustrated in Figure 2.2.

2.2.4 Group delay

The group delay of $A(z)$, normalized to the sampling period T_s, is given by :

$$\tau_A(\Omega) = \frac{d\beta_A(\Omega)}{d\Omega} = -\left[N + 2\cdot\tau_P(\Omega)\right], \tag{2.10}$$

$\tau_P(\Omega)$ being the group delay of polynomial $P(z)$. A compact expression of $\tau_P(\Omega)$ is best achieved introducing the auxiliary variables $u(\Omega)$ and $w(\Omega)$:

$$u(\Omega) = \mathrm{Im}\left\{\sum_{\nu=0}^{N} p_\nu \cdot e^{j\nu\Omega}\right\}, \quad w(\Omega) = \mathrm{Re}\left\{\sum_{\nu=0}^{N} p_\nu \cdot e^{j\nu\Omega}\right\}; \quad (2.11a,b)$$

and their derivatives :

$$\dot{u}(\Omega) = \frac{du(\Omega)}{d\Omega} = \mathrm{Re}\left\{\sum_{\nu=0}^{N} \nu \cdot p_\nu \cdot e^{j\nu\Omega}\right\}, \quad (2.12a)$$

$$\dot{w}(\Omega) = \frac{dw(\Omega)}{d\Omega} = -\mathrm{Im}\left\{\sum_{\nu=0}^{N} \nu \cdot p_\nu \cdot e^{j\nu\Omega}\right\}. \quad (2.12b)$$

Hence, $\beta_P(\Omega)$ and $\tau_P(\Omega)$ merely become :

$$\beta_P(\Omega) = -\arctan\left(u(\Omega)/w(\Omega)\right), \quad (2.13a)$$

$$\tau_P(\Omega) = -\left(\frac{\dot{u}(\Omega)\cdot w(\Omega) - u(\Omega)\cdot \dot{w}(\Omega)}{u^2(\Omega) + w^2(\Omega)}\right). \quad (2.13b)$$

An example is provided in Figure 2.2d.

2.2.5 Biconjugate of complex allpass functions

Using equations (A.8) and (2.5), the biconjugate $\overline{A(z)}$ of $A(z)$ is observed to verify :

$$\overline{A(z)} = A^{-1}(z^{-1}), \quad (2.14a)$$

which, in terms of the corresponding phase response $\beta_{\overline{A}}(\Omega)$ of $\overline{A(z)}$, leads to the following symmetry [3] :

$$\beta_{\overline{A}}(\Omega) = -\beta_A(-\Omega). \quad (2.14b)$$

This result can as well be derived from equations (2.6) and (2.8). The group delay $\tau_{\overline{A}}(\Omega)$ of $\overline{A(z)}$ is finally characterized by :

$$\tau_{\overline{A}}(\Omega) = +\tau_A(-\Omega). \quad (2.14c)$$

For real allpass functions, $\overline{A(z)} = A(z)$, i.e. $\beta_{\overline{A}}(\Omega) = \beta_A(\Omega)$, and (2.14b) reduces then to the odd symmetry $\beta_A(\Omega) = -\beta_A(-\Omega)$, implying in turn the even symmetry $\tau_A(\Omega) = \tau_A(-\Omega)$ in (2.14c).

---

[3] This symmetry is a direct consequence of the para-odd nature of the complex phase response, as can be demonstrated in the ψ-domain from (A.55), (A.11), (A.31), and (A.56b).

Example

The frequency responses and poles configuration of the biconjugate $\overline{A(z)}$ of the allpass $A(z)$ specified in Table 2.2 and Figure 2.2 are represented in Figure 2.3. The poles of $\overline{A(z)}$ are merely the complex conjugates of the poles of $A(z)$.

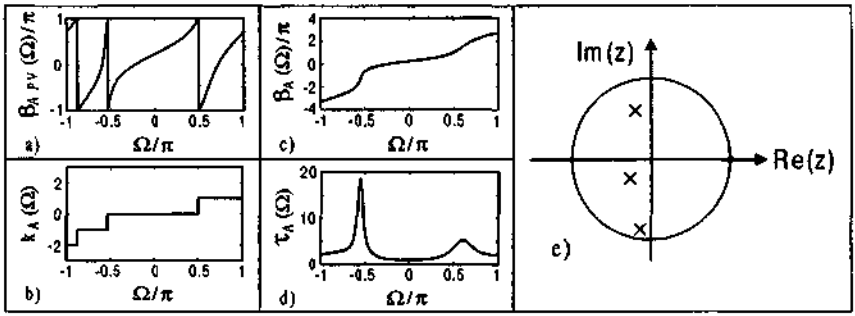

Figure 2.3: Biconjugate of the complex allpass presented in Figure 2.2:
a) PV of the phase response; c) Unwrapped phase response;
b) Phase unwrapping factor; d) Group delay;
e) Poles configuration.

2.2.6 Pathological allpass functions

Adopting the terminology defined in [Henk81a] for real arbitrary-phase polynomials, a complex or real allpass function is said to be *pathological* when at least one of its poles, including possible multiplicity, lies on the unit-circle. In such a case, the associated zeros coincide with the poles located on the unit-circle, cf (2.5), and the allpass bebaves like a lower-order allpass function.

Precisely stated, let us split $A(z)$ in (2.5) into a non-pathological allpass $A_1(z)$, and a purely pathological one $A_2(z)$, respectively :

$$A(z) = A_1(z) \cdot A_2(z), \tag{2.15a}$$

$$A_1(z) = \lambda \cdot \prod_{\mu=1}^{n_1} \left(\frac{1 - z_{\infty 1\mu}^{*} \cdot z}{z - z_{\infty 1\mu}} \right), \quad A_2(z) = \prod_{\nu=1}^{n_2} \left(\frac{1 - z_{\infty 2\nu}^{*} \cdot z}{z - z_{\infty 2\nu}} \right), \tag{2.15b}$$

with $N = n_1 + n_2$; $\quad |z_{\infty 1\mu}| \neq 1, \quad |z_{\infty 2\nu}| = 1, \quad \forall \mu, \nu$.

Defining

$$z_{\infty 2\nu} = \exp(j \cdot \delta_\nu), \tag{2.16}$$

the next formulas are obtained :

$$A_2(z) = (-1)^{n_2} \cdot \prod_{\nu=1}^{n_2} \exp(-j \cdot \delta_\nu), \quad z \neq \exp(j \cdot \delta_\nu), \forall \nu; \tag{2.17a}$$

$$\beta_{A2}(\Omega) = \sum_{\nu=1}^{n_2} \delta_\nu \pm n_2 \cdot \pi; \quad \tau_{A2}(\Omega) = 0; \quad \Omega \neq \delta_\nu, \forall \nu. \tag{2.17b,c}$$

Moreover, applying L'Hospital's rule [Abra70, Youn73], (2.17a,b,c) are shown to be also valid for $z = \exp(j \cdot \delta_\nu)$ and $\Omega = \delta_\nu$, $\forall \nu$, respectively, so that finally :

$$A_2(z) = (-1)^{n_2} \cdot \prod_{\nu=1}^{n_2} \exp(-j \cdot \delta_\nu), \ \forall z; \tag{2.18a}$$

$$\beta_{A2}(\Omega) = \sum_{\nu=1}^{n_2} \delta_\nu \pm n_2 \cdot \pi; \quad \tau_{A2}(\Omega) = 0; \quad \forall \Omega. \tag{2.18b,c}$$

In conclusion, $A_2(z)$ reduces to a complex unimodular constant, and the global allpass $A(z)$ behaves like an allpass of degree $(N - n_2)$.

In practice, the net effect of $A_2(z)$ is indistinguishable from the contribution of λ. Moreover, besides of being non-economic, pathological allpass functions should be imperatively avoided, because [4] :

- their phase response is highly sensitive near to $\Omega = \delta_\nu$, $\forall \nu \in [1,2,\ldots,n_2]$;
- they are prone to spurious internal signal states (non-controllable and/or non-observable states [Bele68]), depending on their implementation structure.

---

[4] It is however noticed that pathological allpass functions may harmlessly occur within *intermediate* steps of certain constructive design methods, as long as the *final* allpass is non-pathological.
For instance in [Henk81a], real arbitrary-phase polynomials are genecated by original recurrence formulae. The method proceeds systematically, starting from a set of zeroth and first-order polynomials, constructing higher-order polynomials by interpolation, with inheritance of former interpolation points. Depending on the problem formulation, i.e. preliminary organization of design parameters, pathological polynomials may without problem occur in *intermediate* design steps. Most important in the present context, it is demonstrated in [Henk81a] that the pathological character is *not* propagated to the next higher-order polynomial using the proposed recurrence formulae.

In the remainder of this report, only *non-pathological* allpass functions are considered.

2.2.7 Losslessness of complex allpass functions

According to (2.2), the input and output signals of a stable unit-magnitude allpass network, denoted by $x(n)$ and $y(n)$, respectively, are related by $|Y(e^{j\Omega})|=|X(e^{j\Omega})|$, $\forall\Omega$. Hence, one verifies for any $x(n)$:

$$\int_{\alpha}^{\alpha+2\pi}\left|Y\left(e^{j\Omega}\right)\right|^2\frac{d\Omega}{2\pi}=\int_{\alpha}^{\alpha+2\pi}\left|X\left(e^{j\Omega}\right)\right|^2\frac{d\Omega}{2\pi} \tag{2.19}$$

where α is an arbitrary real constant. Applying Parseval's theorem results in :

$$E_y=\sum_{n=-\infty}^{\infty}|y(n)|^2=\sum_{n=-\infty}^{\infty}|x(n)|^2=E_x\ , \tag{2.20}$$

and one observes that the energy of the output signal E_y equals the energy of the input signal E_x. Allpass functions are therefore considered as *lossless* functions, or *pseudo-lossless* functions according to the terminology introduced in [Fett72b].

2.3 Even/odd phase response constituents of complex allpass functions

This section aims at deriving for any complex allpass network an equivalent allpass composed of elementary allpass functions with even and odd phase response. The purpose of this operation is threefold. First, the basic pole structure of allpass functions with purely even pbase response is identified, and will give rise to a detailed discussion in Section 2.4. Second, the relationship between the original complex allpass and the related elementary allpass functions with even/odd symmetry is analyzed, providing in particular the basis for simplified allpass design methods, as examplified in Subsection 2.3.4. Finally, the achieved relationships will serve in Section 2.5 to develop original stability criteria. Most of the results produced in the present section were published in [Anso99].

2.3.1 Decomposition of complex allpass functions

Making use of equation (2.14b), the even and odd parts of the phase response β_A, i.e. β_{AE} and β_{AO}, respectively, are specified as :

$$\beta_{AE}(\Omega) = 0.5 \cdot [\beta_A(\Omega) + \beta_A(-\Omega)] = 0.5 \cdot [\beta_A(\Omega) - \beta_{\overline{A}}(\Omega)] \,, \qquad (2.21a)$$

$$\beta_{AO}(\Omega) = 0.5 \cdot [\beta_A(\Omega) - \beta_A(-\Omega)] = 0.5 \cdot [\beta_A(\Omega) + \beta_{\overline{A}}(\Omega)] \,, \qquad (2.21b)$$

with $$\beta_A(\Omega) = \beta_{AE}(\Omega) + \beta_{AO}(\Omega). \qquad (2.22)$$

For reasons that will be explained later, it is *not* possible to assign rational allpass functions to β_{AE} or β_{AO} in the most general case of $A(z)$. However, rational allpass filters can always be allocated to *twice* the value of β_{AE} and β_{AO}. The next functions are thus introduced :

$$A'_E\left(e^{j\Omega}\right) = e^{-j\cdot 2\cdot\beta_{AE}(\Omega)}, \quad A'_O\left(e^{j\Omega}\right) = e^{-j\cdot 2\cdot\beta_{AO}(\Omega)}, \qquad (2.23a,b)$$

fulfilling $$A^2(z) = A'_E(z) \cdot A'_O(z), \qquad (2.24)$$

according to (2.22). Finally, the next useful formulas are achieved from (2.21) and (2.23) :

$$A'_E(z) = A(z) / \overline{A(z)}, \quad A'_O(z) = A(z) \cdot \overline{A(z)}. \qquad (2.25a,b)$$

2.3.2 Allpass functions with purely even/odd phase response

Obviously, a complex allpass [5] $A(z)=A_E(z)$ featuring a purely *even* phase response verifies $\beta_{AO}(\Omega)\equiv 0$, $\forall\Omega$, resulting in $A'_O(z)\equiv 1$ due to (2.23b). Equation (2.25b) thus involves :

$$A(z)=A_E(z)=1/\overline{A_E(z)}. \tag{2.26}$$

Consequently, any pole $z_{\infty i}$ of $A=A_E$ is necessarily paired to another pole $z_{\infty i+1}=1/z_{\infty i}$ as depicted in Figure 2.4. Excluding any pole configuration that would lead to a collapse between poles and zeros, complex allpass filters with a purely *even* phase response are consequently demonstrated to be:

1) necessarily of even degree $N=N_E=2k$, with $k=0,1,2,...$;
2) precisely composed of $N_E/2$ stable and as many unstable poles for $N_E\geq 2$; and
3) devoid of any constituent allpass filter of *real* type.

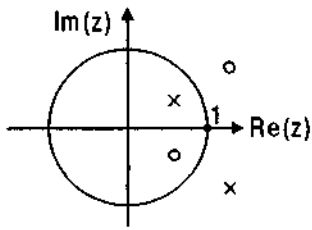

Figure 2.4: Pole/zero configuration for a 2nd-order complex allpass featuring a purely even phase response.

Clearly, allpass filters [6] $A(z)=A_O(z)$ featuring a purely *odd* phase response, except for a possible phase shift $\theta=\pm\pi$, are of real type with $\beta_{AE}(\Omega)\equiv 0$, $\forall\Omega$, and $A'_E(z)\equiv 1$. Equation (2.25a) implies then :

$$A(z)=A_O(z)=\overline{A_O(z)}. \tag{2.27}$$

---

[5] The function A_E is distinct from A'_E in (2.23a) and (2.25a).

[6] The function A_O is distinct from A'_O in (2.23b) and (2.25b).

2.3.3 Refined decomposition of allpass functions

The case of a general complex allpass $A(z)$ is now reconsidered by factorizing it into three parts, namely an allpass $A_1(z)$ collecting all real constituents of $A(z)$, a complex allpass $A_2(z)$ gathering all components of $A(z)$ featuring a purely even pbase response, and a residual complex allpass $A_3(z)$ whose phase response is neither even nor odd :

$$A(z)=\lambda\cdot A_1(z)\cdot A_2(z)\cdot A_3(z). \tag{2.28}$$

To render later developments clearer, the unimodular constant λ is explicitly extracted in (2.28) from the elementary $A_i(z)$, $i=1,2,3$, thus fixing $\lambda_i=1$, $\forall i$, in (2.5).

Denoting the degree of A_i by N_i, it is observed that $N=N_1+N_2+N_3$, where N_1 and N_3 are of any parity, whereas N_2 is necessarily even. Moreover, $A_1(z)$ and $A_2(z)$ are satisfying :

$$A_1(z)=\overline{A_1(z)}, \qquad A_2(z)=1/\overline{A_2(z)}, \tag{2.29a,b}$$

due to (2.27) and (2.26), so that equations (2.25a,b) result in :

$$A'_E(z)=\lambda^2\cdot A_2^2(z)\cdot A_3(z)/\overline{A_3(z)}, \tag{2.30a}$$

$$A'_O(z)=A_1^2(z)\cdot A_3(z)\cdot\overline{A_3(z)}. \tag{2.30b}$$

One notices that for $N_3>0$, neither $A'_E(z)$ nor $A'_O(z)$ correspond to the true square of a rational function, which explains a posteriori the reason of splitting the *square* of $A(z)$ into constituents featuring an even/odd phase response, cf equation (2.24).

The degrees of polynomials $A^2(z)$, $A'_E(z)$, and $A'_O(z)$ in (2.24) and (2.30) amount to :

$$\deg\{A^2(z)\}=2N=2(N_1+N_2+N_3), \tag{2.31a}$$

$$\deg\{A'_E(z)\}=2(N_2+N_3), \quad \deg\{A'_O(z)\}=2(N_1+N_3), \tag{2.31b,c}$$

leading to :

$$\begin{aligned}\deg\{A^2(z)\}&=\deg\_\text{Reduced}\{A'_E(z)\cdot A'_O(z)\}\\&\le\deg\{A'_E(z)\}+\deg\{A'_O(z)\},\end{aligned} \tag{2.32}$$

where $\deg\_{\text{Reduced}}\{A'_E(z)\cdot A'_O(z)\}$ measures the degree of the *reduced* term $A'_E(z)\cdot A'_O(z)$ achieved after cancellation of matching poles and zeros. Clearly, equality in (2.32) only holds for $N_3=0$.

Example

A decomposition example based on the allpass specified in Table 2.3 is illustrated in Figure 2.5, including the unwrapped phase response and its even/odd constituents, and the group delay. The pole constellations of $A(z)$, $A'_E(z)$, and $A'_O(z)$ are also represented, where distinct labels are used to identify the poles assigned to $A_i(z)$, $i=1,2,3$.

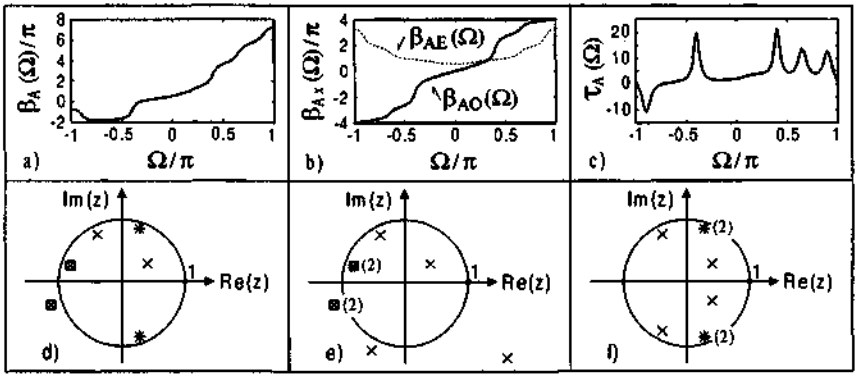

Figure 2.5: Decomposition of a 6th-order complex allpass function
(with ✱ : poles of $A_1(z)$, ◙ : poles of $A_2(z)$, × : poles of $A_3(z)$):
a) Unwrapped phase response; d) Pole configuration of $A(z)$;
b) Even/odd parts of phase; e) Pole configuretion of $A'_E(z)$;
c) Group delay; f) Pole configuration of $A'_O(z)$.

	ν	θ/π, $\mathrm{Re}\{z_{\infty\nu}\}$	$\mathrm{Im}\{z_{\infty\nu}\}$
θ/π	—	0.85	—
$z_{\infty\nu}$	1	$0.90\cdot\exp(\mathrm{j}\cdot 0.40\cdot\pi)$	
	2	$z_{\infty 2} = z_{\infty 1}^{*}$	
	3	$0.85\cdot\exp(\mathrm{j}\cdot 0.90\cdot\pi)$	
	4	$z_{\infty 4} = 1/z_{\infty 3}^{*}$	
	5	$0.85\cdot\exp(\mathrm{j}\cdot 0.65\cdot\pi)$	
	6	$0.50\cdot\exp(\mathrm{j}\cdot 0.20\cdot\pi)$	

Table 2.3: Parameters specifying the allpass $A(z)$ in Figure 2.5.

2.3.4 Design of complex allpass functions using the decomposed form

Following the former discussions, one observes that complex allpass functions without pure even or odd phase symmetry, can be designed (i.e. approximated) :

1) either directly from their phase specification, in which case an approximation tool for complex allpasses is requested, or
2) indirectly from the even/odd parts of the specified phase, making use of (2.28) – (2.30a,b), together with approximation tools for allpass networks featuring purely even/odd phase responses.

Usually, the optimization criteria are different for the direct and indirect design methods, so that the corresponding residual approximation errors will differ as well.

When applying the second method, it is in general necessary to perform a *joint* approximation of $A'_E(z)$ and $A'_O(z)$, cf (2.30a,b), including the factorization of the constituent networks $A_i(z)$, $i=1,2,3$, to have a better control of the residual error distribution.

In particular cases, it is possible to proceed to a rough approximation of complex allpasses using approximation tools previewed for real allpass functions only, as illustrated in the next example.

Example

A 5th-order complex allpass $A(z)$ fulfilling the next phase response specifications :

$$\beta_{As}(\Omega)=(N-0.5)\cdot\Omega, \quad \text{for} \quad \Omega\in[-\pi,\ 0.4\cdot\pi], \tag{2.33a}$$

$$\beta_{As}(\Omega)=(N-0.5)\cdot\Omega+\pi, \quad \text{for} \quad \Omega\in[0.6\cdot\pi,\ \pi]; \tag{2.33b}$$

as depicted in Figure 2.6a), should be designed. Such allpass functions are useful to realize antimetric lattice-type wave digital filters, cf Chapter 3, featuring an almost linear phase response.

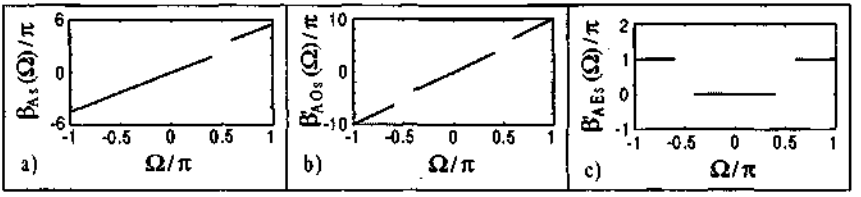

Figure 2.6: Phase specification of a 5th-order complex allpass :
a) Phase specification for $A(z)$; b) Phase specification for $A'_O(z)$;
c) Phase specification for $A'_E(z)$.

Referring to (2.23), Figures 2.6b) and 2.6c) show the specified phase response of $A'_O(z)$ and $A'_E(z)$, corresponding to twice the odd/even parts of $\beta_{As}(\Omega)$. According to Corollary 3 of Property 3 to be seen in Section 2.5, the allpass is known beforehand to be stable, the range of the specified phase response being $\beta_{As}(\pi)-\beta_{As}(-\pi)=2N$. Consequently, referring to (2.28) – (2.30), $N_2=0$, $A_2(z)\equiv 1$.

In a further step, $A(z)$ is indirectly designed through approximation of the 10th-order real allpass $A'_O(z)$, following the specified phase $\beta'_{AOs}(\Omega)$ in Figure 2.6b). The results are provided in Figure 2.7 and Table 2.4. Figures 2.7a1) and 2.7a2) represent the achieved phase response and residual approximation error $\varepsilon_{\beta' AO}(\Omega)$, defined by :

$$\varepsilon_{\beta' AO}(\Omega)=\beta'_{AO}(\Omega)-\beta'_{AOs}(\Omega), \tag{2.34}$$

whereas Figure 2.7d) depicts the pole configuration of $A'_O(z)$. Clearly, since there are no poles occurring twice within given tolerances, $N_1=0$, $A_1(z)\equiv 1$, and thus $N=N_3$, $A(z)=A_3(z)$. The poles belonging to $A_3(z)$ are then carefully selected, confronting the corresponding phase response to the specified one $\beta_{As}(\Omega)=\beta_{A3s}(\Omega)$, performing if necessary trial and error iterations.

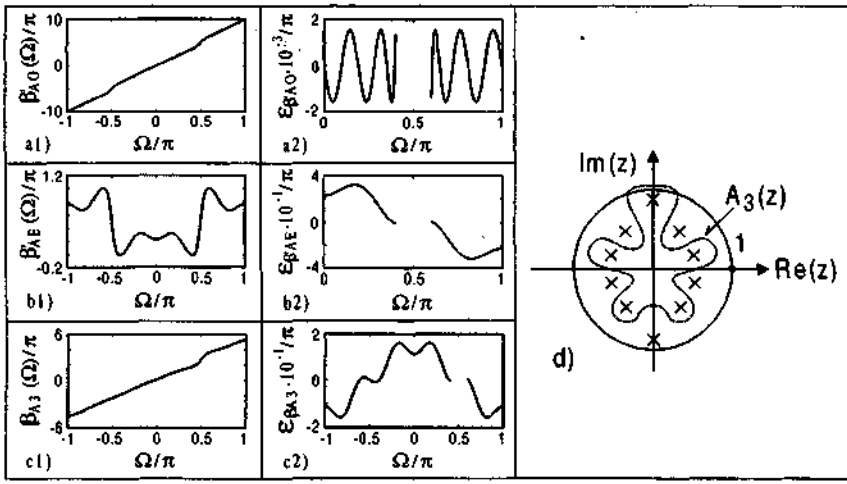

Figure 2.7: Indirect design of 5th-order complex allpass from the odd part of the phase specification :
a1) Approximated $\beta'_{AO}(\Omega)$; a2) Residual error of $\beta'_{AO}(\Omega)$;
b1) Measured $\beta'_{AE}(\Omega)$; b2) Measured error of $\beta'_{AE}(\Omega)$;
c1) Measured $\beta_{A3}(\Omega)$; c2) Measured error of $\beta_{A3}(\Omega)$;
d) Pole configuration of $A'_O(z)$, with indication of poles of $A_3(z)$.

	ν	θ/π, $\mathrm{Re}\{z_{\infty\nu}\}$	$\mathrm{Im}\{z_{\infty\nu}\}$
θ/π	—	0	—
$z_{\infty\nu}$	1	0	0.87494816536732
	2	0.52727953136742	0.17302611885221
	3	$z_{\infty 3} = -z^*_{\infty 2}$	
	4	0.34298463301594	−0.47628633440593
	5	$z_{\infty 5} = -z^*_{\infty 4}$	
	6 ~ 10	$z_{\infty\nu} = z^*_{\infty(11-\nu)}$	

Table 2.4: Parameters specifying the allpass $A'_O(z)$ in Figure 2.7.

	ν	θ/π, $\mathrm{Re}\{z_{\infty\nu}\}$	$\mathrm{Im}\{z_{\infty\nu}\}$
θ/π	—	−0.25	—
$z_{\infty\nu}$	1 − 5	$z_{\infty\eta}$, $\eta = 1,\ldots,5$, from Table 2.4	

Table 2.5: Parameters specifying the allpass $A_3(z)$ in Figure 2.7.

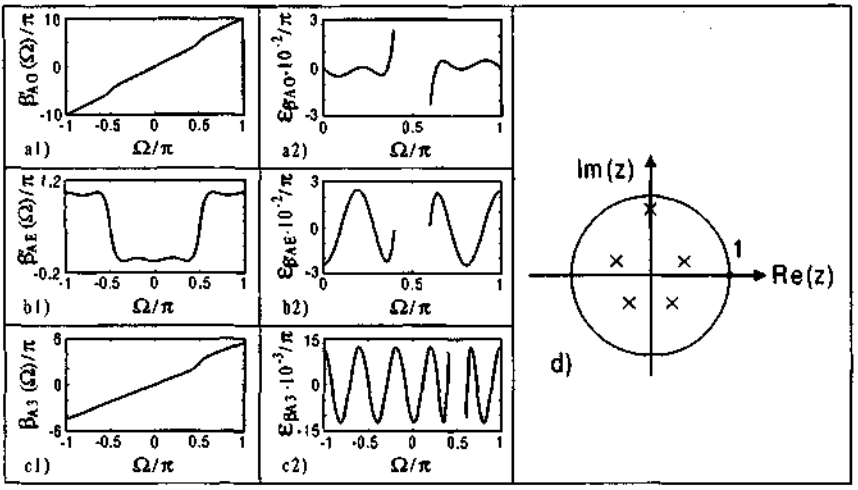

Figure 2.8: Design of 5th-order complex allpass :
a1) Measured $\beta'_{AO}(\Omega)$; a2) Measured error of $\beta'_{AO}(\Omega)$;
b1) Measured $\beta'_{AE}(\Omega)$; b2) Measured error of $\beta'_{AE}(\Omega)$;
c1) Approximated $\beta_{A3}(\Omega)$; c2) Residual error of $\beta_{A3}(\Omega)$;
d) Pole configuration of $A_3(z)$.

	ν	θ/π, Re$\{z_{\infty\nu}\}$	Im$\{z_{\infty\nu}\}$
θ/π	—	−0.25	—
$z_{\infty\nu}$	1	0	0.83103852841610
	2	0.42947066493390	0.17862887686643
	3	$z_{\infty 3} = -z^*_{\infty 2}$	
	4	0.26975615538154	−0.34662547930327
	5	$z_{\infty 5} = -z^*_{\infty 4}$	

Table 2.6: Parameters specifying the allpass $A_3(z)$ in Figure 2.8.

Once the poles of $A_3(z)$ are identified, cf Figure 2.7d), the constant λ in (2.28) and (2.30a) is determined minimizing either the measured error $\varepsilon_{\beta' AE}(\Omega)$ of $\beta'_{AE}(\Omega)$, or the measured error $\varepsilon_{\beta A3}(\Omega)$ of $\beta_{A3}(\Omega)$, where $\varepsilon_{\beta' AE}(\Omega)$ and $\varepsilon_{\beta A3}(\Omega)$ are defined similarly to (2.34). The parameters of $A_3(z)$ being established, cf Table 2.5, the assessment of the achieved allpass can be complemented as depicted in Figures 2.7b1) to 2.7c2). It should be noticed tbat the obtained

results could be further improved performing additional approximation iterations involving both odd and even parts of the phase response. These improvements were not undertaken in this work.

The allpass $A(z)=A_3(z)$ was also directly approximated for comparison purposes, resulting in Figure 2.8 and Table 2.6.

It is observed that the indirectly designed allpass provides a correct estimation of the targeted allpass, but should be improved to get a usable solution. Moreover, the residual phase approximation errors in Figures 2.7a2), b2), c2) and Figures 2.8a2), b2), and c2) are noticed to differ depending on the used approximation criterion, in particular regarding the respective number and size of the ripples.

2.4 Explicit form of allpass functions with purely even phase response

Referring to Subsection 2.3.2, a non-pathological complex allpass $A_E(z)$ featuring a purely even phase response $\beta_{AE}(\Omega)$, and being thus of necessarily even degree N, can be written as :

$$A_E(z)=\lambda\cdot\prod_{\nu=1}^{N/2}\left(\frac{1-z_{\infty\nu}^{*}\cdot z}{z-z_{\infty\nu}}\right)\cdot\left(\frac{1-z/z_{\infty\nu}^{*}}{z-1/z_{\infty\nu}}\right)=\lambda\cdot\frac{z^N\cdot\tilde{P}(z)}{P(z)}\,, \qquad (2.35)$$

where the poles $z_{\infty\nu}$ are necessarily complex with $\mathrm{Im}\{z_{\infty\nu}\}\neq 0$, $|z_{\infty\nu}|\neq 1$, $\forall\nu$. Clearly, $P(z)$ is a *circularly symmetric* polynomial, cf Subsection A.2.8, as can be verified from :

$$P(z)=\prod_{\nu=1}^{N/2}\left(z^2-(z_{\infty\nu}+1/z_{\infty\nu})\cdot z+1\right), \qquad (2.36)$$

inducing that $P(z)$ can be reformulated as :

$$P(z)=\sum_{\mu=0}^{N}p_\mu\cdot z^\mu\,,\quad \text{with}\quad p_0=p_N=1, \qquad (2.37)$$

and $\qquad p_\mu=p_{N-\mu}\,,\quad \mu=1,2,\ldots,N/2.$

Moreover, extracting from $P(z)$ the factor $z^{N/2}$:

$$P(z)=z^{N/2}\cdot P'(z)\,, \qquad (2.38)$$

it is possible to specify an auxiliary rational function $P'(z)$:

$$P'(z) = p_{N/2} + \sum_{\mu=0}^{(N/2)-1} p_\mu \cdot \left[z^{((N/2)-\mu)} + z^{-((N/2)-\mu)} \right]$$

$$= p_{N/2} + \sum_{\eta=1}^{N/2} p_{N/2-\eta} \cdot \left(z^{\eta} + z^{-\eta} \right) \qquad (2.39)$$

which can be rearranged in the following compact form :

$$P'(z) = \sum_{\eta=0}^{N/2} p'_\eta \cdot \left(\frac{z^{\eta} + z^{-\eta}}{2} \right), \qquad (2.40a)$$

with $p'_0 = p_{N/2}, \quad p'_\eta = 2 \cdot p_{N/2-\eta}$ for $\eta = 1,2,....,(N/2-1)$, (2.40b)

and $p'_{N/2} = 2 \cdot p_0 = 2.$

Hence, using (2.40a) together with (2.38) and (2.35), $A_E(z)$ and its corresponding phase response $\beta_{AE}(\Omega)$ can be expressed in the next canonic form :

$$A_E(z) = \lambda \cdot \frac{z^N \cdot \widetilde{P}(z)}{P(z)} = \lambda \cdot \frac{\widetilde{P'}(z)}{P'(z)}, \qquad (2.41)$$

$$\beta_{AE}(\Omega) = -\left[\theta + 2 \cdot \beta_{P'}(\Omega)\right], \quad \theta = \mathrm{Arg}\{\lambda\}, \qquad (2.42a)$$

with $$\beta_{P'}(\Omega) = -\arctan\left(\frac{\sum_{\eta=0}^{N/2} p'_{I\eta} \cdot \cos(\eta\Omega)}{\sum_{\eta=0}^{N/2} p'_{R\eta} \cdot \cos(\eta\Omega)} \right), \qquad (2.42b)$$

and $$p'_\eta = p'_{R\eta} + j \cdot p'_{I\eta}, \qquad (2.42c)$$

$$p'_{N/2} = 2 \quad \Rightarrow \quad p'_{R(N/2)} = 2, \quad p'_{I(N/2)} = 0. \qquad (2.42d)$$

Clearly, it is verified from equations (2.42b) and (2.42a) that $\beta_{P'}(\Omega)$ and thus $\beta_{AE}(\Omega)$ are even functions of Ω.

Moreover, the number of real parameters fully specifying $A_E(z)$ is the same as for real allpass functions, namely $(N+1)$, corresponding to the real and imaginary components of p'_η, $\eta = 0,1,...,(N/2-1)$, together with θ, cf Table 2.1.

Finally, the design steps to achieve an allpass with even phase response are tbe following :

1) Select an even degree N.

2) Approximate $\beta_{AE}(\Omega)$ according to the specified phase response $\beta_{AEs}(\Omega)$ using (2.42a) – (2.42d) together with a selected approximation method. The rational function $P'(z)$ of degree $N/2$ and λ or θ are then established.

3) Derive the polynomial $P(z)$ in (2.37) applying :

$$\begin{aligned} &p_0 = 1; \quad p_{N/2-\eta} = p'_\eta/2 \quad \text{for } \eta = 1,2,\ldots,(N/2-1); \\ &p_{N/2} = p'_0; \quad \text{and} \quad p_k = p_{N-k} \quad \text{for } k = (N/2+1),\ldots,N. \end{aligned} \tag{2.43}$$

Examples

Figure 2.9 and Table 2.7 present a 6th-order complex allpass with even phase and thus odd group delay.

Figures 2.10 – 2.12, with corresponding Tables 2.8 – 2.10, are in turn showing 6th-order allpass functions $A_E(z)$ featuring an even and almost linear phase response over $|\Omega| \in [0, 0.9 \cdot \pi]$, approximated in the equiripple sense. The figures represent the unwrapped phase $\beta_{AE}(\Omega)$, the corresponding group delay, the unwrapped phase of the constituent allpass $A_{E1}(z)$ collecting the stable poles of $A_E(z)$, the residual approximation error :

$$\varepsilon_{\beta AE}(\Omega) = \beta_{AE}(\Omega) - \beta_{AEs}(\Omega), \tag{2.44}$$

where $\beta_{AEs}(\Omega)$ is the specified phase response, and the poles configuration of $A_E(z)$.

Interestingly, one notices that the poles tend to collapse with the real axis for rather low slopes, cf Figure 2.11, whereas the poles lean to become all pathological for higher slope values, cf Figure 2.12, with a quasi-regular distribution along the unit-circle within the specified frequency range.

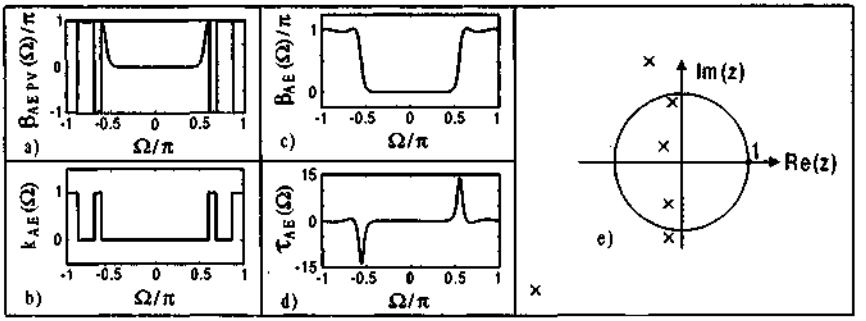

Figure 2.9: 6th-order complex allpass with purely even phase response:
a) PV of the phase response;
b) Phase unwrapping factor;
c) Unwrapped phase response;
d) Group delay;
e) Poles configuration.

	ν	θ/π, Re$\{z_{\infty\nu}\}$	Im$\{z_{\infty\nu}\}$
θ/π	—	0.08941355286258	—
$z_{\infty\nu}$	1	−0.20068185138151	−0.60886993992255
	2	−0.15354945297270	0.87488889993960
	3	−0.26422833019066	0.22649405639718
	4, 5, 6	$z_{\infty\nu} = 1 / z_{\infty(7-\nu)}$	

Table 2.7: Parameters specifying the allpass illustrated in Figure 2.9.

It is further remarked for allpass networks featuring an even pbase, that the spanned phase range $[\beta_A(\pi)-\beta_A(0)]$ can be specified in a very flexible way, namely that it is not constrained to $k\cdot\pi$, $|k|\leq N$, $k\in\mathbb{Z}$, compared to the real allpass case, cf (2.58). This property can be in particular well exploited in the realm of allpass-based filter transformation methods [Anso00].

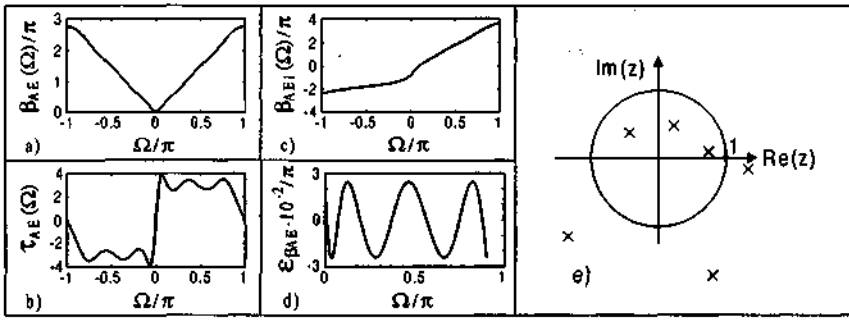

Figure 2.10: 6th-order complex allpass with even and almost linear phase response with $\beta_{AE}(\Omega) \cong 3 \cdot |\Omega|$, $|\Omega| \in [0, 0.9 \cdot \pi]$:
a) Unwrapped phase response; c) Unwrapped phase of $A_{E1}(z)$;
b) Group delay; d) Residual approximation error;
e) Poles configuration.

	ν	θ/π, $\mathrm{Re}\{z_{\infty\nu}\}$	$\mathrm{Im}\{z_{\infty\nu}\}$
θ/π	—	−1.83510972898010	—
$z_{\infty\nu}$	1	0.74388651897665	0.09236788798514
	2	0.22551516611338	0.47668290476940
	3	−0.43048106800464	0.36843269843914
	4, 5, 6	$z_{\infty\nu} = 1 / z_{\infty(7-\nu)}$	

Table 2.6: Parameters specifying the allpass illustrated in Figure 2.10.

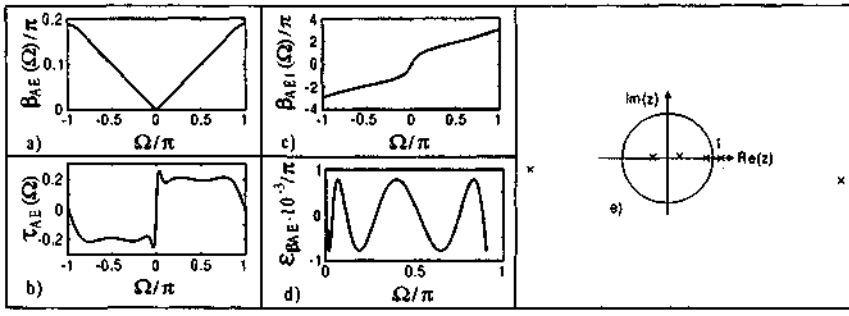

Figure 2.11: 6th-order complex allpass with even and almost linear phase response with $\beta_{AE}(\Omega) \cong 0.2 \cdot |\Omega|$, $|\Omega| \in [0, 0.9 \cdot \pi]$:
a) Unwrapped phase response; c) Unwrapped phase of $A_{E1}(z)$;
b) Group delay; d) Residual approximation error;
e) Poles configuration.

	ν	θ/π, $\mathrm{Re}\{z_{\infty\nu}\}$	$\mathrm{Im}\{z_{\infty\nu}\}$
θ/π	—	−0.12826397587580	—
$z_{\infty\nu}$	1	0.85166346668685	0.00176400940432
	2	−0.32875734449001	0.02791122713453
	3	0.25763874038248	0.03312962170538
	4, 5, 6	$z_{\infty\nu} = 1 / z_{\infty(7-\nu)}$	

Table 2.9: Parameters specifying the allpass illustrated in Figure 2.11.

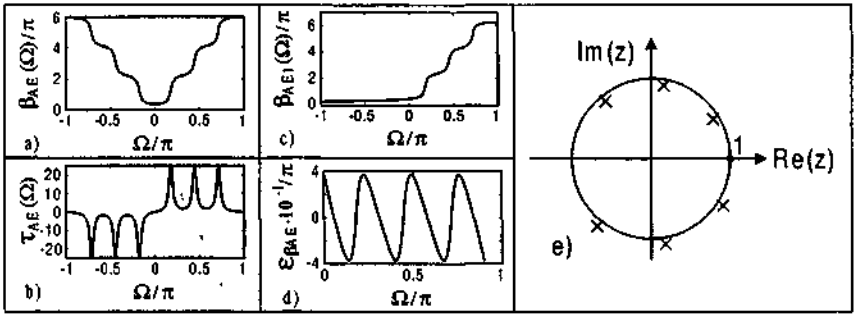

Figure 2.12: 6th-order complex allpass with even and almost linear phase response with $\beta_{AE}(\Omega) \cong 7.0 \cdot |\Omega|$, $|\Omega| \in [0, 0.9 \cdot \pi]$:
a) Unwrapped phase response; c) Unwrapped phase of $A_{E1}(z)$;
b) Group delay; d) Residual approximation error;
e) Poles configuration.

	ν	θ/π, $\mathrm{Re}\{z_{\infty\nu}\}$	$\mathrm{Im}\{z_{\infty\nu}\}$
θ/π	—	−0.11225369076380	—
$z_{\infty\nu}$	1	0.78161237133097	0.49396122657832
	2	−0.57845621521259	0.72015627456241
	3	0.15354645535954	0.90894345006201
	4, 5, 6	$z_{\infty\nu} = 1 / z_{\infty(7-\nu)}$	

Table 2.10: Parameters specifying the allpass illustrated in Figure 2.12.

2.5 Stability-related properties of complex allpass functions

This section aims at discussing in detail the relationship between the stability of complex allpass functions and their phase or group delay responses. These properties are for instance useful to determine the strict stability of allpass networks by measuring their phase/group delay responses over the whole frequency domain, without having to explicitly compute the poles. In addition to assessing the strict stability of an allpass, these properties provide an easy way to establish the number of stable and unstable poles belonging to any allpass, by observation of its phase response over the whole frequency domain. Moreover, in the frame of an allpass approximation problem, it is then possible to check the consistency of the specified phase response to be achieved, before actually launching the approximation.

This section is structured as follows. A non-exhaustive synopsis of known stability-related properties is first provided as background to the discussed developments. Next, the connection between the stability and the monotone increasing character of the phase response of an allpass is recalled, before making the link with the spanned range of the phase response, which is central to this section. The features of the allpass mean group delay are then handled. Finally, stability conditions are established in relation with the even and odd parts of the allpass phase response. Part of the results achieved in this section were published in [Anso99].

Clearly, the stability-related properties presented in this section directly apply to complex polynomials as well, considering the straight link between allpass functions and their denominator, cf (2.4).

2.5.1 Known stability related properties

There exist of course many different definitions of the stability, according to the classes of problems to be handled. Important taxonomy criteria are [Levi96, Lopa96, Khal96]: 1) the linearity/non-linearity of the considered system; 2) the type of mathematical model best representing the behavior of the system (i.e. total or partial differential equations for systems with lumped or distributed parameters, respectively); 3) the deterministic or stochastic character of the system;

4) the time invariant, time varying, or periodically time varying nature of the system; 5) the type of signals handled within the system and at its interfaces, including time-continuous, time-discrete, digital, or mixed signals; 6) others.

This report is focusing on linear time-invariant (LTI) systems only, modeled by rational functions, so that the notion of stability is exclusively linked to the pole constellation of the systems [7]. Numerous different stability criteria and test methods were elaborated in the literature to cover general or specific cases, e.g. [Bish96], in particular to reduce computation costs, which is most often achieved by avoidance of the explicit calculation of the poles.

In this section, the link between the stability and the phase/group delay responses of polynomials and allpass functions is considered, centering the discussion on the case of digital systems. The results extend however directly to time-discrete systems, or to time-continuous systems with either lumped or commensurate distributed parameters using the bilinear transform.

Table 2.11 provides a selected set of stability criteria for polynomials and allpass functions that were discussed in the literature. This list is by far non-exhaustive. The known stability criteria corresponding to Cases 7 and 8 in Table 2.11 are recalled in Subsections 2.5.2 and 2.5.3, and will serve as basis for the elaboration of new criteria.

---

[7] It is recalled that any (complex) rational function $F(z)$ is said to be *strictly stable* when all its poles lie within the *open* unit-circle in the z-plane. $F(z)$ is on the contrary denoted *unstable* when at least one of its poles is outside the *closed* unit-circle, whereas it becomes *strictly unstable* when all poles are confined outside the *closed* unit-circle. Poles *on* the unit-circle are not considered here.

	Case	Stability criteria / test methods	Time continuous ψ -domain		Time discrete z -domain	
			Real case	Complex case	Real case	Complex case
General	1	Lyapunov, Popov, etc.	[Khal96]	X		
Linear Time Invariant Cases	2	Polynomial: Routh-Hurwitz	[Bose85, Vaid87c, Baue95, Bish96]	X	–	–
	3	Schur-Cohn-Fujiwara-Jury	–	–	[Bose85, Vaid87c, Baue95, Bish96]	X
		...				
	4	Pseudo-lossless function based	[Dels85]	[Dels85]	[Dels84]	[Dels84]
		...				
	5	Phase properties of polynomials	[Bose94, Keel96]	[Bose94, Keel96]	[Bose94]	[Bose94]
	6	Polynomial phase approximation based	[Henk81b]	–	([Henk81b])	–
		...				
	7	Allpass monotooe phase response	[Bele68]	[Bele68]	([Bele68]), [Vaid93]	([Bele68]), [Vaid93]
	8	Allpass spanned range of phase response	[Bele68]	[Bele68]	([Bele68]), [Vaid93]	([Bele68]), [Vaid93]
	9	Allpass monotone phase response with even / odd response decomposition	–	([Anso99], and this report)	–	[Anso99], and this report

Table 2.11: Selected set of stability criteria and related references [8, 9].

[8] Entries marked with an "X" correspond to cases that are known to be covered in the literature, without explicit provision of a reference in this report.

[9] Entries mentioned in parenthesis are horizontally achieved in Table 2.11 through bilinear transform of the problem from the time continuous ψ -domain to the time discrete z -domain or conversely, cf (A.50), and (A.51).

2.5.2 Stability and monotone phase-response

Case of first-order allpass functions

Property 1 [Bele68, p. 167], [Vaid93, p. 76], (Table 2.11, Case 7) : A necessary and sufficient condition for a first-order complex allpass $A(z)$ to be strictly stable (strictly unstable) is that its group delay $\tau_A(\Omega)$ is strictly positive (strictly negative) over the whole frequency axis, or equivalently, that its *unwrapped* phase response is a monotone increasing (decreasing) function over the whole frequency range.

Proof of necessity : A first-order allpass with pole $z_\infty = \rho \cdot e^{j\delta}$, $\rho \geq 0$, is considered :

$$A(z) = \lambda \cdot \frac{1 - z_\infty^* \cdot z}{z - z_\infty} = \lambda \cdot z^{-1} \cdot \frac{1 - z_\infty^* \cdot z}{1 - z_\infty \cdot z^{-1}}. \tag{2.45}$$

From the frequency response :

$$A\left(e^{j\Omega}\right) = e^{-j(\Omega-\theta)} \cdot \frac{1 - \rho \cdot e^{j(\Omega-\delta)}}{1 - \rho \cdot e^{-j(\Omega-\delta)}}, \tag{2.46}$$

one derives directly the phase response [10] and group delay :

$$\beta_A(\Omega) = \Omega - \theta + 2 \cdot \beta_P(\Omega), \quad \beta_P(\Omega) = \arctan\left(\frac{\rho \cdot \sin(\Omega - \delta)}{1 - \rho \cdot \cos(\Omega - \delta)}\right), \tag{2.47}$$

$$\tau_A(\Omega) = \frac{d\beta_A(\Omega)}{d\Omega} = \frac{1 - \rho^2}{(1-\rho)^2 + 2\rho \cdot [1 - \cos(\Omega - \delta)]}, \tag{2.48}$$

which are defined for all parameter values, except in the pathological case $\{\rho = 1, \Omega = \delta\}$ already handled in Subsection 2.2.6, and for which $\tau_A(\Omega) = 0$, $\forall\, \Omega$. For non-pathological cases, the denominator of τ_A is observed from (2.48) to fulfill :

$$\text{Denom}\{\tau_A(\Omega)\} > 0, \quad \forall \Omega, \ \forall \rho \mid (\rho \geq 0) \cap (\rho \neq 1), \tag{2.49}$$

---

[10] The phase response is here defined slightly differently than in (2.6) – (2.8) in order to render later considerations easier; the group delay and unwrapped phase response remain clearly unaffected.

so that the next relationships are achieved from (2.48) :

$$\begin{cases} \tau_A(\Omega) > 0, \ \forall \Omega & \Leftrightarrow \quad 0 \le \rho < 1; \qquad (2.50a) \\ \tau_A(\Omega) < 0, \ \forall \Omega & \Leftrightarrow \quad \rho > 1. \qquad (2.50b) \end{cases}$$

Hence, the group delay of a causal and strictly stable first-order allpass, i.e. $0 \le \rho < 1$, is strictly positive over the whole frequency domain. As a result, the corresponding unwrapped phase response is a monotone increasing function of Ω. Similarly, for a strictly unstable allpass, i.e. $\rho > 1$, $\tau_A(\Omega) < 0$, $\forall \Omega$, and the unwrapped phase becomes a monotone decreasing function of Ω, $\forall \Omega$. *Necessity* conditions are thus read in (2.50a) from right to left. ■

Proof of sufficiency : Conversely, a first-order allpass featuring a monotone increasing (decreasing) phase response – or equivalently a strictly positive (negative) group delay – is necessarily stricly stable (strictly unstable), as can be readily verified from (2.48) and (2.50a,b). *Sufficiency* conditions are consequently read from left to right in (2.50a,b). ■

Case of Nth-order allpass functions

Property 2 (Table 2.11, Case 7) :
For an Nth-order complex or real allpass $A(z)$, the condition of strictly positive (strictly negative) group delay $\tau_A(\Omega)$ over the whole frequency axis, or equivalently, the observation of a monotone increasing (decreasing) response of the *unwrapped* phase $\beta_A(\Omega)$, are necessary but insufficient conditions to guarantee the strict stability (strict instability) of $A(z)$.

Proof of necessity : Decomposing an Nth-order complex or real allpass filter into a cascade of elementary (complex) first-order cells :

$$A(z) = \prod_{\nu=1}^{N} A_\nu(z) \ , \ \beta_A(\Omega) = \sum_{\nu=1}^{N} \beta_{A\nu}(\Omega) \ , \ \tau_A(\Omega) = \sum_{\nu=1}^{N} \tau_{A\nu}(\Omega) \qquad (2.51)$$

where $A_\nu(z)$, $\beta_{A\nu}(\Omega)$, and $\tau_{A\nu}(\Omega)$ represent the transfer function, phase response, and group delay of each elementary cell, and assuming that every pole $z_{\infty\nu}$ of $A(z)$ is located within the open unit-circle, one deduces from (2.50a) that :

$$0 \le \rho_\nu < 1, \ \forall \nu \ \Rightarrow \ \tau_A(\Omega) > 0, \ \forall \Omega, \tag{2.52a}$$

namely, that the phase response of $A(z)$ is monotone increasing. Similarly, when every pole of $A(z)$ is lying outside the closed unit-circle, (2.50a) is implying :

$$\rho_\nu > 1, \forall \nu \ \Rightarrow \tau_A(\Omega) < 0, \forall \Omega, \tag{2.52b}$$

the phase response of $A(z)$ becoming then monotone decreasing. These features are verified for both complex and real $A(z)$. ■

Proof of insufficiency : The reciprocal assertion to the former demonstration would be misleading for Nth-order allpass functions, since compensation effects may occur between the contributions of the constituent cells. ■

Example

The next example illustrates the proof of insufficiency. A 4th-order complex allpass $A(z)$ counting three stable poles, and an unstable one is specified in Figure 2.13 and Table 2.12. Altbough $A(z)$ features a strictly positive group delay and thus a monotone increasing phase response, this allpass is undoubtedly unstable.

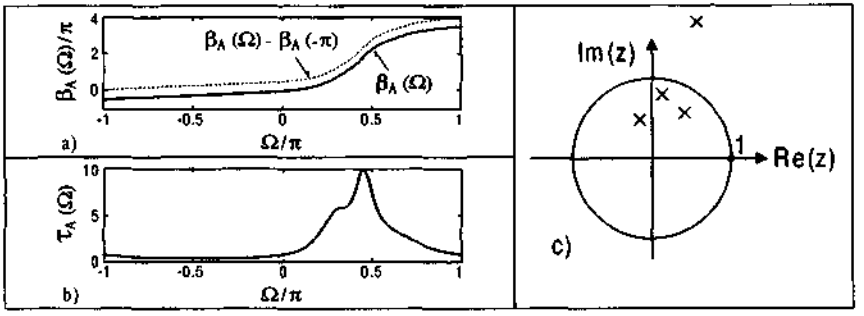

Figure 2.13: Unstable 4th-order complex allpass function featuring a monotone increasing phase response:
a) Unwrapped phase response; c) Poles configuration.
b) Group delay;

	ν	θ/π, $\mathrm{Re}\{z_{\infty\nu}\}$	$\mathrm{Im}\{z_{\infty\nu}\}$
θ/π	—	0	—
$z_{\infty\nu}$	1	$0.70\cdot\exp(\mathrm{j}\cdot 0.30\cdot\pi)$	
	2	$0.80\cdot\exp(\mathrm{j}\cdot 0.45\cdot\pi)$	
	3	$0.50\cdot\exp(\mathrm{j}\cdot 0.60\cdot\pi)$	
	4	$1.80\cdot\exp(\mathrm{j}\cdot 0.40\cdot\pi)$	

Table 2.12: Parameters specifying the allpass illustrated in Figure 2.13.

2.5.3 Spanned range of the phase response

Case of first-order allpass functions

Property 3 (Table 2.11, Case 8) :
The necessary and sufficient condition for a first-order complex allpass $A(z)$ to be strictly stable (unstable) is that the range spanned by its *unwrapped* phase response verifies for any constant $\alpha\in\mathbb{R}$:

$$\beta_A(\pi)-\beta_A(-\pi)=\beta_A(\alpha+2\pi)-\beta_A(\alpha)=\pm 2\pi,\quad \forall\alpha\in\mathbb{R}, \tag{2.53}$$

where the positive (negative) sign applies in the stable (unstable) case in the right hand-sided part of the formula.

Proof of necessity : Starting from (2.47), we specify :

$$\beta_A(\Omega)=\Omega-\theta+2\cdot\beta_P(\Omega),\quad \beta_P(\Omega)=\arctan\left(U_P(\Omega)/W_P(\Omega)\right), \tag{2.54a}$$
$$U_P(\Omega)=\rho\cdot\sin(\Omega-\delta),\qquad W_P(\Omega)=1-\rho\cdot\cos(\Omega-\delta). \tag{2.54b}$$

In the *stable* case, i.e. $0\le\rho<1$, $W_P(\Omega)>0$ is clearly verified $\forall\Omega$, whereas $U_P(\Omega)$ evolves with changing sign. $U_P(\Omega)/W_P(\Omega)$ is obviously an odd cyclic function of period 2π centered on $\Omega=\delta$, and so does $\beta_P(\Omega)$. Moreover, the min/max values of $U_P(\Omega)/W_P(\Omega)$ are observed to be *finite*, due to $W_P(\Omega)>0$, so that the min/max values of $\beta_P(\Omega)$ are confined to $0<\beta_{P\max}=-\beta_{P\min}<\pi/2$. Consequently, $\beta_P(\Omega)\equiv\beta_{P\,\mathrm{PV}}(\Omega)$, and $\beta_P(\alpha+2\pi)-\beta_P(\alpha)=0$, $\forall\alpha\in\mathbb{R}$, due to periodicity. (2.53) is thus demonstrated from (2.54a) in the stable case. An example is presented in Figure 2.14 and Table 2.13.

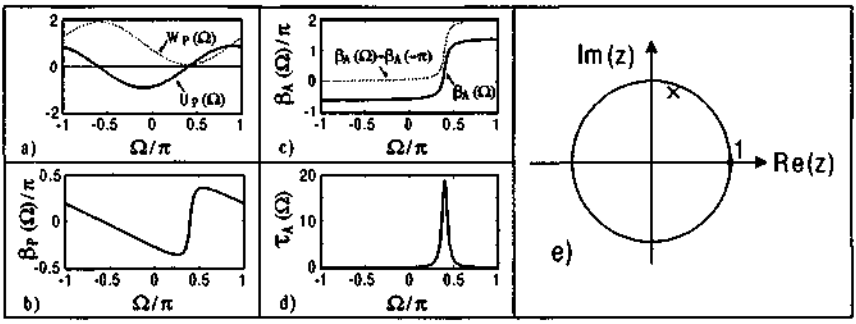

Figure 2.14: Spanned range of the phase response of a stable 1st-order complex allpass with $\rho = 0.90$, $\delta = 0.40 \cdot \pi$:
a) Functions $U_P(\Omega)$, $W_P(\Omega)$; c) Unwrapped phase of $A(z)$;
b) Phase $\beta_P(\Omega)$; d) Group delay of $A(z)$;
e) Pole configuration.

	ν	θ/π, $\mathrm{Re}\{z_{\infty\nu}\}$	$\mathrm{Im}\{z_{\infty\nu}\}$
θ/π	—	0	—
$z_{\infty\nu}$	1	$0.90 \cdot \exp(\mathrm{j} \cdot 0.40 \cdot \pi)$	

Table 2.13: Parameters specifying the allpass illustrated in Figure 2.14.

In the *unstable* case, i.e. $\rho > 1$, $U_P(\Omega)$ and $W_P(\Omega)$ are both evolving with changing sign, $U_P(\Omega)/W_P(\Omega)$ and $\beta_P(\Omega)$ remaining odd cyclic functions of period 2π centered on $\Omega = \delta$. The derivative of U_P/W_P is now demonstrated to be strictly negative, except at $W_P(\Omega) = 0$, cf (2.55), so that $U_P(\Omega)/W_P(\Omega)$ and thus the unwrapped $\beta_P(\Omega)$ become monotone decreasing functions of Ω.

$$\frac{d}{d\Omega}\left(\frac{U_P(\Omega)}{W_P(\Omega)}\right) = \frac{-\rho \cdot [\rho - \cos(\Omega - \delta)]}{W_P^2(\Omega)}, \tag{2.55}$$

Furthermore, assuming provisionally that $0 \le \delta < \pi/2$, it is noticed that the frequencies Ω_1 and Ω_3 verifying $U_P(\Omega) = 0$ alternate with the frequencies [11] Ω_2 and Ω_4 at which $W_P(\Omega) = 0$, so that :

$$-\pi < \Omega_1 < \Omega_2 < \Omega_3 < \Omega_4 < \pi, \tag{2.56a}$$

with $$\Omega_1 = \delta - \pi, \quad \Omega_2 = \delta - \xi, \quad \Omega_3 = \delta, \quad \Omega_4 = \delta + \xi, \tag{2.56b}$$

[11] $W_P(\Omega) = 0$ has clearly two solutions in the non-pathological case $\rho > 1$.

and $$\xi = \arccos(1/\rho), \quad 0 < \xi < \pi/2 .$$

The values of the unwrapped $\beta_P(\Omega)$ are then fulfilling :

$$\beta_P(-\pi) > \beta_P(\Omega_1) > \beta_P(\Omega_2) > \beta_P(\Omega_3) > \beta_P(\Omega_4) > \beta_P(\pi), \quad (2.56c)$$

with $$\beta_P(\Omega_1) = 0, \quad \beta_P(\Omega_2) = -\pi/2, \quad \beta_P(\Omega_3) = -\pi, \quad (2.56d)$$
$$\beta_P(\Omega_4) = -3\pi/2, \quad \beta_P(\pi) = \beta_P(-\pi) - 2\pi .$$

There is hence precisely one wrapping point at Ω_3 within the frequency domain $\Omega \in [-\pi, \pi]$, so that $\beta_P(\Omega) \equiv \beta_{P\,PV}(\Omega)$. Consequently, $\beta_P(\pi) - \beta_P(-\pi) = -2\pi$, the spanned range of $A(z)$ becoming $\beta_A(\pi) - \beta_A(-\pi) = -2\pi$. When assigning δ to other quadrants than $0 \le \delta < \pi/2$, i.e. $(k-2)\cdot\pi/2 \le \delta < (k-1)\cdot\pi/2$, $k = 0,1,3$, the frequencies Ω_i, $i = 1,2,3,4$, are cyclicly reordered, so that precisely one wrapping point is still encountered within $\Omega \in [-\pi, \pi]$, and the former results remain valid. This concludes the proof of (2.53) in the unstable case. An example is presented in Figure 2.15 and Table 2.14.

The demonstration of the necessity condition is thus completed. ■

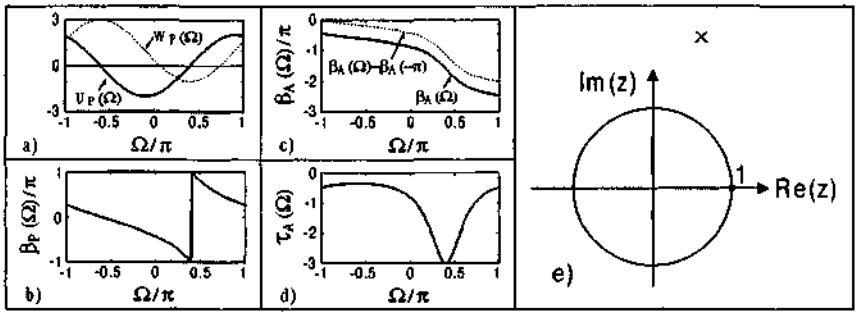

Figure 2.15: Spanned range of the phase response of an unstable 1st-order complex allpass with $\rho = 2.00$, $\delta = 0.40\cdot\pi$:
a) Functions $U_P(\Omega)$, $W_P(\Omega)$; c) Unwrapped phase of $A(z)$;
b) Phase $\beta_P(\Omega)$; d) Group delay of $A(z)$;
e) Pole configuration.

	ν	θ/π, $\mathrm{Re}\{z_{\infty\nu}\}$	$\mathrm{Im}\{z_{\infty\nu}\}$
θ/π	—	0	—
$z_{\infty\nu}$	1	$2.00\cdot\exp(\mathrm{j}\cdot 0.40\cdot\pi)$	

Table 2.14: Parameters specifying the allpass illustrated in Figure 2.15.

Proof of sufficiency : The proof proceeds in the reverse sense and is thus omitted. ■

Case of mixed stable/unstable Nth-order allpass functions

Corollary 1 to Proparty 3 :
Extending the result of Property 3 to Nth-order allpass functions $A(z)$ that are non-pathological but possibly featuring a mixed stable/unstable poles configuration, and denoting by N_1 and N_2 the number of stable and unstable poles, respectively, the next formulas are established from (2.53) :

$$\beta_A(\pi)-\beta_A(-\pi)=\beta_A(\alpha+2\pi)-\beta_A(\alpha)=2\pi\cdot n, \qquad (2.57a)$$

with $n=N_1-N_2,\ |n|\le N,\ n\in\mathbb{Z}$,

and $$N_1=(N+n)/2,\quad N_2=(N-n)/2,\quad N_1+N_2=N. \qquad (2.57b)$$

Proof : The proof is omitted due to evidence. ■

Example

Figure 2.13 shows the example of a 4th-order allpass with $N_1=3$ and $N_2=1$, inducing $n=2$, so that $\beta_A(\pi)-\beta_A(-\pi)=4\pi$.

Real Nth-order allpasa : In the real case, (2.57a) can be replaced by the simpler form :

$$\beta_A(\pi)-\beta_A(0)=\beta_A(\pi)-\theta=\pi\cdot n\ , \qquad (2.58)$$

the definition of n remaining the same than in (2.57a,b).

Complex allpass with even phase response : In this case, since the numbers of stable and unstable poles are by essence the same, $n=0$ in (2.57), with N even.

Remark on the parity nf the parameter n : Recalling that $A(z)$ is assumed non-pathological, it is observed from (2.57a,b) that $n=N_1-N_2=2\cdot N_1-N$, namely that n has the same parity than N regardless of the poles distribution among stable/unstable ones [12].

---

[12] The assumption of the non-pathological character of $A(z)$ in (2.57) is essential to verify $N_1+N_2=N$, involving 1) that the spanned range of the phase is

Spanned phase range over extended frequency domain

Corollary 2 to Property 3 :
Expressions (2.57a,b) evaluated over an extended frequency domain are verifying the next formula that is in particular useful in the frame of allpass-based filter transformation methods [Anso00] :

$$\beta_A(K\cdot 2\pi+\alpha)-\beta_A(\alpha)=2\pi\cdot K\cdot n\ ,\qquad K\in\mathbb{Z}\ ,\ \alpha\in\mathbb{R}\ , \tag{2.59}$$

the parameter n remaining specified as in (2.57a,b).

Proof :
Performing the substitution $\alpha\mapsto(k-1)\cdot 2\pi+\alpha$, $k\in\mathbb{N}_+$, in (2.57a), one achieves :

$$\beta_A(k\cdot 2\pi+\alpha)-\beta_A((k-1)\cdot 2\pi+\alpha)=2\pi\cdot n\ ,\quad k\in\mathbb{N}_+,\ \alpha\in\mathbb{R}\ . \tag{2.60}$$

Evaluating recurrently (2.60) for $k=K,K-1,K-2,...,1$, with $K\in\mathbb{N}_+$, and summing up all resulting equations, one gets :

$$\beta_A(K\cdot 2\pi+\alpha)-\beta_A(\alpha)=2\pi\cdot K\cdot n\ ,\qquad K\in\mathbb{N}_+,\ \alpha\in\mathbb{R}\ . \tag{2.51}$$

It is then remarked that the arguments of $\beta_A(.)$ occur in decreasing order when reading (2.57a) from left to right. This is also the case in (2.60) for $k\in\mathbb{N}_+$, but not any more when assigning negative values to k, in which case it is necessary to change as well the sign of the right hand-sided part of (2.60). It is thus demonstrated that (2.61) can be generalized as specified in (2.59). ■

Case of strictly stable/unstable Nth-order allpass functions

Corollary 3 to Property 3 [Bele68, p. 167], [Vaid93, p. 76], (Table 2.11, Case 8) :
The necessary and sufficient condition for an Nth-order complex allpass $A(z)$ to be strictly stable (strictly unstable) is that the range spanned by its *unwrapped* phase verifies for any constant $\alpha\in\mathbb{R}$:

$$\beta_A(\pi)-\beta_A(-\pi)=\beta_A(\alpha+2\pi)-\beta_A(\alpha)=\pm 2\pi\cdot N\ ,\quad \forall\alpha\in\mathbb{R}\ . \tag{2.62}$$

---

decreasing by steps of 2π with every unstable pole; and 2) that n and N share the same parity.

where the positive (negative) sign applies in the stable (unstable) case in the right hand-sided part of the formula.

Proof of necessity : Assuming that $A(z)$ is strictly stable (strictly unstable), $n=N_1=N$ and $N_2=0$ $(n=-N_2=-N$ and $N_1=0)$ are verified in (2.57), resulting in (2.62) with appropriate sign. ■

Proof of sufficiency : The proof proceeds in the reverse sense and is thus omitted. ■

Remarks :
Considering the pbase $\beta_A(\Omega)=\beta_{AE}(\Omega)+\beta_{AO}(\Omega)$ of an Nth-order allpass, where $\beta_{AO}(\Omega)$ is assumed purely odd, and noting that by essence $\beta_{AE}(-\pi)=\beta_{AE}(\pi)$, (2.57) can be restated as :

$$\beta_A(\pi)-\beta_A(-\pi)=\beta_{AO}(\pi)-\beta_{AO}(-\pi)=2\cdot\beta_{AO}(\pi)=2\pi\cdot n,$$
$$\Rightarrow \quad \beta_{AO}(\pi)=\pi\cdot n \tag{2.63}$$

showing that for a complex allpass, it suffices to consider the spanned range of $\beta_{AO}(\Omega)$ over $\Omega\in[0,\ \pi]$, similarly to the case of real allpass networks [13], cf (2.58). This remark applies also to (2.59), and, as mentioned in [Anso99], to (2.62) to assess the strict stability/unstability of a complex allpass.

Discussion
The publications [Bele68] and [Vaid93] are covering Property 1, and Corollary 3 of Property 3, limiting the last to the case of strictly stable Nth-order allpass filters, and proving it by the sole invocation of the monotone increasing character of the phase, without explicit provision of a thorough analysis of the spanned phase range as provided in Property 3 in this document.
It is believed that the discussion proposed in the report offers an enlarged insight into the stability-relatad features of complex allpass functions. Hence, Property 2 is catching the attention to avoid undue extension of Property 1 from the 1st-order to the Nth-order case [14].

---

[13] The only difference is that $\beta_{AO}(\Omega)$ is by definition assumed to be purely odd, i.e. $\beta_{AO}(\Omega)=-\beta_{AO}(-\Omega)$, whereas for a real allpass network, $\beta_A(\Omega)$ can be affected by a possible phase shift $\theta=\pm\pi$.

[14] There is no originality claim with this respect.

Moreover, Corollary 1 to Property 3 is of much richer use to assess the number of stable/unstable poles of an Nth-order allpass. Finally, Corollary 2 to Property 3, representing the most general formulatioo of tbe spanned phase range derived in this report, is useful in the realm of allpass-based filter transformation methods [Anso00].

2.5.4 Mean group delay

Cnrollary 4 to Property 3 :
Given an Nth-order allpass $A(z)$ that is non-pathological but possibly featuring a mixed stable/unstable poles configuration. The mean group delay of $A(z)$ measured over $\Omega \in [\alpha, (\alpha+2\pi)]$, $\forall \alpha \in \mathbb{R}$, fulfills:

$$\overline{\tau_A} = n, \quad \text{with } |n| \leq N,\ n \in \mathbb{Z}, \tag{2.64}$$

the parameter n remaining specified as in (2.57a,b).

Proof : The mean group delay is specified by :

$$\overline{\tau_A} = \frac{1}{2\pi} \int_{\alpha}^{\alpha+2\pi} \tau_A(\Omega) \cdot d\Omega = \frac{1}{2\pi} \cdot [\beta_A(\alpha+2\pi) - \beta_A(\alpha)], \tag{2.65}$$

where $\beta_A(\alpha+2\pi)$ and $\beta_A(\alpha)$ are evaluated along the unwrapped function $\beta_A(\Omega)$, $\forall \alpha \in \mathbb{R}$. (2.64) results then by direct application of (2.57a). ■

Corollary 5 to Property 3 :
The necessary and sufficient condition for an Nth-order allpass $A(z)$ to be strictly stable (strictly unstable) is that its meao group delay measured over $\Omega \in [\alpha, (\alpha+2\pi)]$, $\forall \alpha \in \mathbb{R}$, verifies.

$$\overline{\tau_A} = \pm N, \tag{2.66}$$

the positive (negative) sign applying in the stable (unstable) case.

Proof : (2.66) is a particular case of (2.64), the demonstration proceeding similarly to the proof of Corollary 3 to Property 3. ■

Examples

Three application examples of (2.64) are proposed in Figure 2.16, referring to the allpass networks $A(z)$ specified in Tables 2.13, 2.14,

and 2.12, respectively. The depicted mean values $\overline{\tau_A} = n$ were numerically processed over all measured values of $\tau_A(\Omega)$, $\Omega \in [-\pi, \pi)]$, producing results that are correct within a marginal error which can be cancelled out by rounding the achieved value. In practice, if the density of measured values $\tau_A(\Omega)$ is sufficient, (2.64) provides an accurate assessment on the stable/unstable pole distribution of $A(z)$.

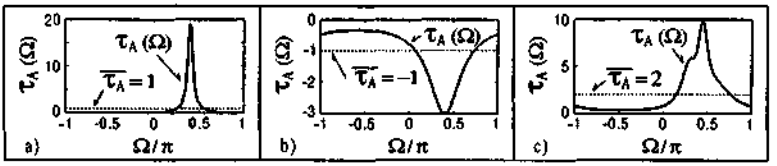

Figure 2.16: Examples of group delay and mean group delay :
a) Stable 1st-order complex allpass specified in Table 2.13;
b) Unstable 1st-order complex allpass specified in Table 2.14;
c) Unstable 4th-order complex allpass specified in Table 2.12.

Remarks :
Let us decompose the group delay of a complex allpass into its even and odd parts :

$$\tau_A(\Omega) = \tau_{AE}(\Omega) + \tau_{AO}(\Omega), \tag{2.67}$$

with $\tau_{AE}(\Omega) = \mathrm{d}\beta_{AO}(\Omega)/\mathrm{d}\Omega$, $\tau_{AO}(\Omega) = \mathrm{d}\beta_{AE}(\Omega)/\mathrm{d}\Omega$, (2.68a,b)

since the first derivative of an even (odd) real and continuous function is odd (even), cf Table A.1. It is observed that the mean value of $\tau_{AO}(\Omega)$ measured over $\Omega \in [\alpha, \alpha + 2\pi]$, $\forall \alpha \in \mathbb{R}$, equals zero by essence, so that (2.64) can be restated :

$$\overline{\tau_A} = \overline{\tau_{AE}} = n, \quad \text{with } |n| \le N,\ n \in \mathbb{Z}, \tag{2.69}$$

where the integration interval is limited to $\Omega \in [\alpha, \alpha + \pi]$. The same remark applies to (2.66) as well.

Discussion
The literature is usually limiting itself to Corollary 6 to Property 3 in the strict stable case, while (2.64) is observed to be more general and powerful.

2.5.5 Stability conditions related to the constituent parts of complex allpass networks

The demonstrations discussed below are based on the results developed in Section 2.3, and more specifically in Subsection 2.3.3.

Lemma 1 [Anso99] :
A necessary but insufficient condition for a complex allpass $A(z)$ in (2.28) to be stable is that $N_2 = 0$, i.e. $A_2(z) \equiv 1$, so that $A(z)$ is devoid of any constituent allpass featuring a purely even phase response.

Proof of necessity : According to Subsection 2.3.2, $A_2(z)$ counts by essence $N_2/2$ unstable poles. Stability is therefore only granted for $N_2 = 0$. ■

Proof of inaufficiency : Obviously, no constraint has been expressed witb respect to $A_1(z)$ and $A_3(z)$ that are also affecting the stability of $A(z)$ in (2.28). ■

Theorem 1 [Anso99] :
A necessary and sufficient condition for a complex allpass $A(z)$ in (2.28) to be strictly stable is that $N_2 = 0$, and that $A'_O(z)$ in (2.30b) is strictly stable.

Proof of necesaity : The strict stability of $A(z)$ implies strict stability of $A_1(z)$, $A_2(z)$, and $A_3(z)$. However, stability of A_2 is only granted for $N_2 = 0$. Finally, strict stability of $A_1(z)$ and $A_3(z)$, and thus of $\overline{A_3(z)}$, implies strict stability of $A'_O(z)$ in (2.30b). ■

Proof of sufficiency : The proof is evident and thus omitted. ■

Remark : It is furthermore observed from (2.28), (2.30), and (2.31), that a stable complex allpass $A(z)$ fulfills :

$$\deg\{A^2(z)\} = \deg\{A'_O(z)\} \geq \deg\{A'_E(z)\}. \tag{2.70}$$

where deg(.) denotes the non-reduced degree of a rational function.

2.5.6 Stability conditions deduced from the even and odd group delay symmetries

Case of first-order allpass functions

Theorem 2 [Anso99], (Table 2.7, Case 9) :
Considering the even and odd parts of the group delay, i.e. $\tau_{AE}(\Omega)$ and $\tau_{AO}(\Omega)$, respectively, a necessary and sufficient condition for a first-order complex allpass $A(z)$ to be strictly stable is given by:

$$\tau_{AE}(\Omega) > |\tau_{AO}(\Omega)| \geq 0, \quad \forall \Omega, \tag{2.71a}$$

or equivalently, using (2.68a,b), by :

$$d\beta_{AO}(\Omega)/d\Omega > |d\beta_{AE}(\Omega)/d\Omega| \geq 0, \quad \forall \Omega. \tag{2.71b}$$

Proof of necessity : The strict stability of $A(z)$ involves $\tau_A(\Omega) > 0$, $\forall \Omega$, according to (2.50a), and thus :

$$\tau_A(\alpha \cdot \Omega) = \tau_{AE}(\Omega) + \alpha \cdot \tau_{AO}(\Omega) > 0, \quad \text{witb } \alpha = \pm 1, \tag{2.72}$$

which is equal to $\tau_{AE}(\Omega) > |\tau_{AO}(\Omega)|$, $\forall \Omega$, and thus to (2.71a). The derivation of (2.71b) from (2.71a) is obvious due to (2.68). Hence, it is observed that for a strictly stable first-order allpass, the odd phase component necessarily exists, is monotone increasing, and is steeper than the absolute value of the even phase component variation. ■

Proof of aufficiency : The demonstration is direct, proceeding in the reverse order than just developed, and is therefore omitted. ■

Remarks : First, it is observed in (2.71a) that $\tau_{AE}(\Omega)$ and $|\tau_{AO}(\Omega)|$ are both even functions of Ω, so that it suffices to apply (2.71a) to the reduced interval $\Omega \in [\alpha, \alpha+\pi]$, $\forall \alpha \in \mathbb{R}$. Second, (2.71a) confirms that an allpass featuring a purely odd group delay, i.e. $\tau_{AE}(\Omega) \equiv \beta_{AO}(\Omega) \equiv 0$ is necessarily unstable. Finally, for a real allpass, $\tau_{AO}(\Omega) \equiv 0$, and (2.71a) reduces to $\tau_A(\Omega) = \tau_{AE}(\Omega) > 0$, $\forall \Omega$.

Examples

Theorem 2 is illustrated through two examples. The first one is depicted in Figure 2.17 and refers to the stable first-order allpass

specified in Table 2.13. Figure 2.18 presents the second example covering the unstable case according to the specifications provided in Table 2.14.

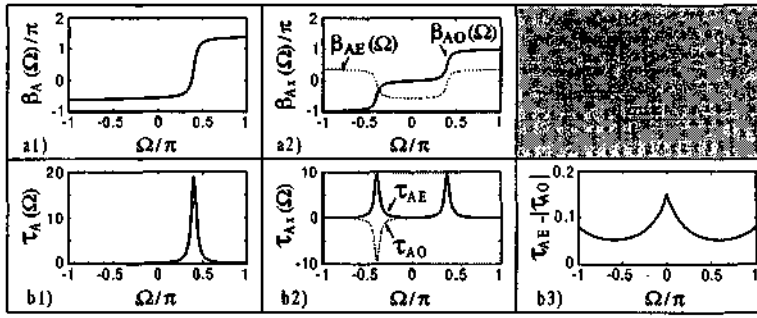

Figure 2.17: Stable 1st-order complex allpass specified in Table 2.13:
a1) Unwrapped phase; b2) Even/odd parts of group delay;
a2) Even/odd parts of phase; b3) $\tau_{AE}(\Omega)-|\tau_{AO}(\Omega)|$.
b1) Group delay;

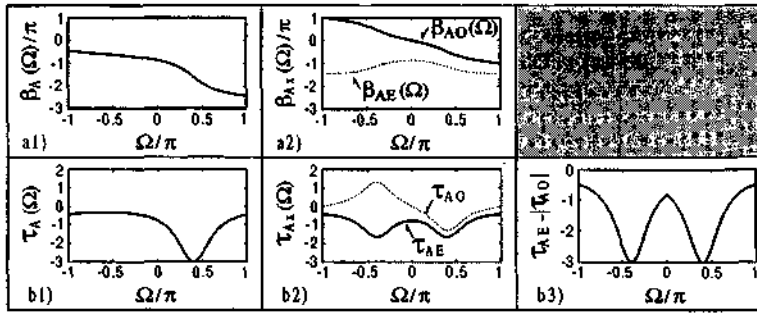

Figure 2.18: Unstable 1st-order complex allpass sperified in Table 2.14:
a1) Unwrapped phase; b2) Even/odd parts of group delay;
a2) Even/odd parts of phase; b3) $\tau_{AE}(\Omega)-|\tau_{AO}(\Omega)|$.
b1) Group delay;

Case of Nth-order allpass functions

Property 4 [Anso99] :
The conditions (2.71a,b) are necessary but insufficient to ensure strict stability of Nth-order complex allpass functions.

Proof of necessity : Adopting (2.51), the strict stability of every elementary allpass $A_\nu(z)$ involves :

$$\tau_{AE\nu}(\Omega) > |\tau_{AO\nu}(\Omega)| \geq 0, \quad \nu = 1,2,...,N, \quad \forall \Omega, \tag{2.73a}$$

resulting in the oext relationship after summation of all formulas :

$$\tau_{AE}(\Omega) = \sum_{\nu=1}^{N} \tau_{AE\nu}(\Omega)$$

$$> \sum_{\nu=1}^{N} |\tau_{AO\nu}(\Omega)| > \left| \sum_{\nu=1}^{N} \tau_{AO\nu}(\Omega) \right| = |\tau_{AO}(\Omega)| \geq 0, \quad \forall \Omega, \tag{2.73b}$$

which concludes the demonstration. ■

Proof of inaufficiency : The reasoo of insufficiency stems from the fact that compeosation effects may occur between the constituent even/odd parts in the unstable case, similarly to the situation encountered in Property 2. ■

Remark : Theorem 2 and Property 4 are the counterparts of Properties 1 and 2, respectively, expressed in terms of tbe even/odd parts of the allpass phase and group delay.

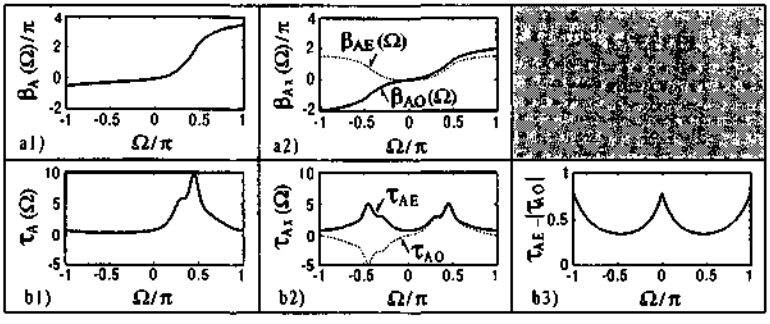

Figure 2.19: Unstable 4th-order complex allpass specified in Table 2.12:
a1) Unwrapped phase; b2) Even/odd parts of group delay;
a2) Even/odd parts of phase; b3) $\tau_{AE}(\Omega) - |\tau_{AO}(\Omega)|$.
b1) Group delay;

Example

The proof of insufficiency is examplified in Figure 2.19, using the unstable 4th-order allpass $A(z)$ specified in Table 2.12. It is observed that (2.73a) is fulfilled despite of the obvious instability of $A(z)$.

2.6 Half-band symmetric allpass functions

This section is devoted to complex half-band symmetric allpass funtions that are by essence featuring a midband phase symmetry over both positive and negative frequency ranges. In their most *general form*, such networks offer a certain degree of freedom in the specification of the phase response over the positive frequency range with respect to the negative one, whereas this degree of freedom drops in the case of *constrained* half-band symmetric allpass functions.

Half-band symmetric allpasses are interesting for the implementation simplifications they provide due to their specific pole constellations, and they play an important role as constitutive networks of amplitude/phase selective half-band filters, cf Chapters 4 and 5.

In the sequel of this section, the definition and general form of half-band symmetric allpass networks are first provided. The corresponding allpass expression and related pole configurations are next specified. The implied implementation simplifications are then discussed, followed by a short presentation of the constrained case. Finally several examples are illustrated.

2.6.1 Definition of the phase response of half-band symmetric allpass functions in the general case

In its most general form, the phase response of a complex half-band symmetric allpass $A(z)$ is specified as follows for $\Omega \in [-\pi, \pi]$:

$$\beta_A(\Omega) - \beta_A(0) = \beta_A(\pi) - \beta_A(\pi - \Omega), \tag{2.74a}$$

implying : $$\tau_A(\Omega) = \tau_A(\pi - \Omega). \tag{2.74b}$$

Expression (2.74a) is known for real allpass networks, and shows that the phase response is necessarily verifying :

$$\beta_A(\pi/2) = 0.5 \cdot [\beta_A(0) + \beta_A(\pi)]. \tag{2.75a}$$

Considering (2.74a) over the negative frequency range $\Omega \in [-\pi, 0]$, and applying (2.57a) to $\beta_A(\pi)$ and $\beta_A(\pi - \Omega)$:

$$\beta_A(\pi) = \beta_A(-\pi) + 2\pi \cdot n, \tag{2.76a}$$

$$\beta_A(\pi - \Omega) = \beta_A(-\pi - \Omega) + 2\pi \cdot n, \tag{2.76b}$$

one achieves :

$$\beta_A(\Omega) - \beta_A(0) = \beta_A(-\pi) - \beta_A(-\pi - \Omega), \tag{2.76c}$$

demonstreting that the phese response is fulfilling:

$$\beta_A(-\pi/2) = 0.5 \cdot [\beta_A(-\pi) + \beta_A(0)]. \tag{2.75b}$$

Figure 2.20 depicts the phase response of general form complex half-band symmetric allpass functions.

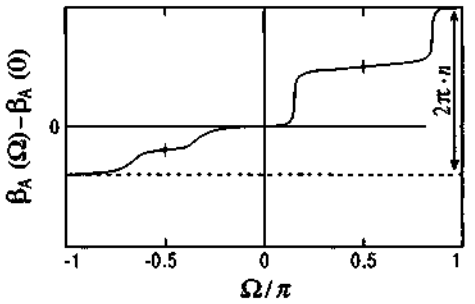

Figure 2.20: Phase response of half-band symmetric allpass networks (general case).

2.6.2 Explicit form of half-band symmetric allpass functions in the general case

This subsection aims at identifying the explicit form of the constituent denominator of complex allpass networks verifying the condition (2.74a). The development is processed in two steps, establishing first in Lemme 2 an equivalent expression for (2.74a), before deriving the explicit form of the allpass denominator in Theorem 3, which represents the central part of this subsection.

Lemma 2 : Reformulating (2.74a) as specified in (2.77a), equations (2.77a) and (2.77b) are demonstrated to be equivalent, $\beta_P(\Omega)$ being defined in (2.6) – (2.8).

$$\beta_A(\Omega)+\beta_A(\pi-\Omega)=\beta_A(0)+\beta_A(\pi) \quad \Leftrightarrow \tag{2.77a}$$

$$\Leftrightarrow \quad \beta_P(\Omega)+\beta_P(\pi-\Omega)=\beta_P(0)+\beta_P(\pi). \tag{2.77b}$$

Proof: The demonstration is merely achieved applying (2.6) to each of the four terms appearing in (2.77a), resulting in (2.77b). ■

Theorem 8 :
The necessary and sufficient condition for an N th-order complex allpass $A(z)$ to feature a general form half-band symmetric phase response as specified in (2.77a,b) is that $P(z)$ is para-even for N even, and para-odd for N odd, cf Table A.3 :

$$N \text{ even:} \quad P(z)=\sum_{\nu=0}^{N/2} p_{R2\nu}\cdot z^{2\nu}+j\cdot\sum_{\nu=0}^{N/2-1} p_{I(2\nu+1)}\cdot z^{2\nu+1}, \tag{2.78a}$$

$$\text{with} \qquad p_{R(2\nu+1)}=p_{I2\nu}=0, \quad \nu=0,\ldots,N/2-1;$$

$$N \text{ odd:} \quad P(z)=\sum_{\nu=0}^{(N-1)/2}\left[p_{R(2\nu+1)}\cdot z^{2\nu+1}+j\cdot p_{I2\nu}\cdot z^{2\nu}\right], \tag{2.78b}$$

$$\text{with} \qquad p_{R2\nu}=p_{I(2\nu+1)}=0, \quad \nu=0,\ldots,(N-1)/2;$$

$$\text{verifying in each case:} \qquad p_{RN}=1, \quad p_{IN}=0. \tag{2.78c}$$

Proof of necessity : The proof of necessity is elaborated starting from equation (2.77b), and taking the tangent of both left and right hand-sided parts of it, as specified in (2.79a). The expressions being rather involved, it is useful to rewrite the left and right hand-sided parts of (2.79a) as provided in (2.79b,c) :

$$\tan[\beta_P(\Omega)+\beta_P(\pi-\Omega)]=\tan[\beta_P(0)+\beta_P(\pi)], \tag{2.79a}$$

$$\text{with} \qquad \tan[\beta_P(\Omega)+\beta_P(\pi-\Omega)]=\frac{Num_1(\Omega)}{Den_1(\Omega)}, \tag{2.79b}$$

$$\text{and} \qquad \tan[\beta_P(0)+\beta_P(\pi)]=\frac{Num_2}{Den_2}. \tag{2.79c}$$

Next, applying (2.79b,c) jointly with (2.8), one obtains formulas (2.80a) – (2.80d) after a longer development that is omitted for conciseness.

$$Num_1(\Omega) = -\sum_{\nu=0}^{N}\sum_{\mu=0}^{N}\left\{\left[(-1)^{\mu}+(-1)^{\nu}\right]\cdot p_{R\nu}\,p_{I\mu}\cdot\cos[(\nu-\mu)\Omega]\right.$$
$$\left.+\left[(-1)^{\mu}-(-1)^{\nu}\right]\cdot\left[p_{R\nu}\,p_{R\mu}-p_{I\nu}\,p_{I\mu}\right]\cdot\sin\nu\Omega\cdot\cos\mu\Omega\right\}, \quad (2.80a)$$

$$Den_1(\Omega) = \sum_{\nu=0}^{N}\sum_{\mu=0}^{N}\left\{(-1)^{\mu}\cdot\left[p_{R\nu}\,p_{R\mu}-p_{I\nu}\,p_{I\mu}\right]\cdot\cos[(\nu-\mu)\Omega]\right.$$
$$\left.-\left[(-1)^{\mu}+(-1)^{\nu}\right]\cdot p_{R\nu}\,p_{I\mu}\cdot\sin[(\nu-\mu)\Omega]\right\}, \quad (2.80b)$$

$$Num_2 = -\sum_{\nu=0}^{N}\sum_{\mu=0}^{N}\left[(-1)^{\mu}+(-1)^{\nu}\right]\cdot p_{R\nu}\,p_{I\mu}, \quad (2.80c)$$

$$Den_2 = \sum_{\nu=0}^{N}\sum_{\mu=0}^{N}(-1)^{\mu}\cdot\left[p_{R\nu}\,p_{R\mu}-p_{I\nu}\,p_{I\mu}\right]. \quad (2.80d)$$

One notices that when ν and μ share the same parity, i.e. for $(\nu+\mu)$ even, (2.81a) is verified, whereas (2.81b) applies when ν and μ are of different parity, i.e. for $(\nu+\mu)$ odd :

$$\text{for } (\nu+\mu) \text{ even}: \quad (-1)^{\mu}+(-1)^{\nu} = 2\cdot(-1)^{\mu}, \quad (2.81a)$$
$$(-1)^{\mu}-(-1)^{\nu} = 0;$$

$$\text{for } (\nu+\mu) \text{ odd}: \quad (-1)^{\mu}+(-1)^{\nu} = 0, \quad (2.81b)$$
$$(-1)^{\mu}-(-1)^{\nu} = 2\cdot(-1)^{\mu}.$$

Consequently, equations (2.80a,c) can be rewritten as follows:

$$Num_1(\Omega) = -\sum_{\substack{\nu=0\\(\nu+\mu)\text{ even}}}^{N}\sum_{\mu=0}^{N}2\cdot(-1)^{\mu}\cdot p_{R\nu}\,p_{I\mu}\cdot\cos[(\nu-\mu)\Omega]$$
$$-\sum_{\substack{\nu=0\\(\nu+\mu)\text{ odd}}}^{N}\sum_{\mu=0}^{N}2\cdot(-1)^{\mu}\cdot\left[p_{R\nu}\,p_{R\mu}-p_{I\nu}\,p_{I\mu}\right]\cdot\sin\nu\Omega\cdot\cos\mu\Omega, \quad (2.82a)$$

$$Num_2 = -\sum_{\substack{\nu=0\\(\nu+\mu)\text{ even}}}^{N}\sum_{\mu=0}^{N}2\cdot(-1)^{\mu}\cdot p_{R\nu}\,p_{I\mu}. \quad (2.82b)$$

According to (2.82b), $Num_2 \equiv 0$ for $(\nu+\mu)$ odd, implying that Num_1 should do the same for $(\nu+\mu)$ odd. Consequently :

$$\sum_{\substack{\nu=0 \\ (\nu+\mu)\,\text{odd}}}^{N} \sum_{\mu=0}^{N} (-1)^{\mu} \cdot \left[p_{R\nu}\, p_{R\mu} - p_{I\nu}\, p_{I\mu} \right] \cdot \sin\nu\Omega \cdot \cos\mu\Omega \equiv 0$$

$\forall \Omega \in [-\pi, \pi]$, which involves :

$$p_{R\nu}\, p_{R\mu} - p_{I\nu}\, p_{I\mu} = 0, \quad \text{for } (\nu+\mu) \text{ odd.} \tag{2.83}$$

Case 1) N **even** : Assuming first that N is even, and introducing (2.78c) in (2.83) with $\nu = N$, one achieves:

$$p_{R\mu} = 0, \quad \text{for } \mu \text{ odd.} \tag{2.84}$$

Considering in a second step any even ν, and inserting (2.84) into (2.83), results in :

$$p_{I\nu} \cdot p_{I\mu} = 0, \quad \text{for } \nu \text{ even, } \mu \text{ odd,} \tag{2.85}$$

meaning that at least every second coefficient $p_{I\eta}$ in the sequence $\eta = 0,1,2,...,N$ is zero valued. Equation (2.84) remaining valid, this leads a priori to two possible solutions, namely:

$$p_{I\mu} = 0, \quad \text{for } \mu \text{ even} \quad \Rightarrow \quad P(z) \text{ para-even;} \tag{2.86a}$$

$$p_{I\mu} = 0, \quad \text{for } \mu \text{ odd} \quad \Rightarrow \quad P(z) \text{ even;} \tag{2.86b}$$

In case $P(z)$ is para-even, one verifies $p_{R\nu}\, p_{I\mu} = 0$ for $(\nu+\mu)$ even, implying that both terms Num_1 and Num_2 in (2.82a,b) become identically zero $\forall \Omega \in [-\pi, \pi]$, thus fulfilling (2.77a,b).

Regarding the denominators Den_i, $i = 1,2$, it is noticed in (2.77b) that $\beta_P(\Omega) + \beta_P(\pi - \Omega) = \beta_P(0) + \beta_P(\pi)$ corresponds to a finite value, so that the tangents in (2.79b,c) are properly defined. Accordingly, the numerators and denominators in (2.79b,c) cannot be simultaneously zero valued. Since $Num_1 \equiv Num_2 \equiv 0$, it is confirmed that $Den_i(\Omega) \neq 0$, $\forall \Omega \in [-\pi, \pi]$, $i = 1,2$. Additionally, Den_i are observed to be non-identically zero in (2.80b,d). The solution (2.86a) is thus validated.

If instead one is considering $P(z)$ as an even polynomial following (2.86b), no solution can be derived from (2.82a,b) except in the real case to be discussed later in the Corollary 3 of Theorem 3. In addition, (2.77b) cannot be found back from an even complex $P(z)$. The solution (2.86b) is consequently rejected.

Case 2) N odd : Proceeding similarly for N odd, the only solution is given by :

$$p_{Rv} = p_{I\mu} = 0 \quad \text{for } v \text{ even, } \mu \text{ odd} \quad \Rightarrow \quad P(z) \text{ para-odd.} \quad (2.87)$$

The demonstration of the necessity condition of Theorem 3 is thus completed. ■

Pronf nf sufficiency : Assuming that polynomial $P(z)$ is fulfilling either (2.78a) or (2.78b) in addition to (2.78c), one establishes from (2.8) :

$$\beta_P(\Omega) = -\beta_P(\pi - \Omega) \quad \Rightarrow \quad \beta_P(0) = -\beta_P(\pi). \quad (2.88a,b)$$

Subtracting (2.88b) from (2.88a) results in (2.77b), and therefore in the equivalent expression (2.77a). The sufficiency condition of Theorem 3 is thus demonstrated. ■

Cnrollary 1 to Theorem 3 :
Consequently to the para-even/odd nature of $P(z)$ in Theorem 3, the N th-order complex allpass $A(z)$ is taking the values listed in Table 2.15 for $z = \pm j$, involving the indicated values for the phase response $\beta_A(\pm\pi/2)$ specified in (2.75a,b).

Pronf: Introducing $z = \pm j$ into (2.78a,b) involves (2.89a), and thus (2.89b) using (2.77a). The values of $A(\pm j)$ and $\beta_A(\pm\pi/2)$ in Table 2.15 are then directly derived in function of N. ■

$$P(\pm j) = (-1)^N \cdot \tilde{P}(\pm j) \quad \Rightarrow \quad A(\pm j) = \lambda \cdot (\mp j)^N ; \quad (2.89a,b)$$

N	$A(\pm j)/\lambda = (\mp j)^N$	$\beta_A(\pm\pi/2) + \theta$
$4k$	1	$2\pi \cdot \eta$
$4k+1$	$\mp j$	$\pm\pi/2 + 2\pi \cdot \eta$
$4k+2$	-1	$\pi + 2\pi \cdot \eta$
$4k+3$	$\pm j$	$\mp\pi/2 + 2\pi \cdot \eta$

Table 2.15: Specific values of $A(\pm j)$ and $\beta_A(\pm\pi/2)$, for $N \geq 1$, $k \in N$, $\eta \in Z$ (η selected according to the unwrapped phase $\beta_A(\Omega) + \theta$).

Corollary 2 to Theorem 3 :
In case the N th-order allpass $A(z)$ in Theorem 3 is real, then $P(z)$ reduces to an even (odd) polynomial for N even (odd), respectively.

Proof: The demonstration is evident and thus omitted. ■

2.6.3 Pole configurations of half-band symmetric allpass functions in the general case

Based on Theorem 3 and its Corollary 2, the pole configurations of half-band symmetric allpass networks are established. This is done considering elementary first-order para-odd, and second-order para-even polynomials. Higher-order para-even/odd polynomials are then achieved by a mere product of lower-order polynomials, following the rules described in (A.15).

The N th-order polynomial $P(z)$ being monic by definition ($p_N = 1$), and considering the conditions to be fulfilled by a polynomial to get para-even/odd, cf Table A.3, it is observed that $P(z)$ can only become para-even for N even, and para-odd for N odd.

Case of 1st-order para-odd polynomials

The condition to be verified by a first-order monic polynomial $P_1(z)$ specified in (2.90a) to become para-odd is $\mathrm{Re}\{z_{\infty 1}\} = 0$, resulting in (2.90b), including the real case $\alpha = 0$.

$$P_1(z) = z - z_{\infty 1}; \tag{2.90a}$$

$P_1(z)$ para-odd: $$z_{\infty 1} = j \cdot \alpha, \quad \text{with} \quad \alpha \in \mathbb{R}. \tag{2.90b}$$

Case of 2nd-order para-even polynomials

In case of a second-order para-even polynomial $P_2(z)$, cf (2.91a), the conditions to satisfy are $\mathrm{Re}\{z_{\infty 1} + z_{\infty 2}\} = \mathrm{Im}\{z_{\infty 1} \cdot z_{\infty 2}\} = 0$. Two subcases are considered according to the fulfillment of $\mathrm{Re}\{z_{\infty 1} + z_{\infty 2}\} = 0$.

Subcase 1: $\mathrm{Re}\{z_{\infty 1}\} = \mathrm{Re}\{z_{\infty 2}\} = 0$: This subcase merely corresponds to the product of two para-odd first-order polynomials, cf (2.90b), resulting in (2.91b). $\mathrm{Im}\{z_{\infty 1} \cdot z_{\infty 2}\} = 0$ is then necessarily satisfied. It is noticed that the two factors α_i, $i = 1,2$, encompassing the value $\alpha_i = 0$, are in general independent of each other.

Subcase 2: $\mathrm{Re}\{z_{\infty 1}\} = -\mathrm{Re}\{z_{\infty 2}\} \neq 0$: In this subcase, $z_{\infty 1} = \alpha + j \cdot \gamma_1$ and $z_{\infty 2} = -\alpha + j \cdot \gamma_2$, with $\alpha, \gamma_1, \gamma_2 \in \mathbb{R}$, and $\alpha \neq 0$ by assumption. The condition $\mathrm{Im}\{z_{\infty 1} \cdot z_{\infty 2}\} = 0$ is then inducing (2.91c).

$$P_2(z) = (z - z_{\infty 1}) \cdot (z - z_{\infty 2}) = z^2 - (z_{\infty 1} + z_{\infty 2}) \cdot z + z_{\infty 1} \cdot z_{\infty 2}; \qquad \textbf{(2.91a)}$$

$P_2(z)$ para-even:

Subcase 1: $z_{\infty i} = j \cdot \alpha_i$, with $\alpha_i \in \mathbb{R}$, $i = 1,2$; (2.91b)

Subcase 2: $z_{\infty 2} = -z_{\infty 1}^*$, with $\mathrm{Re}\{z_{\infty i}\} \neq 0$, $i = 1,2$. (2.91c)

Allpass pole configurations for complex para-even/odd $P(z)$

The allpass pole constellations corresponding to elementary complex para-even/odd polynomials $P(z)$ following (2.90b) and (2.91b,c) are represented in the left column of Figure 2.21, parts a) and b). Higher-order complex para-even/odd $P(z)$ are obtained by multiplication of elementary complex para-even/odd polynomials, including elementary real even/odd polynomials $P(z)$ discussed below.

Allpass pole configurations for real even/odd $P(z)$

In the real case, the relationship (2.90b) becomes (2.92a), whereas (2.91b,c) result in (2.92b,c,d). Tbe corresponding allpass pole configurations are illustrated in the right column of Figure 2.21, parts a), b), and c).

$P_1(z)$ odd: $z_{\infty 1} = 0$; (2.92a)

$P_2(z)$ even:

Subcase 1: $z_{\infty 1} = j \cdot \alpha$, $z_{\infty 2} = z_{\infty 1}^*$, with $\alpha \in \mathbb{R}$; (2.92b)

Subcase 2: $z_{\infty 1} \in \mathbb{R}$, $z_{\infty 2} = -z_{\infty 1}$, with $z_{\infty 1} \neq 0$; (2.92c)

$P_4(z)$ even: $z_{\infty 1} \in \mathbb{C}$, $z_{\infty 2} = -z_{\infty 1}$, $z_{\infty 3} = z_{\infty 1}^*$, $z_{\infty 4} = -z_{\infty 1}^*$. (2.92d)

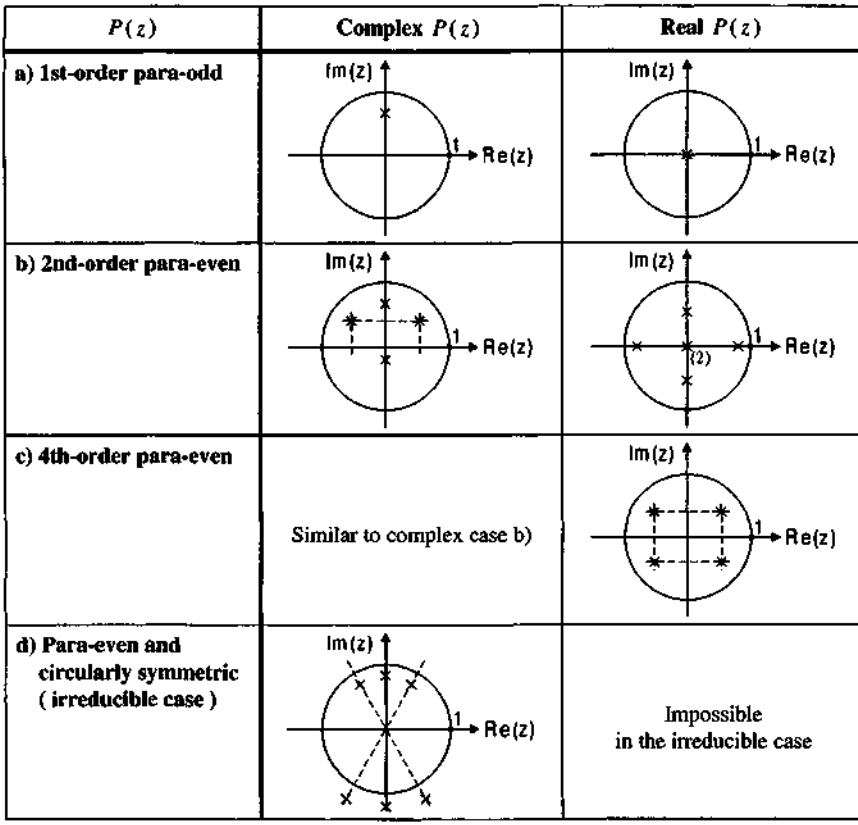

Figure 2.21: Pole configurations for elementary half-band symmetric allpass functions (general case).

2.6.4 Para-even and circularly symmetric case

The case where the denominator $P(z)$ of a half-band symmetric allpass $A(z)$ is para-even and circularly symmetric is handled by splitting $A(z)$ into two allpasses, namely $A_\alpha(z)$ collecting all real pole configurations, the remaining complex poles being taken over by $A_\beta(z)$, the related denominators being labeled $P_\alpha(z)$ and $P_\beta(z)$:

$$A(z) = A_\alpha(z) \cdot A_\beta(z); \quad A_\alpha(z) \text{ real}, \quad A_\beta(z) \text{ complex}; \tag{2.93}$$

the factor λ of $A(z)$ being assigned to $A_\beta(z)$. Clearly, the circular symmetry involves a necessarily paired occurrence of poles verifying $z_{\infty i+1} = 1/z_{\infty i}$, excluding poles at the origin because their inverse would be rejected to infinity. The elementary real pole configurations of $P_\alpha(z)$ obtained from Figures 2.21b and 2.21c are thus represented in Figure 2.22. Obviously, every pole in Figure 2.22 is precisely cancelled out by a zero of the same configuration, so that, whatever its degree, $A_\alpha(z)$ is demonstrated to be fully reducible to the degenerate allpass $A'_\alpha(z) \equiv 1$.

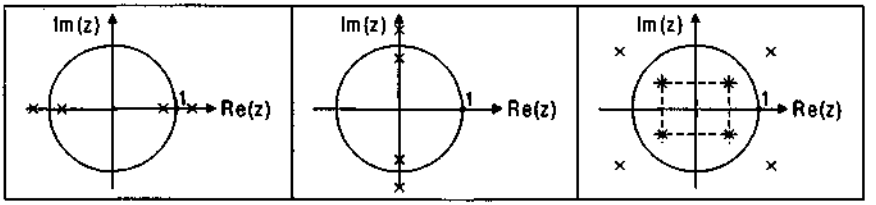

Figure 2.22: Pole configurations for real elementary half-band symmetric allpass functions with even and circularly symmetric denominator.

Considering $A_\beta(z)$, whose poles are necessarily non-real by assumption, i.e. $\mathrm{Im}\{z_{\infty i}\} \neq 0$, the relationships (2.91b) and (2.91c) are replaced by (2.94a) and (2.94b), respectively, as depicted in Figure 2.21, part d).

$P_2(z)$ para-even:

$$z_{\infty 1} = j \cdot \alpha, \; z_{\infty 2} = 1/z_{\infty 1}, \quad \text{with} \quad \alpha \neq 0, \; \alpha \in \mathbb{R}; \tag{2.94a}$$

$P_4(z)$ para-even:

$$z_{\infty 1} \in \mathbb{C}, \; z_{\infty 2} = -z^*_{\infty 1}, \; z_{\infty 3} = 1/z_{\infty 1}, \; z_{\infty 4} = -1/z^*_{\infty 1}. \tag{2.94b}$$

The next corollary can thus be formulated.

Corollary 3 to Theorem 3 :
Referring to Theorem 3, an *irreducible* N-th order (N even) complex allpass $A(z)$ owning a para-even and circularly symmetric denominator $P(z)$ is: 1) necessarily devoid of real pole configurations; and thus 2) featuring a purely even phase response. Moreover, the

auxiliary rational function $P'(z)$ defined in (2.40a,b) is para-even for $N/2$ even, and para-odd for $N/2$ odd.

Proof: The fact that an irreducible complex allpass $A(z)$ with para-even and circularly symmetric denominator $P(z)$ is necessarily devoid of real pole configurations follows from the developments made at beginning of this subsection. According to Subsection 2.3.2, $A(z)$ is then certified to feature a purely even phase response, in addition to the half-band symmetry. Finally, the para-even/odd property of $P'(z)$ in function of the parity of $N/2$ is a consequence of (2.40b). ■

2.6.5 Implementation simplifications

Due to the para-even/odd nature of the denominator $P(z)$ of a general case half-band symmetric allpass $A(z)$, a (limited) implementation simplification is rendered possible making use of (A.28). Indeed, specifying:

$$\hat{z} = j \cdot z, \tag{2.95}$$

equations (2.78a,b) can be rewritten:

N even:

$$P(z) = \sum_{\nu=0}^{N/2} p_{R2\nu} \cdot (-1)^{\nu} \cdot \hat{z}^{2\nu} + \sum_{\nu=0}^{N/2-1} p_{I(2\nu+1)} \cdot (-1)^{\nu} \cdot \hat{z}^{2\nu+1}, \tag{2.96a}$$

N odd:

$$P(z) = j \cdot \sum_{\nu=0}^{(N-1)/2} \left[p_{R(2\nu+1)} \cdot (-1)^{\nu+1} \cdot \hat{z}^{2\nu+1} + p_{I2\nu} \cdot (-1)^{\nu} \cdot \hat{z}^{2\nu} \right]. \tag{2.96b}$$

$\tilde{P}(z)$ behaving similarly, $A(z)$ can be realized using *real* allpass structures, except for the j factors introducing a mere swap between the real and imaginary parts of the signals, and which occur in particular in connection with the complex delays. This implementation simplification was already cited in [Meer83, Vaid87a]. More explicitly, the transfer function of $A(z)$ can be expressed as :

$$A(z) = \lambda \cdot z^{-N_0} \cdot \prod_{\mu=1}^{N_1} \left(\frac{1 + j \cdot \alpha_\mu \cdot z}{z - j \cdot \alpha_\mu} \right) \cdot \prod_{\nu=1}^{N_2} \left(\frac{1 - z_{\infty\nu}^{*} \cdot z}{z - z_{\infty\nu}} \right) \cdot \left(\frac{1 + z_{\infty\nu} \cdot z}{z + z_{\infty\nu}^{*}} \right), \tag{2.97a}$$

with $N = N_0 + N_1 + 2 \cdot N_2$; $\quad \alpha_\mu \in \mathbb{R}$, $\alpha_\mu \neq 0$; (2.97b)

where N_0 represents the number of poles at the origin, N_1 denoting the number of purely imaginary poles following (2.90b) and (2.91b), whereas N_2 specifies the number of paired poles according to (2.91c). Finally, one achieves :

$$A(z)=\lambda\cdot j^{N-N_0}\cdot z^{-N_0}\cdot\prod_{\mu=1}^{N_1}\left(\frac{1+\alpha_\mu\cdot\hat{z}}{\hat{z}+\alpha_\mu}\right)\cdot\prod_{\nu=1}^{N_2}\left(\frac{1+d_\nu\cdot\hat{z}+e_\nu\cdot\hat{z}^2}{\hat{z}^2+d_\nu\cdot\hat{z}+e_\nu}\right), \tag{2.98a}$$

with $d_\nu=2\cdot\mathrm{Im}\{z_{\infty\nu}\};\quad e_\nu=|z_{\infty\nu}|^2.$ (2.98b)

Implementation simplifications in the real case

Clearly, $P(z)$ and thus $A(z)$ are both becoming even or odd functions in the real case. Hence, $A(z)$ can be reformulated as :

N even: $$A(z)=\hat{A}(z^2); \tag{2.99a}$$

N odd: $$A(z)=z^{-1}\cdot\hat{A}(z^2); \tag{2.99b}$$

a feature that is well known for the realization of real half-band allpass-based networks [Noss83, Gazs85a, Fett86, Vaid93], $\hat{A}(z^2)$ representing an even degreed allpass. The form of $A(z)$ is leading to drastic reductions in hardware resources, computation throughput, and power consumption, especially for multirate filterbank implementations, as cited in the mentioned references.

2.6.6 Half-band symmetric allpass functions in the constrained case

Two conditions are introduced in [Fett85] for the design of half-band symmetric allpasses used to realize specific amplitude and mixed amplitude/phase selective half-band filters. These conditions are:

N even: $$A(z)=-A^{-1}(-z); \tag{2.100a}$$

N odd: $$A(z)=-A(-z). \tag{2.100b}$$

Inserting (2.78a,b) into (2.100a,b), respectively, results in :

N even: $A(z)$ with para-even and circularly symmetric denominator $P(z)$; with $\lambda = \pm j$; (2.101a)

N odd: $A(z)$ with real and odd $P(z)$; with $\lambda = \pm 1$; (2.101b)

so that $A(z)$ is featuring either a purely even phase response for N even if irreducible (cf Corollary 3 to Theorem 3), or a purely odd phase response. The subject is discussed in detail in Chapter 4.

Moreover, inserting the values of λ specified in (2.101a,b) into (2.89b) results in :

$$A(\pm j) = \pm j, \ \forall N, \quad \Leftrightarrow \quad \beta_A(\pm\pi/2) = \pm\pi/2 + 2\pi\cdot\eta, \ \forall N; \quad (2.102a,b)$$

thus replacing Table 2.15. The upper/lower signs appearing on botb sides of every equation (2.102a,b) are not any more correlated. Tbe factor η is selected according to tbe unwrapped phase $\beta_A(\Omega)$.

2.6.7 Examples

A first example illustrating a general case half-band symmetric allpass was already discussed in Figure 2.8 and Table 2.6. Several further examples are described below, the first corresponding to a 5th-order complex para-odd allpass depicted in Figure 2.23 with parameters specified in Table 2.16.

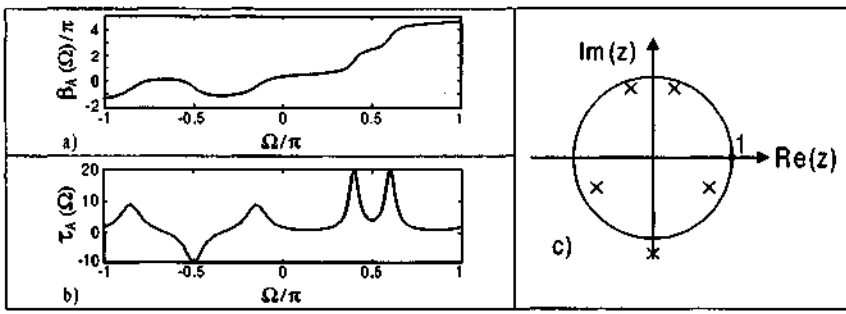

Figure 2.23: 5th-order complex half-band symmetric allpass function with para-odd denominator $P(z)$:
a) Unwrapped phase response; c) Poles configuration.
b) Group delay;

	ν	θ/π, $\mathrm{Re}\{z_{\infty\nu}\}$	$\mathrm{Im}\{z_{\infty\nu}\}$
θ/π	—	0	—
$z_{\infty\nu}$	1	$1.20\cdot\exp(-j\cdot 0.50\cdot\pi)$	
	2	$0.90\cdot\exp(j\cdot 0.40\cdot\pi)$	
	3	$0.80\cdot\exp(-j\cdot 0.15\cdot\pi)$	
	4, 5	$z_{\infty\nu}=-z^{*}_{\infty(7-\nu)}$	

Table 2.16: Parameters specifying the allpass illustrated in Figure 2.23.

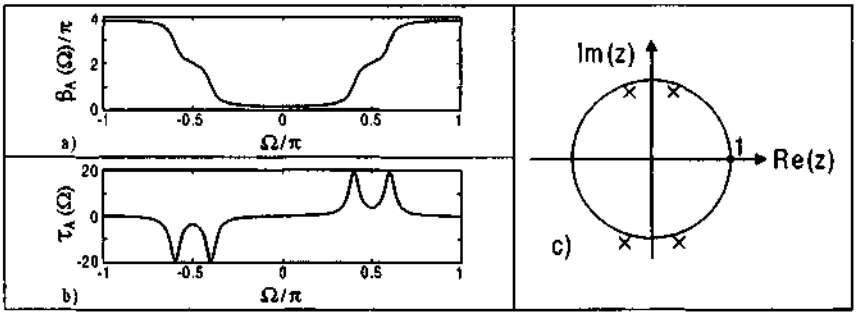

Figure 2.24: 4th-order complex half-band symmetric allpass function featuring an even phase response, and thus a para-even and circularly symmetric denominator $P(z)$:
a) Unwrapped phase response; c) Poles configuration.
b) Group delay;

	ν	θ/π, $\mathrm{Re}\{z_{\infty\nu}\}$	$\mathrm{Im}\{z_{\infty\nu}\}$
θ/π	—	0	—
$z_{\infty\nu}$	1	$0.90\cdot\exp(j\cdot 0.40\cdot\pi)$	
	2	$z_{\infty 2}=-z^{*}_{\infty 1}$	
	3, 4	$z_{\infty\nu}=1/z_{\infty(5-\nu)}$	

Table 2.17: Parameters specifying the allpass illustrated in Figure 2.24.

The two next examples present complex allpass networks featuring an even phase response. A general case is depicted in Figure 2.24 with parameters given in Table 2.17, whereas Figure 2.25 and Table 2.18 correspond to an allpass with almost linear phase response $\beta_{AE}(\Omega)\cong 3\cdot|\Omega|$ over $|\Omega|\in[0,\pi]$, the adopted legend and represented characteristics being the same than in Figure 2.7.

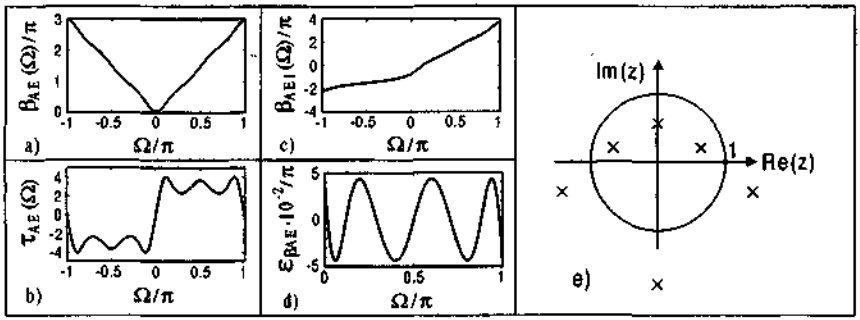

Figure 2.25: 6th-order complex half-band symmetric allpass with even and almost linear phase with $\beta_{AE}(\Omega) \cong 3 \cdot |\Omega|$, $|\Omega| \in [0, \pi]$:
a) Unwrapped phase response; c) Unwrapped phase of $A_{E1}(z)$;
b) Group delay; d) Residual approximation error;
e) Poles configuration.

	ν	θ/π, $\mathrm{Re}\{z_{\infty\nu}\}$	$\mathrm{Im}\{z_{\infty\nu}\}$
θ/π	—	− 0.5	—
$z_{\infty\nu}$	1	0	0.55943181755232
	2	0.64830915709478	0.19851187299565
	3	$z_{\infty 3} = -z_{\infty 2}^{*}$	
	4, 5, 6	$z_{\infty\nu} = 1/z_{\infty(7-\nu)}$	

Tahle 2.18: Parameters specifying the allpass illustrated in Figure 2.25.

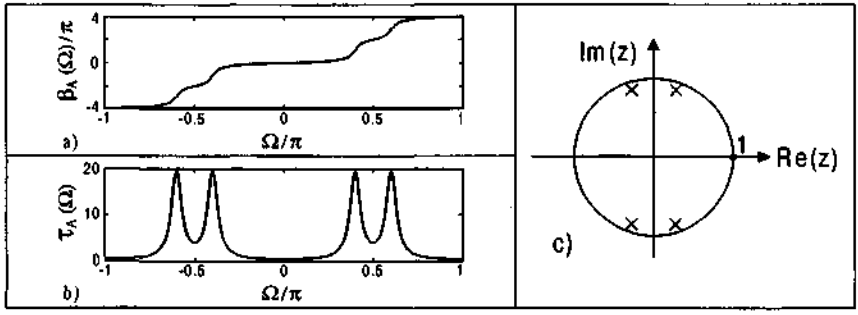

Figure 2.26: 4th-order real half-band symmetric allpass function with even denominator $P(z)$:
a) Unwrapped phase response; c) Poles configuration.
b) Group delay;

	ν	θ/π, $\mathrm{Re}\{z_{\infty\nu}\}$	$\mathrm{Im}\{z_{\infty\nu}\}$
θ/π	—	0	—
$z_{\infty\nu}$	1	$0.90\cdot\exp(\mathrm{j}\cdot 0.40\cdot\pi)$	
	2	$z_{\infty 2} = -z_{\infty 1}^{*}$	
	3, 4	$z_{\infty\nu} = z_{\infty(5-\nu)}^{*}$	

Table 2.19: Parameters specifying the allpass illustrated in Figure 2.26.

Finally, Figure 2.26 and Table 2.19 illustrate the case of a real even-ordered allpass.

2.7 Allpass properties in the ψ-domain

It is observed that all elementary properties of allpass functions that were identified or demonstrated in the z-domain in this chapter, bave their direct counterpart in the ψ-domain, and vice-versa, both domains being related through the bilinear transform.

2.8 Conclusion

In tbis chapter, various elementary properties of allpass functions were discussed in detail. After recall of basic definitions, a detailed analysis of the even/odd allpass phase response constituents was undertaken in Section 2.3, allowing for a factorization of allpass functions into elementary allpasses. The explicit form of allpass networks with purely even phase response was then derived, whicb is in particular useful to perform the approximation of sucb filters. Next, the stability of allpass functions, and by extension of polynomials, was discussed in Section 2.5, focusing on the relationship between stability and phase or group delay responses. Finally, complex half-band symmetric allpass filters were handled in Section 2.6.

It is observed that an important part of the results achieved in the chapter is merely based on the analysis of the even/odd allpass phase constituents, with exploitation of the identified properties.

Contributions

The main contributions [15] of the chapter considered as original to the best knowledge of the author are :

- **C2–I**: Establishment of the refined decomposition of complex allpass functions (2.28) and their correspondence to related purely even and odd phase response constituents (2.30a,b), including their potential use for simplified approximation of complex allpass filters as described in Subsection 2.3.4, and the provision of the explicit form of allpass functions featuring a purely even phase response as discussed in Section 2.4.
- **C2–II**: Systematic study of stability-related properties of complex and real allpass functions as presented in Section 2.5, with gradual progression of the features analysis. Results of particular interest are :
  - **C2–II/1**: Provision of a new proof of the known Property 3 in Subsection 2.5.3.
  - **C2–II/2**: Expression (2.59) specifying the spanned phase range over extended frequency domain, representing a generalization of known spanned phase range expressions [Bele68, Vaid93], that is in particular useful in the frame of allpass-based filter transformation methods [Anso00], and allows for a precise enumeration of stable and unstable poles belonging to the assessed allpass, provided the applied phase unwrapping technique is secure.
  - **C2–II/3**: Identified stability conditions related to the constituent parts of complex allpass networks in Subsection 2.5.5, with contribution of Lemma 1 and Theorem 1.
  - **C2–II/4**: Identified stability conditions deduced from the even and odd group delay symmetries as discussed in Subsection 2.5.6, with contribution of Theorem 2 and Property 4.

---

[15] In this report, contributions that are claimed to be original are listed adopting the following numbering scheme :
Cx-y/z, where "C" stands for *claimed original contribution*, "x" specifies the concerned report chapter, "y" corresponds to the index of the claimed contribution, whereas "z" is potentially used for numbering the constituent parts of the claimed contribution.

- **C2-III**: Systematic study of half-band symmetric allpass functions as handled in Section 2.6, with identification of the fact that complex half-band allpass filters are featuring two separate symmetries in the positive and negative frequency ranges, cf (2.74a), (2.76c), and Figure 2.20, the main contribution being provided by Theorem 3 and related corollaries. Moreover, a restricted version of Theorem 3 is discussed in Subsection 2.6.6 for the case of constrained half-band symmetric allpass functions.

A further contribution is given by the observation made along the examples described in Subsection 2.4, that purely even phase response allpass functions offer a remarkable flexibility to diversely shape their phase response, since the spanned phase range $[\beta_A(\pi)-\beta_A(0)]$ is unconstrained. This fact can in particular be exploited in allpass-based transformation methods to partially shift out (or shift in) portions of the frequency response of transformed filters [Anso00], rendering non-circular transformations possible.

Further potential research

Based on the former considerations, the next subjects are proposed for potential further research:

- Systematic *study of the available design space of allpass functions* with purely even phase response, and general complex allpass functions, by approximating classes of phase responses, establishing guidelines if appropriate.
- Study of *further elementary properties* featured by complex allpass functions, in relation with particular filter configurations. As an example, the formal and practical study of complex filters for analytic signal processing could be envisaged, based on the refined allpass decomposition (2.28).
- Systematic study of *allpass-based filter transformations*, exploiting the results developed in the chapter, e.g. along already collected ideas [Anso00].
- Others.

Chapter 3

Complex and Real Wave Digital Filters

3.1 Introduction

The concept of Wave Digital Filters was introduced in 1971 by A. Fettweis [Fett71] as a basis for designing what we will call "robust" time-discrete filters. It is remarkable to observe, after almost 30 years of regular progress, how many – diversely oriented – theoretical and practical results, including industrial applications, were elaborated from these seminal ideas.

Hence, the WDF principle can be perceived as a true *paradigm* for robust digital signal processing, offering original solutions to a wide range of signal processing problems, including :

- *Real linear time-invariant filtering, using :*
  - *Classical WDF structures (e.g. ladder, lattice)* [Fett86];
  - *Power WDF structures* [1] [Hahn85, Host85, Zhan88];
  - *Orthogonal WDF structures* [2] [Fett90, Depr80, Suzu91];
  - *Lattice structured FIR filters* [Fett86, Zaln89, Vaid88];

---

[1] Filter structures essentially based on classical networks, but using power wave signal quantities.

[2] Recent filter configurations resulting from original factorization methods.

- *Complex linear time-invariant filters* [Fett81a, Meer83, Schü91, Jarm94, Scar94];
- *Hypercomplex linear time-invariant filters* [Kant89, Ebbi90, Schü90, Schü91, Fuku95, Kama97];
- *Signal modulation and multirate processing* [Fett82, Gazs86a], *in particular with retrieval of reflected power* [Dabr87a, Dabr87b];
- *Bidimensional and N-Dimensional signal processing* [Zou89, Doma91, Fett94, ICAS94, Gu94], *in particular using complex networks* [Fett87, Blej90, Janc93];
- *Adaptive signal processing* [Kubi85b, Zaln90, Tan92, Tan94];
- *Numerical integration and modelling of linear and non-linear time-variant processes described by Partial Differential Equations* [Fett89, Fett92b, Fett92c, Nits93, Fett94, ICAS94, Sche98];

and many more topics, dealing e.g. with practical DSP and VLSI implementation aspects.

However, one should also mention the numerous contributions originating from complementary approaches. These include design methods relying on various types of analog-to-digital transformations [Tant95] for the mapping of classical analog networks onto digital filters (e.g. backward difference approximation, impulse invariant method, matched z-transformation, etc.), in particular LDI-based methods [Brut75, Turn86, Nowr90, Nowr93].

Other contributions concern the Markel and Gray lattice filter structures [Gray79], resonator-based orthogonal filters and filter-banks [Péce88, Péce89, Padm91, Padm96], contributions proposed by Vaidyanathan and al. [Vaid84, Vaid88], and many others.

This chapter is dealing with complex and real WDF design limited to the linear time-invariant case. The sequel of the chapter is organized as follows. Section 3.2 is first recalling the fundamental properties of real WDFs, whereas complex WDFs are introduced in Section 3.3. Section 3.4 is then presenting in detail complex lossless two-ports, mainly focusing on lattice-type networks. In addition to reminding the essential features of symmetric and antimetric lossless two-ports, this section discusses in particular: i) achievement of higher-order

lossless two-ports by cascading lower-order symmetric/antimetric ones, including the scalar case; ii) doubly magnitude-complementary networks offering an interesting low-sensitivity to mismatches; iii) transformations of lossless two-ports; iv) equivalent implementations of real antimetric lossless two-ports. Next, the canonic number of design parameters characterizing lossless two-ports is handled in Section 3.5, discussing also their use to achieve different filter responses. Section 3.6 is then devoted to the mapping procedure of complex lossless two-ports from the ψ-domain into the z-domain, followed by the conclusions drawn in Section 3.7.

3.2 Real Wave Digital Filters

The concept of WDFs introduces a framework consisting in a rule-based mapping of classical analog networks (i.e. passive lumped element-based filter structures, or commensurete distributed networks), either onto analog time-discrete networks (e.g. switched capacitor filters), or onto digital filters [Fett71, Fett86]. Only digital filters are considered in this report.

The Wave Digital Filters achieved after mapping are featuring the following properties :

- They are fulfilling the *realizability* – or *computability* – conditions, [Fett84a, Fett86, Croc75], in the sense that the resulting digital networks : (i) are organized in ordered sequences of computation operations (precedence dependencies, etc.), and (ii) are devoid of any delay-free loop.
- They inherit the properties of the analog reference network they are derived from, which most importantly involves preservation of *passivity* and *losslessness* [Fett88, Fett72a, Fett72b, Fett75, Fett86, Deso75, Doma84, Vaid85a], which in turn implies further essential characteristics, including *low sensitivity*, *low round-off noise*, and *stability under finite-precision arithmetic conditions*. These properties will be discussed in Subsections 3.2.2 and 3.2.3.

A comprebensive tutorial paper on Wave Digital Filters and their design can be found in [Fett86], whereas complementary introductory

material is available in [Boit90, Laws90, Suzu90, Anto93], and [Schü94].

3.2.1 Mapping procedure to achieve real WDFs from analog reference filters

The mapping procedure recalled below applies to real networks [Fett86]. This method proceeds similarly to derive complex WDFs [Fett81a, Schü91].

Three frequency domains are considered for designing WDFs [Fett86], cf Section A.3 :

- the *p-domain*, where p is the actual complex frequency;
- tbe *ψ-domain*, ψ corresponding to Richards' variable used for the design of commensurate distributed reference filters;
- the *z-domain*, where z is the standard complex frequency variable used in digital signal processing; z is related to ψ through the bilinear transform, cf (A.50).

The transfer of analog reference filters into the digital domain should be performed using convenient signal variables. Hence, a first attempt based on the digitization of voltages and currents of the analog network fails very soon, because this leads to unrealizable filters containing delay-free loops. To circumvent this problem, *wave quantities* as known from the *scattering parameter theory* [Bele68, Youl71, Fett92a] are used instead for designing WDFs [Fett86].

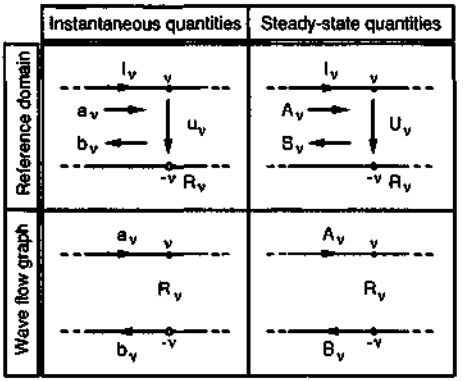

Figure 3.1: Representation of a port (real networks).

These wave quantities are defined with respect to each *port* of the reference network, where a port is characterized by a *voltage*, a *current*, and a constant *port resistance* R for real networks (Figure 3.1). One distinguishes *incident* waves (denoted by a or A), which propagate in the *forward* direction, and *reflected* waves (denoted by b or B), propagating in the *backward* direction. The port quantities can moreover be considered either as *instantaneous* quantities in the time domain (lower case symbols a and b), or *steady-state* quantities in the frequency domain (upper case symbols A and B).

The incident and reflected waves can be defined as *power*, *voltage* or *current wave quantities* [Fett86], where the power waves correspond to the usual wave quantities known from the classical scattering parameter theory. The difference between these quantities being marginal [Kubi85a], and considering the related implementation simplifications [Fett86], only voltage wave quantities are considered in the report.

The mapping procedure applied for the derivation of WDFs proceeds now as follows (Figure 3.2). A passive reference filter is first selected and specified in the ψ-plane. This reference filter is characterized by voltage quantities, elementary one-port and two-port components, and basic parallel / serial interconnection networks fufilling Kirchhoff's interconnection laws. If necessary, the reference filter includes also compact second and fourth-order filter sections (Brune, Darlington C, D, and E cells).

The elementary one- and two-port components are subdivided into *frequency dependent* components (equivalent capacitances and inductances, Unit Elements, etc.), and *frequency independent* components (resistances, ideal transformers, etc.).

The interconnection network as a whole is frequency independent, and is usually decomposed into elementary parallel and serial interconnections, or into more general interconnections when required. These interconnection networks are all defined as multiports to get a consistent description in the wave domain.

In a second step, the reference filter is described using wave quantities in the ψ-plane, cf Figure 3.2. The elementary components are then defined by a reflectance coefficient $S(\psi)$ for one-ports, and by a scattering matrix $S(\psi)$ for two-ports or multiports. Furthermore, the

interconnection networks are converted into so-called *adaptors* characterized by a frequency independent multiport scattering matrix [Fett86].

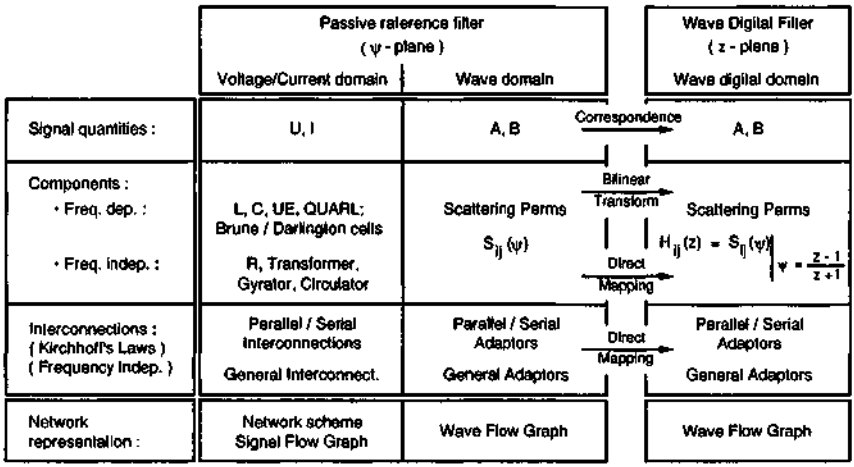

Figure 3.2: Mapping procedure from analog reference filters onto WDFs (real networks).

The last step consists in transferring the achieved wave filter from the analog domain into the digital domain using the bilinear transform. Obviously, all frequency independent building blocks (concerned components, adaptors) are directly mapped into the digital domain (Figure 3.2).

An example of the procedure is given in Figure 3.3 for an elementary doubly-terminated third-order ladder structure. The internal structure of the adaptors can be found in [Fett86].

As can be observed from Figure 3.3, WDFs achieved from classical two-ports are featuring two input and two output signals, making the four entries – i.e. transfer functions – of the scattering matrix *simultaneously* available. This property, which extends directly to multiports, is appreciated for many applications (e.g. branching filters, analysis and synthesis filter banks), and leads to economic solutions.

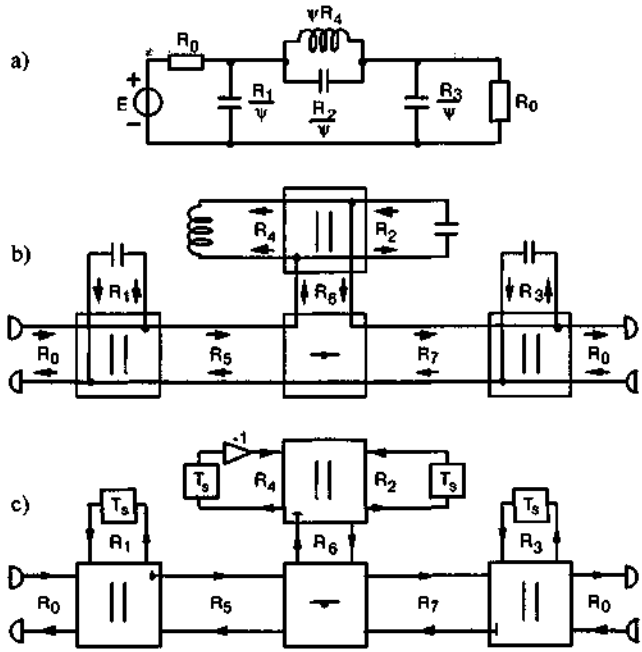

Figure 3.3: Example of mapping procedure for a 3rd-order ladder filter: a) Analog reference filter; b) Intermediate step; c) Derived Ladder WDF.

A further advantage for WDFs is that the extended corpora available for the design of classical filters, including design tables and charts [Zver67, Saal79], or elaborated approximation tools, e.g. [Szen77], can all be (re-)used for WDFs, resulting in a rich framework. It should be emphasized that the phase distortion introduced by the bilinear transform occurring in the WDF design process, is by no means a limitation for applications requiring fulfillment of a specified phase response, since the distortion can be pre-compensated prior to performing the approximation, e.g. [Henk81a, Föld91].

3.2.2 Passivity and losslessness

When applied to digital circuits, the notions of passivity and losslessness are referring to a measure of *instantaneous power* (time domain), or a measure of *steady-state power* (frequency domain) assigned to all input/output terminals of the circuit, and to all internal

signals corresponding to the leads of the basic building blocks composing the network, cf [Fett88, Fett72b, Boyd82]. When the (instantaneous or steady-state) total power *absorbed* by a digital circuit is proved to be nonnegative or equal to zero for any choice of input signals, it is said to be passive or lossless, respectively.

External passivity and *external losslessness* are further distinguished from *internal passivity* and *internal losslessness*, respectively [Fett88]. External passivity and losslessness refers to the balance of the absorbed (steady-state) power of a digital circuit as observed from input/output terminals only, and corresponds to a *behavioural* characteristic of the network. External losslessness is essential to achieve low-sensitive digital networks, and is sufficient to ensure input/output stability under linear conditions.

A digital circuit is in turn denoted as *internally passive* or *lossless* when it is comprehensively composed of passive or lossless building blocks, which corresponds to a *structural* property of the network. Internal passivity or losslessness is the only one which may guarantee stability under finite-precision operational conditions (i.e. avoidance of small and large scale limit-cycles, forced response stability, marginal parasitic oscillations occurring with periodic input signals, stability under looped conditions) [Fett88], provided the digital network is properly designed.

Due to the principle of power conservation, it is observed that internal passivity or losslessness involves external passivity or losslessness, respectively, whereas the converse assertion is not necessarily verified [Fett88].

Considering the mapping procedure applied for the derivation of WDFs, it turns out that WDFs are *by construction* only composed of passive or lossless building blocks, and are therefore internally – and by extension also externally – passive or lossless. Applying in addition well-defined signal quantization and overflow handling rules [Fett75, Meer79, Meer80a] in case of finite-precision arithmetic implementation, where the signals under consideration are precisely selected at the ports of the constituent building blocks, WDFs are shown to present all the desired features for robust digital filtering.

3.2.3 Sensitivity, round-off noise, and stability

WDFs are thus characterized by the next interrelated features :

- *Low sensitivity to filter coefficients* :
  Due to the Orchard-Fettweis Theorem [Orch66, Hasl81a], the attenuation response of *terminated* classical lossless analog networks is particularly insensitive to parameter variations within the *passband*. Hence, the resulting WDFs are characterized by a very low sensitivity to filter coefficients, allowing for coarsely quantized coefficients and reduced implementation complexity [Fett73, Fett74b, Yang81, Fett86].
  It is noticed that the sensitivity observed in the *stopband* of both analog and corresponding WDF networks is depending on the underlying filter structure [Rega88a, Pras87]. Lattice filters are for instance known for their perceptible sensitivity in the stopband, compared e.g. to ladder networks – a reason why they are usually avoided in the analog domain [3].
  Finally, it is mentioned that *singly terminated* reference filters are leading to more sensitive WDF structures [Fett86].
- *Low round-off noise* :
  Connected to their low passband sensitivity [Fett72a, Fett73, Fett74b, Ullr76], WDFs are characterized by a performant signal-to-noise ratio, allowing for shorter signal wordlengths (cf fixed-point implementation).
- *Stability under linear conditions* :
  This property is automatically fulfilled due to internal passivity / losslessness of WDFs.
- *Stability under finite-precision arithmetic conditions* :
  The stability under finite-precision operational conditions, including avoidance of small and large scale limit-cycles through controlled signal quantization and overflow handling, stability for

---

[3] Another reason why analog lattice filters are normally avoided for filtering purposes is because of their implementation costs : the structure is either non-canonic (cf basic lattice, T-, and Π-networks), or it requires a transformer (cf Jaumann, bridged-T networks) [Bele88, Blin76]. The stopband sensitivity of analog lattice structures is on the other hand of crucial importance for instrumentation and measurement purposes, e.g. the Wheatstone bridge.

periodic input signals, forced response stability, and the strong conditions of stability under looped conditions, can be shown to be fulfilled by WDFs, provided specific design guidelines are followed [Fett75, Meer79, Meer80a, Noss83, Fett86, Dabr86, Fett88, Butt88, Butt89].

3.2.4 Factorization methods and related WDF structures

Basically, the Wave Digital Filter structures essentially differ according to the *factorization method* used to synthesize the lossless N-port to be designed. Hence, starting from the abstract mathematical description of the N-port to be synthesized, expressing the relationship between the externally ingoing and outgoing signal quantities, the factorization consists in systematically extracting from the original mathematical description elementary (zero-, first-, second-, or fourth-order) sections, allowing for a gradual degree reduction of the N-port description, until it has been fully handled. This process is influenced by important aspects, such as the reciprocal or non-reciprocal nature of the N-port to design, or the possible necessity to achieve a canonic implementation.

The factorization is done using either the rational impedance/admittance matrices of the lossless N-port, or its chain matrix, scattering matrix, scattering transfer matrix [4], or one out of its two scattering hybrid matrices [Bele68, Fett90] [5, 6].

Finally, apart from possible (local) transformations aiming at simplifying the N-port implementation, e.g. to avoid the use of costly components, the overall structure of the resulting N-port is fixed associating to each elementary (zero-, first-, second-, or fourth-order) section a corresponding physically realizable network.

---

[4] The scattering transfer matrix is also termed scattering chain matrix.

[5] The factorization of the scattering matrix or scattering hybrid matrices results in networks that are costly to implement in the time-continuous domain, since they involve many circulators; conversely, the corresponding WDF structures are simple to realize [Fett90].

[6] For lossless one-ports, the mathematical description reduces either to a scalar impedance/admittance (in fact a reactance due to losslessness), or to a reflectance [Bele68].

		Time continuous filters		Time discrete filters		Wave Digital Filters		
		Real	Complex (including real case)	Real	Complex	Real	One-real complex	Complex (including one-real case)
General	Foster 1+2	[Bahe84], pp. 48-49.	[Bele68], pp. 135-138.			[Fett86]	[Fett81a, Meer80b]	[Schü91]
	Cauer 1+2	[Bele68], pp. 141-143; [Bahe84], pp. 51-57.	[Bele68], pp. 143-149.			[Fett86]	[Meer80b, Fett81a]	[Schü91]
	Richards	[Bahe84], pp. 142-146.				[Fett86]	[Meer80b]	[Schü91]
	(Mixed)	...	...			([Fett86])		
Specific	Chain of circulator-type allpass sections	—	—	—	—	[Fett86]	[Meer80b, Fett81a]	[Schü91]
	Complex reactance interpreted as real antimetric two-port	—	—	—	[Vaid87a, Sara87, Rega88b]			[Meer83]
	Other allpass implementations	—	—	[Nowr93]	[Rega88b]			

Table 3.1: Factorization methods and related lossless one-port implementation structures.

		Time continuous filters		Time discrete filters		Wave Digital Filters		
		Real	Complex (including real case)	Real	Complex	Real	One-real complex	Complex (including one-real case)
Reciprocal	Darlington insertion loss method + Scattering transfer matrix factorization	[Darl39, Youl71]	[Bele68, Naga90b]	[Turn86, Cort92]	[Acha90]			[Naga90b]
	Lattice-type structures	*(Very sensitive to parms. variations)*	[Bele68] *(Very sensitive to parms. variations)*	[Vaid87a [7], Sara87 [7], Rega88b [7], Nowr90. Cort92]		[Fett74a, Nout74, Meer83 [7], Fett86]	[Meer80b, Fett81a] [8]	[Schü91]
	Power WDF structures [1]	—	—	—	—	[Hahn85. Host85, Zhan88]		
Reciprocal and non-reciprocal	Extended Darlington method + Scatt. transfer matrix factorization	[Fett69. Tan88, Unbe89. Jarm91]	[Bele68, Tan88, Jarm94, Scar94]			[Nout75, Suzu90, Jarm91]	[Fett81a, Jarm94]	[Jarm94]
	Orthogonal structures [2, 9]			[Depr80, Vaid85b, Rao87, Padm96]		[Vaid85b, Fett90, Suzu91]		

Table 3.2: Factorization methods and related doubly terminated lossless two-port implementation structures.

[7] Real antimetric lossless two-ports realized with a single complex allpass.

[8] Referring to [Fett81a]: Complex Lattice-type WDFs are not always implementable in *true* one-real form, as explained in the paper.

[9] Inclusion of the non-reciprocal case should be checked separately for each mentioned reference.

			Time discrete filters		Wave Digital Filters		
			Real	Complex	Real	One-real complex	Complex (including one-real case)
Reciprocal	Two-port implementations						
	Scalar transfer functions	Leapfrog	[Cort92]				
Reciprocal and non-reciprocal	Two-port implementations	Scattering matrix factorization	—	—	[Fett86]		
		EESS WDFs [10]	—	—	[Wanh81, Sjös93]		
	Scalar transfer functions	State-Space WDFs	—	—	[Fett86]		
		Parallel form WDFs	—	—	[Göck90]		
		Resonator-based WDFs	—	—	[Padm96]		
		GIC-based WDFs [11]	—	—	[Anto93]		
		Other		[Ragh91]			

Table 3.3: Specific lossless two-port implementation structures not represented in Table 3.2.

[10] Essentially Equivalent State Space (EESS) WDFs correspond to state-space implementations that are behaviorally operating like the original WDF structures they are derived from, including location and processing of signal quantization (bit-true level), and they offer a highly regular structure amenable to efficient hardware implementations. When internal filter signals undergoing a quantization in the original WDF are merged in the EESS structure, the latter offers even a reduced quantization noise level.

[11] Generalized-Immittance Converter (GIC) based WDFs can be implemented in two forms, using either voltage- or current-conversion GICs. The latter is discussed in detail in [Anto93].

Clearly, considering the number of factorization methods, including mixed approaches, considering also the variety of possible implementations for the elementary sections involving different components, and the available (local) transformation techniques that can be applied, e.g. Kuroda-Levy methods [Frai69], it turns out that the number of achievable lossless analog reference N-ports, and of the Wave Digital Filters derived thereof, is significant.

Obviously, under strict linear and nominal operational conditions, all these different lossless N-port implementation structures are equivalent, the same remark applying to all corresponding WDF structures. However, under real life operational conditions, involving :

- for classical analog N-ports: sensitivity to component tolerances with respect to nominal value, including loss effects; sensitivity to varying physical quantities (temperature, humidity, others); sensitivity to (small-scale) component non-linearities; component implementation costs and sizes; others;
- for WDFs: sensitivity to filter coefficients, allowing for more / less coarsely quantized coefficients; level of round-off noise (type of quantization rule adopted; number of internal signals quantized, etc.); implementation costs related to regularity of the structure; others;

important qualitative and quantitative differences are observed. Regarding the WDF realization procedure, the designer can follow three approaches:

- either he already disposes of existing WDF structures fulfilling the needs of the considered application, in which case it suffices to adjust their degree and coefficients to the application problem (simplest case);
- or he disposes of an appropriate analog reference N-port he can map into the WDF domain applying the correspondence rules (more involved situation, but avoiding the factorization process);
- or he proceeds otherwise to the factorization, producing the final WDF without necessarily generating the reference N-port (most involved situation, but offering the marginal possibility to achieve original WDF structures, although many were already published).

Table 3.1 provides a non-exhaustive list of factorization methods and implementation structures obtained for lossless one-ports (i.e. reactances), considering the analog reference networks, and related digital and WDF structures.

Table 3.2 is in turn presenting a non-exhaustive list of factorization methods and related implementation structures for doubly resistor terminated lossless two-ports, further structures being referred to in Table 3.3. It is recalled that Darlington's insertion loss synthesis technique, originally elaborated for reciprocal lossless two-ports only [Darl39, Youl71], and later extended to the non-reciprocal case by Youla, was playing a central role in the filter synthesis field.

3.2.5 WDF design procedure

Schematically, the WDF design procedure involves the next steps, whose effective execution depends on the encountered situation and the objectives of the handled application :

Phase 1: Unquantized filter design (floating point):

- Set the specifications, including selection of filter degree, identify the reciprocal/non-reciprocal nature of the filter, including the lattice-type case, determine the constraints and available degrees of freedom regarding the requested amplitude/phase response, with possibly prescribed transmission zeros, etc.;
- Approximate the filter, selecting an optimization criterion (e.g. maxflat, minimax, others) and the approximation method, to establish the filter coefficients (floating point precision);
- Determine the corresponding lossless two-port scattering matrix, or equivalent description of the two-port;
- If necessary, perform the factorization to synthesize the detailed implementation structure of the lossless reference two-port;
- If necessary, apply equivalence transformations (e.g. Kuroda-Levy's method), or select alternative implementations of Brune sections, or Darlington C–, D–, and E–sections, etc.;
- Map the lossless reference two-port onto the corresponding WDF structure, possibly including *careful* simplifications/modifications of the structure that are preserving the fundamental properties of

the original WDF (e.g. mapping onto Essentially Equivalent State-Space WDFs [10] [Wanh81, Sjös93]);

- Thoroughly assess the functionality of the obtained WDF.

Phase 2: Finite wordlength implementation (fixed point):

- Optimize the quantized value of the filter coefficients according to the target implementation platform;
- Apply a scaling to all authorized filter signals;
- Quantize all authorized filter signals, either individually, or globally according to the target implementation platform;
- Thoroughly assess the functionality of the achieved WDF.

Phase 3: Physical (software/hardware) implementation:

- Perform the physical realization of the filter and check the results.

A detailed discussion of the design procedure, including provision of examples, can be found in [Fett86, Laws90, Wanh99], and [Sjös93].

3.3 Complex Wave Digital Filters

The extension of filtering methods to the complex numbering field presents several interests. First at conceptual level, expressing (certain) filtering problems in the complex field often provides a more regular and compact – sometimes even elegant – description of the situation, which helps in getting a better insight of the problem, in specifying solution strategies and elaborating design/approximation tools, or in handling specific applications. This motivation certainly holds also in case the final target filter is real.

Second, selected practical applications undoubtedly do also benefit from the use of complex filters, as will be seen in Subsection 3.3.3, and this even if the handled signals are real (e.g. analytic signal processing).

The question to be answered then in case of *digital* signal processing is to know if there is a reason to physically implement filters in complex form, since the networks dealt with in the present context are linear – at least under ideal operational conditions – and can thus be

equivalently represented by a real network, considering complex signals as a mere arrangement of real signal pairs following specific mathematical rules [Meer80b]. Tbe answer to this question is then given by the actual implementation costs related to the application, and should be handled case by case. Indeed, the relationship between the original complex filter and its real counterpart is more complicated than it might seem, and can affect issues like the selection of the filter structure, regularity and modularity of the solution, clustering of operations, roundoff-noise since signal quantization is not necessarily processed equally in both cases, ease of software/hardware realization, etc.. A definite answer is tbus not given here.

The remainder of this section is organized as follows. The equivalence between complex and real networks is first discussed in Subsection 3.3.1. A classification is then estsblished in Subsection 3.3.2 to distinguish situations according to the (non-) realness of the considered filters and related inpnt/output signals. Next, Snbsection 3.3.3 motivates the use of complex filters, furnishing a short list of application examples. In Subsection 3.3.4, several categories of filtering problems are differentiated in terms of real/complex classical filtering and broadband matching problems. The additional components needed to realize complex WDFs are then introduced in Subsection 3.3.5, before discussing in Subsection 3.3.6 the concept of one-realness related to the implementation of complex WDFs.

3.3.1 Equivalence between complex and real networks

Given any (not necessarily lossless) complex two-port N as represented in Figure 3.4a. The two-port is featuring incident and reflected waves $A_i(\psi)$ and $B_i(\psi)$, $i=1,2$, respectively, together with the scattering matrix $S(\psi)=\{S_{kl}(\psi)\}$, $k,l=1,2$, where $S_{kl}(\psi)$ correspond to the scattering parameters. All quantities are related by :

$$A=\begin{pmatrix} A_1 \\ A_2 \end{pmatrix}, \quad B=\begin{pmatrix} B_1 \\ B_2 \end{pmatrix}, \quad S=\begin{pmatrix} S_{11} & S_{12} \\ S_{21} & S_{22} \end{pmatrix}, \quad B=S\cdot A, \qquad (3.1a,b,c,d)$$

explicit mention of the variable ψ being dropped for simplicity. All quantities being complex, they can be decomposed into their constitutive real analytic and imaginary analytic parts, cf Subsections A.2.2 and A.2.6 :

$$A_i = A_{i\,Ra} + j \cdot A_{i\,Ia};\ B_i = B_{i\,Ra} + j \cdot B_{i\,Ia};\ S_{kl} = S_{kl\,Ra} + j \cdot S_{kl\,Ia}; \quad (3.2a,b,c)$$

which applies by extension to the matrix forms :

$$A = A_{Ra} + j \cdot A_{Ia};\quad B = B_{Ra} + j \cdot B_{Ia};\quad S = S_{Ra} + j \cdot S_{Ia}; \quad (3.3a,b,c)$$

Clearly, introducing (3.3a,b,c) into (3.1d) leads to :

$$\left(\frac{B_{Ra}}{B_{Ia}}\right) = \left(\begin{array}{c|c} S_{Ra} & -S_{Ia} \\ \hline S_{Ia} & S_{Ra} \end{array}\right) \cdot \left(\frac{A_{Ra}}{A_{Ia}}\right), \quad (3.4)$$

thus demonstrating that any complex two-port can be equivalently expressed by a real 4-port [Meer80b]. The next topic of interest concerns the relationship between the degree of the original complex scattering matrix S, and the real equivalent one specified by the degrees of S_{Ra} and S_{Ia}, due to their impact on the implementation complexity. Since the scattering parameters are rational functions, they will be considered first.

Degree of the real and imaginary analytic parts of rational functions

Given a complex scattering parameter S with dropped indices for simplicity, which is considered in *reduced* form, i.e. the numerator and denominator are coprime. Moreover, S is factorized into two terms S_α and S_β, S_α collecting all real zero/pole configurations, S_β gathering the remainder part of S :

$$S = S_\alpha \cdot S_\beta, \quad \text{with } S_\alpha = \overline{S_\alpha}, \quad (3.5a,b)$$

so that the real analytic and imaginary analytic parts of S become :

$$S_{Ra} = \frac{S_\alpha \cdot S_\beta + \overline{S_\alpha \cdot S_\beta}}{2} = \frac{S_\alpha \cdot S_\beta + \overline{S_\alpha} \cdot \overline{S_\beta}}{2} = S_\alpha \cdot S_{\beta\,Ra}\ , \quad (3.6a)$$

and similarly : $$S_{Ia} = S_\alpha \cdot S_{\beta\,Ia}\ ; \quad (3.6b)$$

$S_{\beta\,Ra}$ and $S_{\beta\,Ia}$ being the real and imaginary analytic parts of S_β. Denoting by Num_X and Den_X the numerator and denominator of any reduced rational function X, respectively, so that $X = Num_X / Den_X$, one establishes :

$$\deg(Num_{S_{Ra}}) \le \deg(Num_S) + \deg(Den_{S_\beta}), \tag{3.7a}$$

$$\deg(Den_{S_{Ra}}) = \deg(Den_S) + \deg(Den_{S_\beta}) \le 2 \cdot \deg(Den_S). \tag{3.7b}$$

deg(.) indicating the degree of the polynomials. Possible common factors between the numerator and denominator of S_{Ra} generated during the process, and which could be cancelled out, are here not taken into account. Clearly, similar results hold for S_{Ia}. In case the considered two-port is lossless, the additional condition :

$$\deg(Num_S) \le \deg(Den_S), \quad (\text{N lossless}); \tag{3.8a}$$

is verified for each of the scattering parameters in (3.1c), the degree of which being then specified by the degree of the denominator.

Degree of the real and imaginary analytic parts of the scattering matrix of lossless two-ports

Focusing on lossless two-ports, and referring to Subsections 3.4.4 to 3.4.7, it is observed that :

- *Non-reciprocal case*: The degree of the scattering parameters of S_{Ra} and S_{Ia} evolve individually along (3.7), so that the prediction of the degrees of S_{Ra} and S_{Ia} is limited in precision to :

$$\deg(S) \le \deg(S_{Ra}) \le 2 \cdot \deg(S), \quad \deg(S) \le \deg(S_{Ia}) \le 2 \cdot \deg(S); \tag{3.9a,b}$$

  the degree of the matrices being specified by the common denominator in S. (3.9a,b) also apply to the *general reciprocal* case.

- *Lattice-type reciprocal case*: S_{Ra} and S_{Ia} are remarked to be themselves of lattice-type. According to Subsection 3.4.13, the scattering matrix of lattice-type lossless two-ports can be factorized into a product of lower-order scattering matrices of same type. It is then possible to apply (3.5) and (3.6) at matrix level, so that :

$$\deg(S_{Ra}) = \deg(S_{Ia}) = \deg(S) + \deg(S_\beta). \tag{3.10}$$

3.3.2 Classification according to (non-) realness of networks and signals

Different situations are distinguished depending on the complex or real nature of the filter networks on one hand, and of the input/output signals assigned to them on the other hand, cf Table 3.4 and

Figure 3.4. The two-ports N considered in this subsection are not necessarily lossless. Cases 1 and 4 in Table 3.4 are classical, and are both illustrated in Figure 3.4a, selecting the appropriate real / complex interpretation for the network and signals.

Case 2 may occur when a real filter network N is embedded in a larger system that is processing complex signals. Referring to (3.4) with $S_{Ia} \equiv 0$ since the two-port N is real, it is observed that two instances of N are needed, namely one to handle the real part of the signals, and a second one to process separately the imaginary components of the signals [Meer80b], as represented in Figure 3.4b.

Case 3 is to be considered differently, two typical examples being listed in Table 3.4. Finally, Case 5 refers to the situation where the two-port N becomes degenerate complex, in the sense that it reduces to a real network N' using an appropriate set of complex constants at its inputs/outputs, as illustrated in Figure 3.4c. One of the constants α_i, β_i, $i=1,2$, should at least be complex. An example is given in Figure 3.4d for $\alpha_1 = \beta_1 = 1$, $\alpha_2 = \beta_2 = \pm j$, where the multiplications by $\pm j$ merely correspond to swapping the real and imaginary parts of the bandled signals, in addition to a sign change (upper and lower signs in Figure 3.4d are matching with those of $\alpha_2 = \beta_2 = \pm j$).

Case	Network N	Network N'	Signals	Figure	Examples
1	Real	—	Real	3.4a	Classical situation
2			Complex	3.4b	Occurs when N is part of a complex system
3	Complex	—	Real	—	1) Analytic signal processing based algorithms (cf Subsection 3.3.1) 2) Complex allpass N implementing a real antimetric lossless 2-port
4			Complex	3.4a	Classical situation
5 (Degenerate complex)	Complex	Real	Complex	3.4c 3.4d	Cf Subsection 3.4.15 and Chapter 4

Table 3.4: Classification according to (non-)realness of two-ports and signals.

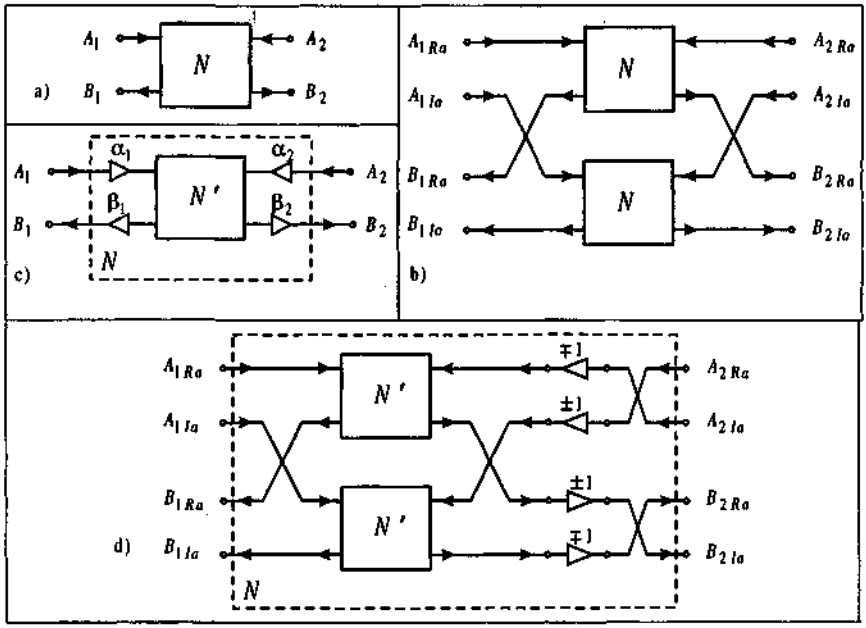

Figure 3.4: Interpretation of the different cases listed in Table 3.4.

3.3.3 Usefulness of complex signal filtering methods

The motivations for extending filtering techniques to the complex domain are multiple :

- At formal mathematical and circuit theory levels:
  - Establishment of a compact filter description formalism rendering the design and approximation procedures often simpler, and helping in better identifying the fundamental features of different filter structures, including real ones.
  - Others;
- At applied mathematical and circuits and systems levels:
  - Enriched mathematical support to design filters, that can open new possibilities even when the target filter is real (e.g. allpass-based transformation techniques [Anso00]);

- Disposal of the necessary network theoretic background in view of elaborating filter approximation tools, including the case of real antimetric target filters handled through approximation of a complex allpass [12];
- Others;

➢ At application level, to perform (examples):

- Analytic signal processing:
  - Filtering of communication signals, where complex solutions are suited to achieve asymmetric amplitude and group delay responses by offering independent control of the lower/upper stopband rolloff rates, while maintaining low intersymbol interference (e.g. single-sideband bandpass filters [Lind96]);
  - Phase or group delay equalization to compensate signal distortions induced either by dispersive processes or communication channels, or to partly restore signals suffering from non-linear distortions [13];
  - Same as above, extended to tunable filters [Take80];
  - Hilbert Transform-based signal transmultiplexing [IEEE82];
  - Others, cf Chapter 6;
- Wideband stereo audio coding relying on complex signal processing, the left/right audio channels appearing, respectively, on the positive/negative frequencies of the complex-valued coder signal [Härm97b, Härm98];
- Multiscale signal analysis for fractal-type signals, or images, e.g. [Bhar98];
- Multidimensional filtering, e.g. image filtering involving non-separable filter kernels;
- Beamforming, radar, and sonar processing, etc.;
- Others.

---

[12] In this case, the complex allpass is not necessarily implemented but serves as a means to process the target filter coefficients.

[13] It is in particular noted that complex allpass networks can offer a two-sided sharp selectivity at low passband frequencies, with respect to real allpasses whose performance is limited by the presence of the complex conjugate poles.

3.3.4 Categories of filtering problems

Referring to Figure 3.7, different categories of filtering problems are distinguished depending on the real/complex essence of the lossless two-port, and the nature of the terminations $Z_{Ei}(\psi)$, $i=1,2$, which should in any case be *strictly positive real functions* [14], cf Table 3.5.

Case	Problem category	Lossless two-port (filter)	Termination impedances [14] $Z_{E1}(\psi)$	$Z_{E2}(\psi)$	Voltage source E_2	References
1	Classical filtering	Real	$Z_{E1}=Z_{E2}=R_E>0$		Unconstrained	(*many*)
2			$R_{E1}>0$	$R_{E2}>0$		(*many*)
3		Complex	$Z_{E1}=Z_{E2}=R_E>0$			(*many*)
4			$R_{E1}>0$	$R_{E2}>0$		(*many*)
5			$Z_{E1}=Z_{E2}=Z_E$ [15]			[Schü91]
6	Single broadband matching	Real	$R_{E1}>0$	$Z_{E2}(\psi)$	$E_2\equiv 0$	[Youl64, Chen95b]
7		Complex				*Seemingly not covered*
8	Double broadband matching	Real	$Z_{E1}(\psi)$	$Z_{E2}(\psi)$	$E_2\equiv 0$	[Carl83, Yarm88, Paul89, Dedi94]
9			Other non-standard terminations			[Hasl81b]
10		Complex	$Z_{E1}(\psi)$	$Z_{E2}(\psi)$		*Seemingly not covered*

Table 3.5: Categories of real and complex filtering problems, referring to the doubly terminated lossless two-port in Figure 3.7.

Classical filtering problems correspond to cases where both termination impedances are assigned a *constant* real/complex value, whereas one is dealing with *single* (or *double*) *broadband matching* problems when Z_{E2} (or both Z_{E1} and Z_{E2}) become frequency dependent terminations. Single (double) broadband matching consists in matching the generator impedance Z_{E1} to the load impedance Z_{E2} over a specified frequency band through a lossless two-port, often denoted as a "tuner" in this context. It is observed that the single/double

[14] Only real passive termination impedances $Z_{Ei}(\psi)$, $i=1,2$, are considered here. These impedances are necessarily dissipative, and are thus *strictly positive real functions*, i.e. $\mathrm{Re}\{Z_{Ei}(\psi)\}>0$, $i=1,2$, for $\mathrm{Re}\{\psi\}\geq 0$ [Bele68], p. 131.

[15] Z_E is a complex-valued constant verifying $\mathrm{Re}\{Z_E\}>0$.

broadband matching problems involving a complex lossless two-port have apparently not been covered in the literature.

This report is considering cases 1 to 4, with focus on cases 1 and 3.

3.3.5 Complex WDF components and structures

The design of complex WDFs proceeds similarly to the real case, except that: i) additional components are introduced, ii) factorization methods are adapted, and iii) care should be taken with respect to the use of complex adaptors and finite-precision WDF implementation in order to guarantee all stability conditions. The third issue will be addressed in the next subsection.

Components of the complex reference two-port		Derived components of the complex WDF	
		One-real complex [Fett81a]	Complex (excl. one-real case)
Imaginary resistance [16] [Bele68]	⇒	Complex unimodular multiplication [Meer80b, Fett81a, Naga90b, Schü91]	
Complex transformer [17] [Bele68]	⇒	[Meer80b, Fett81a, Schü91]	
Complex gyrator [17]	⇒	[Meer80b, Schü91, Naga90b]	
Complex Unit Element [17]	⇒	[Naga90b]	
Serial / parallel interconnection networks [16]	⇒	Real adaptors [Fett81a]	Complex adaptors [Schü91]

Table 3.6: Additional components used to design complex doubly terminated lossless reference two-ports and related WDFs.

Referring to Table 3.6, the design of complex lossless reference two-ports and WDFs derived thereof involves the following additional components with respect to the real case :

- Imaginary resistances [Bele68], p. 57, which are necessarily occurring, and are implemented as unimodular multiplications in the WDF domain;
- Complex ideal transformers [18] [Bele68 (p. 120), Meer80b, Fett81a, Schü91];

[16] Requested in all cases.

[17] Requested according to desired lossless reference two-port / WDF structure.

- Complex gyrators [19] [Meer80b, Schü91, Naga90b]; and
- Complex Unit Elements [Naga90b];

the latter three appearing according to the considered network. Informations on factorization methods and associated implementation structures can be found in Tables 3.1 – 3.3.

3.3.6 One-realness and related topics

An important issue concerns the mutual adaptation of the interconnected components. To solve this problem, Fettweis introduced the notion of *one-realness* – known from Richards' Theorem [Bahe84] – into the WDF framework to implement complex impedances [Fett81a]. A complex impedance $Z(\psi)$ in the reference network is called one-real when $Z(\psi=1)=R$ is real and positive. Under this condition, the corresponding reflectance $S(\psi)=[Z(\psi)-R]/[Z(\psi)+R]$ features a transmission zero at $\psi=1$, i.e. at $z=\infty$, thus ascertaining that the component is devoid of any delay-free loop between its leads in the WDF domain (realizability condition) [20]. Furthermore, and this has a direct impact on the WDF implementation, it is then possible to realize the series/parallel network interconnections using *real* adaptors in the WDF domain, all stability properties known for real WDFs extending then to the complex case [Fett81a]. This approach avoids thus the elaboration of complex adaptors, and, more important, the specific study of all stability conditions (cf Subsection 3.2.3) in the complex case, at cost of the (mild) one-real constraint.

In [Schü91], Schütte is establishing the following:

a) First, he derives the overall formulas for complex serial/parallel adaptors in the *unconstrained* case [21], and demonstrates further that *constrained* complex serial/parallel adaptors become structurally identical to real ones, including the same real adaptor coeffi-

---

[18] Ideal complex transformers were originally considered as a pure mathematical concept, being physically unrealizable as a real passive network [Carl62]. It was later shown in [Meer80b, Schü91] that ideal complex N-port transformers can certainly be physically implemented as real 2N-port transformers.

[19] Although not labeled as such, complex gyrators were already discussed in [Bele68], pp. 213-214.

[20] Internal avoidance of delay-free loops should though be checked separately.

cient, the only difference being that their port resistances are complex [22].

b) Second, Schütte considers complex reactances implemented in a Foster 1-type configuration, involving by construction constrained three-port serial adaptors only. From there, he demonstrates in detail that the Foster 1-type WDF implementation of any complex reactance results in precisely the same WDF structure when deriving it: 1) either as a general (i.e. non one-real) complex reactance involving complex adaptors with complex port resistances in the WDF domain, or 2) as an equivalent one-real complex reactance implemented with real adaptors featuring real port resistances, the adaptor coefficients being real and identical in both cases. Clearly, only the interpretation of the port resistances changes from one implementetion to the other [23].

c) Consequently, he deduces that one-realness is *not* introducing any functional constraint regarding the implementation of single reactances [24].

Regarding point c), it is though recalled that one-realness can marginally affect the functionality of implemented *two-ports*, as it may happen for lattice-type filters realized as Lattice WDFs [Fett81a].

---

[21] Serial/parallel adaptors are termed *unconstrained* when all their port resistances can take arbitrary positive values. The adaptore are called *conetrained* when one of their ports is reflection free, involving that the corresponding port resistance is fixed by the other port resistances [Fett86].

[22] According to the terminology used, WDF "port resistances" are labeled as such irrespective of the real/complex constent value assigned to them.

[23] Notes of the author: i) The logical link between points a) and b) above is not explicitly presented as such in [Schü91]. Instead a rether detailed but informative development is done based on the Foster 1-type implementetion, making implicitly use of constrained serial adaptore. ii) Implementing instead the complex reactances in Foster 2-type structure would require constrained three-port *parallel* adaptors only, featuring again real adaptor coefficients, thus leading to the same conclusions.

[24] Note of the author: The generalization expressed in c) out of the observations made on the Foster 1-type WDF implementation of complex reactances is justified by the fact that *every* complex reactance can be represented in the complex Foster 1-type form, cf [Bele68], Section 3, p. 135.

It turns out that any kind of one-real/non one-real complex reactance and lossless two-port requires numerous complex unimodular multiplications located next to adaptors when implemented in the WDF domain. These unimodular multiplications are not exactly realizable in finite-precision arithmetic (quantization of filter *coefficients* only is considered here), so that the lossless character of WDFs cannot be preserved in the strict sense when realized in this form.

Starting with a complex WDF reactance involving adaptors with real coefficients, this problem is circumvented in [Scbü89, Schü91] by integrating the complex unimodular multiplications into the adaptors. This procedure is particularly attractive in case of two-port adaptors, which can then be replaced by a two-port cross-adaptor [25] [Schü89], requiring two successive Multiply-and-Accumulate (MAC) operations, involving the corresponding complex adaptor coefficient in its true and complex conjugate forms, thus allowing for a lossless realization of the cross-adaptor in finite precision (two's complementary number representation) [Schü89, Schü91]. In addition, this cross-adaptor can be assembled into serial/parallel 3-port adaptors which are all efficiently implementable on MAC-based processors, cf performance data in [Schü91]. The proposed solution is particularly appealing for reactances realized with Richards' structure. Although the *signal* quantizations could be performed at the same locations in the cross-adaptor based WDF than in the original one (same signals undergoing same scaling factors), which would *in principle* imply the same behaviour for both WDF structures with respect to stability issues, it would be mandatory to assess the stability question explicitly, including scaling and coefficient sensitivity, a topic that was unfortunately not covered in [Schü91].

Finally, Schütte proposes an extension to Darlington's insertion loss synthesis method to handle the case of lossless two-ports terminated on constant complex impedances, cf Case 5 in Table 3.5.

In conclusion, complex WDFs can be realized either in one-real form, or in general complex form, the latter providing for a lossless and efficient implementation of certain WDF structures on signal processors, while requiring an explicit verification of the stability.

---

[25] This cross-adaptor corresponds to the complex extension of the classical Markel and Gray two-multiplier lattice section.

3.4 Complex lossless two-ports

This section represents the core part of the chapter, recalling fundamental properties of lossless two-ports (directly applicable to corresponding WDFs), and elaborating new results.

3.4.1 Notion of complex power

The *total steady-state complex power* $P(\psi)$ entering a complex passive N-port (cf Figure 3.5) is given by [Bele68, Bahe84] :

$$P(\psi) = \sum_{k=1}^{N} U_k(\psi) \cdot I_k^*(\psi). \tag{3.11}$$

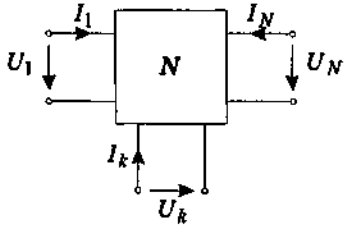

Figure 3.5: Complex passive N-port.

$P(\psi)$ can be decomposed into the *total average active power* $P_a(\psi)$ and the *total average reactive power* $P_r(\psi)$, respectively [Bele68] :

$$P(\psi) = P_a(\psi) + j \cdot P_r(\psi) \tag{3.12a}$$

$$P_a(\psi) = \mathrm{Re}\{P(\psi)\} \; ; \; P_r(\psi) = \mathrm{Im}\{P(\psi)\} \; ; \; \forall \psi \in \mathbb{C}. \tag{3.12b, c}$$

Since the active and reactive powers supplied by the external sources to a Kirchhoff network are respectively equal to the total active and reactive power absorbed by the constitutive elements, P_a and P_r can be reformulated as follows [Bahe84, Bele68] :

$$P_a(\psi) = P_d(\psi) + 2 \cdot [T_m(\psi) + T_e(\psi)] \cdot \mathrm{Re}\{\psi\} \tag{3.13a}$$

$$P_r(\psi) = P_x(\psi) + 2 \cdot [T_m(\psi) - T_e(\psi)] \cdot \mathrm{Im}\{\psi\}, \tag{3.13b}$$

where P_d corresponds to the total average power dissipated by real resistances, P_x to the total average reactive power absorbed by imaginary resistances [Bele68], whereas T_m and T_e are correspon-

ding to the total average magnetic and electric energy stored within inductances and capacitances, respectively. It is observed that $P_d(\psi)$, $T_m(\psi)$ and $T_e(\psi)$ are by essence non-negative real functions $\forall \psi \in \mathbb{C}$, while $P_x(\psi)$ can take any real value for $\psi \in \mathbb{C}$. Moreover, $P_a = P_d$ for $\psi = j \cdot \phi$.

Categories of complex N-ports

In view of (3.13a), the following categories of N-ports are considered [Bele68, Bahe84, Fett72b] :

Passive complex N-ports :	$P_a(\psi) \geq 0$	for	$\mathrm{Re}\{\psi\} \geq 0$	(3.14a)
Lossless complex N-ports :	$P_a(\psi) = 0$	for	$\psi = j \cdot \phi$	(3.14b)
Non-energic complex N-ports :	$P_a(\psi) = 0$		$\forall \psi \in \mathbb{C}$.	(3.14c)

Noticing that P_d, T_m, T_e, and P_x are all para-even quantities, and introducing (3.13) into (3.12a), the para-even part of $P(\psi)$ yields :

$$P_e(\psi) = 0.5 \cdot \left[P(\psi) + P_*(\psi) \right] = P_d(\psi) \ , \tag{3.15}$$

Consequently, condition (3.14b) characterizing lossless complex N-ports can be equivalently expressed by :

$$P_e(\psi) \equiv 0, \quad \forall \psi \in \mathbb{C} . \tag{3.16}$$

Classification of WDF building blocks

The basic building blocks used for designing WDFs can be classified according to (3.14) [Fett72b, Schü91]. Hence, under linear operational conditions, (complex) ideal transformers ($P(\psi) \equiv 0, \forall \psi \in \mathbb{C}$), (complex) gyrators, circulators, imaginary resistances, and all kinds of (complex) adaptors, are shown to be non-energic. Tbese elements are thus reflecting back all the active power they are receiving.

Capacitances, inductances, (complex) Unit Elements (UEs), and (complex) Quasi-Reciprocal Lines (QUARLs) are in turn lossless under the same conditions. Hence, these elements may temporarily store active power.

3.4.2 Basic properties of complex lossless one-ports

The complex passive one-port represented in Figure 3.6 is terminated on a voltage source featuring a complex internal impedance of *constant* value Z_E with $\mathrm{Re}\{Z_E\} > 0$. The corresponding incident and reflected voltage waves, $A(\psi)$ and $B(\psi)$, respectively, are then defined as [Schü91] :

$$A = U + Z_E \cdot I; \qquad B = U - Z_E^* \cdot I; \qquad \mathrm{Re}\{Z_E\} > 0; \qquad (3.17a,b,c)$$

$$U = \frac{Z_E^* \cdot A + Z_E \cdot B}{Z_E + Z_E^*}; \qquad I = \frac{A - B}{Z_E + Z_E^*}. \qquad (3.18a,b)$$

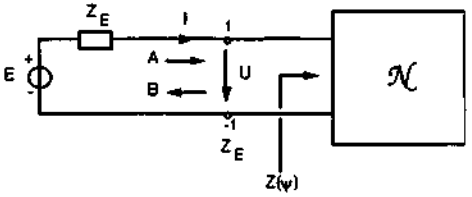

Figure 3.6: Terminated complex passive one-port.

In case Z_E reduces to a real resistance, i.e. $Z_E = R_E$, equations (3.17) and (3.18) are merely replaced by [Fett86] :

$$A = U + R_E \cdot I; \qquad B = U - R_E \cdot I; \qquad R_E > 0; \qquad (3.19a,b,c)$$

$$U = (A + B)/2; \qquad I = (A - B)/(2 \cdot R_E). \qquad (3.20a,b)$$

The reflectance $S(\psi)$ of the complex one-port is then defined :

$$S(\psi) = \frac{B(\psi)}{A(\psi)} = \frac{Z - Z_E^*}{Z + Z_E}; \quad \text{with } Z(\psi) = \frac{U(\psi)}{I(\psi)}, \qquad (3.21a,b)$$

$Z(\psi)$ corresponding to the input impedance of the one-port.

According to (3.12b), (3.11), (3.18), and (3.21a), the total average active power delivered to the one-port is :

$$P_a(\psi) = \mathrm{Re}\{U \cdot I^*\} = 0.5 \cdot [U \cdot I^* + U^* \cdot I] = \frac{A \cdot A^* - B \cdot B^*}{2 \cdot (Z_E + Z_E^*)} = \frac{A \cdot A^* \cdot (1 - S \cdot S^*)}{2 \cdot (Z_E + Z_E^*)} \tag{3.22}$$

where the argument ψ has been dropped for simplicity in the right-hand sided part of (3.22).

It is noted that tbe active power delivered by the voltage source becomes maximum for $B(\psi) = 0$, namely when the one-port is said to be *matched*, or *adapted* to the source. Under these circumstances, one verifies from (3.17b) and (3.21b), or directly from (3.21a), that :

$$Z(\psi) = Z_E^*(\psi) \quad \Rightarrow \quad P_{a\,\max}(\psi) = \frac{A \cdot A^*}{2 \cdot (Z_E + Z_E^*)} . \tag{3.23}$$

The normalized active power transferred from tbe source to the complex one-port is thus determined by :

$$p_a(\psi) = P_a(\psi) / P_{a\,\max}(\psi) = 1 - S(\psi) \cdot S^*(\psi) . \tag{3.24}$$

Hence, (3.14a,b) can be reformulated in function of $S(\psi)$:

Passive complex one-port : $S(\psi) \cdot S^*(\psi) \le 1$ for $\mathrm{Re}\{\psi\} \ge 0$ (3.25a)

Lossless complex one-port : $S(\psi) \cdot S^*(\psi) = 1$ for $\psi = j \cdot \phi$. (3.25b)

Clearly, for lossless (complex) one-ports, the reflectance becomes a (complex) allpass function, and the one-port collapses to a pure (complex) reactance. In this case, (3.25b) can be equally represented by :

$$S(\psi) \cdot S_*(\psi) = 1, \quad \forall \psi \in \mathbb{C}, \tag{3.26}$$

proceeding similarly to the replacement of (3.14b) by (3.16).

3.4.3 Basic properties of complex lossless two-ports

A doubly terminated complex lossless two-port as illustrated in Figure 3.7 is considered. The two-port is terminated on botb sides on *constant* complex impedances Z_{E1}, Z_{E2}, with $\mathrm{Re}\{Z_{Ek}\} > 0$, $k = 1,2$.

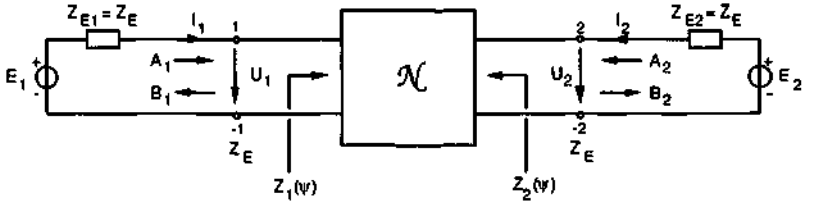

Figure 3.7: Doubly terminated complex lossless two-port.

Grouping the incident waves A_k and the reflected waves B_k, $k=1,2$, into vectors :

$$A=[A_1 \quad A_2]^T, \quad B=[B_1 \quad B_2]^T, \tag{3.27}$$

their relation can be expressed introducing the *scattering matrix* S :

$$B=S\cdot A, \qquad S=\begin{pmatrix} S_{11} & S_{12} \\ S_{21} & S_{22} \end{pmatrix}, \tag{3.28}$$

where S_{11} corresponds to the *input reflection coefficient* (or *input reflectance*), and S_{22} to the *output reflection coefficient* (or *output reflectance*). Similarly, S_{21} is defined as the *forward transmission coefficient* (or *transmittance*), and S_{12} as the *backward transmission coefficient* (or *backward transmittance*). For complex lossless lumped element-based two-ports, the entries of $S(\psi)$ are all rational functions of ψ, and are analytic for $\mathrm{Re}\{\psi\}\geq 0$.

In the remainder of the report, and without limitation of the results, cf [Schü91, Fett86, Paul86], the constant termination impedances are assumed to be equal, i.e. $Z_{E1}=Z_{E2}=Z_E$, so that the voltage and power scattering matrices become identical [Fett86, Schü91].

Under this assumption, and according to (3.12b), (3.11), and (3.22), the total active power dissipated by the two-port is given by :

$$P_a(\psi)=\frac{\sum_{k=1}^{2}(A_k\cdot A_k^*-B_k\cdot B_k^*)}{2\cdot(Z_E+Z_E^*)}. \tag{3.29}$$

Using (3.27) and (3.28), $P_a(\psi)$ can be expressed in a matrix form :

$$P_a(\psi) = \frac{(A^{*T} \cdot A - B^{*T} \cdot B)}{2 \cdot (Z_E + Z_E^*)} = \frac{A^{*T} \cdot (I_2 - S^{*T} \cdot S) \cdot A}{2 \cdot (Z_E + Z_E^*)}, \qquad (3.30)$$

where the superscript T indicates matrix transposition, whereas I_2 denotes the 2 x 2 unit-matrix. Consequently to (3.14a), the Hermitian matrix $(I_2 - S^{*T} \cdot S)$ is positive definite for $\mathrm{Re}\{\psi\} \geq 0$ for a *passive* complex two-port, and the corresponding $S(\psi)$ is thus a *bounded* matrix [Bele68]. For *lossless* complex two-ports, the next expression is derived :

$$S_*^T \cdot S = S \cdot S_*^T = I_2 , \qquad (3.31)$$

which is at tbe origin of Feldkeller's equations, and of Belevitch's parameterized form of the scattering matrix [Bele68].

3.4.4 Parameterized form of the scattering matrix

Based on [Bele68], and adopting the modified notation introduced in [Fett69, Fett81b, Fett87], the scattering matrix can be rewritten in the parameterized canonic form :

$$S = \frac{1}{g} \cdot \begin{pmatrix} h & \sigma \cdot f_* \\ f & -\sigma \cdot h_* \end{pmatrix}, \qquad (3.32)$$

wbere the following conditions hold, e.g. [Fett87] :

1) f, g, and h are polynomials in ψ, related by :

$$g \cdot g_* = h \cdot h_* + f \cdot f_* . \qquad (3.33)$$

In one of these polynomials, one of the coefficients may be selected arbitrarily, e.g. equal to 1.

2) g is a scattering Hurwitz polynomial [Fett84b], which means that:
   - $g(\psi) \neq 0$ for $\mathrm{Re}\{\psi\} \geq 0$,
   - g and g_* are relatively prime, i.e. (g_* / g) corresponds to a non-trivial stable allpass function.

3) σ is a unimodular constant, i.e. $|\sigma| = 1$.

4) The subscript asterisk designates the paraconjugate, cf (A.11).

5) If the two-port is real, all coefficients in S may be selected real, i.e. f, g, and h are then real polynomials, and $\sigma = \pm 1$. For real lossless two-ports, (3.33) is equivalent to the analytic continuation of Feldkeller's relations, cf [Bele68].

It is demonstrated from (3.32) and (3.33) that :

$$\det(S(\psi)) = -\sigma \cdot g_*(\psi)/g(\psi), \tag{3.34}$$

i.e. the determinant of $S(\psi)$ corresponds to an allpass function [Bele68]. Furthermore, introducing the unimodular constants α, β, γ, and σ', and defining the polynomials :

$$f' = \alpha \cdot f, \qquad g' = \beta \cdot g, \qquad h' = \gamma \cdot h, \tag{3.35a,b,c}$$

the matrix S' defined by :

$$S' = \frac{1}{g'} \cdot \begin{pmatrix} h' & \sigma' \cdot f'_* \\ f' & -\sigma' \cdot h'_* \end{pmatrix}, \tag{3.36}$$

is shown to satisfy all the conditions 1) – 5) listed above, several network-level interpretations being possible to establish the relationship between S and S'.

Direct extension of the former properties to multidimensional lossless two-ports is possible, cf [Fett87].

One introduces further the *characteristic function* of the two-port :

$$C(\psi) = \frac{S_{11}(\psi)}{S_{21}(\psi)} = \frac{h(\psi)}{f(\psi)}, \tag{3.37}$$

and the attenuation $a_{21}(\phi)$ of S_{21}, processed for $\psi = j \cdot \phi$:

$$a_{21}(\phi) = -20 \cdot \log\{ |S_{21}(j \cdot \phi)| \} = 10 \cdot \log\{ 1 + |C(j \cdot \phi)|^2 \}. \tag{3.38}$$

Hence, the characteristic function is directly related to the amplitude response of S_{21} [26]. $C(\psi)$ is frequently used to solve the amplitude approximation problem of S_{21} for lattice-type reciprocal networks.

---

[26] (3.38) is valid for both reciprocal and non-reciprocal lossless two-ports.

3.4.5 Reciprocal lossless two-ports

Several kinds of lossless two-ports are distinguished. A first classification is made between *reciprocal* and *non-reciprocal* lossless two-ports. By definition, a (complex or real) lossless two-port is said to be reciprocal when it is verifying [Bele68] :

$$S_{21} = S_{12} \ , \tag{3.39}$$

otherwise, the two-port is denoted non-reciprocal. Reciprocal lossless two-ports are then further subdivided into (necessarily reciprocal) *lattice-type* two-ports, owing their name to their basic structure depicted in Figures 3.8 and 3.9, and into *general reciprocal* two-ports, which cannot be reduced to a lattice-type structure, an example being given in [Feis65] by the so-called L-filters (*Laufzeitgeebnet*) suitable for joint amplitude and phase approximation, that are offering an advantageous solution for narrow-band Frequency Modulation (FM) systems. In this report, the terms "lattice-type" and "lattice-type reciprocal" are interchangeably used to denote the corresponding lossless two-ports. Finally, lattice-type two-ports are classified into *symmetric* and *antimetric* (or anti-symmetric) lossless two-ports, as specified in Subsections 3.4.6 and 3.4.7.

3.4.6 Complex symmetric lossless two-ports

The next developments are achieved proceeding similarly to [Fett87], which handles the case of antimetric filters.

By definition, a complex lossless two-port is said to be *symmetric* – and thus reciprocal – when it is fulfilling [Bele68, Fett81a] :

$$S_{21} = S_{12}, \quad S_{11} = S_{22} \tag{3.40a,b}$$

which implies :

$$f = \sigma \cdot f_* \ , \quad h = -\sigma \cdot h_* \ , \quad C_* = -C \ . \tag{3.41a,b,c}$$

Conversely, if (3.40a) and (3.41c) hold, then (3.40b) also holds, so that the two-port is demonstrated to be symmetric.

It is observed from (3.41c) that the characteristic function C of a complex symmetric lossless two-port is para-odd. Consequently, according to (A.18b), C becomes a purely imaginary-valued function for real frequencies $\psi = j \cdot \phi$.

Hence, from the former considerations and (3.38), it is demonstrated that the amplitude approximation of S_{21} can be reformulated as a *real* approximation problem in $C(j\cdot\phi)/j$.

The following (complex) functions are next introduced [Fett81a]:

$$S_1 = S_{11} - S_{21}, \quad S_2 = S_{11} + S_{21} \tag{3.42a,b}$$

which can be reformulated as provided hereafter using (3.32):

$$S_1 = (h - f)/g, \quad S_2 = (h + f)/g. \tag{3.43a,b}$$

From equations (3.33) and (3.41a,b), it can be shown that:

$$S_1 \cdot S_{1*} = S_2 \cdot S_{2*} = 1, \tag{3.44}$$

namely, that S_1 and S_2 are (complex) allpass functions.

Let g_1 and g_2 be the lowest-degree denominators of S_1 and S_2, respectively. It is observed from (3.43) that g_1 and g_2 divide g, and are therefore themselves scattering Hurwitz polynomials. Defining $S_1 = f_1/g_1$ and $S_2 = f_2/g_2$, and making use of (3.44), shows that S_1 and S_2 can be rewritten as:

$$S_1 = \sigma_1 \cdot g_{1*}/g_1, \quad S_2 = \sigma_2 \cdot g_{2*}/g_2 \tag{3.45a,b}$$

where σ_1 and σ_2 are unimodular constants, i.e. $|\sigma_1| = |\sigma_2| = 1$. Next, using (3.42) to express S_{11} and S_{21} in function of S_1 and S_2:

$$S_{11} = (S_2 + S_1)/2, \quad S_{21} = (S_2 - S_1)/2 \tag{3.46a,b}$$

and making use of (3.45) together with (3.40), it is possible to process S in the form (3.32):

$$g = g_1 \cdot g_2, \qquad h = (\sigma_2 \cdot g_1 \cdot g_{2*} + \sigma_1 \cdot g_{1*} \cdot g_2)/2 \tag{3.47a,b}$$

$$\sigma = -\sigma_1 \cdot \sigma_2, \quad f = (\sigma_2 \cdot g_1 \cdot g_{2*} - \sigma_1 \cdot g_{1*} \cdot g_2)/2 \tag{3.48a,b}$$

and condition (3.33) is fulfilled.

Using (3.46), the scattering matrix can be reformulated in a canonic form with respect to the number of instanciated allpass functions [Fett86]:

$$S = \frac{1}{2} \cdot \begin{pmatrix} -1 & 1 \\ 1 & 1 \end{pmatrix} \cdot \begin{pmatrix} S_1 & 0 \\ 0 & S_2 \end{pmatrix} \cdot \begin{pmatrix} -1 & 1 \\ 1 & 1 \end{pmatrix}. \tag{3.49}$$

Figure 3.8 illustrates the corresponding structure :

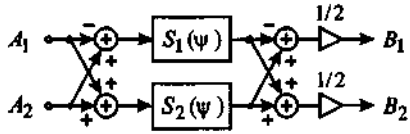

Figure 3.8: Functional description of symmetric lossless two-ports.

3.4.7 Complex antimetric lossless two-ports

A complex lossless two-port is by definition said to be *antimetric* – and thus reciprocal – when it is fulfilling [Bele68, Fett81a, Fett87] :

$$S_{21} = S_{12}, \quad S_{11} = -S_{22} \tag{3.50a,b}$$

which involves :

$$f = \sigma \cdot f_*, \quad h = \sigma \cdot h_*, \quad C_* = C. \tag{3.51a,b,c}$$

Conversely, if (3.50a) and (3.51c) hold, then (3.50b) also holds, so that the two-port is demonstrated to be antimetric [Fett87].

Equation (3.51c) shows that the characteristic function C of a complex antimetric lossless two-port is para-even. C becomes thus a purely real-valued function for real frequencies $\psi = j \cdot \phi$. Hence, similarly to the case of symmetric two-ports, it is demonstrated that the amplitude approximation of S_{21} can be reformulated as a *real* approximation problem in $C(j \cdot \phi)$.

The following (complex) functions are next defined [Fett81a, Fett87] :

$$S_1 = S_{11} - j \cdot S_{21}, \quad S_2 = S_{11} + j \cdot S_{21} \tag{3.52a,b}$$

which can be reformulated as :

$$S_1 = (h - j \cdot f)/g, \quad S_2 = (h + j \cdot f)/g, \tag{3.53a,b}$$

and it can be shown from equations (3.33) and (3.51a,b) that (3.44) still holds, i.e. S_1 and S_2 are (usually complex) allpass functions.

Let g_1 and g_2 be the lowest-degree denominators of S_1 and S_2, respectively. Similarly to the symmetric case, S_1 and S_2 can be rewritten as :

$$S_1 = \sigma_1 \cdot g_{1*}/g_1, \quad S_2 = \sigma_2 \cdot g_{2*}/g_2 \qquad (3.54a,b)$$

where σ_1 and σ_2 are unimodular constants. Using (3.52), S_{11} and S_{21} can be expressed as functions of S_1 and S_2 :

$$S_{11} = (S_2 + S_1)/2, \quad S_{21} = (S_2 - S_1)/(2 \cdot j) \qquad (3.55a,b)$$

and the following formulae can be derived [Fett87] :

$$g = g_1 \cdot g_2, \qquad h = (\sigma_2 \cdot g_1 \cdot g_{2*} + \sigma_1 \cdot g_{1*} \cdot g_2)/2 \qquad (3.56a,b)$$

$$\sigma = \sigma_1 \cdot \sigma_2, \qquad f = (\sigma_2 \cdot g_1 \cdot g_{2*} - \sigma_1 \cdot g_{1*} \cdot g_2)/(2 \cdot j). \qquad (3.57a,b)$$

and (3.33) is shown to be verified.

Using (3.55), the scattering matrix can be reformulated in a canonic form with respect to the number of instanciated allpass functions :

$$S = \frac{1}{2} \cdot \begin{pmatrix} -1 & 1 \\ 1/j & 1/j \end{pmatrix} \cdot \begin{pmatrix} S_1 & 0 \\ 0 & S_2 \end{pmatrix} \cdot \begin{pmatrix} -1 & 1/j \\ 1 & 1/j \end{pmatrix}. \qquad (3.58)$$

Figure 3.9 illustrates the corresponding structure :

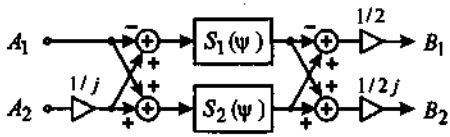

Figure 3.9: Functional description of antimetric lossless two-ports.

3.4.8 Matched lossless two-ports

A complex or real lossless two-port is said to be *matched* when the following condition is fulfilled [Bele68, p. 172] :

$$S_{11} \equiv S_{22} \equiv 0 \quad \Leftrightarrow \quad h \equiv 0. \qquad (3.59)$$

Due to (3.33), S_{12} and S_{21} are then demonstrated to be allpass functions. A reciprocal realization of the matched lossless two-port is merely achieved from symmetric and antimetric lossless two-ports by setting $S_1 = -S_2$ into formulas (3.46a) and (3.55a), respectively.

3.4.9 Power and allpass complementarity of lattice-type lossless two-ports

It follows from (3.32) and (3.33) that the scattering parameters S_{21} and S_{11} of *any* kind of lossless two-port, regardless of reciprocity, symmetry, and antimetry, are power complementary, cf Subsection A.8.2.

Furthermore, equations (3.42a,b) show that S_{21} and S_{11} belonging to a (complex or real) *symmetric* lossless two-port are in addition allpass complementary, cf Subsection A.8.3. S_{21} and S_{11} are thus doubly complementary, cf Subsection A.8.4.

On the contrary, it follows from (3.55a,b) that :

$$S_{11}(\psi) \pm S_{21}(\psi) = \pm \frac{(1-j)}{2} \cdot S_2(\psi) \cdot \left[1 \pm j \cdot \frac{S_1(\psi)}{S_2(\psi)} \right], \qquad (3.60)$$

demonstrating that S_{21} and S_{11} of a (complex or real) *antimetric* lossless two-port are certainly *not* allpass complementary.

3.4.10 Analytic frequency responses of lattice-type lossless two-ports

The analytic frequency responses of the scattering parameters of lattice-type lossless two-ports are derived in this subsection. The resulting expressions are intentionally provided with redundancy.

Hence, the constituent allpass functions S_1 and S_2 of the scattering parameters S_{11} and S_{21} are expressed in function of their respective complex phase variables Φ_1 and Φ_2, cf Subsection A.4.1 :

$$S_1(\psi) = \exp(-\Phi_1(\psi)), \qquad S_2(\psi) = \exp(-\Phi_2(\psi)). \qquad (3.61a,b)$$

Next, the quantities Φ_Σ and Φ_Δ are introduced as the mean value, and mean difference value of Φ_1 and Φ_2 , respectively :

$$\Phi_\Sigma(\psi) = (\Phi_1(\psi) + \Phi_2(\psi))/2; \quad \Phi_\Delta(\psi) = (\Phi_1(\psi) - \Phi_2(\psi))/2. \quad (3.62a,b)$$

Accordingly, considering *symmetric* lossless two-ports first, it follows from (3.46), (3.61), and (3.62) that the analytic frequency responses of S_{11} and S_{21}, and thus C, can be expressed as :

Symmetric : $S_{11}(\psi) = \exp(-\Phi_\Sigma(\psi)) \cdot \cosh(\Phi_\Delta(\psi))$, (3.63)

$$S_{21}(\psi) = \exp(-\Phi_\Sigma(\psi)) \cdot \sinh(\Phi_\Delta(\psi)), \quad (3.64)$$

$$C(\psi) = \coth(\Phi_\Delta(\psi)). \quad (3.65)$$

Similarly, using (3.56), (3.61), and (3.62), the analytic frequency responses of S_{11} and S_{21} are formulated as follows for antimetric lossless two-ports :

Antimetric : $S_{11}(\psi) = \exp(-\Phi_\Sigma(\psi)) \cdot \cosh(\Phi_\Delta(\psi))$, (3.66)

$$S_{21}(\psi) = -j \cdot \exp(-\Phi_\Sigma(\psi)) \cdot \sinh(\Phi_\Delta(\psi)), \quad (3.67)$$

$$C(\psi) = j \cdot \coth(\Phi_\Delta(\psi)). \quad (3.68)$$

3.4.11 Real frequency responses of lattice-type lossless two-ports

According to (A.56b), all phase responses verify $\Phi(j \cdot \phi) = j \cdot \varphi(\phi)$ for real frequencies $\psi = j \cdot \phi$, and the former expressions can be reformulated as given below :

$$S_1(j \cdot \phi) = \exp(-j \cdot \varphi_1(\phi)), \quad S_2(j \cdot \phi) = \exp(-j \cdot \varphi_2(\phi)). \quad (3.69a,b)$$

$$\varphi_\Sigma(\phi) = (\varphi_1(\phi) + \varphi_2(\phi))/2, \quad \varphi_\Delta(\phi) = (\varphi_1(\phi) - \varphi_2(\phi))/2. \quad (3.70a,b)$$

Symmetric : $S_{11}(j \cdot \phi) = \exp(-j \cdot \varphi_\Sigma(\phi)) \cdot \cos(\varphi_\Delta(\phi))$, (3.71)

$$S_{21}(j \cdot \phi) = j \cdot \exp(-j \cdot \varphi_\Sigma(\phi)) \cdot \sin(\varphi_\Delta(\phi)), \quad (3.72)$$

$$C(j \cdot \phi) = -j \cdot \cot(\varphi_\Delta(\phi)); \quad (3.73)$$

Antimetric : $S_{11}(j \cdot \phi) = \exp(-j \cdot \varphi_\Sigma(\phi)) \cdot \cos(\varphi_\Delta(\phi))$, (3.74)

$$S_{21}(j \cdot \phi) = \exp(-j \cdot \varphi_\Sigma(\phi)) \cdot \sin(\varphi_\Delta(\phi)), \quad (3.75)$$

$$C(j \cdot \phi) = \cot(\varphi_\Delta(\phi)). \quad (3.76)$$

Symmetric lossless two-ports

The frequency responses of S_{11} and S_{21} can be rewritten as :

$$S_{i1}(j \cdot \phi) = \left| S_{i1}(j \cdot \phi) \right| \cdot \exp(-j \cdot \varphi_{i1}(\phi)), \quad i = 1,2 \quad (3.77)$$

where φ_{i1} correspond to the phase responses of S_{i1}, $i=1,2$. Hence, in case of (complex or real) *symmetric* lossless two-ports, comparing (3.77) with (3.71) and (3.72), the amplitude responses of S_{11} and S_{21} are specified by :

$$\left| S_{11}(j\cdot\phi) \right| = \left| \cos(\varphi_{\Delta}(\phi)) \right|, \quad \left| S_{21}(j\cdot\phi) \right| = \left| \sin(\varphi_{\Delta}(\phi)) \right|, \quad (3.78a,b)$$

which confirms their power complementarity for real frequencies. Moreover, adopting the notation provided in [Lang93], the phase responses of S_{11} and S_{21} are determined by :

$$\varphi_{11}(\phi) = \phi_{\Sigma}(\phi) \qquad \pm\frac{\pi}{2}\cdot\left[1-\text{sign}\left(\cos(\varphi_{\Delta}(\phi))\right)\right] \qquad (3.79a)$$

$$\varphi_{21}(\phi) = \phi_{\Sigma}(\phi) - \frac{\pi}{2} \pm \frac{\pi}{2}\cdot\left[1-\text{sign}\left(\sin(\varphi_{\Delta}(\phi))\right)\right]. \qquad (3.79b)$$

The terms in brsckets appearing in (3.79a,b) introduce *fixed phase steps* of $\pm\pi$ induced by the transmission zeros of S_{11} and S_{21} that are located on the imaginary axis $\psi = j\cdot\phi$. These terms occur in the stopband(s) of the corresponding functions, and are therefore usually omitted for simplification purposes.

Disregarding these last factors, it is observed from (3.79a,b) that $\varphi_{11}(\phi)$ and $\varphi_{21}(\phi)$ are equal, except for a constant phase lag of $\pi/2$. Hence, for (complex or real) symmetric lossless two-ports, S_{11} and S_{21} are providing *quadratured* phase responses.

Antimetric lossless two-ports

Proceeding similarly for the *antimetric* case, the amplitude responses of S_{11} and S_{21} are still given by (3.78), whereas the phase responses are expressed by :

$$\varphi_{11}(\phi) = \phi_{\Sigma}(\phi) \pm \frac{\pi}{2}\cdot\left[1-\text{sign}\left(\cos(\varphi_{\Delta}(\phi))\right)\right] \qquad (3.80a)$$

$$\varphi_{21}(\phi) = \phi_{\Sigma}(\phi) \pm \frac{\pi}{2}\cdot\left[1-\text{sign}\left(\sin(\varphi_{\Delta}(\phi))\right)\right]. \qquad (3.80b)$$

Disregarding the terms in brackets occurring in (3.80a,b), the phase responses are this time shown to be *in-phase*.

Group delay

Finally, for both (complex or real) symmetric and antimetric lossless two-ports, the group delays $\tau_{11}(\phi)$ and $\tau_{21}(\phi)$ of S_{11} and S_{21} are determined by :

$$\tau_{11}(\phi)=\tau_{21}(\phi)=[\,\tau_1(\phi)+\tau_2(\phi)\,]/\,2 \qquad (3.81)$$

where $\tau_1(\phi)$ and $\tau_2(\phi)$ correspond to the group delay of S_1 and S_2. The Dirac impulses induced by the right hand-sided factors in (3.79) and (3.80) have been ignored in (3.81).

According to (2.52a), an important result of (3.81) is that the group delay of *stable* symmetric and antimetric lossless two-ports is strictly positive at any frequency.

Remark on the amplitude responses

It follows from (3.38) that the amplitude response of S_{21} and the characteristic function C of a (complex or real) symmetric or antimetric lossless two-port are directly interrelated. Equation (3.78b) is further demonstrating that the amplitude response of S_{21} is directly connected to the mean phase difference φ_Δ. Hence, from a conceptual point of view, it is strictly equivalent to perform the amplitude approximation directly on S_{21}, or to process it using either C or φ_Δ [Henk96]. Invoking the power complementarity between S_{21} and S_{11}, the same observations apply to S_{11}.

The formal equivalence between an amplitude approximation relying on C or on φ_Δ is demonstrated in [Henk97a] for real symmetric and antimetric lossless two-ports (lattice-type structure). Application examples on the amplitude approximation based on φ_Δ are presented e.g. in [Tarr95].

3.4.12 Minimum/non-minimum phase response

According to Subsections 3.4.6 and 3.4.7, and later Subsections 3.4.16 and 3.5.1, symmetric and antimetric lossless two-ports are essentially featuring para-even/odd polynomials f and h, except for a unimodular constant.

Due to (A.25), the scattering parameters S_{21} and S_{11} of (complex or real) symmetric/antimetric lossless two-ports are thus shown to be :

- either of minimum phase type, in which case all finite transmission zeros are located on the imaginary axis $\psi = j \cdot \phi$;
- or of non-minimum phase type, in which case the finite transmission zeros that are outside the imaginary axis $\psi = j \cdot \phi$ are evenly distributed over the left and right half-planes in the ψ-domain.

Hence, minimum phase filters with finite transmission zeros located in the *open* left half-plane of the ψ-domain are not realizable with (complex or real) symmetric/antimetric lossless two-ports.

3.4.13 Composition of symmetric and antimetric lossless two-ports

Lossless two-ports can be equivalently represented using their scattering matrix S, scattering *chain* (or *transfer*) matrix K, or scattering *hybrid* matrices of the first and second kind, H and H', respectively, as defined in [Bele68, Fett90].

Accordingly, higher-order lossless two-ports can be assembled in different ways from lower-order ones, merely by cascading the corresponding scattering matrices of the same type (i.e. S, K, H, or H'). Clearly, the same approach can be applied for factorization purposes, e.g. [Fett90].

In this subsection, the assembly of lossless two-ports is considered by cascading their scattering matrices S. A second situation is then discussed where *selected* scattering parameters belonging to different lossless two-ports are cascaded. The results are valid for both real and complex networks.

Cascading the scattering matrix of lossless two-ports

Using (3.40), it is shown that the scattering matrix resulting from cascading (i.e. multiplying) the scattering matrices of two symmetric two-ports is itself symmetric, cf [Fett86] Section IX B :

$$S = S' \cdot S'' = \begin{pmatrix} S'_{11} & S'_{21} \\ S'_{21} & S'_{11} \end{pmatrix} \cdot \begin{pmatrix} S''_{11} & S''_{21} \\ S''_{21} & S''_{11} \end{pmatrix} = \begin{pmatrix} S_{11} & S_{21} \\ S_{21} & S_{11} \end{pmatrix} \qquad (3.82a)$$

$$S_{11} = S'_{11} \cdot S''_{11} + S'_{21} \cdot S''_{21}; \quad S_{21} = S'_{21} \cdot S''_{11} + S'_{11} \cdot S''_{21}. \qquad (3.82b)$$

Equivalently, it is demonstrated that the scattering matrix achieved by cascading the scattering matrices of two antimetric lossless two-ports, is itself antimetric when reversing the sign of the second input signal (an operation which is normally irrelevant), cf [Fett86] :

$$S = S' \cdot S'' = \begin{pmatrix} S'_{11} & S'_{21} \\ S'_{21} & -S'_{11} \end{pmatrix} \cdot \begin{pmatrix} S''_{11} & S''_{21} \\ S''_{21} & -S''_{11} \end{pmatrix} \cdot \begin{pmatrix} 1 & 0 \\ 0 & -1 \end{pmatrix} = \begin{pmatrix} S_{11} & S_{21} \\ S_{21} & -S_{11} \end{pmatrix} \quad (3.83a)$$

$$S_{11} = S'_{11} \cdot S''_{11} + S'_{21} \cdot S''_{21}; \quad S_{21} = S'_{21} \cdot S''_{11} - S'_{11} \cdot S''_{21}. \quad (3.83b)$$

Obviously, the symmetric/antimetric property is preserved when cascading the scattering matrices of two-ports of same type. On the contrary, when cascading the scattering matrices of two mixed symmetric/antimetric two-ports, one achieves a two-port with four different scattering parameters, where the reciprocity is in particular lost [27].

Cascading the scattering parameters of lossless two-ports

A different situation occurs when pairs of scattering parameters belonging to separate (complex or real) two-ports are cascaded. This is useful to realize particular single-input two-output, or two-input single-output filter configurations.

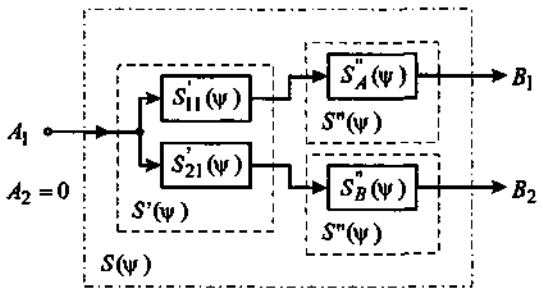

Figure 3.10: Cascaded filters structures.

[27] Following this observation, it seems that at least certain kinds of non-reciprocal lossless two-ports could be designed by cascading the scattering matrices of two mixed symmetric/antimetric two-ports. However, the usefulness of these configurations (e.g. with respect to group delay, implementstion costs, limitations in frequency responses) should be checked, and an appropriate factorization method should be found.

As depicted in Figure 3.10, the whole filter denoted by $S(\psi)$ is composed of a two-port $S'(\psi)$ providing two power-complementary outputs, which are in turn processed by a pair of identical two-ports $S''(\psi)$. $S'(\psi)$ and the pair of two-ports $S''(\psi)$, including their contributing scattering parameters $S''_A(\psi)$ and $S''_B(\psi)$, are selected according to Table 3.7 :

$$S_{11} = S'_{11} \cdot S''_A; \quad S_{21} = S'_{21} \cdot S''_B. \tag{3.84}$$

Using (3.63), (3.64), (3.66), and (3.67), the para-even/odd nature of the characteristic function $C(\psi)$, and thus the symmetric/antimetric-like behavior of the achieved filter configuration $S(\psi)$, are determined in Table 3.7. Replacing $S'(\psi)$ with an antimetric structure produces similar results. It is observed that none of the resulting structures in Table 3.7 is any more power complementary.

Case Index	$S'(\psi)$ Type	$S''(\psi)$ Type	$S''_A(\psi)$	$S''_B(\psi)$	$S(\psi)$ $C(\psi)$	$S(\psi)$ Type
1	Symmetric	Symmetric	S''_{11}	S''_{21}	$C = C_*$	Antimetric-like
2	"	Symmetric	S''_{21}	S''_{11}	$C = C_*$	Antimetric-like
3	"	Antimetric	S''_{11}	S''_{21}	$C = -C_*$	Symmetric-like
4	"	Antimetric	S''_{21}	S''_{11}	$C = -C_*$	Symmetric-like

Table 3.7: Categories of cascaded filters structures.

3.4.14 Doubly magnitude-complementary networks

A particular filter configuration is obtained for the first row of Table 3.7, when $S''(\psi) = S'(\psi)$. In this case, the achieved filter responses are the following :

$$S_{11}(\psi) = [\, S'_{11}(\psi) \,]^2 = \exp(-2 \cdot \Phi_\Sigma(\psi)) \cdot \cosh^2(\Phi_\Delta(\psi)), \tag{3.85a}$$

$$S_{21}(\psi) = [\, S'_{21}(\psi) \,]^2 = \exp(-2 \cdot \Phi_\Sigma(\psi)) \cdot \sinh^2(\Phi_\Delta(\psi)), \tag{3.85b}$$

showing that the responses are in-pbase. Observing that $S_{11}(\psi)$ is a perfect square, its magnitnde is given by :

$$|S_{11}(\psi)| = S'_{11}(\psi) \cdot S'_{11*}(\psi) = \cosh^2(\Phi_{\Delta}(\psi)). \tag{3.86}$$

Proceeding similarly with $S_{21}(\psi)$, it is demonstrated that $S_{11}(\psi)$ and $S_{21}(\psi)$ are magnitude complementary, cf (A.83) :

$$\begin{aligned} |S_{11}(\psi)| + |S_{21}(\psi)| &= S'_{11}(\psi) \cdot S'_{11*}(\psi) + S'_{21}(\psi) \cdot S'_{21*}(\psi) \\ &= \cosh^2(\Phi_{\Delta}(\psi)) - \sinh^2(\Phi_{\Delta}(\psi)) = 1. \end{aligned} \tag{3.87}$$

Similarly, it is demonstrated that the *difference* between $S_{11}(\psi)$ and $S_{21}(\psi)$ results in an allpass response :

$$S_{11}(\psi) - S_{21}(\psi) = \exp(-2 \cdot \Phi_{\Sigma}(\psi)) \ , \tag{3.88}$$

so that these transfer functions are finally proved to be doubly magnitude-complementary, cf Subsection A.8.6. When implementing these filters, one sbould take care of the subtraction occurring in (3.88), because using an addition instead destroys the allpass complementarity. Equations (3.87) and (3.88) were formerly derived in [Rega87] for real systems operating under real frequencies, limited to $\varepsilon = 0$.

It is observed that (e.g. lowpass/highpass) complementary filter pairs $H_i(z)$, $i = 1,2$, designed using linear phase FIR filters implemented in direct form sucb that $H_2(z) = z^{-N/2} - H_1(z)$, are by construction doubly magnitude-complementary, provided the transfer function H_1 is approximated so as to satisfy $0 \le H_1(\exp(j\Omega))/\exp(-N\Omega/2) \le 1$, $\forall \Omega$.

Sensitivity to mismatches of doubly complementary networks

By definition, both kinds of networks, namely (i) doubly complementary and (ii) doubly magnitude complementary networks, are fulfilling tbe allpass complementary condition. For practical applications, the question arises to evaluate in how far the allpass complementarity is preserved when mismatches occur (essentially concerns mixed analog/digital processes).

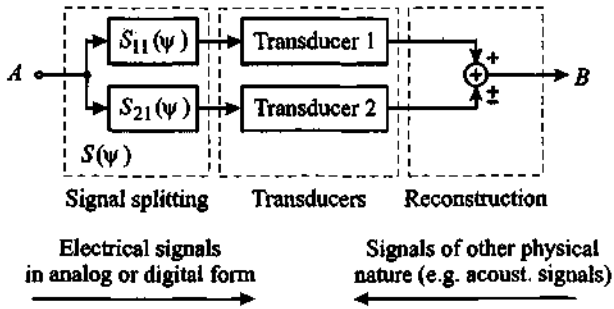

Figure 8.11: Sensitivity to mismatches ; Example of practical situation.

Figure 3.11 depicts a typical practical situation requiring signal splitting into complementary frequency ranges, followed by separate processing of the achieved signals, and a reconstruction. Such a situation is encountered e.g. when complementary transducers are used, each of them best fitting to a certain frequency range. A typical example is given by high quality multiway loudspeaker crossovers, considering the two-way system with a woofer/midrange speaker and a tweeter as a particular case [Rega87]. For technological reasons (in the given example : e.g. non-coincidental driver mounting), or for operational reasons (in the example : e.g. off-axis listening), a mismatch in phase – and more generally also in magnitude – may occur between the signal components before reconstruction.

Figure 3.12 represents a model of the situation considered at a *fixed* frequency. The constant parameters ε and θ correspond to the magnitude and phase mismatches between the two branches.

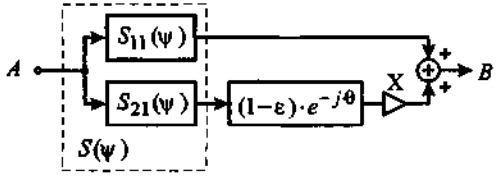

Figure 3.12: Sensitivity to mismatches ; Model for :
- **symmetric doubly complementary networks** ($X = \pm 1$);
- **antimetric doubly magnitude complementary networks** ($X = -1$).

For (complex or real) symmetric lossless two-ports, and according to (3.71) and (3.72), the overall transfer function as illustrated in Figure 3.12 is given by :

$$Q(\varepsilon,\theta,\phi) = \left| Q(\varepsilon,\theta,\phi) \right| \cdot \exp(-j \cdot \varphi_Q(\varepsilon,\theta,\phi)) = B / A \tag{3.89}$$

$$Q(\varepsilon,\theta,\phi) = \exp(-j \cdot \varphi_\Sigma) \cdot \{[\cos(\varphi_\Delta) + X \cdot (1-\varepsilon) \cdot \sin(\varphi_\Delta) \cdot \sin(\theta)] + X \cdot j \cdot (1-\varepsilon) \cdot \sin(\varphi_\Delta) \cdot \cos(\theta)\}. \tag{3.90}$$

with $\varphi_\Sigma = \varphi_\Sigma(\phi)$ and $\varphi_\Delta = \varphi_\Delta(\phi)$. The variation of the magnitude and phase responses is then provided by :

$$\Delta|Q| = \left| Q(\varepsilon,\theta,\phi) \right| - \left| Q(0,0,\phi) \right| = \sqrt{1 + (\varepsilon^2 - 2\cdot\varepsilon) \cdot \sin^2(\varphi_\Delta) + X \cdot (1-\varepsilon) \cdot \sin(2\cdot\varphi_\Delta) \cdot \sin(\theta)} \; - 1 \tag{3.91}$$

$$\Delta\varphi_Q = \varphi_Q(\varepsilon,\theta,\phi) - \varphi_Q(0,0,\phi) = X \cdot \left\{ \varphi_\Delta - \arctan\left[\frac{(1-\varepsilon) \cdot \cos(\theta) \cdot \tan(\varphi_\Delta)}{1 + X \cdot (1-\varepsilon) \cdot \sin(\theta) \cdot \tan(\varphi_\Delta)} \right] \right\}. \tag{3.92}$$

For magnitude and phase mismatches situated within $(-0.2 \le \varepsilon \le 0.2)$ and $(-\pi/4 \le \theta \le \pi/4)$, respectively, the greatest variation of $\Delta|Q|$ and $\Delta\varphi_Q$ is achieved for $\varphi_\Delta = \pm\pi/4$, i.e. $|S_{11}| = |S_{21}| = \sqrt{2}/2$. Figure 3.13 displays the results for $\varphi_\Delta = \pi/4$ and $X = 1$. It is observed that $\Delta|Q|$ is strongly sensitive to a phase mismatch θ, whereas $\Delta\varphi_Q$ is sensitive to both magnitude and phase mismatches.

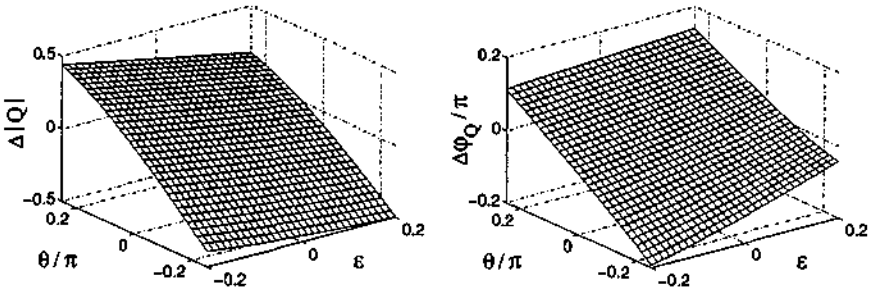

Figure 3.13: Sensitivity of symmetric doubly complemeotary networks ($\varphi_\Delta = \pi/4$; $X = 1$) : a) Variation of $\Delta|Q|$; b) Variation of $\Delta\varphi_Q$.

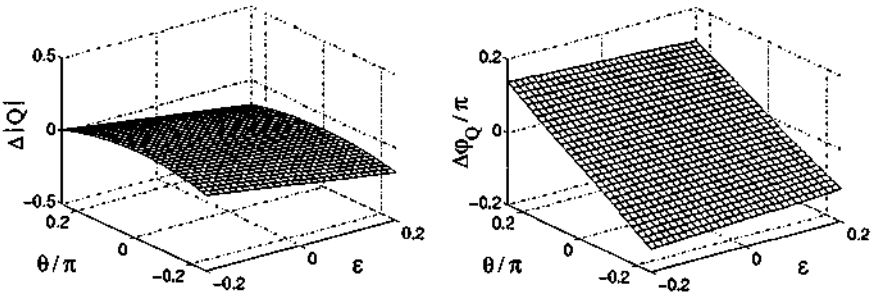

Figure 3.14: Sensitivity of antimetric doubly magnitude compl. networks ($\varphi_\Delta = \pi/4$; $X=-1$) : a) Variation of $\Delta|Q|$; b) Variation of $\Delta\varphi_Q$.

Sensitivity of doubly magnitude complementary networks to mismatches

For an antimetric doubly magnitude complementary network (first case in Table 3.7), the transfer function Q is expressed as follows using (3.85a,b) :

$$Q(\varepsilon,\theta,\phi)=\exp(-2\cdot j\cdot\varphi_\Sigma)\cdot\{[\cos^2(\varphi_\Delta)+(1-\varepsilon)\cdot\sin^2(\varphi_\Delta)\cdot\cos(\theta)] - j\cdot(1-\varepsilon)\cdot\sin^2(\varphi_\Delta)\cdot\sin(\theta)\}. \tag{3.93}$$

$\Delta|Q|$ and $\Delta\varphi_Q$ are then determined by :

$$\Delta|Q| = |Q(\varepsilon,\theta,\phi)| - |Q(0,0,\phi)| = \sqrt{1+(\varepsilon^2-2\varepsilon)\cdot\sin^4(\varphi_\Delta)+0.5[(1-\varepsilon)\cdot\cos(\theta)-1]\cdot\sin^2(2\varphi_\Delta)} - 1 \tag{3.94}$$

$$\Delta\varphi_Q = \varphi_Q(\varepsilon,\theta,\phi)-\varphi_Q(0,0,\phi) = \arctan\left[\frac{(1-\varepsilon)\cdot\sin(\theta)\cdot\tan^2(\varphi_\Delta)}{1+(1-\varepsilon)\cdot\cos(\theta)\cdot\tan^2(\varphi_\Delta)}\right]. \tag{3.95}$$

For $(-0.2\le\varepsilon\le 0.2)$ and $(-\pi/4\le\theta\le\pi/4)$, the greatest variation of $\Delta|Q|$ and $\Delta\varphi_Q$ occurs again for $\varphi_\Delta=\pm\pi/4$ $(X=-1)$. Figure 3.14 displays the results for $\varphi_\Delta=\pi/4$.

It is observed that $\Delta|Q|$ is this time much less sensitive to a phase mismatch θ. Furthermore, for $\varepsilon=$ constant in Figure 3.14a, it is

observed that any phase mismatch caused by θ *decreases* the magnitude $|Q|$, which corresponds to a minimum sensitivity situation [Rega87]. Moreover, $\Delta\varphi_Q$ is less sensitive to ε.

In summary, qualitetively extending these observations to cases where ε and θ are time-varying, it is shown that doubly complementary filter pairs are much more sensitive to phase and magnitude mismatches than doubly magnitude complementary filter pairs. Hance, the latter should be selected for applications needing a low sensitivity, such as in the example of the multiway loudspeaker crossover, whereas the former should be used in applications requiring a high sensitivity, e.g. for instrumentation and measurement.

It is however noted that for a given filter order, doubly magnitude complementary filter pairs are featuring a less selective amplitude response, because S_{11} and S_{21} are expressed as perfect squares, cf (3.85a,b).

3.4.15 Elementary transformations of complex lossless two-ports

Preliminary note

The transformations discussed in this subsection assume that the *signals* processed by the lossless two-port are complex. Hence, referring to Table 3.4, only Cases 2, 4, and 5 are authorized.

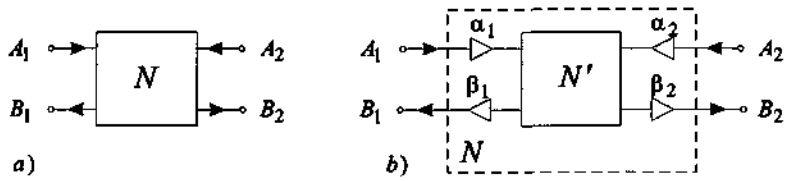

Figure 3.15: Equivalent two-port configurations, with identical incident and reflected waves.

General equivalence transformation

An *arbitrary* – not necessarily reciprocal – complex or real lossless two-port N featuring a scattering matrix $S(\psi)$ (3.32) is considered in Figure 3.15a, with complex input/output signals.

Introducing the unimodular constants α_1, α_2, β_1, and β_2, the two-port N can be decomposed as shown in Figure 3.15b, where the internal two-port N' is characterized by the scattering matrix [Fett81a] :

$$S' = \begin{pmatrix} \alpha_1^* \cdot \beta_1^* \cdot S_{11} & \alpha_2^* \cdot \beta_1^* \cdot S_{12} \\ \alpha_1^* \cdot \beta_2^* \cdot S_{21} & \alpha_2^* \cdot \beta_2^* \cdot S_{22} \end{pmatrix} = \frac{1}{g'} \cdot \begin{pmatrix} h' & \sigma' \cdot f'_* \\ f' & -\sigma' \cdot h'_* \end{pmatrix} \tag{3.96a}$$

with

$$g' = g \,. \tag{3.96b}$$

Transformations preserving the symmetry / antimetry

A symmetric or antimetric lossless two-port N can be mapped onto a two-port N' of the same type, that is featuring purely para-even/odd constitutive polynomials f' and h'. Conversely, N' can be mapped onto N. This is achieved by forcing $\sigma' = \pm 1$ in (3.96a). The corresponding transformations are provided in Table 3.8a. They are specified both for the notation defined in (3.35) and (3.36), and for (3.96).

These transformations will in particular serve in Section 3.5 to identify the number of independent design parameters available in lossless two-ports.

Transformations for general reciprocal and non-reciprocal two-ports

Still forcing $\sigma' = \pm 1$, Table 3.8b and Table 3.8c are provided for the general reciprocal and non-reciprocal cases, respectively.

Transformation from symmetric to antimetric lossless two-ports and vice-versa

Similarly, it is possible to map a symmetric (antimetric) lossless two-port N onto an antimetric (symmetric) lossless two-port N' using the transformation specified in Table 3.8d [28].

---

[28] Adapted from [Bele68, p. 298], and [Fett69, Fett81b, Fett87].

Hence, in case of *complex* lattice-type lossless two-ports, a direct correspondence exists between symmetric and antimetric type two-ports. Therefore, from a filtering (i.e. frequency discrimination) point of view, *complex symmetric and antimetric lossless two-ports are shown to be equivalent*, except for the constant phase shifts of $\pm\pi/2$ specified in Table 3.8d. For filtering applications requiring the realization of a *single* transfer function, i.e. S_{11} or S_{21}, the difference between the two kinds of networks is conceptually irrelevant. However, for applications requiring the simultaneous realization of several transfer functions, e.g. S_{11} together with S_{21} for a single-input two-output filter configuration, the selection of the type of two-port affects the phase shift *between* the output signals of the filter, as was established in Subsection 3.4.11.

Transformation of lossless two-ports into one-real two-ports

Referring to [Fett81a], an *arbitrary* (not necessarily reciprocal) complex lossless two-port N can be mapped onto a one-real complex two-port N', with $S'(\psi=1)=S'^{*}(\psi=1)$, applying the parameters :

$$\alpha=\sqrt{\frac{f^{*}(\psi=1)}{f(\psi=1)}};\qquad \beta=\sqrt{\frac{g^{*}(\psi=1)}{g(\psi=1)}};\qquad \gamma=\sqrt{\frac{h^{*}(\psi=1)}{h(\psi=1)}},\qquad \text{(3.97a,b,c)}$$

$$\sigma'=\sqrt{\frac{f^{*}(\psi=1)\cdot f(\psi=-1)}{f(\psi=1)\cdot f^{*}(\psi=-1)}},\qquad \text{(3.97d)}$$

to the transformation specified in (3.35) and (3.36). The condition for this transformation to succeed in achieving a one-real two-port N' is given by [Fett81a] :

$$C(\psi=1)\cdot C^{*}(\psi=-1)=C^{*}(\psi=1)\cdot C(\psi=-1).\qquad (3.98)$$

Using (3.97), the same result can alternatively be obtained applying (3.96) with parameters [Fett81a] :

$$\alpha_1=\beta;\quad \alpha_2=\sigma'^{*}\cdot\sigma\cdot\alpha\cdot\beta\cdot\gamma;\quad \beta_1=\gamma^{*},\quad \beta_2=\alpha^{*}.\qquad (3.99a\text{–}d)$$

Part	Two-ports N and N'	Considered two-ports		S' specified by (3.35) and (3.36)				S' specified by (3.96)				Features of S'			
		S	S'	α	β	γ	σ'	α_1	α_2	β_1	β_2	f'	h'	C'	σ'
a)	Lattice-type (reciprocal)	Sym.	Sym.	$\frac{1}{\sqrt{\sigma}}$	1	$\frac{1}{\sqrt{\sigma}}$	1	$\sqrt{\sigma}$		1		f'_e	h'_o	C	1
		Anti.	Anti.										h'_e		
		Sym.	Sym.	$\frac{\pm j}{\sqrt{\sigma}}$	1	$\frac{\pm j}{\sqrt{\sigma}}$	-1	$\mp j\sqrt{\sigma}$		1		f'_o	h'_e	C	-1
		Anti.	Anti.										h'_o		
b)	General reciprocal			$\frac{1}{\sqrt{\sigma}}$	1	$\frac{1}{\sqrt{\sigma}}$	1	$\sqrt{\sigma}$		1		f'_e		C	1
				$\frac{\pm j}{\sqrt{\sigma}}$	1	$\frac{\pm j}{\sqrt{\sigma}}$	-1	$\mp j\sqrt{\sigma}$		1		f'_o		C	-1
c)	Non-reciprocal			$\frac{1}{\sqrt{\sigma}}$	1	$\frac{1}{\sqrt{\sigma}}$	1	$\sqrt{\sigma}$		1				C	1
				$\frac{\pm j}{\sqrt{\sigma}}$	1	$\frac{\pm j}{\sqrt{\sigma}}$	-1	$\mp j\sqrt{\sigma}$		1				C	-1
d)	Lattice-type (reciprocal)	Sym.	Anti.	$\mp j$	1	1	$-\sigma$	1	$\pm j$	1	$\pm j$			$\pm j \cdot C$	$-\sigma$
		Anti.	Sym.												

Table 3.8: Elementary transformations for lossless two-port with complex signals
(Application of transformations are restricted to Cases 2, 4, and 5 according to Table 3.4; Sym.: Symmetric two-ports; Anti.: Antimetric two-ports).

Observations

Coming back to the restrictions made in the application of Table 3.8 to Cases 2, 4, and 5 only, according to Table 3.4, it becomes obvious why these restrictions have been established. Indeed, in Case 1 from Table 3.4, real lossless two-ports of symmetric and antimetric type are of totally different nature. This can be deduced from (3.43) and (3.53), where the constituent allpass functions of real symmetric lossless two-ports are themselves real, whereas they become complex for real antimetric lossless two-ports.

Despite of this, when the two-port N is real with *complex* input/output signals, Table 3.8 applies without problem. Taking for example the transformations in Table 3.8d, N is then mapped onto a degenerate complex lossless two-port N', and vice-versa. Figure 3.4d illustrates the case where N' is real, and N degenerete complex.

The expressed restrictions extend to Case 3 of Table 3.4 handling real signals.

3.4.16 Phase response of polynomials f and h

Para-even/odd polynomials are featuring a *constant* phase response for $\psi = j \cdot \phi$, except for possible phase steps, cf (A.30).

Referring to the network transformations in Table 3.8a, the polynomials f' and h' belonging to the transformed lattice-type two-port N' are para-even/odd. Since f' and h' are related to the polynomials f and h of network N by unimodular constants – cf Table 3.8a – it is demonstrated that f and h of symmetric and antimetric lossless two-ports are featuring a constant phase response, except for possible local phase steps.

3.4.17 Real lossless two-ports

Clearly, referring back to (3.28), the condition to fulfil to get real lossless two-ports, including non-reciprocal networks, reduces to :

$$\mathrm{Ia}\{S\} = 0; \tag{3.100}$$

cf (A.8) and (A.9), which implies :

$$\mathrm{Ia}\{S_{ij}\} = 0 \quad \Leftrightarrow \quad S_{ij}(\psi) = \overline{S_{ij}(\psi)}; \qquad i, j = 1,2. \tag{3.101}$$

Real symmetric lossless two-ports

Applying (3.101) to (3.46), it is observed that the constitutive allpass networks of real symmetric lossless two-ports are necessarily real, and vice-versa :

$$\mathrm{Ia}\{S_i\}=0 \quad \Leftrightarrow \quad S_i(\psi)=\overline{S_i(\psi)}; \qquad i=1,2. \tag{3.102}$$

Real antimetric lossless two-ports

Similarly, introducing (3.101) into (3.55), it is demonstrated that the constitutive allpass functions of real antimetric two-ports necessarily verify the following condition [Meer83, Fett87] :

$$S_i(\psi)=\overline{S_{(3-i)}(\psi)}; \qquad i=1,2; \tag{3.103}$$

which induces, cf (A.10) :

$$S_{11}(\psi)=\overline{S_{11}(\psi)}=\mathrm{Ra}\{S_2(\psi)\}=\mathrm{Ra}\{S_1(\psi)\} \tag{3.104a}$$

$$S_{21}(\psi)=\overline{S_{21}(\psi)}=\mathrm{Ia}\{S_2(\psi)\}=-\mathrm{Ia}\{S_1(\psi)\}. \tag{3.104b}$$

Hence, the allpass functions S_1 and S_2 are normally complex for real antimetric two-ports, except for trivial networks not retained here, e.g. $S_{21}\equiv 0$. The complete form of the resulting scattering matrix is given below for later reuse :

$$S=\begin{pmatrix} \mathrm{Ra}\{S_2\} & \mathrm{Ia}\{S_2\} \\ \mathrm{Ia}\{S_2\} & -\mathrm{Ra}\{S_2\} \end{pmatrix} \tag{3.105a}$$

$$=\begin{pmatrix} \mathrm{Ra}\{S_1\} & -\mathrm{Ia}\{S_1\} \\ -\mathrm{Ia}\{S_1\} & -\mathrm{Ra}\{S_1\} \end{pmatrix}. \tag{3.105b}$$

Real equivalent scattering matrix of complex allpass functions

Let us consider the response $B=S\cdot A$ of a complex allpass, with scattering function $S(\psi)$. The real analytic part of the response can be written :

$$\begin{aligned}\mathrm{Ra}\{B\}&=[B+\overline{B}]/2=[S\cdot A+\overline{S}\cdot\overline{A}]/2\\ &=[(S+\overline{S})\cdot(A+\overline{A})+(S-\overline{S})\cdot(A-\overline{A})]/4.\end{aligned}$$

Proceeding similarly for the imaginary analytic part, and simplifying the results, one achieves :

$$\mathrm{Ra}\{B\} = \mathrm{Ra}\{S\}\cdot\mathrm{Ra}\{A\} - \mathrm{Ia}\{S\}\cdot\mathrm{Ia}\{A\} \tag{3.106a}$$

$$\mathrm{Ia}\{B\} = \mathrm{Ia}\{S\}\cdot\mathrm{Ra}\{A\} + \mathrm{Ra}\{S\}\cdot\mathrm{Ia}\{A\}. \tag{3.106b}$$

Accordingly, the response of a complex allpass can be equally expressed by a real scattering matrix :

$$\begin{pmatrix} \mathrm{Ra}\{B\} \\ \mathrm{Ia}\{B\} \end{pmatrix} = \begin{pmatrix} \mathrm{Ra}\{S\} & -\mathrm{Ia}\{S\} \\ \mathrm{Ia}\{S\} & \mathrm{Ra}\{S\} \end{pmatrix} \cdot \begin{pmatrix} \mathrm{Ra}\{A\} \\ \mathrm{Ia}\{A\} \end{pmatrix}, \tag{3.107}$$

which, following (A.10), is identical to :

$$\begin{pmatrix} \mathrm{Ra}\{B\} \\ \mathrm{Ia}\{B\} \end{pmatrix} = \begin{pmatrix} 0 & 1 \\ 1 & 0 \end{pmatrix} \cdot \begin{pmatrix} \mathrm{Ra}\{\bar{S}\} & -\mathrm{Ia}\{\bar{S}\} \\ \mathrm{Ia}\{\bar{S}\} & \mathrm{Ra}\{\bar{S}\} \end{pmatrix} \cdot \begin{pmatrix} 0 & 1 \\ 1 & 0 \end{pmatrix} \cdot \begin{pmatrix} \mathrm{Ra}\{A\} \\ \mathrm{Ia}\{A\} \end{pmatrix}. \tag{3.108}$$

The equivalence represented in Figure 3.16 is thus established.

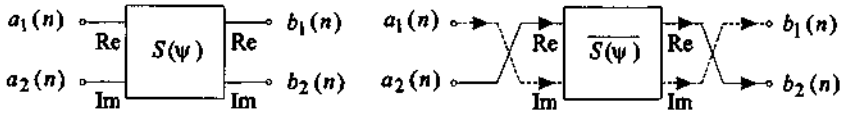

Figure 3.16: Equivalent implementations of a complex allpass function.

Equivalence between real antimetric lossless two-ports and complex allpass functions

Comparing (3.107) with (3.105a), and setting $\mathrm{Ra}\{B\} = B_1$, $\mathrm{Ia}\{B\} = B_2$, $\mathrm{Ra}\{A\} = A_1$, $\mathrm{Ia}\{A\} = A_2$, and $S = S_2$, one observes that a real antimetric lossless two-port of degree n can be realized by a complex allpass S_2 of degree $n/2$, provided that the sign of A_2 is changed [Meer83], cf Figure 3.17a :

$$S = \begin{pmatrix} \mathrm{Ra}\{S_2\} & -\mathrm{Ia}\{S_2\} \\ \mathrm{Ia}\{S_2\} & \mathrm{Ra}\{S_2\} \end{pmatrix} \cdot \begin{pmatrix} 1 & 0 \\ 0 & -1 \end{pmatrix}. \tag{3.109}$$

Of course, this sign change can be simply dropped when $A_2 \equiv 0$ [Vaid87a], as it often occurs in *analysis* branching filters.

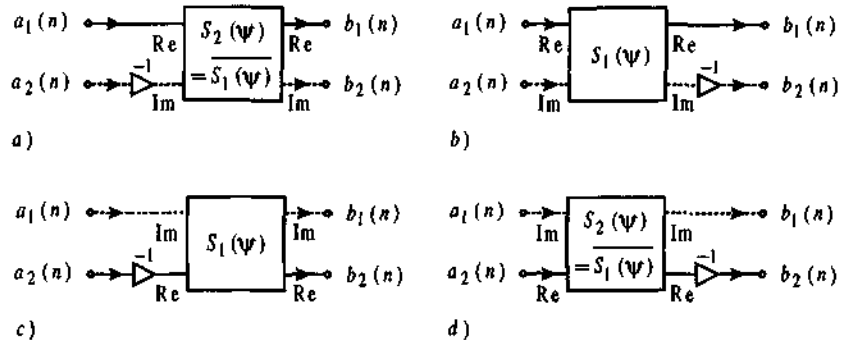

Figure 3.17: Networks equivalent to a real antimetric lossless two-port.

Alternatively, introducing $S = S_1$ into (3.107) and comparing with (3.105b), it is demonstrated that a real antimetric lossless two-port can be equally implemented by the allpass S_1, making sure that B_2 is changed in sign, cf Figure 3.17b :

$$S = \begin{pmatrix} 1 & 0 \\ 0 & -1 \end{pmatrix} \cdot \begin{pmatrix} \mathrm{Ra}\{S_1\} & -\mathrm{Ia}\{S_1\} \\ \mathrm{Ia}\{S_1\} & \mathrm{Ra}\{S_1\} \end{pmatrix}. \tag{3.110}$$

Again, the sign change can be dropped when B_2 is ignored, as it is usually the case in *synthesis* branching filters.

Finally, making use of the identity given in Figure 3.16, two further variants can be obtained for the implementation of real antimetric lossless two-ports [29], cf Figure 3.17c,d.

3.5 Independent parameters characterizing lossless two-ports

This section aims at determining the maximum number of real and independent parameters fully specifying a lossless two-port N of degree n, emphasizing the lattice-type case. These parameters basi-

[29] The purpose of establishing the exhaustive list of implementations for real antimetric lossless two-ports is in providing the basis for a precise comparison of implementation structures described in the literature, in particular regarding the implementetion of Quasi-Mirror Filterbanks, cf Chapter 4.

cally correspond to the coefficients of the scattering matrix polynomials f, h, g, including the constant σ, or to any equivalent set of parameters (e.g. zero/poles configurations, or the parameters of the constituent allpass functions specifying lattice-type two-ports, etc.).

The identification of these independent parameters, considered in relationship with the filter type and degree, provides an insigbt of the kind of filter responses that can be realized, and furnishes essential informations for the elaboration of filter approximation methods and tools.

3.5.1 Independent parameters of complex lossless two-ports

Canonic form of lattice-type lossless two-ports

According to Table 3.8a, a symmetric/antimetric lossless two-port N can be mapped onto a two-port N' of same type featuring purely para-even/odd polynomials f' and h', and conversely. The characteristic function – and thus the amplitude response – remains invariant to this transformation, i.e. $C(\psi)=C'(\psi)$. Moreover, the phase responses of both networks are the same, except for a *constant* phase shift specified by σ.

Consequently, the two-port N' involving para-even/odd polynomials only – and thus the maximum number of *free* parameters – corresponds to the *canonic* form of the network to be designed for a specified amplitude *and/or* phase response, except for the parameter σ fixing the constant phase shift between the responses of N and N'.

The approximation of symmetric and antimetric lossless two-ports should therefore be performed in two steps, determining the two-port N' first, and mapping it in a second step onto the network N according to the application specifications.

Degree of two-port and polynomials f, h, and g

Next, the degree of polynomials f, h, and g, denoted by n_f, n_h, and n, respectively, are introduced, deg(.) indicating the degree :

$$n_f = \deg(f), \quad n_h = \deg(h), \quad n = \deg(g). \qquad (3.111a,b,c)$$

Due to (3.33), the degrees of the polynomials are verifying :

$$n = \max(n_f, n_h), \quad n_f \le n, \quad n_h \le n, \tag{3.112a,b,c}$$

$n = \deg(g)$ corresponding to the degree of the two-port. Considering further the relationship between two-ports N and N', one derives :

$$n_{f'} = n_f, \quad n_{h'} = n_h, \quad n' = n. \tag{3.113a,b,c}$$

Maximum number of independent parameters characterizing lattice-type lossless two-ports

Given the degree of the two-port N, the maximum number of real and independent parameters available in the set $\{\sigma, f, h, g\}$ that are fully characterizing N, is looked for.

Considering the canonic equivalent N' of N, and referring to Table 3.8a, it is observed that both parameters σ and $\sigma' = \pm 1$ should be fixed to have a one-to-one correspondence between N and N'. Moreover, σ' plays a particular role, since it decides upon the para-even/odd nature of f' and h'. Both σ and σ' should thus be fixed separately by the application.

Hence, three different measures of the maximum number of free parameters are introduced, namely *tot_nb_parms_N* for N, counting σ and σ', *tot_nb_parms_N'* for N', counting σ', and *nb_parms_N'*, excluding σ' [30] :

$$tot\_nb\_parms\_N = tot\_nb\_parms\_N' + 1, \quad \textit{(only complex } N, N') \tag{3.114a}$$

$$tot\_nb\_parms\_N = tot\_nb\_parms\_N', \quad \textit{(only real } N, N';\ N \equiv N') \tag{3.114b}$$

$$tot\_nb\_parms\_N' = nb\_parms\_N' + 1, \quad \textit{(complex + real } N, N') \tag{3.114c}$$

Complex symmetric lossless two-ports

The following expression is derived from (3.33) and (3.41) for N' :

$$g' \cdot g'_* = -\sigma' \cdot (h'^2 - f'^2) = -\sigma' \cdot (h' - f') \cdot (h' + f'); \quad \sigma' = \pm 1. \tag{3.115a,b}$$

Factors $(h' - f')$ and $(h' + f')$ are then fixed with (3.47b) and (3.48b):

$$h' - f' = \sigma'_1 \cdot g'_{1*} \cdot g'_2; \quad h' + f' = \sigma'_2 \cdot g'_1 \cdot g'_{2*}; \tag{3.116a,b}$$

---

[30] Equation (3.114b) is valid for Case 1 in Table 3.4.

with $g' = g'_1 \cdot g'_2$; $\sigma'_i = -\sigma' / \sigma'_{(3-i)}$; $i = 1,2$. (3.117a,b)

The polynomial g' is arbitrarily assumed monic [31], cf Subsection 3.4.4. The same assumption is made for g'_1 and g'_2, agreeing with (3.117a). Besides these constraints, g', g'_1, and g'_2 are general complex polynomials, and are thus counting $2 \cdot n' = 2 \cdot (n'_1 + n'_2)$, $2 \cdot n'_1$, and $2 \cdot n'_2$ real free parameters, respectively, with $n'_i = \deg(g'_i)$, $i = 1,2$.

Hence, the right-hand sided parts of (3.116a,b), which are completely interrelated, are counting $2 \cdot n' + 1$ real free parameters, including $\mathrm{Arg}\{\sigma'_1\}$ or $\mathrm{Arg}\{\sigma'_2\}$, where σ'_1 and σ'_2 are linked by (3.117b) [32].

Clearly, the left-hand sided parts of (3.116a,b), i.e. $(h' \pm f')$, count the same amount of real independent parameters. This is easily verified taking into account that $\deg(h' \pm f') = n'$, and that the leading coefficient of $(h' \pm f')$ is unimodular. The polynomials f' and h' being respectively para-even (-odd) and para-odd (-even) for symmetric lossless two-ports, it is observed that they are precisely and separately contributing to the real and imaginary part of each coefficient in the factors $(h' \pm f')$, cf (A.26).

It is further noticed from (3.116) and (3.117b) that it suffices to know either both polynomials f' and h', or one of the right-hand sided terms in (3.116), to fully determine N', without costly use of (3.33). Moreover, when designing strictly stable networks, i.e. both g'_1 and g'_2 are strictly Hurwitz, and assuming that f' and h' are known, it suffices to use only one expression of (3.116a,b) to uniquely determine g'_1 and g'_2 by factorization. On the contrary, both equations (3.116a,b) are requested to handle unsteble networks.

Finally, $nb\_parms\_N' = (2 \cdot n + 1)$ for complex symmetric lossless two-ports, cf Table 3.9.

Complex antimetric lossless two-ports

For complex antimetric lossless two-ports, equations (3.115) – (3.117) are replaced by :

---

[31] A polynomial is *monic* when its leading coefficient, associated to the highest power of the independent variable, is equal to +1 [Bele68, p. 406].

[32] It is recalled that parameter $\sigma' = \pm 1$ is not counted in nb_parms_N', cf (3.114c).

$$g' \cdot g'_* = \sigma' \cdot (h'^2 + f'^2) = \sigma' \cdot (h' - j \cdot f') \cdot (h' + j \cdot f'); \; \sigma' = \pm 1; \quad (3.118a,b)$$

$$h' - j \cdot f' = \sigma'_1 \cdot g'_{1*} \cdot g'_2; \quad h' + j \cdot f' = \sigma'_2 \cdot g'_1 \cdot g'_{2*}; \quad (3.119a,b)$$

with $$g' = g'_1 \cdot g'_2; \quad \sigma'_i = \sigma' / \sigma'_{(3-i)}; \quad i = 1,2. \quad (3.120a,b)$$

The development proceeds very similarly to the symmetric case, and is dropped for conciseness. The number of design parameters is exactly the same than for the symmetric case, cf Table 3.9.

	nb_parms_N'	
	Complex N'	**Real N'**
Lattice-type N' (Symmetric or antimetric)	$2 \cdot n + 1$	$n + 1$
General reciprocal N'	$3 \cdot n + 1$	For n odd: $(3 \cdot n - 1)/2 + 1$ For n even: $3 \cdot n/2 + 1$
Non-reciprocal N'	$4 \cdot n + 2$	$2 \cdot n + 1$

Table 3.9: Maximum number of real independent parameters of lossless two-ports [32].

Max. number of independent parameters characterizing non-reciprocal and general reciprocal lossless two-ports

For the sake of completeness, the non-reciprocal and general reciprocal cases are briefly handled. Complex non-reciprocal lossless two-ports N' are best designed by directly approximating the irreducible and unit-bounded coefficient $S'_{21} = f'/g'$. Assuming that g' is monic, whereas f' is a general unconstrained complex polynomial, the maximum number of real independent parameters is $(4 \cdot n + 2)$ [32].

The factor $(h' \cdot h'_*)$ is then uniquely determined from (3.33). However, h' cannot be uniquely obtained from $(h' \cdot h'_*)$, due to the multiple factorization possibilities [Bele68, p. 284]. Moreover, an arbitrary unimodular constant can be assigned to h' without affecting $(h' \cdot h'_*)$, cf (3.35c). The factorization is thus observed to be much more intricate than for lattice-type networks, $(h' \cdot h'_*)$ being of degree $2 \cdot n_h$.

Finally, the data for the general reciprocal case are also provided in Table 3.9, noticing that $f' = \sigma' \cdot f'_* = \pm f'_*$ is verified due to reciprocity, involving that f' is para-even/odd, cf Table 3.8b.

Authorized/prohibited network configurations for lattice-type lossless two-ports

It is observed from Subsection 3.4.4 that polynomials f and h can't simultaneously possess a (single or multiple) zero at $\psi = 0$, otherwise polynomial g should own the same zero(s) due to (3.33), which would be in contradiction with the strictly Hurwitz nature of g.

Applying this rule to the transformed two-port N', a list of prohibited network configurations can be establisbed using (A.26), cf Table 3.10. The mentioned polynomials $F_i'(\psi)$, $H_i'(\psi)$, $i = 1,...,4$, are specified by the notation introduced in (A.26), and are all evaluated at $\psi = 0$.

	$C'(\psi)$	Lattice-type lossless two-port N'		
		Complex	Imaginary	Real
Symmetric case	$C' = h_o'/f_e'$	$F_1' = H_4' = 0$	$H_4' = 0$	$F_1' = 0$
	$C' = h_e'/f_o'$	$F_4' = H_1' = 0$	$F_4' = 0$	$H_1' = 0$
Antimetric case	$C' = h_e'/f_e'$	$F_1' = H_1' = 0$	Prohibited	$F_1' = H_1' = 0$
	$C' = h_o'/f_o'$	$F_4' = H_4' = 0$	$F_4' = H_4' = 0$	Prohibited

Table 3.10: Prohibited configurations for lattice-type lossless two-ports (all polynomials $F_i'(\psi)$, $H_i'(\psi)$, $i = 1,...,4$, are evaluated at $\psi = 0$).

Purely imaginary and real lossless two-ports N' are defined for $F_1' \equiv F_3' \equiv H_1' \equiv H_3' \equiv 0$, and $F_2' \equiv F_4' \equiv H_2' \equiv H_4' \equiv 0$, respectively. In the real case, the two-ports N and N' become identical, with $\sigma' = \sigma = \pm 1$.

3.5.2 Independent parameters of real lattice-type lossless two-ports

Real lattice-type lossless two-ports are featuring $\sigma = \pm 1$, and the two-ports N' and N are thus identical, polynomials f and h becoming necessarily para-even/odd. It is recalled that symmetric and antimetric two-ports correspond to fundamentally different filter configurations in the real case. The maximum number of real independent parameters is provided in Table 3.9 using (3.114b,c).

Degree of two-port and polynomials f, h, and g

The definitions provided in (3.111) and (3.112) clearly apply to real two-ports. For classification purposes, the terms n_{f0} and n_{h0} are further introduced, indicating the number of zeros of f and h lying at $\psi = 0$. Finally, the number of transmission zeros of $S_{21} = f/g$ and $S_{11} = h/g$ located at infinity, denoted by $n_{f\infty}$ and $n_{h\infty}$, respectively, are specified by :

$$n_{f\infty} = n - n_f, \quad n_{h\infty} = n - n_h. \tag{3.121}$$

Real symmetric lossless two-ports

Real para-even/odd polynomials merely reduce to even/odd polynomials. From (3.41), f and h are respectively even and odd for $\sigma = 1$, whereas they become odd and even for $\sigma = -1$ [Bele68].

		Odd degree n		Even degree n	
		$f(\psi)$	$h(\psi)$	$f(\psi)$	$h(\psi)$
$\sigma = 1$	Typ. resp. of S_{21}	**Lowpass**		**Bandstop**	
	Parity of f, h	Even	Odd	Even	Odd
	Monic f, h [31,33]	–	Yes	Yes	–
	Degree	$n_f \le n-1$ (n_f even)	$n_h = n$ (n_h odd)	$n_f = n$ (n_f even)	$n_h \le n-1$ (n_h odd)
	Zeros at origin	$n_{f0} = 0$	$n_{h0} \ge 1$	$n_{f0} = 0$	$n_{h0} \ge 1$
	Zeros at infinity	$n_{f\infty} \ge 1$	$n_{h\infty} = 0$	$n_{f\infty} = 0$	$n_{h\infty} \ge 1$
$\sigma = -1$	Typ. resp. of S_{21}	**Highpass**		**Bandpass**	
	Parity of f, h	Odd	Even	Odd	Even
	Monic f, h [31,33]	Yes	–	–	Yes
	Degree	$n_f = n$ (n_f odd)	$n_h \le n-1$ (n_h even)	$n_f \le n-1$ (n_f odd)	$n_h = n$ (n_h even)
	Zeros at origin	$n_{f0} \ge 1$	$n_{h0} = 0$	$n_{f0} \ge 1$	$n_{h0} = 0$
	Zeros at infinity	$n_{f\infty} = 0$	$n_{h\infty} \ge 1$	$n_{f\infty} \ge 1$	$n_{h\infty} = 0$

Table 3.11: Elementary paremeters for real symmetric lossless two-ports.

[33] The polynomial g was assumed monic for the establishment of this table, which contains an entry to indicate whether f or h are monic as well. No indication, i.e. "–", means that the situation is application dependent.

Clearly, real even (odd) polynomials are necessarily of even (odd) degree. Hence, one deduces that f and h are of different degree for real symmetric lossless two-ports, the parity of their degree being specified by their even/odd nature.

Furthermore, the polynomial f or h that is of odd degree has necessarily an odd number of zeros at the origin, but at least one. Conversely, the polynomial f or h that is of even degree should be devoid of any zero at the origin, cf Table 3.10.

		$n_f = n_h = n$			
		$f(\psi)$	$h(\psi)$	$f(\psi)$	$h(\psi)$
Typical resp. of S_{21}		**LP, HP, BP, BS**		**LP, HP, BP, BS**	
Monic f, h (31, 33)		No	No	–	–
Zeros at origin		$n_{f0} = 0$	$n_{h0} = 0$	$n_{f0} \cdot n_{h0} = 0$ (34)	
Zeros at infinity		$n_{f\infty} = 0$	$n_{h\infty} = 0$	$n_{f\infty} = 0$	$n_{h\infty} = 0$
Examples of amplitude approximated filters	Butterworth	–		–	
	Chebyshev	BS Chebyshev		HP Chebyshev	
	Inverse Cheb.	BP Inv. Chebyshev		LP Inv. Chebyshev	
	Elliptic	Elliptic		Modified elliptic (35)	

Table 3.12a: Basic parameters for real antimetric lossless two-ports
(LP: Lowpass; HP: Highpass; BP: Bandpass; BS: Bandstop).

Considering the behavior at infinity, cf (3.121), the polynomial f or h that has lower degree than n is associated to a necessarily odd number of transmission zeros at infinity, but at least one. Inversely, the polynomial f or h of degree n does not induce any transmission

---

[34] In all generality, zeros may be located at the origin, in which case they should be assigned to exactly one of the polynomials f and h in accordance with the filter response. The zeros should necessarily occur pairwise.

[35] Even ordered filtere can be modified to feature paire of attenuation zeros/poles at the origin or/and at infinity. The modification can be performed using a particular transformation [Sedr78], or other approximation methods. Note that modified elliptic filtere achieved by transformation are not any more equiripple in both passband and stopband, and that they are suboptimal with respect to frequency selectivity.
In the present case, the modification provides either attenuation zeros *or* attenuation poles at the origin.

zero at infinity. Hence, analyzing the asymptotic behavior of polynomials f and h at the origin and infinity, it is possible to collect the parameters corresponding to typical filter responses assigned to S_{21}, cf Table 3.11.

Real antimetric lossless two-ports

According to Table 3.10, the polynomials f and h belonging to real antimetric lossless two-ports are necessarily even, i.e. $\sigma = 1$ [Youl71, Fett84b]. Consequently, f and h are both of even degree.

Furthermore, the results achieved in Subsection 3.4.16, in particular formulas (3.103) and (3.104), directly apply. Hence, the next expressions are derived from (3.54) :

$$g_2 = \overline{g_1} \; ; \qquad \sigma_2 = \sigma_1^* . \tag{3.122}$$

The basic parameters for designing real antimetric lossless two-ports are provided in Table 3.12a for the case where f and h are of same (even) degree. Table 3.12b completes the figure for situations where f and h are of different (even) degree.

		$n_f = n-2k$, $n_h = n$		$n_f = n$, $n_h = n-2k$	
		$f(\psi)$	$h(\psi)$	$f(\psi)$	$h(\psi)$
Typical resp. of S_{21}		**Lowpass, Bandpass**		**Highpass, Bandstop**	
Monic f, h (31,33)		–	Yes	Yes	–
Zeros at origin		$n_{f0} \cdot n_{h0} = 0$ (34)		$n_{f0} \cdot n_{h0} = 0$ (34)	
Zeros at infinity		$n_{f\infty} \geq 2$	$n_{h\infty} = 0$	$n_{f\infty} = 0$	$n_{h\infty} \geq 2$
Examples of amplitude approximated filters	Butterworth	LP/BP Butterworth		HP/BS Butterworth	
	Chebyshev	LP/BP Chebyshev		–	
	Inverse Cheb.	–		HP/BS Inv. Chebyshev	
	Elliptic	Modified elliptic (36)		Modified elliptic (36)	

Table 3.12b: Basic parameters for real antimetric lossless two-ports ($k = 1,\ldots, n/2$).

[36] These modified elliptic filters are featuring attenuation zeros/poles at the origin *and* at infinity. Hence, these filters can be realized with equally-valued termination resistances.

3.6 Mapping of lossless two-ports into the z-domain

The mapping of the complex or real lossless two-ports is performed by application of the forward bilinear transform T_B defined in (A.50). Details on the procedure are provided in Section A.6. The following discussion concentrates on *lattice-type* lossless two-ports, in which case one is essentially interested in the T_B transformation of allpass functions, cf (A.77) and (A.78).

		Forward bilinear transform T_B →		
		ψ-domain		z-domain
Signal quantities	Incident waves	$A_i(\psi),\ a_i(n\cdot T_s)$	$\Rightarrow$	$A_i(z),\ a_i(n)$
	Reflected waves	$B_i(\psi),\ b_i(n\cdot T_s)$	$\Rightarrow$	$B_i(z),\ b_i(n)$
Parameter-ized scattering matrix	Polynomials	$f(\psi)$	$\Rightarrow$	$P(z)$
		$h(\psi)$	$\Rightarrow$	$R(z)$
		$g(\psi)$	$\Rightarrow$	$Q(z)$
	Unitary constant	σ	$\Rightarrow$	λ
Network functions	Allpass functions	$S_i(\psi)$	$\Rightarrow$	$H_i(z)$
	Transfer functions	$S_{i1}(\psi)$	$\Rightarrow$	$H_{i1}(z)$
	Characteristic fct.	$C(\psi)=S_{11}/S_{21}$	$\Rightarrow$	$C_z(z)=H_{11}/H_{21}$

Table 3.13: Bilinear transformation of canonic lattice-type lossless two-ports N $(i=1,2)$.

The correspondence between the signal quantities, polynomials, and network functions when passing from the ψ-domain to the z-domain, is defined in Table 3.13. It is observed that the incident and reflected waves are represented with the same symbols in both domains, although they are mathematically not equal when proceeding from one domain to the other. This shouldn't be a problem, the distinction being usually clearly indicated by the context.

Clearly, all formulas elaborated in the ψ-domain for lattice-type lossless two-ports have their counterpart in the z-domain under T_B transformation conditions.

According to (A.78b), the unimodular constants λ_i belonging to the (stable) allpass functions $H_i(z)$, $i=1,2$, are related to those of $S_i(\psi)$ by :

$$\lambda_i = \sigma_i \cdot \prod_{\nu=1}^{n_{i2}} \left(\frac{1-\psi^*_{\infty i\nu}}{1-\psi_{\infty i\nu}} \right), \qquad \text{with } n_i = n_{i1} + n_{i2}, \tag{3.123}$$

$$\psi_{\infty i\nu} \neq -1, \quad \nu = 1,2,\ldots,n_{i2};$$

$H_i(z)$ and $S_i(\psi)$ being of same degree n_i, n_{i1} corresponding to the number of poles located at $\psi=-1$ (i.e. $z=0$), whereas n_{i2} indicates the number of poles verifying $\psi_{\infty i\nu} \neq -1$ (i.e. $z_{\infty i\nu} \neq 0$), $\nu = 1,2,\ldots,n_{i2}$.

The z-domain counterpart of (3.48a) and (3.57a) is then achieved defining :

$$\lambda = \sigma = \pm\sigma_1 \cdot \sigma_2 = \pm\eta \cdot \lambda_1 \cdot \lambda_2, \tag{3.124a}$$

with

$$\eta = \prod_{\nu=1}^{n_{12}} \left(\frac{1-\psi_{\infty 1\nu}}{1-\psi^*_{\infty 1\nu}} \right) \cdot \prod_{\nu=1}^{n_{22}} \left(\frac{1-\psi_{\infty 2\nu}}{1-\psi^*_{\infty 2\nu}} \right), \tag{3.124b}$$

and

$$\psi_{\infty i\nu} \neq -1, \quad \nu = 1,2,\ldots,n_{2i};$$

where the upper (lower) sign in (3.124a) holds for symmetric (antimetric) two-ports.

		Modified forward bilinear transform T_{BP} →		
		ψ-domain		z-domain
Symmetric lossless two-ports	Case 1 : $(\lambda' = \sigma' = 1)$	$f'(\psi) = f'_e(\psi)$ $h'(\psi) = h'_o(\psi)$	⇒	$P'(z) = P'_{PCS}(z)$ $R'(z) = R'_{PCA}(z)$
	Case 2 : $(\lambda' = \sigma' = -1)$	$f'(\psi) = f'_o(\psi)$ $h'(\psi) = h'_e(\psi)$	⇒	$P'(z) = P'_{PCA}(z)$ $R'(z) = R'_{PCS}(z)$
Antimetric lossless two-ports	Case 1 : $(\lambda' = \sigma' = 1)$	$f'(\psi) = f'_e(\psi)$ $h'(\psi) = h'_e(\psi)$	⇒	$P'(z) = P'_{PCS}(z)$ $R'(z) = R'_{PCS}(z)$
	Case 2 : $(\lambda' = \sigma' = -1)$	$f'(\psi) = f'_o(\psi)$ $h'(\psi) = h'_o(\psi)$	⇒	$P'(z) = P'_{PCA}(z)$ $R'(z) = R'_{PCA}(z)$

Table 3.14: Bilinear transformation of canonic latice-type lossless two-ports N'.

Considering now the canonic form N' of lattice-type lossless two-ports, cf Subsection 3.5.1, the complementary relations given in Table 3.14 are established, cf Section A.7. It is noticed that the network transformation defined in (3.96) and Table 3.8a in the ψ-domain, which provide the rules for passing from a non-canonic two-port N to its canonic form N' and conversely, applies without change in the z-domain, since only constants are involved.

3.7 Conclusion

This chapter is providing a survey on complex and real WDF filter design. Starting with a detailed review of real WDF design, a gradual introduction to complex filtering is proposed, recalling that complex and real filters are formally equivalent, but may differ in practice, thus relegating the question of the choice between both solutions to case by case selections fixed by the applications. A review of available complex WDF structures is then proposed, including a discussion on the important concept of one-realness elaborated by Fettweis.

The essential part of the chapter is then devoted to recalling basic properties of complex and real lossless two-ports WDFs are derived from, putting the emphasis on *lattice-type* structures, and proposing specific contributions along the presented matter. It is in particular demonstrated using elementary equivalence transformations that complex lattice-type lossless filters are belonging to a single class of networks, with a marginal difference between symmetric and antimetric implementations which is not affecting the amplitude response, the phase response of both structures differing only by a constant phase shift. Conversely, but this fact was of course well known before, real symmetric and antimetric filters are fundamentally different.

Further issues introduced in the chapter are listed below among the contributions.

Contributions

Chapter 3 holds a particular place in the report, since it is furnishing an extended review on complex and real Wave Digital Filter design, recalling numerous essential properties of lossless two-ports WDFs are relying on, and providing a sound basis of knowledge for succeeding chapters. Logically, most of the material presented in this chapter is of course well known.

However, the structured survey proposed in the chapter helps in ordering the subject, classifying problems, and identifying topics deserving attention for further research beyond those mentioned later in the conclusions.

C3–I: As such, the systematic review proposed in Chapter 3 is considered as original.

In addition, to the best knowledge of the author, the next specific contributions are considered as original :

- **C3–II**: Analysis of cascaded scattering parameters of lattice-type lossless two-ports as handled in Subsection 3.4.I3, cf Table 3.7, and study of *complex* doubly magnitude-complementary networks treated in Subsection 3.4.I4 which are identified to have much lower amplitude sensitivity to mismatches, compared to classical doubly-complementary networks.
- **C3–III**: Establishment of an exhaustive list of complex allpass configurations that are equivalent to a real antimetric lossless two-port, cf Figure 3.17, useful to compare published filter structures.
- **C3–IV**: Detailed discussion of the independent parameters of complex lossless two-ports, including identification of allowed / prohibited configurations of lattice-type lossless two-ports, cf Table 3.10, and provision of synoptic design tables for real symmetric and antimetric lossless two-ports, cf Tables 3.11, 3.12a, and 3.12b.

C3–V: Moreover, based on the survey of diverse filtering problems handled in Subsection 3.3.4, the field of single/double broadband matching is recognized as interesting for WDF implementations, noticing in particular that the complex case was seemingly not covered in the literature.

Further potential research

Based on the former reflections, the next subjects are proposed for potential further research:

- Following the discussion held in Subsection 3.3.6, detailed *study of the implementation of non-one-real complex WDFs to* get lossless and economic realizations of WDFs, using in particular the cross-adaptor proposed in [Schü89, Schü91], with mandatory assessment of all stability conditions related to the finite-precision implementation.
- Detailed study of *single and double broadband matching networks* implemented as WDFs, analyzing in particular the reason why *complex* broadband matching was seemingly not covered before.
- Systematic study of *(complex) non-reciprocal and general reciprocal networks* implemented as WDFs, whereas it is noticed that the subject is already generously covered in the literature for standard filter configurations of real type.
- Application of *case studies* exploiting the identified lower amplitude sensitivity of *(complex) doubly-magnitude complementary networks* to parameter mismatches, cf Subsection 3.4.14.
- Others.

Chapter 4

Bireciprocal-Type Wave Digital Filters

4.1 Introduction

Bireciprocal WDFs [1] correspond to half-band filters realizing power complementary lowpass and highpass filter pairs used to design multirate IIR-based Quasi-Mirror Filters (QMFs) [Vaid87d], or tree-shaped filterbanks, to perform signal analysis and synthesis in the frame of applications renging from communications, to spectral signal analysis/estimation, bearing aids design, subband speech/audio/image coding [Sauv90], elementary signal transmultiplexing, and also pattern recognition, to mention some of them. Half-band filters are of course also intensively applied to signal decimation and interpolation, in particular in connection with (oversampled) analog-to-digital converters (ADCs) [Dijk88] and digital-to-analog converters (DACs), in which case the lowpass filter response is used alone.

Half-band filters have been intensively studied in the literature. They rely either on Finite Impulse Response (FIR) filters [Croc83, Nuss83, Gala84, Vaid93, Vaid90, Vaid88], or on IIR filters [Vaid87a, Rega88b, Vaid90], with few extensions to complex half-band filtering, e.g. [Fett85].

---

[1] The meaning of the term "bireciprocal" will be explained in Section 4.3.

Many contributions have been published on bireciprocal WDFs, especially in the real symmetric case [Noss83, Gazs85a, Fett86], considering the significant implementation simplifications incurred in terms of hardware, number of processed operations, etc., cf e.g. [Fett86]. However, the real antimetric case is covered as well [Meer83], including also complex bireciprocal WDFs [Fett85].

The objectives of this chapter are twofold. The first objective, acting as a complementary contribution to [Fett85], aims at formally demonstrating that any IIR-based half-band filter realized as a lattice-type lossless two-port is precisely composed of a *real* symmetric or *real* antimetric lossless two-port. Any complex half-band filter configuration derived thereof is achieved through elementary transformations resulting in degenerate complex two-ports. This result clarifies the interpretation of many properties established in [Fett85], while removing reservations expressed in the same paper for the complex case.

The second objective is to provide a detailed list of possible half-band signal analysis and synthesis arrangements, still based on lattice-type lossless two-ports, and including the corresponding implementation structures. It is then shown that half-band filters relying on a real antimetric lossless two-port, can be interpreted and realized in two different ways under multirate operational conditions, with related constraints guiding the actual choice to be made according to the application requirements.

The chapter is organized as follows. Section 4.2 recalls shortly the structure of cascaded half-band analysis and synthesis networks operating under multirate conditions and realized with lossless two-ports, including the condition for perfect reconstruction of the original signal. In Section 4.3, the perfect reconstruction condition is specialized for lattice-type lossless two-ports, leading to a bireciprocal form of the corresponding characteristic function, which in turn implies that bireciprocal WDFs are essentially real, complex cases being derived thereof. The relationship between real and complex bireciprocal WDFs is described in Section 4.4. Section 4.5 is then furnishing details on real bireciprocal WDF configurations, including degree of the constituent allpass functions, and pole constellation. These data are then compiled in Section 4.6 to establish synoptic

tables valid in both real and complex cases. The corresponding implementation structures are discussed in Section 4.7, before drawing the conclusions in Section 4.8.

4.2 Cascaded half-band analysis / synthesis networks realized with lossless two-ports

Referring to [Fett85], the network arrangement illustrated in Figure 4.1 is considered, where N corresponds to a lossless two-port of reciprocal or non-reciprocal type [2], with scattering matrix S. The transpose network of N is indicated by N^T, and features $\boldsymbol{B} = \boldsymbol{S}^T \cdot \boldsymbol{A}$. N is a priori considered real or complex.

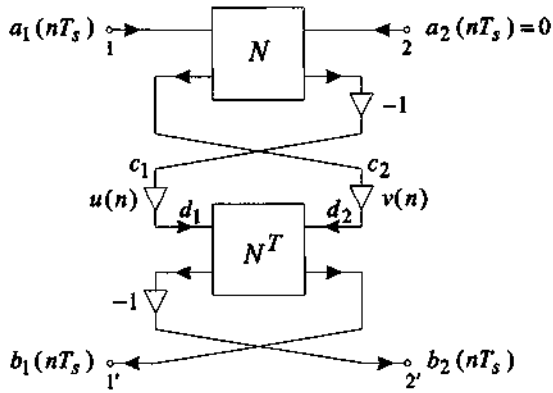

Figure 4.1: Network configuration involving multipliers $u(n)$ and $v(n)$ for halving the sampling rate [Fett85].

The functions $u(n)$ and $v(n)$ occurring in Figure 4.1 take alternately the values 1 and 0, either in the same or in opposite phases. The two situations are distinguished by the parameter $q = \pm 1$:

$$u(n) = [1 + (-1)^n]/2 = [1 + e^{j \cdot n\Omega/2}]/2, \tag{4.1a}$$

$$v(n) = [1 + q \cdot (-1)^n]/2 = q \cdot u(n) + (1 - q)/2. \tag{4.1b}$$

[2] The two-ports referred to in this chapter correspond to the normalized two-ports N' specified in Subsection 3.5.1. However, the apostrophe is dropped for simplicity.

Clearly, $v(n)=u(n)$ for $q=1$, and $v(n)=1-u(n)$ for $q=-1$. As demonstrated in [Fett85], applying to the entrance of the network arrangement in Figure 4.1 the signals :

$$a_1(nT_s)=A_1\cdot e^{p\cdot nT_s}, \quad a_2(nT_s)=0 \tag{4.2a,b}$$

where A_1 is a complex constant, and assuming that the reciprocal or non-reciprocal two-port N fulfills the condition [3] :

$$C(1/\psi)=-q/C_*(\psi), \tag{4.3}$$

then the following output signals are achieved :

$$b_1(nT_s)=0.5\cdot A_1\cdot \det(S(\psi))\cdot e^{p\cdot nT_s}, \tag{4.4a}$$

$$b_2(nT_s)=\frac{-S_{11}(1/\psi)}{S_{12}(\psi)}\cdot e^{j\Omega\cdot n/2}\cdot b_1(nT_s), \tag{4.4b}$$

where the determinant $\det(S(\psi))$ corresponds to an allpass function, cf (3.34). It is remarked from (4.4a) that, except for an allpass-type distortion, the input signal a_1 can be perfectly reconstructed under condition (4.3), and this irrespective of: i) the filtering performance of N, and ii) the fact that every second sample of signals d_1 and d_2 in Figure 4.1 is reduced to zero [Fett85].

4.3 Bireciprocal WDFs

For lattice-type lossless two-ports N, the characteristic function is verifying (3.41c) and (3.51c) in the symmetric and antimetric cases, respectively, which can be rewritten in a compact form :

$$C(\psi)=-r\cdot C_*(\psi), \quad \text{with} \quad \begin{matrix} r=1 & \text{for symmetric } N, \text{ and} \\ r=-1 & \text{for antimetric } N, \end{matrix} \tag{4.5}$$

so that (4.3) can be reformulated as :

$$C(1/\psi)=q\cdot r/C(\psi). \tag{4.6}$$

Hence, except for the sign introduced by the factor $q\cdot r=\pm 1$, the characteristic function of lattice-type lossless two-ports is observed to

[3] The assumption made in Subsection 3.4.3, stating that the termination impedances of the lossless two-port N are equal, i.e. $Z_{E1}=Z_{E1}=Z_E$, is recalled.

be of *bireciprocal* (or *self-reciprocal*) type, explaining in the same time the name assigned to the corresponding WDFs. Although the characteristic function of lattice-type lossless two-ports was originally termed bireciprocal or self-reciprocal only for $q \cdot r = 1$ [Fett85], the definition is extended in this report to $q \cdot r = \pm 1$. This choice will be commented later in Section 4.4.

Furthermore, $C(\psi)$ (and by extension the corresponding network N) will be called :

- *bireciprocal of the first kind* for $q = 1$, and
- *bireciprocal of the second kind* for $q = -1$.

The degree n of the two-port N is linked to q as follows [Fett85], page 897 :

$$\text{for } q = 1 : \ n \text{ odd}; \quad \text{for } q = -1 : \ n \text{ even}; \quad \text{with } \ n = n_1 + n_2; \tag{4.7}$$

where n_1 and n_2 correspond to the degree of the constituent allpass functions $S_i(\psi)$, $i = 1,2$, cf Figures 3.8 and 3.9.

Replacing $C(\psi)$ in (4.6) with (3.37), and applying (3.46) and (3.55) for symmetric and antimetric two-ports, respectively, the next result is obtained [Fett85] :

$$\text{for } q = 1 : \quad S_2(1/\psi) \cdot S_1(\psi) = -S_1(1/\psi) \cdot S_2(\psi); \tag{4.8a}$$

$$\text{for } q = -1 : \quad S_2(1/\psi) \cdot S_2(\psi) = -S_1(1/\psi) \cdot S_1(\psi). \tag{4.8b}$$

which is noticed to be independent of r, i.e. (4.8a,b) are valid for both symmetric and antimetric two-ports [4]. Assuming without limitation that $S_i(\psi)$, $i = 1,2$, are stable, the unstable allpass :

$$S'(\psi) = S_1(\psi) / S_2(\psi); \tag{4.9}$$

is defined and introduced into (4.8a,b), which are then replaced by :

$$\text{for } q = 1 : \quad S'(\psi) = -S'(1/\psi); \tag{4.10a}$$

$$\text{for } q = -1 : \quad S'(\psi) = -1/S'(1/\psi) \cdot. \tag{4.10b}$$

Moreover, denoting by $H'(z)$ and $H_i(z)$ the bilinear transform of $S'(\psi)$, and $S_i(\psi)$, respectively, i.e. :

---

[4] Starting from here, the discussion proceeds more directly than in [Fett85].

$$H'(z)=T_B\{S'(\psi)\},\quad H_i(z)=T_B\{S_i(\psi)\},\quad i=1,2; \tag{4.11a,b}$$

and making use of Table A.6, (4.10a,b) is equivalenty expressed by :

for $q=1$ (i.e. n odd) : $H'(z)=-H'(-z)$; (4.12a)

for $q=-1$(i.e. n even) : $H'(z)=-1/H'(-z)$. (4.12b)

Referring to Subsection 2.6.6, it is demonstrated that :

1) if $H'(z)$ is fulfilling (4.12a), then $H'(z)$ is certified to be real with odd denominator due to (2.101b), to feature an odd phase, and to belong to a real lossless two-port N of symmetric type; or
2) if $H'(z)$ is verifying (4.12b), then $H'(z)$ has a para-even and circularly symmetric denominator following (2.101a), such that the phase response of $H'(z)$ is purely even if $H'(z)$ is irreducible. Moreover, assigning the stable poles of $H'(z)$ to $H_1(z)$, and the unstable ones to $1/H_2(z)$, and specifying the constants λ_i of $H_i(z)$, $i=1,2$, as follows according to (2.101a) :

$$\lambda_1=\lambda_2^*=\pm\exp(\pm j\cdot\pi/4),\quad \text{with } \lambda_1^2=\lambda'=\pm j; \tag{4.13a,b}$$

one achieves : $H_1(z)=\overline{H_2(z)}$. (4.13c)

Consequently, considering (3.103) which applies directly to the z-domain, it is proved that $H_i(z)$, $i=1,2$, are belonging to a real lossless two-port N of antimetric type.

In conclusion, it is proved that, irrespective of their possible complex nature, lattice-type bireciprocal WDFs are necessarily and precisely composed of a real symmetric or a real antimetric lossless two-port whenever (4.12a) or (4.12b) are respectively applying, including any equivalent form thereof as (4.10a,b) :

for $q=1$ (i.e. n odd) : N real symmetric two-port; (4.14a)

for $q=-1$(i.e. n even) : N real antimetric two-port. (4.14b)

Complex bireciprocal WDFs are then merely achieved by direct extension of the real network to process complex signals, or using elementary transformations leading to degenerate complex two-ports, as will be seen in the next section.

4.4 Relationships between real and complex bireciprocal WDFs

Following the former considerations, the relationship between the basic real lattice-type lossless two-ports with bireciprocal characteristic function, and the configurations derived thereof to handle complex signals, is indicated in Table 4.1. The vertical mappings merely correspond to passing from filter configurations of Case 1 in Table 3.4 to filters of Case 2 in Table 3.4. From there, it is then possible to transform originally real symmetric (antimetric) filters into degenerate complex antimetric (symmetric) filters proceeding horizontally in Table 4.1, applying the transformations indicated in Table 3.8d. The resulting filters correspond to Case 5 configurations in Table 3.4, an example of their structure being provided in Figure 3.4d.

	Applied I/O signals	Symmetric N		Antimetric N
Bireciprocal of 1st kind (q=1)	Real	Original real symmetric N (Case 1, Table 3.4)		Impossible configuration
		⇓		
	Complex	Derived real symmetric N (Case 2, Table 3.4)	(5) ⇒	Derived degenerate complex antimetric N (Case 5, Table 3.4)
Bireciprocal of 2nd kind (q=−1)	Real	Impossible configuration		Original real antimetric N (Case 1, Table 3.4)
				⇓
	Complex	Derived degenerate complex symmetric N (Case 5, Table 3.4)	(5) ⇐	Derived real antimetric N (Case 2, Table 3.4)

Table 4.1: Relationship between original real bireciprocal WDFs and WDFs derived thereof to process complex signals.

The possibility of realizing the real antimetric lossless two-port N as a complex allpass (cf Subsection 3.4.17 and Case 3 in Table 3.4) is reserved, and does not affect the results above.

---

[5] Horizontal mappings in Table 4.1 imply application of transformations specified in Table 3.8d.

Discussion

The relationships established in Table 4.1 clarify many points regarding bireciprocal filters :

1) It was observed that (4.8a,b), and thus (4.10a,b), and (4.12a,b), are independent of the factor r, although r appears explicitly in (4.6). The reason is that for the original real two-port, q and r are tightly connected, with $q = r = 1$ in the symmetric case, and $q = r = -1$ for the antimetric case. When transforming the original real symmetric (antimetric) WDF into an antimetric (symmetric) one using the transformation in Table 3.8d, $C(\psi) \mapsto \pm j \cdot C(\psi)$, so that (4.6) is replaced by (4.15a), and thus (4.15b) introducing the r' factor of the achieved WDF, with $r' = -r$.

$$C(1/\psi) = -q \cdot r / C(\psi) \quad \Rightarrow \quad C(1/\psi) = q \cdot r' / C(\psi). \qquad (4.15a,b)$$

Hence, the result depends on the interpretation of the same situation. Either one considers (4.15a) when referring to the original real WDF, or one is retaining (4.15b) taking the transformed degenerate complex WDF as reference, in which case the sign change drops. This explains why r has no effect on (4.8), (4.10), and (4.12).

2) Accordingly, the extension of the definition of bireciprocal $C(\psi)$ and bireciprocal WDFs to $q \cdot r = -1$ in (4.6) is not critical.

3) According to (3.38), the filter amplitude response is linked to $|C(j \cdot \phi)|$ which is invariant to the transformation in Table 3.8d. Hence, in case of bireciprocal WDFs, the notion of lowpass/highpass filtering, which is otherwise not well defined for complex filters, applies without problem to the derived degenerate complex WDFs.

4) In [Fett85], many properties that were derived/verified individually for complex bireciprocal WDFs could be achieved more easily recognizing that complex WDFs are obtained through elementary transformations from real bireciprocal WDFs according to Table 4.1. As an example, on p. 898 of [Fett85], one-realness of complex bireciprocal WDFs is proved by showing that (4.6) satisfies the condition (3.98), which is of course true. But demonstrating that (4.6) involves realness of the core bireciprocal WDF is stronger, because this fact implies that many properties are automatically extended to the complex case.

5) As a complement to topic 4), reservations expressed for the complex case can be removed. In [Fett85], p. 896, end of Section III.A, it is stated that the poles of *real* symmetric bireciprocal WDFs designed under specific conditions, e.g. properly designed lowpass/highpass responses (cf Appendix 1 in [Fett85]), are all lying on the unit circle $|\psi|=1$, with negative real part to ensure stability. Later, on p. 897, it is explained that this property does no longer have to be correct for *complex* symmetric bireciprocal WDFs. Again, based on Table 4.1, it is certified that this property extends without restriction to the (degenerate) complex case.

4.5 Configuration of real bireciprocal WDFs

This section aims at establishing the elementary properties of real bireciprocal WDFs of both symmetric and antimetric type.

4.5.1 Phase response of half-band symmetric allpass functions in the ψ-domain

Equations (2.74a,b) and (2.75a) characterizing half-band symmetric allpass functions are equivalently expressed as follows in the ψ-domain, referring to $S'(\psi)$:

$$\varphi_{S'}(\phi)-\varphi_{S'}(0)=\varphi_{S'}(\infty)-\varphi_{S'}(1/\phi);\quad \tau_{S'}(\phi)=\tau_{S'}(1/\phi); \tag{4.16a,b}$$

$$\varphi_{S'}(1)=0.5\cdot[\varphi_{S'}(0)+\varphi_{S'}(\infty)]. \tag{4.16c}$$

where $\varphi_{S'}(\phi)$ and $\tau_{S'}(\phi)$ are the phase and group delay of $S'(j\cdot\phi)$. Furthermore, the ψ-domain counterpart of (2.102a,b) is :

$$S'(\psi=\pm j)=\pm j,\ \forall n,\quad \Leftrightarrow\quad \varphi_{S'}(\phi=\pm 1)=\pm\pi/2+2\pi\cdot\eta,\ \forall n. \tag{4.17a,b}$$

Specifying the phase response of $S_i(j\cdot\phi)$ by $\varphi_i(\phi)$, $i=1,2$, one deduces from (4.9) and (3.70b) :

$$\varphi_{S'}(\phi)=\varphi_1(\phi)-\varphi_2(\phi)=2\cdot\varphi_\Delta(\phi); \tag{4.18}$$

Clearly, due to (3.71) – (3.76), $\varphi_{S'}(\phi=\pm 1)$ in (4.17b) is located in the center of a transition band, implying $|S_{11}(\pm j)|=|S_{21}(\pm j)|$ for both symmetric/antimetric cases, resulting in :

$$|S_{11}(\psi=\pm j)|^2=|S_{21}(\psi=\pm j)|^2=1/2 \tag{4.19}$$

due to the power complementarity of S_{i1}, $i=1,2$. To get proper half-band filters, involving a lowpass (highpass) response for S_{11} (S_{21}) or vice-versa, a single transition band should only exist within $|\phi| \in [0,\infty]$, so that $\eta = 0$ is fixed in (4.17b), leading with (4.16c) to :

$$|\varphi_{S'}(0) + \varphi_{S'}(\infty)| = \pi . \tag{4.20}$$

Finally, $\varphi_{S'}(\phi)$ is specified as indicated in Table 4.2, ϕ_{pass} and ϕ_{stop} corresponding to the passband and stopband edge frequencies, with $\phi_{pass} < 1 < \phi_{stop}$.

Case	$S_{11}(j\cdot\phi)$	$S_{21}(j\cdot\phi)$	$\lvert\phi\rvert \in [0,\phi_{pass}]$	$\lvert\phi\rvert \in [\phi_{stop},\infty]$
1	Lowpass	Highpass	$\varphi_{S'}(\phi) \cong 0$	$\varphi_{S'}(\phi) \cong \pm\pi$
2	Highpass	Lowpass	$\varphi_{S'}(\phi) \cong \pm\pi$	$\varphi_{S'}(\phi) \cong 0$

Table 4.2: Specification of $\varphi_{S'}(\phi)$ according to the desired response of $S_{i1}(j\cdot\phi)$, $i=1,2$.

4.5.2 Real symmetric bireciprocal WDFs

$S'(\psi)$ being real in this case, $\varphi_{S'}(0) = 0, \pm\pi$, so that $\varphi_{S'}(\infty)$ is specified according to Table 4.3. Since $\varphi_{S'}(\infty) - \varphi_{S'}(0) = \pm\pi$ is then verified in any case, and recalling that S_1 (S_2) is assumed stable (unstable), it follows from (2.58) that the degree difference between S_1 and S_2 is 1. n_i, $i=1,2$, are then interrelated as indicated in Table 4.3.

Case	λ	$\varphi_{S'}(\phi=0)$	$\varphi_{S'}(\phi=+1)$	$\varphi_{S'}(\phi=\infty)$	n_i, $i=1,2$.
1	-1	$+\pi$	$+\pi/2$	0	$n_1 = n_2 - 1$
2	1	0	$-\pi/2$	$-\pi$	
3	1	0	$+\pi/2$	$+\pi$	$n_1 = n_2 + 1$
4	-1	$-\pi$	$-\pi/2$	0	

Table 4.3: Specifications of $\varphi_{S'}(0)$, $\varphi_{S'}(\infty)$, and interrelation between n_i, $i=1,2$.

Pole configurations in the z-domain

The pole configurations of $H'(z)$ are verifying (2.92a-d), as illustrated in Figure 2.21 (real case). Since the degree n of $H'(z)$ is odd, there is at least one pole at $z=0$, which is stable, and thus assigned to $H_1(z)$ that was assumed stable. According to this scheme, the

degree of H_1 (H_2) is necessarily odd (even), resulting in the specifications (4.21a,b) examplified in Table 4.4.

$$n=2k+1; \quad n_1=n_2+(-1)^k=[n+(-1)^k]/2; \quad \text{with } k\in\mathbb{N}_+. \qquad (4.21a,b)$$

k	1	2	3	4	5	6
n	3	5	7	9	11	13
n_1	1	3	3	5	5	7
n_2	2	2	4	4	6	6

Table 4.4: Specification of n_i, $i=1,2$, in function of k and n (low degrees).

All remaining poles of $H'(z)$ are allocated to H_1 and $1/H_2$ according to their stability [6]. Clearly, H_1 and H_2 can be reformulated as follows using (2.99):

$$H_1(z)=z^{-1}\cdot\hat{H}_1(z^2), \quad H_2(z)=\hat{H}_2(z^2); \qquad (4.22a,b)$$

so that :

$$H_1(z)=-H_1(-z), \quad H_2(z)=H_2(-z); \qquad (4.23a,b)$$

$H'(z)=H_1(z)/H_2(z)$ verifying again (4.12a).

The form of H_1 and H_2 in (4.22) is quite well known for real symmetric bireciprocal networks [Noss83, Gazs85a, Fett86, Vaid93], and leads to drastic reductions in terms of hardware resources, computation throughput, and power consumption, especially for multirate filterbank implementations, as cited in the mentioned references.

Pole configurations in the ψ-domain

For consistency, the pole configurations (2.92a,b,c,d) are provided below in the ψ-domain :

$$\psi_{\infty 1}=-1 \quad \Rightarrow \quad \text{self-reciprocal poles;} \qquad (4.24a)$$

$$\psi_{\infty 1}\in\mathbb{C}, \ |\psi_{\infty 1}|=1, \text{ and } \psi_{\infty 2}=\psi_{\infty 1}^*, \text{ with } \psi_{\infty 1}\neq -1 \quad \Rightarrow \quad \text{complex conjugate poles;} \qquad (4.24b)$$

---

[6] According to the described pole allocation scheme, all remaining poles potentially located at the origin, occurring in this case pairwise, would be logically assigned to H_1. This avoids a simultaneous appearance of identical poles within both H_i, $i=1,2$, which could then be factorized out of the filter.

$$\psi_{\infty 1} \in \mathbb{R},\ \psi_{\infty 1} \neq -1, \text{ and } \psi_{\infty 2} = 1/\psi_{\infty 1} \quad \Rightarrow \text{ paired reciprocal poles;} \tag{4.24c}$$

$$\psi_{\infty 1} \in \mathbb{C},\ |\psi_{\infty 1}| \neq 1, \text{ and } \psi_{\infty 2} = 1/\psi_{\infty 1},\ \psi_{\infty 3} = \psi_{\infty 1}^*,\ \psi_{\infty 4} = 1/\psi_{\infty 1}^* \quad \Rightarrow \text{ quadruplet poles;} \tag{4.24d}$$

where the poles (4.24a) belong to $S_1(\psi)$ only, according to the former convention. Consequently to (4.24), it is noted that the denominators of (stable) S_i are circularly symmetric, cf (A.36a).

Tbe ψ-domain pole constellations and their z-domain counterparts are represented in Table 4.5a and Table 4.5d, respectively, the relative position of the poles matching from one domain to the other (only stable poles are considered in Table 4.5).

Finally, it is demonstrated that (4.23a,b) is equally expressed by :

$$S_i(1/\psi) = (-1)^i \cdot S_i(\psi), \quad i = 1,2. \tag{4.25}$$

4.5.3 Real antimetric bireciprocal WDFs

For real antimetric bireciprocal WDFs, the degree n of $H'(z)$, and thus $S'(\psi)$, is even, with an equal number of stable and unstable poles, cf Figure 2.21d, to be distributed over H_i (S_i), $i = 1,2$, so that the next formulas are established :

$$n = 2k; \quad n_1 = n_2 = n/2; \quad \text{with } k \in \mathbb{N}_+. \tag{4.26a,b}$$

Table 4.6 is then specifying $\varphi_{S'}(0)$ and $\varphi_{S'}(\infty)$ in accordance with (4.20). Two new terms appear with respect to the symmetric situation in Table 4.3, namely δ and k.

Case	λ	$\varphi_{S'}(\phi = 0)$	$\varphi_{S'}(\phi = +1)$	$\varphi_{S'}(\phi = \infty)$	$S'(\psi)$
1	$-(-1)^k\, j$	$+\pi - (-1)^k \cdot \delta$	$+\pi/2$	$(-1)^k \cdot \delta$	Same poles for Cases 1 + 2
2	$(-1)^k\, j$	$-(-1)^k \cdot \delta$	$-\pi/2$	$-\pi + (-1)^k \cdot \delta$	
3	$-(-1)^k\, j$	$(-1)^k \cdot \delta$	$+\pi/2$	$+\pi - (-1)^k \cdot \delta$	Same poles for Cases 3 + 4 (conjugate of Cases 1 + 2)
4	$(-1)^k\, j$	$-\pi + (-1)^k \cdot \delta$	$-\pi/2$	$-(-1)^k \cdot \delta$	

Table 4.6: Specifications of $\varphi_{S'}(0)$, $\varphi_{S'}(\infty)$, in connection with factor k from (4.26a), and with $\delta \geq 0$ (Table valid for prototype filters).

	In the ψ-domain	In the z-domain
Bireciprocal $C(\psi)$ **of 1st kind** $(q=1)$	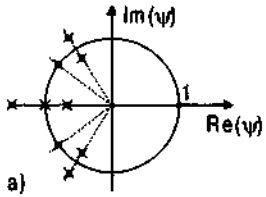 a) *Pole configurations for* S_i [7]	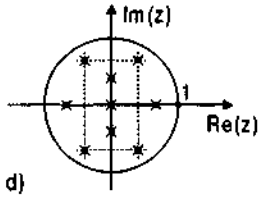 d) *Pole configurations for* H_i [8]
Bireciprocal $C(\psi)$ **of 2nd kind** $(q=-1)$	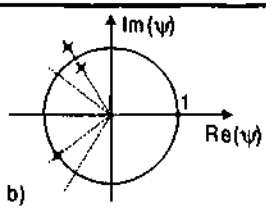 b) *Pole configurations for* S_1 ⇕ 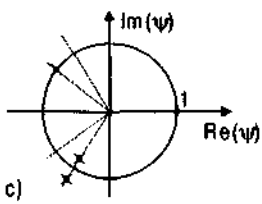 c) *Pole configurations for* S_2	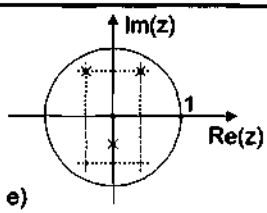 e) *Pole configurations for* H_1 [9] ⇕ 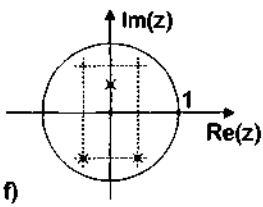 f) *Pole configurations for* H_2 [9]

Table 4.5: Pole arrangements for lattice-type lossless two-ports featuring a bireciprocal characteristic function in the ψ-domain, and their counterpart expressed in the z-domain ($i=1,2$).

---

[7] The denominators of stable S_i are circularly symmetric (CS) polynomials.

[8] The denominator of H_1 is an odd polynomial containing at least one zero at the origin. Conversely, the denominator of H_2 is even and devoid of any zero at the origin.

[9] The denominators of H_i are para-even (para-odd) polynomials for an even (odd) number of purely imaginary poles.

The factor $\delta \geq 0$ takes into account the fact that the even phase response of $S'(\psi)$ is not constrained to go through an integer multiple of π at $\phi = 0, \infty$. The factor k, specifying the degree of $S'(\psi)$ in (4.26a), determines the number of possible phase ripples occurring within the passband/stopband, and influences therefore $\varphi_{S'}(\phi = 0, \infty)$. Examples explaining the relationship are given in Figure 4.2 and 4.3. k is in addition also affecting λ due to sign changes indicated in Table 2.15.

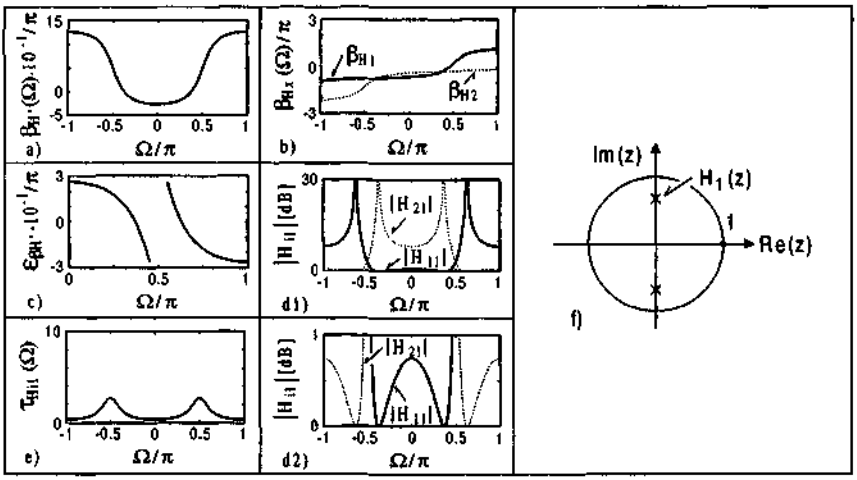

Figure 4.2: 2nd-order real antimetric bireciprocal WDF (prototype resp.) (specifications: $\beta_{H'S}(\Omega) = 0$, for $|\Omega| \in [0, 0.45 \cdot \pi]$ and $\beta_{H'S}(\Omega) = \pi$, for $|\Omega| \in [0.55 \cdot \pi, \pi]$):

a) Unwrapped phase $\beta_{H'}$;
b) Unwrapped β_{H1}, β_{H2};
c) Residual approx. error;
d1) Attenuation $|H_{11}|$, $|H_{21}|$;
d2) Passband attenuation;
e) Group delay of H_{i1};
f) Pole configuration of H_1, H_2.

		ν	θ_i/π, $\mathrm{Re}\{z_{\infty i\nu}\}$	$\mathrm{Im}\{z_{\infty i\nu}\}$
H_1	θ_1/π	—	+ 0.25	—
	$z_{\infty 1\nu}$	1	0	0.67985845889550
H_2	θ_2/π	—	− 0.25	—
	$z_{\infty 2\nu}$	1	$z_{\infty 21} = z^*_{\infty 11}$	

Table 4.7: Parameters specifying the filter illustrated in Figure 4.2.

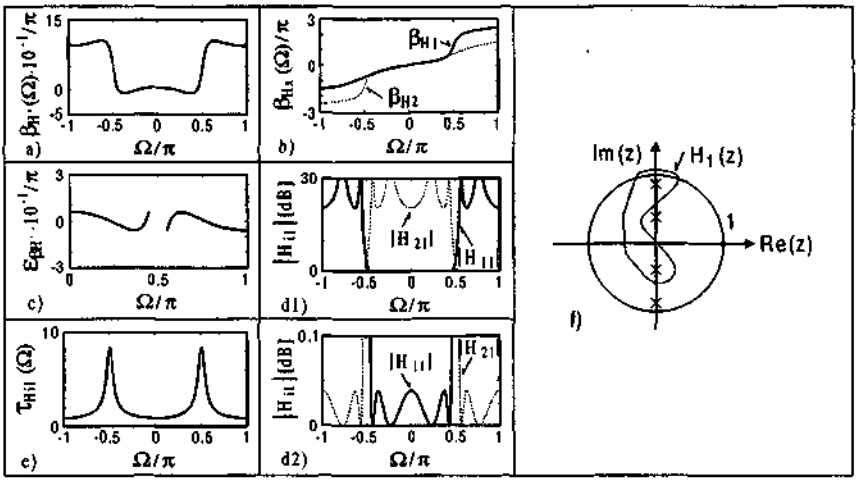

Figure 4.3: **4th-order real antimetric bireciprocal WDF** (prototype resp.) (specifications: $\beta_{H'_S}(\Omega)=0$, for $|\Omega| \in [0, 0.45\cdot\pi]$ and $\beta_{H'_S}(\Omega)=\pi$, for $|\Omega| \in \{0.55\cdot\pi, \pi]$):
a) Unwrapped phase $\beta_{H'}$; d1) Attenuation $|H_{11}|$, $|H_{21}|$;
b) Unwrapped β_{H1}, β_{H2}; d2) Passband attenuation;
c) Residual approx. error; e) Group delay;
f) Pole configuration of H_1, H_2.

		ν	θ_i/π, $\mathrm{Re}\{z_{\infty i\nu}\}$	$\mathrm{Im}\{z_{\infty i\nu}\}$
H_1	θ_1/π	—	−0.25	—
	$z_{\infty 1\nu}$	1	0	0.86771611627277
		2	0	−0.38691676301199
H_2	θ_2/π	—	+0.25	—
	$z_{\infty 2\nu}$	1	$z_{\infty 21} = z^*_{\infty 11}$	
		2	$z_{\infty 22} = z^*_{\infty 12}$	

Table 4.8: **Parameters specifying the filter illustrated in Figure 4.3.**

Pole configurations in the z-domain

The pole configurations of $H'(z)$ are satisfying (2.94a,b), as shown in Figure 2.21d, the stable (unstable) poles being allocated to H_1 $(1/H_2)$, while applying (4.13a) and (4.13c). Figures 4.2 and 4.3 illustrate the effect of parameters δ and k, based on simple examples of second- and fourth-order allpass filters $H'(z)$ approximated in the equiripple sense, corresponding both to Case 3 of Table 4.6.

Based on (2.97a) but excluding real poles, so that $N_0 = 0$ in (2.97a), one demonstrates :

$$H_i(-z) = (-1)^{n_i} \cdot \lambda_i^2 \cdot \overline{H_i(z)}; \tag{4.27}$$

which results in the next equations making use of (4.13) :

$$H_1(z) = (-1)^{n/2} \cdot \lambda' \cdot H_2(-z) = \pm j \cdot H_2(-z), \tag{4.28a}$$

$$H_2(z) = (-1)^{n/2} \cdot \lambda'^* \cdot H_1(-z) = \mp j \cdot H_1(-z). \tag{4.28b}$$

so that $H'(z) = H_1(z)/H_2(z)$ is confirmed to satisfy (4.12b). The implementation simplifications of H_1 and H_2 are discussed in Subsection 2.6.5 [Meer83, Vaid87a].

Pole configurations in the ψ-domain

The pole configurations (2.94a,b) become in the ψ-domain :

$$\psi_{\infty 1\nu} \in \mathbb{C}, \; |\psi_{\infty 1\nu}| = 1 \quad \Rightarrow \quad \text{self-para-reciprocal pole } \psi_{\infty 1\nu}; \tag{4.29a}$$

$$\psi_{\infty 1\nu} \in \mathbb{C}, \; |\psi_{\infty 1\nu}| \neq 1 \quad \Rightarrow \quad \text{paired poles}(\psi_{\infty 1\nu}, 1/\psi^*_{\infty 1\nu}). \tag{4.29b}$$

Moreover, (4.13a) and (4.28) result in :

$$S_i(\psi) = \overline{S_{(3-i)}(\psi)}; \quad i = 1,2 \tag{4.30}$$

$$S_1(\psi) = \pm j \cdot S_2(1/\psi), \quad S_2(\psi) = \mp j \cdot S_1(1/\psi) \tag{4.31a,b}$$

The denominators of stable S_i are shown to be para-circularly symmetric, cf (A.42a). The ψ-domain pole configurations and their corresponding z-domain counterparts are represented in Table 4.5b,c and Table 4.5e,f, respectively.

4.6 Configuration of complex bireciprocal WDFs

Based on the real bireciprocal WDF configurations described in Section 4.5, and on the relationships linking complex to real bireciprocal WDFs as described in Table 4.1, it is possible to establish the synoptic Tables 4.9 and 4.10 covering all cases.

4.6.1 Output signals achieved for a cascade of analysis and synthesis bireciprocal WDFs

Hence, the output signals $b_i(nT_s)$, $i=1,2$, of the half-band filter network depicted in Figure 4.1 and specified in (4.4a,b), are taking the next form in the real and complex lattice-type case :

$$b_1(nT_s) = 0.5 \cdot r \cdot S_1(\psi) \cdot S_2(\psi) \cdot [A_1 \cdot e^{p \cdot n \cdot T_s}], \tag{4.32a}$$

which is independent of q, and :

$$b_2(nT_s) = (-1)^{n_1} \cdot r \cdot e^{j\Omega \cdot n/2} \cdot b_1(nT_s), \quad \text{for } q=1; \tag{4.32b}$$

$$b_2(nT_s) = \mp j \cdot r \cdot e^{j\Omega \cdot n/2} \cdot b_1(nT_s), \quad \text{for } q=-1. \tag{4.32c}$$

Usually, the output $b_2(nT_s)$ is dropped.

		Bireciprocal filters of first kind ($q=+1$)		Bireciprocal filters of second kind ($q=-1$)	
		Characteristic function	**Constitutive allpass fcts**	**Characteristic function**	**Constitutive allpass fcts** [10]
Degree of two-port *(cf [Fett85], page 897)*		n **odd**		n **even**	
Degree of constitutive allpass functions		$n=n_1+n_2=2\cdot k+1,\quad k\in\mathbb{N}_+$: $n_1=n_2+(-1)^k=[\,n+(-1)^k\,]/2$		$n=n_1+n_2,\quad n_1=n_2=n/2$	
Symmetric case	**Complex I/O signals**	$C(1/\psi)=+1/C(\psi)$ with $C(\psi=\pm1)\in\mathbb{R}$	$S_i(1/\psi)=$ $=(-1)^i\cdot S_i(\psi)$	$C(1/\psi)=-1/C(\psi)$ [11] with $j\cdot C(\psi=\pm1)\in\mathbb{R}$	$S_1(1/\psi)=\pm j\cdot S_2(\psi)$ $S_2(1/\psi)=\mp j\cdot S_1(\psi)$
	Real I/O signals				
Antimetric case	**Complex I/O signals**	$C(1/\psi)=-1/C(\psi)$ [11] with $j\cdot C(\psi=\pm1)\in\mathbb{R}$	$S_i(1/\psi)=$ $=(-1)^i\cdot S_i(\psi)$	$C(1/\psi)=+1/C(\psi)$ with $C(\psi=\pm1)\in\mathbb{R}$	$S_1(1/\psi)=\pm j\cdot S_2(\psi)$ $S_2(1/\psi)=\mp j\cdot S_1(\psi)$
	Real I/O signals				$S_1(1/\psi)=\pm j\cdot\overline{S_1(\psi)}$ $S_i(\psi)\quad=\overline{S_{(3-i)}(\psi)}$

Table 4.9: Lattice-type lossless two-ports featuring a bireciprocal characteristic function (ψ -domain, $i=1,2$).

[10] S_1 and S_2 should be both selected either with upper, or with lower sign.

[11] The perfect signal reconstruction condition is expressed in function of the original real bireciprocal WDF, cf (4.15a).

		Bireciprocal filters of first kind ($q=+1$)		Bireciprocal filters of second kiod ($q=-1$)	
		Characteristic function	Constitutive allpass fcts	Characteristic function	Constitutive allpass fcts [12]
Degree of two-port *(cf [Fett85], page 897)*		n odd		n even	
Degree of constitutive allpass functions		$n=n_1+n_2=2\cdot k+1, \quad k\in\mathbb{N}_+$: $n_1=n_2+(-1)^k=[\,n+(-1)^k\,]/2$		$n=n_1+n_2, \quad n_1=n_2=n/2$	
Symmetric case	Complex I/O signals	$C_z(-z)=+1/C_z(z)$ with $C_z(z=0,\infty)\in\mathbb{R}$	$H_i(-z)=$ $=(-1)^i\cdot H_i(z)$	$C_z(-z)=-1/C_z(z)$ [11] with $jC_z(z=0,\infty)\in\mathbb{R}$	$H_1(-z)=\pm j\cdot H_2(z)$ $H_2(-z)=\mp j\cdot H_1(z)$
	Real I/O signals				
Antimetric case	Complex I/O signals	$C_z(-z)=-1/C_z(z)$ [11] with $jC_z(z=0,\infty)\in\mathbb{R}$	$H_i(-z)=$ $=(-1)^i\cdot H_i(z)$	$C_z(-z)=+1/C_z(z)$ with $C_z(z=0,\infty)\in\mathbb{R}$	$H_1(-z)=\pm j\cdot H_2(z)$ $H_2(-z)=\mp j\cdot H_1(z)$
	Real I/O signals				$H_1(-z)=\pm j\cdot\overline{H_1(z)}$ $H_i(z)=\overline{H_{(3-i)}(z)}$

Table 4.10: Lattice-type lossless two-ports featuring a bireciprocal characteristic function, expressed in the z-domain ($i=1,2$).

[12] H_1 and H_2 are simultaneously chosen either with upper, or with lower sign.

4.7 Implementation structures

Knowing all features of complex / real bireciprocal lossless two-ports/ WDFs, it is possible to determine their implementation structure.

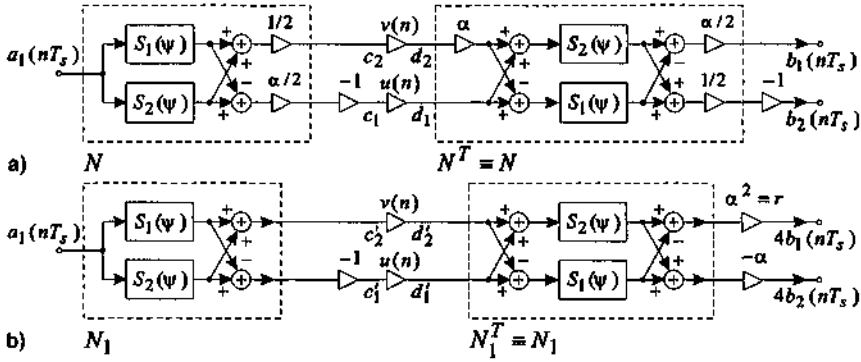

Figure 4.4: General coofiguratioo according to Fig. 4.1 for bireciprocal lossless two-ports (lattice-type case only) (ψ-domain, $\forall\, q, r$): a) Complete structure; b) Simplified represention.

Figure 4.4a preseots the general network after Figure 4.1, when replacing the two-port N by the detailed structure of symmetric or antimetric two-ports, according to Fig. 3.8 and Fig. 3.9. Figure 4.4 is valid for any q and r, with constant α defined as :

$$\alpha = 1/\sqrt{r} \quad \Leftrightarrow \quad \alpha = \begin{cases} 1, & \text{for } r = 1 \quad \text{(symmetric case)} \\ 1/j, & \text{for } r = -1 \quad \text{(antimetric case).} \end{cases} \tag{4.33}$$

Figure 4.4b is achieved after elemeotary rescaling [13] performed only to simplify later figures on tbe discrete-time network implemeotation. The two-port N is relabeled N_1 due to rescaling. The same is done for the signals c_i, d_i, which become c_i', d_i', $i = 1,2$. It is noted that the analysis and synthesis two-ports are kept identical in their internal structure io Figure 4.4, so as to preserve implementation modularity (nsage of same components for time-multiplexed or

[13] Optimal signal scaling of the whole network configuration in Fig. 4.4b and later figures derived thereof should be explicitly done for each application.

duplicated instanciation). Further modifications could otherwise be introduced into Figure 4.4b, e.g. to ensure proper intermediate signal scaling.

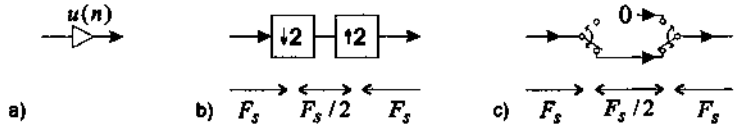

Figure 4.5: Equivalent representations of signal multiplication by $u(n)$:
a) Original operation in the ψ-domain;
b) Decimation / interpolation stage in the z-domain;
c) Representation involving memoryless switches [Croc83].

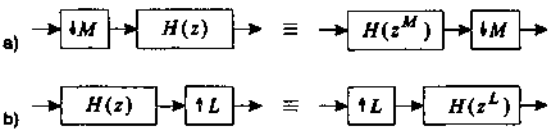

Figure 4.6: Noble identities for multirate networks [Vaid93] :
a) First identity; b) Second identity.

The different representations for signal multiplication, and the noble identities used for multirate signal processing, are recalled in Figures 4.5 and 4.6, respectively. It is important to notice that when using decimation and interpolation operators in the z-domain, as illustrated in Figure 4.5b and Figure 4.6, all signals of the network are assumed to be synchronized, i.e. *in phase*, with respect to the highest sampling signal. This feature is ensured for $q=1$, whereas care should be taken for $q=-1$.

4.7.1 Bireciprocal networks of first kind (complex and real cases)

The discrete-time implementation is then achieved from Figure 4.4b and Figure 4.5b for bireciprocal networks of the first kind ($q=1$), as depicted in Figure 4.7a. The digital network is labelled N_2, and tbe actual sampling frequency is mentioned below the corresponding structures. According to (4.21b), the two-port N_2 illustrated in Fig. 4.7a features odd and even degrees n_1 and n_2 for the constituent

allpass functions H_1 and H_2, respectively [14], which are labeled according to (4.22a,b).

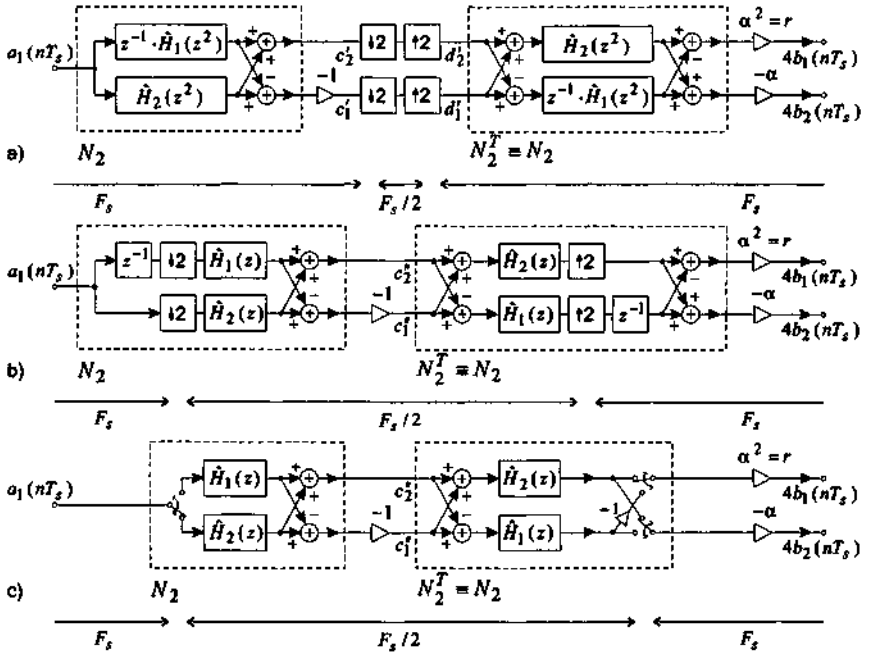

Figure 4.7: Discrete-time implementation for $q = 1$, $\forall r$:
a) z-domain representation of Fig. 4.4b (n_1 odd, n_2 even);
b) Structure after use of noble identities (n_1 odd, n_2 even);
c) Switch-level representation (switches with memory effect; structure independent of the relative parity of n_1 and n_2).

Figure 4.7b is then obtained after application of the noble identities, and the switch-level representation of the discrete-time implementation is finally provided in Figure 4.7c. Figure 4.7c was formerly presented in [Fett85] for symmetric networks only.

An important notice has to be made here regarding the behavioral interpretation of switches occurring in multirate networks. Indeed,

[14] It is noted that the odd (even) degree allocated to n_1 (n_2) does not affect at all the final implementation structure depicted in Figure 4.7c, which is general.

the switches are sometimes assumed to operate memoryless, transferring the data instantaneously from input to output, whereas they are supposed to include a memory effect in other situations.

In case of Figure 4.7c, the switches are incorporating a memory function. While the closed path of each switch is transferring the data, the disconnected lead is actually memorizing the signal value provided at the former sampling period, referring to the highest sampling rate related to the switch (valid for both decimation and interpolation stages). In terms of a concrete realization, this means that the corresponding data should be stored in a memory or register.

4.7.2 Bireciprocal networks of second kind (complex and real cases)

For bireciprocal-type two-ports of the second kind ($q=-1$), there are two implementation possibilities, depending on whether the signals c_1' and c_2' in Figure 4.4b should be conveyed synchronously from the analysis to the synthesis two-port, or not.

The asynchronous case, i.e. where c_1' and c_2' are transferred out of phase, is discussed first. The implementation structure is merely obtained by noticing that only one of the signals c_1' and c_2' in Figure 4.4b is actually transmitted at a time. As shown in Figure 4.8, the path between the analysis and synthesis two-ports can thus be time-multiplexed. Any intermediate signal processing, e.g. signal conditioning for communication purposes, or signal compression/decompression, could be performed similarly. Further simplifications e.g. relying on noble identities, are not possible for $q=-1$, as already mentioned before. Finally, it is remarked that the switches occurring in Fig. 4.8 are devoid of any memory effect, and that the whole network configuration, including transfer channel between analysis and synthesis two-ports, is operating at highest sampling frequency F_s.

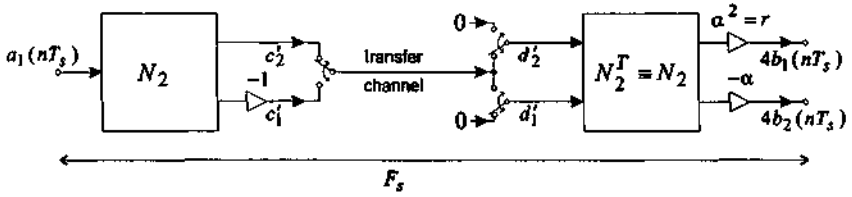

Figure 4.8: Discrete-time implementation of first type for $q = -1$, $\forall r$ (memoryless switches).

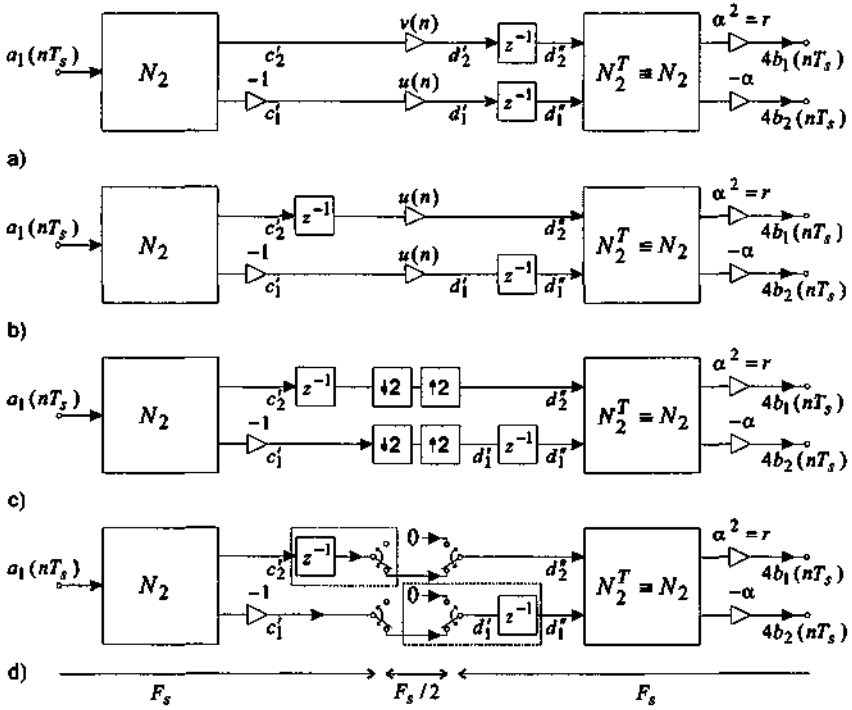

Figure 4.9: Discrete-time implementation of second type for $q = -1$, $\forall r$;
a) z-domain representation of Fig. 4.4b, with delay insertion;
b) Modified structure letting appear two multipliers $u(n)$;
c) Replacement of multipliers by decimator/interpolation stages;
d) Switch-level representation (memoryless switches, cf text).

The second approach for implementing bireciprocal two-ports of the second kind consists in transforming the structure in Figure 4.4b so that both paths between the analysis and synthesis two-ports operate in phase, replacing $v(n)$ by $u(n)$. Therefore, two unit-delays are first introduced at the cross-section of the whole structure, at level of signals d_1' and d_2', cf Figure 4.9a. The output signals of the unit-delays are labeled d_1'' and d_2''. Next, observing that the *steady-state* values of $v(n)$ and $u(n)$ fulfill $v(n)=u(n\pm1)$ [15], the following expression is verified :

$$\begin{aligned} d_2''(n) &= d_2'(n-1) = v(n-1)\cdot c_2'(n-1) \\ &= u(n)\cdot c_2'(n-1), \end{aligned} \tag{4.38}$$

leading to Figure 4.9b [Gala84, Fig. 10]. Clearly, the signals c_1' and c_2' can now be conveyed *in phase* from the analysis to the synthesis two-ports, at cost of two delay elements, and an increase of the overall group delay by one sampling period. The data transfer is performed using two channels operating at half the sampling rate.

Figures 4.9c and 4.9d are then merely obtained using Figure 4.5. Again, further simplifications relying on noble identities are not possible ($q\approx-1$). It is noticed that the switch-level representation provided in Figure 4.9d relies on memoryless-type switches [16].

4.7.3 Case of real antimetric bireciprocal networks

The results provided in Figures 4.8 and 4.9 can be specialized for real antimetric networks as depicted in Figure 4.10. Figure 4.10a shows the basic configuration in the ψ-domain. It is derived directly from Figure 4.4a, where Figures 3.17b and 3.17d were selected for illustration purposes for the analysis and synthesis two-ports, respectively. Figure 4.10b presents the discrete-time implementation of first type according to Figure 4.8, whereas the second type of

---

[15] Causality is here of no concern since $v(n)$ and $u(n)$ are deterministic signals.

[16] The dashed areas in Fig. 4.9d involving each a unit-delay and a switch, could as well be interpreted as switches with memory effect. This notation would however be problematic, because of the simultaneous occurrence of two different types of switches in the same schematic, namely with and without memory effect. The representation of Fig. 4.9d is therefore preferred in this report.

implementation is drawn Figures 4.10c1 and 4.10c2, which are respectively equivalent to Figures 4.9c and 4.9d.

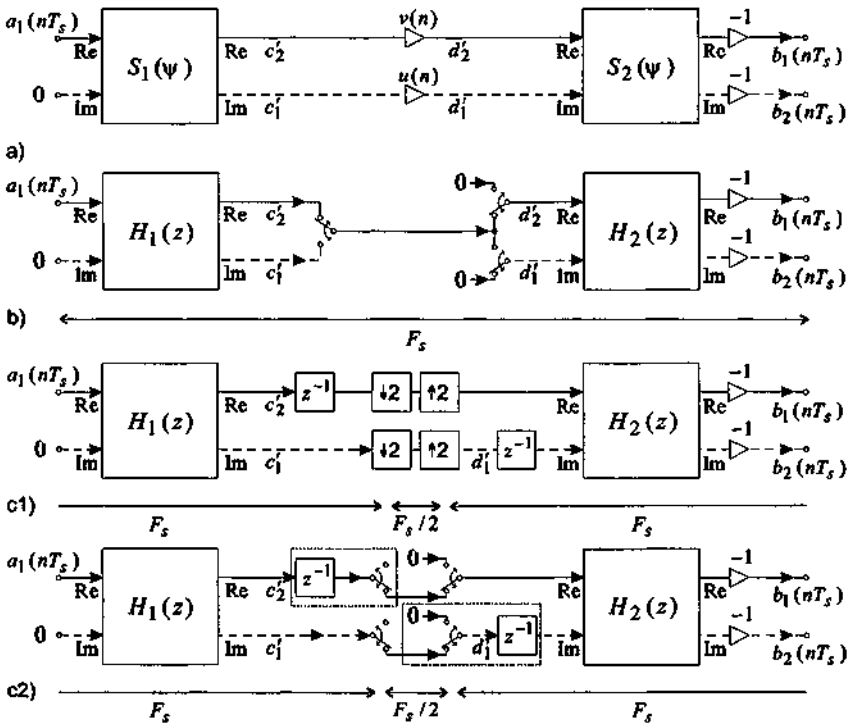

Figure 4.10: Real antimetric case $q = r = -1$:
a) Original structure after Fig. 4.4a (selected allpass fcte);
b) Discrete time implementation of 1st type (memoryless switches);
c) Discrete time implementation of 2nd type :
c1) Structure corresponding to Fig. 4.9c;
c2) Switch-level representation (memoryless switches).

4.7.4 Discussion

It was found that some publications dealing with the discrete-time implementation of analysis/synthesis networks based on real antimetric bireciprocal filters, are intermixing the switch-level represen-

tations of Figure 4.10b and Figure 4.10c2, i.e. of the first and second types of implementation structures.

Indeed, Figure 19a in [Vaid87a] is noticed to be identical to Figure 4.10c1, taking into account the factor $r=-1$ in (4.32a), letting think that the referred structure is based on the implementation of second type according to the classification of this report, with synchronized data transfer between analysis and synthesis two-ports, and additional delay. However, the switch-level representation provided in Figure 19b of [Vaid87a] corresponds to a direct implementation of the original structure in Figure 4.4a, functionally equivalent to the first implementation in Figure 4.10b, without additional delay, i.e. where the data are transferred out of phase over the channel. Hence, both implementation structures were mixed up in that paper.

In a later publication of the same authors, the switch-level implementation of Figure 4.10b is mentioned again in Figure 18 of [Rega88b], but without explicit reference to Figure 4.10c1, so that no conclusion can be drawn from that paper [17].

4.7.5 Comparison of half-band filter structures at signal processing level

A signal processing level comparison of bireciprocal half-band filter structures is made in Table 4.11. It is observed that bireciprocal WDFs of the first kind ($q=1$) naturally offer a synchronized data transfer of both channels at decimated rate, thus allowing for potential joint signal processing between the sub-sampled channel signals. This feature can be exploited in certain speech and image subband compression algorithms exploiting channel cross-correlation, e.g. [Wong97], which can be processed at decimated rate.

On the other hand, bireciprocal WDFs of the second kind ($q=-1$) are essentially conveying data that are out of phase, since the original signals c_1' and c_2' were sampled out phase. However, inserting a delay into each path, it is possible to synchronize the channel signals for data transfer purposes only, without changing the fact that the original signals c_1' and c_2' were acquired out of phase. Hence, in case

[17] Opportunity to discuss the subject directly with the authors of [Vaid87a, Rega88b] was not given.

the sub-sampled channel signals are undergoing a joint signal processing algorithm operated at decimated rate, it may be necessary to re-synchronize the data, e.g. using a costly signal interpolation filter approximating a fractional delay of $T_s/2$ [Laak96], with (considerably) increased group delay.

Clearly, it becomes apparent from this discussion that to achieve an overall optimal solution, it is essential to choose the type of bireciprocal network configuration – selection of a bireciprocal WDF of first/second kind, and in the latter case, selection of the first/second type of structure, cf Figures 4.8 and 4.9 – according to the *global* application requirements.

q	Type	c_1', c_2' sampled in phase	Path between analysis and synthesis two-ports			Overall group delay [T_s]	Fig. ref.
			In phase data transfer	Nb requested channels x rate	Signals can be jointly processed [18]		
+1		Yes	Yes	$2 \times F_s/2$	Yes	τ_{g1}	4.7
−1	1	No	No	$1 \times F_s$	cf [19]	τ_{g2}	4.8
	2	No	Yes	$2 \times F_s/2$	cf [19]	$\tau_{g2}+1$	4.9

Table 4.11: Synopsis of properties related to complex/real bireciprocal network configurations based on Fig. 4.4 ($\forall r$).

[18] Joint signal processing between the sub-sampled channel signals, processed at decimated rate (e.g. speech and image compression algorithms exploiting channel cross-correlation).

[19] The original signals c_1' and c_2' being sampled out of phase, it may be necessary to adjust the joint signal processing algorithms operating on the sub-sampled signals, e.g. using a signal interpolation filter approximating a fractional delay of $T_s/2$, at cost of increased group delay.

4.8 Conclusion

Motivated by the former publication [Fett85], the main object of the chapter was to study the class of complex bireciprocal WDFs, emphasizing lattice-type structures. Initially perceived as a generalization of real bireciprocal WDFs which are currently used for multirate signal processing, but also for economic implementations of monorate filters, the subject of complex bireciprocal WDFs rised interesting questions concerning the distribution of the spectral signal energy with respect to the real case, possible pole constellations, and detailed implementation structures.

Actually, based on Theorem 3 from Chapter 2, it is demonstrated in Chapter 4 that any kind of lattice-type WDF featuring a biraciprocal characteristic function is necessarily relying on a *real* bireciprocal network, which may undergo elementary two-port transformations resulting then in *degenerate* complex bireciprocal WDFs, as was illustrated in Table 4.1. This result helped in clarifying the interpretation of former achievements elaborated in [Fett85], while removing reservations that were expressed in the same reference.

Simultaneously, the same result rises the question of the usefulness of degenerate complex bireciprocal WDFs, a topic that was not handled in the report, further studies on application fields being needed.

The chapter proposes additionally synoptic tables specifying all possible bireciprocal WDF arrangements, including corresponding pole configurations, and discusses in detail the available discrete time implementation structures.

Contributions

To the best knowledge of the author, the next contributions proposed in the chapter are considered as original:

- **C4–I**: As a complementary contribution to [Fett85], formal demonstration establishing that any IIR-based half-band filter realized in form of a lattice-type lossless two-port is precisely composed of a real symmetric or real antimetric lossless two-port (Section 4.3), including identification of the relationships between all possible bireciprocal WDF configurations, cf Table 4.1.

- **C4–II**: Elaboration of synoptic tables summarizing all possible configurations of lattice-type lossless networks featuring a bireciprocal characteristic function, expressed in both ψ- and z-domains, cf Tables 4.9 and 4.10, including precise list of possible pole constellations provided in Table 4.5.
- **C4–III**: Detailed analysis of discrete-time implementation structures for bireciprocal networks of the second kind (Subsection 4.7.2), distinguishing two implementation structures depicted in Figures 4.8 and 4.9, including specialization thereof for the real antimetric case presented in Figure 4.10. Moreover, a comparison at signal processing level of half-band filter structures is provided in Subsection 4.7.5, resulting in Table 4.11.

Further potential research

The following subjects are proposed for potential further research:

- Study of *non-reciprocal* and *general reciprocal* lossless signal analysis/synthesis pairs offering a perfect signal reconstruction, identifying their properties and possible fields of application.
- Identify applications that could benefit from implementations relying on bireciprocal networks of the second kind, potentially including joint processing between sub-sampled channel signals executed at decimated rate.
- Identify possible applications needing *degenerate complex bireciprocal filters*.
- Others.

Chapter 5
Design of Lattice-Type WDFs

5.1 Introduction

This chapter proposes two extensions of the filter design framework that was devised in [Gazs85a] for symmetric lattice WDFs. The first extension, discussed in Section 5.2, concerns the design of prototype antimetric lattice-type WDFs, obtained by revising a subset of the design equations used in [Gazs85a], and adapting the pole distribution scheme to the antimetric case, providing a series of examples to illustrate the results.

The second extension handled in Section 5.3 covers the design of so-called warped bireciprocal lattice-type WDFs, which can be perceived as a generalization of bireciprocal filters, and offer an interesting approach to achieve multiplierless filter implementations in the symmetric case [Gazs85b, Güll86, Mili97, Mili99]. Section 5.3 recalls specific formulas characterizing warped bireciprocal filters, and furnishes the fundamental equation these filters rely on, before explaining how their design can be embedded in the framework described in [Gazs85a]. Both symmetric and antimetric cases are treated, whereas it is noticed that suitable antimetric lattice-type WDF implementations are presently not identified to fully exploit the potentialities offered by warped bireciprocal filters.

The contributions of Sections 5.2 and 5.3 can be merged, leading to an enriched design framework that is easy to use also for non-

specialists, and presents a general interest that is not exclusively connected to the realization of Wave Digital Filters.

At the end of the chapter, conclusions are drawn in Section 5.4, with a discussion of further possible research activities related to the subject.

5.2 Design of prototype antimetric lattice-type WDFs

Based on his former publication [Darl70], Darlington proposed in [Darl78] a remarkably simple and efficient method for the approximation of odd-degreed elliptic lowpass filters. This method proceeds by elementary transformation of the original filter into a modified filter with enlarged transition band, the procedure being recursively applied several times until the transition band is considered sufficiently wide (or equivalenty until both pass- and stopbands become suitably narrow) to approximate the passband and stopband in the minimax sense using formulas for Cbebyshev filters. The achieved filters are then transformed back into the original domain, the quality of the approximation being excellent in most cases.

Hence, the method described in [Darl78] proposes :

i) an algebraic solution for the approximation of odd-ordered prototype lowpass elliptic filters, thus rendering the approximation of elliptic filters possible, e.g. on pocket calculators or on compact DSP platforms, without necessary recourse to complicated Jacobian elliptic functions;

ii) a unified design framework for prototype lowpass filters, including Butterworth, Chebyshev, and elliptic filters, where inverse Chebyshev filters are also covered using simple filter transformations;

iii) explicit provision of all critical frequencies for elliptic filters, including frequencies of minimum and maximum passband loss, transmission zeros, and frequencies of minimum stopband loss.

Later, Gazsi neatly integrated these results into a design framework [Gazs85a] for odd-degreed prototype symmetric Lattice WDFs, with a thorough exploitation of the available design margins to achieve best

frequency and amplitude selectivity, covering the bireciprocal case as well. The regularly cited publication [Gazs85a] can be considered as a reference for prototype filter design as such, without necessary connection to lattice WDF implementation. The framework described in [Gazs85a] was integrated in various academic and commercial filter design tools such as Falcon [Gazs86], and Filter Architect ™ from Frontier Design [Fron00].

It should be noticed for completeness that other contributions to the analytic design of elliptic filters were also proposed, e.g. [Luto93, Rabr93, Luto92].

This section aims at extending the approach of [Darl78, Gazs85a] to antimetric lossless two-ports referring to even-ordered lowpass prototype filters, including the bireciprocal case. Examples of antimetric lattice-type WDF designs are provided.

5.2.1 Notation

For practical reasons, the notation adopted in this section complies with [Gazs85a], thus differing from the remainder of the report. Various definitions from [Gazs85a] are recalled for consistency.

Referring to Figure 5.1a, the next quantities are introduced :

a_s : Specified minimum attenuation in the stopband in [dB];
a_p : Maximum allowable attenuation spread in the passband in [dB];
f_s : Lower edge frequency of the stopband;
f_p : Upper edge frequency of the passband;
F : Sampling frequency.

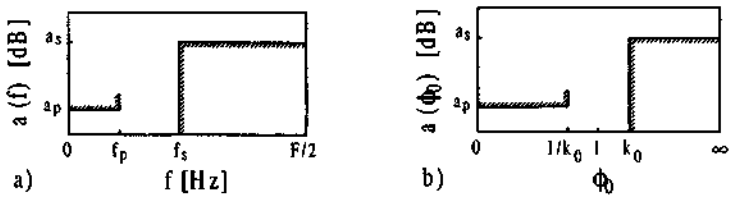

Figure 5.1: Design specifications for lowpass filters :
a) Original filter specifications; b) Normalized specifications.

The stopband and passband ripple factors ε_s and ε_p are defined by :

$$\varepsilon_s = \sqrt{10^{a_s/10} - 1}\,, \qquad \varepsilon_p = \sqrt{10^{a_p/10} - 1}\,; \tag{5.1a,b}$$

$$a_s = 10 \cdot \log\left(1 + \varepsilon_s^2\right), \qquad a_p = 10 \cdot \log\left(1 + \varepsilon_p^2\right); \tag{5.2a,b}$$

whereas the ψ-plane real frequencies ϕ_s and ϕ_p are fixed by :

$$\phi_s = \tan\left(\pi \cdot f_s / F\right), \qquad \phi_p = \tan\left(\pi \cdot f_p / F\right); \tag{5.3a,b}$$

$$f_s = \frac{F}{\pi} \cdot \arctan\left(\phi_s\right), \qquad f_p = \frac{F}{\pi} \cdot \arctan\left(\phi_p\right). \tag{5.4a,b}$$

The following relationships are thus clearly verified :

$$a_s \gg a_p \quad \Leftrightarrow \quad \varepsilon_s \gg \varepsilon_p\,; \tag{5.5a,b}$$

$$f_s > f_p \quad \Leftrightarrow \quad \phi_s > \phi_p\,. \tag{5.6a,b}$$

5.2.2 Darlington's design method for elliptic filters

Table 5.1 furnishes the definition of all necessary filter design parameters and quantities to apply Darlington's design method for elliptic filters. The normalized frequency variable ϕ_0, and normalized stopband/passband edge frequencies k_0 and $1/k_0$, respectively, are in particular introduced, cf Table 5.1 and Figure 5.1b :

$$\phi_0(\phi_s) = k_0; \qquad \phi_0(\phi_p) = 1/k_0\,. \tag{5.7a,b}$$

The rational function $F_0(\phi_0)$ determining the filter response, and all related critical frequencies, are defined for both symmetric and antimetric cases. $F_0(\phi_0)$ is a self-reciprocal function verifying :

$$F_0(1/\phi_0) = 1/F_0(\phi_0); \qquad F_0(k_0) = r_0; \qquad F_0(1/k_0) = 1/r_0\,. \tag{5.8a,b,c}$$

Starting with the normalized quantities in Table 5.1, it is possible to recursively map the original filter into new filter configurations using the forward transformation defined in Table 5.2, the index i indicating the number of successively applied transformations. Most important, the width of the transition band and the amplitude discrimination factor are both observed to increase at each iteration :

$$k_0 > 1 \quad \Rightarrow \quad k_{i+1} > k_i; \qquad r_0 \gg 1 \quad \Rightarrow \quad r_{i+1} \cong 2 \cdot r_i^2 \gg r_i; \tag{5.9a,b}$$

Quantities		Definition	Remarks
Variables	Frequency	ϕ	
	Normalized frequency	$\phi_0 = \phi \Big/ \sqrt{\phi_s \cdot \phi_p}$	
Functions	Rational function	$F_0(\phi_0) = \phi_0 \cdot \prod_{\nu=1}^{(N-1)/2} \frac{1-\phi_{0\nu}^2 \cdot \phi_0^2}{\phi_0^2 - \phi_{0\nu}^2}$	– Symmetric case; – Does not explicitly appear in [Gazs85a]
		$F_0(\phi_0) = \prod_{\nu=1}^{N/2} \frac{1-\phi_{0\nu}^2 \cdot \phi_0^2}{\phi_0^2 - \phi_{0\nu}^2}$	– Antimetric case [this report]
	Transfer function	$\lvert S_{11}(j\phi_0)\rvert^2 = \frac{1}{1+\varepsilon_p^2 \cdot r_0^2 \cdot F_0^2(\phi_0)}$	– Does not explicitly appear in [Gazs85a]
	Characteristic function	$\lvert C(j\phi_0)\rvert^2 = \frac{1}{\varepsilon_p^2 \cdot r_0^2 \cdot F_0^2(\phi_0)}$	– Does not explicitly appear in [Gazs85a]
Constants	Edge frequencies	$\phi_s,\ \phi_p$	
	Normalized edge freq.	$\phi_s \mapsto k_0 = \sqrt{\phi_s/\phi_p} > 1,\ \phi_p \mapsto 1/k_0$	
	Amplitude discrimination factor	$r_0 = \sqrt{\varepsilon_s/\varepsilon_p} \gg 1$	

Table 5.1: Definition of filter design parameters / quantities [Darl78].

Quantities	Forward transformation	Backward transformation
Normalized frequency	$\phi_{i+1} = k_i \cdot \phi_i + \sqrt{(k_i \cdot \phi_i)^2 - 1}$	$\phi_{i-1} = \frac{1}{k_i}(\phi_i + 1/\phi_i),\ \lvert\phi_i\rvert \geq 1$
Rational function	$F_{i+1}(\phi_{i+1}) =$ $= r_i \cdot F_i(\phi_i) + \sqrt{\left(r_i \cdot F_i(\phi_i)\right)^2 - 1}$	$F_{i-1}(\phi_{i-1}) =$ $= \frac{1}{2r_i}\left(F_i(\phi_i) + 1/F_i(\phi_i)\right)$
Critical frequencies	$\phi_{(i+1)\nu} = k_i \cdot \phi_{i\nu} + \sqrt{(k_i \cdot \phi_{i\nu})^2 - 1}$	$\phi_{(i-1)\nu} = \frac{1}{k_i}(\phi_{i\nu} + 1/\phi_{i\nu}),\ \lvert\phi_{i\nu}\rvert \geq 1$
Normalized edge freq.	$k_{i+1} = k_i^2 + \sqrt{k_i^4 - 1}$	$k_{i-1} = \sqrt{0.5 \cdot (k_i + 1/k_i)},\ \lvert k_i\rvert > 1$
Amplitude discrimination factor	$r_{i+1} = r_i^2 + \sqrt{r_i^4 - 1} \cong 2 \cdot r_i^2 \gg 1$	$r_{i-1} = \sqrt{0.5 \cdot (r_i + 1/r_i)}$

Table 5.2: Forward and backward transformations [Darl78].

so that the passband (stopband) response can be approximated in the minimax sense by a Chebyshev (inverse Chebysbev) filter response after $i=4$ iterations. The parameters of the achieved filter are then retrieved in the original domain using the backward transformation specified in Table 5.2 [Darl78].

At each iteration, the rational function is verifying :

$$F_i(1/\phi_i)=1/F_i(\phi_i);\quad F_i(k_i)=r_i;\quad F_i(1/k_i)=1/r_i. \tag{5.10a,b,c}$$

and

$$F_i(\phi_i)=\phi_i\cdot\prod_{\nu=1}^{(N-1)/2}\frac{1-\phi_{i\nu}^2\cdot\phi_i^2}{\phi_i^2-\phi_{i\nu}^2};\quad F_i(\phi_i)=\prod_{\nu=1}^{N/2}\frac{1-\phi_{i\nu}^2\cdot\phi_i^2}{\phi_i^2-\phi_{i\nu}^2}; \tag{5.11a,b}$$

in the symmetric and antimetric cases, respectively. After $i=4$ iterations, the frequency range $\phi_4\geq k_4$ corresponds to an inverse Chebyshev stopband in $F_4(\phi_4)$, the behavior in the stopband being approximately proportional to $1/T_N(k_4/\phi_4)$, where $T_N(.)$ denotes the Chebyshev polynomial of degree N [Darl78]. Hence, with $k_4\gg 1$:

$$T_N(k_4/\phi_4)\Big|_{\phi_4=k_4}=1;\quad T_N(k_4/\phi_4)\Big|_{\phi_4=1}\cong 2^{N-1}\cdot k_4^N \tag{5.12a,b}$$

so that :

$$\frac{F_4(k_4)}{F_4(1)}=r_4=\frac{T_N(1)}{T_N(k_4)}\cong 2^{N-1}\cdot k_4^N\quad\Rightarrow\quad r_4\cong\frac{(2\cdot k_4)^N}{2}\gg 1. \tag{5.13a,b}$$

Equation (5.13b) is essential for the design of elliptic filters. It is used: i) to fix the minimum filter degree $N_{\min}$ requested by the specifications; and ii) once the effective filter degree is selected, to systematically distribute the design margin to achieve best frequency and amplitude selectivity, cf [Gazs85a].

$N_{\min}$ is established from (5.13b) noting that $r_{i+1}\cong 2\cdot(r_i)^2$ for $i=0,1,2,3$, leading to (5.14a), and thus to (5.14b), complying with [Gazs85a]. The effectively selected filter degree N should be an odd (even) integer for symmetric (antimetric) filters, fulfilling $N\geq N_{\min}$.

$$(2\cdot k_4)^N=\left(4\cdot r_0^2\right)^8\quad\Rightarrow\quad N_{\min}=\frac{8\cdot\ln(4\cdot\varepsilon_s/\varepsilon_p)}{\ln(2\cdot k_4)}. \tag{5.14a,b}$$

5.2.3 Design method for prototype antimetric lattice-type WDFs

The design procedure applying to antimetric lattice-type WDFs is described in Table 5.3.

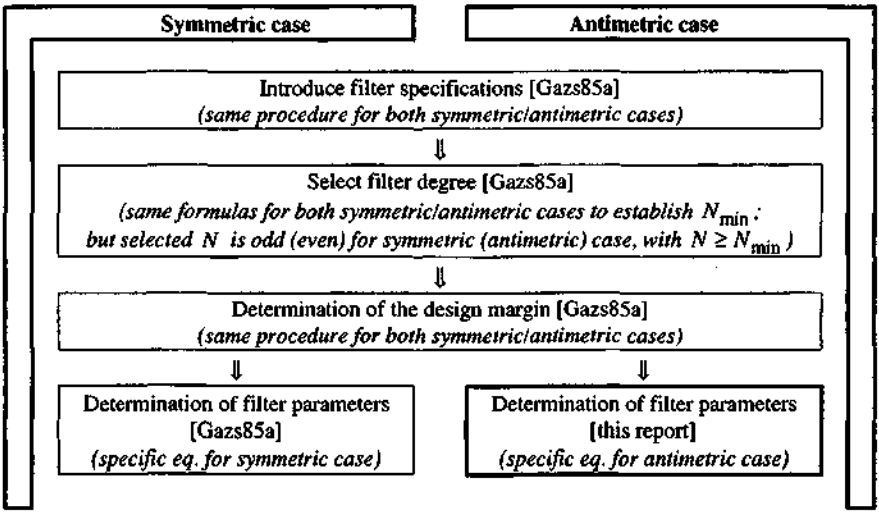

Table 5.3: Design procedure for symmetric/antimetric lattice-type WDFs (for Butterworth, Chebyshev, and elliptic filters, including bireciprocal Butterworth and elliptic filters).

Most of the framework developed in [Gazs85a] applies directly to the antimetric case, except the determination of the filter parameters which are specific to the symmetric and antimetric cases. The remainder of this section essentially concentrates on the determination of antimetric filter parameters.

Pole distribution over the lattice branches for prototype antimetric lowpass filters

From Subsection 3.4.17 and equation (A.77a) the form of the constituent allpass networks of antimetric WDFs is recalled :

$$S_1(\psi) = \sigma_1 \cdot \prod_{\nu=1}^{N_1} \left(\frac{\psi + \psi^*_{\infty 1\nu}}{\psi - \psi_{\infty 1\nu}} \right), \quad S_2(\psi) = \overline{S_1(\psi)}, \quad \sigma_1 = e^{j\cdot\xi_{S1}} ; \qquad (5.15a,b,c)$$

where $S_1(\psi)$ and thus $S_2(\psi)$, of filter degree :

$$N_1 = N_2 = N/2; \quad N = 2m; \quad \text{with } m \in N_+; \tag{5.16a,b}$$

are devoid of real pole configurations. In Subsections 5.2.4 to 5.2.6, the poles of S_1 and S_2 will be produced simultaneously without distinction of their attribution to S_1 or S_2. A pole distribution strategy among the lattice branches should therefore be defined.

Proceeding similarly to Section 4.3 and Subsections 4.5.1 and 4.5.3, both allpass functions $S_1(\psi)$ and $S_2(\psi)$ are assumed stable, whereas the allpass :

$$S'(\psi) = S_1(\psi)/S_2(\psi), \tag{5.17a}$$

with phase response :

$$\varphi_{S'}(\phi) = \varphi_1(\phi) - \varphi_2(\phi) = 2 \cdot \varphi_\Delta(\phi), \tag{5.17b}$$

is clearly unstable. Referring to (3.74) – (3.76), a lowpass response is assigned to $S_{11}(\psi)$ according to Tables 5.4 and 5.1.

$S_{11}(j \cdot \phi)$	$S_{21}(j \cdot \phi)$	$\lvert\phi\rvert \in [0, \phi_p]$	$\lvert\phi\rvert \in [\phi_s, \infty]$
Lowpass	Highpass	$\varphi_{S'}(\phi) \equiv 0$	$\varphi_{S'}(\phi) \equiv \pm\pi$

Table 5.4: Specification of $\varphi_{S'}(\phi)$.

Constraining further $\varphi_{S'}(\phi)$ so that $\varphi_{S'}(\infty) \equiv +\pi$, results in the next specifications :

$$\varphi_{S'}(\phi = 0) = (-1)^m \cdot \delta_p, \quad \varphi_{S'}(\phi = \infty) = +\pi - (-1)^m \cdot \delta_s; \tag{5.18a,b}$$

involving the factor m from (5.16b), and the phase ripple factors $\delta_p \geq 0$, $\delta_s \geq 0$. Equations (5.18a,b) can be compared with Case 3 in Table 4.6, and are valid for prototype Butterworth, Chebyshev, and elliptic lowpass filter responses.

For prototype lowpass filters, the poles of $S_{11}(\psi)$ are known to be alternately distributed over $S_1(\psi)$ and $S_2(\psi)$. Assuming S_{11} and thus S_1 and S_2 to be stable, (5.18a,b) imply that the poles of S_{11} are cyclically distributed over S_1 and S_2, by sorting the poles in increasing order of their argument (trigonometric orientation), and assigning the first pole with lowest argument to S_1. The described distribution scheme is independent of the factor m in (5.16b), and applies thus to all even filter degrees. Two examples are provided in Figure 5.2.

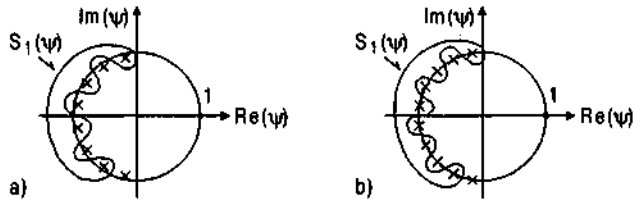

Figure 5.2: Cyclic pole distribution of $S_{11}(\psi)$ over the lattice branches $S_1(\psi)$ and $S_2(\psi)$ of prototype antimetric lowpass filters (unmarked poles being assigned to $S_2(\psi)$):
a) Pole distribution of the 8th-order filter described in Figure 5.3;
b) Pole distribution of the 10th-order filter described in Figure 5.4.

Determination of the parameters ξ_1 and δ_S

In addition to the poles, the constant ξ_1 in (5.15c) has to be fixed for every filter, the easiest being to evaluate the filter response at $\phi \to \infty$. The allpass $S_1(\psi)$ features then the next response using (3.69a):

$$\lim_{\phi\to\infty} S_1(j\phi) = e^{-j\cdot\varphi_1(\infty)} = e^{j\cdot\xi_1} \quad \Rightarrow \quad \varphi_1(\infty) = -\xi_1. \tag{5.19a,b}$$

Accordingly, applying (3.55a), $S_{11}(\psi)$ becomes:

$$\lim_{\phi\to\infty} S_{11}(j\phi) = \lim_{\phi\to\infty} 0.5\cdot\left[\, S_1(j\phi) + \overline{S_1(j\phi)} \,\right] = \cos(\xi_1). \tag{5.20}$$

On the other hand, since $\varphi_1(\infty) = -\varphi_2(\infty) = -\xi_1$, (3.70a) results in $\varphi_\Sigma(\infty) = 0$, so that:

$$\lim_{\phi\to\infty} S_{11}(j\phi) = \lim_{\phi\to\infty} \cos\left[\frac{\varphi_{S'}(\phi)}{2}\right] = \cos\left[\frac{\pi - (-1)^m\cdot\delta_S}{2}\right] \tag{5.21a}$$

$$= (-1)^m \cdot \sin(\delta_S/2) \tag{5.21b}$$

is achieved from (3.74). Clearly, δ_S is univocally determined from (5.21b) according to the specified amplitude response:

$$\delta_S = 2\cdot\arcsin\left(\lim_{\phi\to\infty} \left|S_{11}(j\phi)\right|\right), \quad \text{with} \quad 0 \le \delta_S < \pi/2. \tag{5.22}$$

Finally, comparing (5.20) to (5.21a), it is possible to fix the parameter ξ_1, this time with intervention of the factor m:

$$\xi_1 = 0.5 \cdot \left[\pi - (-1)^m \cdot \delta_S \right]. \tag{5.23}$$

Allpass configurations in the z-domain

Once S_1 and thus S_2 are fully determined, the corresponding allpass networks in the z-domain are obtained using (A.78a,b) :

$$H_1(z) = \lambda_1 \cdot \prod_{\nu=1}^{N_1} \left(\frac{1 - z_{\infty 1\nu}^* \cdot z}{z - z_{\infty 1\nu}} \right), \qquad H_2(z) = \overline{H_1(z)}; \tag{5.24a,b}$$

with $$\lambda_1 = e^{j\theta_1} = \sigma_1 \cdot \prod_{\nu=1}^{N_1} \left(\frac{1 - \psi_{\infty 1\nu}^*}{1 - \psi_{\infty 1\nu}} \right). \tag{5.24c}$$

5.2.4 Butterworth antimetric lattice-type WDFs

As indicated in Table 5.3, the filter degree and design margin are determined for the antimetric case exactly in the same way than for symmetric lattice WDFs. The original formulas (31) to (35) provided in [Gazs85a] are thus directly applied to Butterworth antimetric lattice-type WDFs, including the bireciprocal case.

The filter parameters are then established as follows. Having chosen a suitable factor γ in equation (35) of [Gazs85a], the parameters A_i and B_i of the (real) auxiliary allpass sections $S_i(\psi)$:

$$S_i(\psi) = \frac{\psi^2 - A_i \cdot \psi + B_i}{\psi^2 + A_i \cdot \psi + B_i}; \quad \text{with } i = 1,2,\ldots,N/2; \tag{5.25}$$

are processed from :

$$A_i = 2 \cdot \sqrt{\frac{1-\gamma}{1+\gamma}} \cdot \cos\left[\pi \cdot (i - 0.5)/N\right], \qquad B_i = \frac{1-\gamma}{1+\gamma}; \tag{5.26a,b}$$

so that the poles of $S_{11}(\psi)$ are obtained pairwise using :

$$\{ \psi_{2i-1}, \psi_{2i} \} = 0.5 \cdot \left(-A_i \pm \sqrt{A_i^2 - 4 \cdot B_i} \right). \tag{5.27}$$

Since $\cos^2\left[\pi \cdot (i-0.5)/N\right] < 1$, $\forall i = 1,2,\ldots,N/2$, $A_i^2 - 4 \cdot B_i < 0$, and the poles calculated from (5.27) are ascertained to be complex conjugate.

Moreover, in the bireciprocal case, one achieves :

$$\gamma = 0 \quad \Rightarrow \quad A_i = 2 \cdot \cos\left[\pi \cdot (i - 0.5)/N\right], \quad B_i = 1. \tag{5.28a,b}$$

The poles established in (5.27) are distributed over S_1 and S_2 applying the method described in Subsection 5.2.3. Finally, the parameters δ_s and ξ_1 are determined from (5.22) and (5.23) :

$$\lim_{\phi \to \infty} \left| S_{11}(j\phi) \right| = 0 \quad \Rightarrow \quad \delta_s = 0, \quad \xi_1 = \pi/2; \tag{5.29}$$

whereas δ_p in (5.18a) is verifying $\delta_p = 0$.

5.2.5 Chebyshev antimetric lattice-type WDFs

Similarly, the original formulas (31) – (33) and (39) – (42) provided in [Gazs85a] apply directly to design Chebyshev antimetric lattice-type WDFs. The parameters A_i and B_i of the auxiliary allpass sections $S_i(\psi)$ are then obtained from :

$$A_i = r \cdot \cos\left[\pi \cdot (i - 0.5)/N\right], \tag{5.30a}$$

$$B_i = \left\{ w^2 + w^{-2} - 2 \cdot \cos\left[\pi \cdot (i - 0.5)/N\right] \right\} \cdot \varphi_p^2 \Big/ 4; \tag{5.30b}$$

(5.25) remaining valid. The poles of $S_{11}(\psi)$ are again retrieved pairwise using (5.27), and distributed over S_1 and S_2 following the method described in Subsection 5.2.3. Finally, the parameters δ_s and ξ_1 are again fixed by (5.29).

5.2.6 Inverse Chebyshev antimetric lattice-type WDFs

As observed in [Gazs85a], when $\left| S_{11}(j\phi) \right|$ is featuring a Chebysbev lowpass response, then $\left| S_{21}(j\phi) \right|$ has an inverse Chebyshev highpass response. Using adequate frequency transformations, it is possible to design an inverse Chebyshev lowpass filter from a lowpass Chebyshev filter. However, the parameter δ_s should be replaced by :

$$\lim_{\phi \to \infty} \left| S_{11}(j\phi) \right| = \frac{1}{\sqrt{1 + \varepsilon_s^{*2}}} \quad \Rightarrow \quad \delta_s = 2 \cdot \arcsin\left(\frac{1}{\sqrt{1 + \varepsilon_s^{*2}}} \right); \tag{5.31a,b}$$

in the inverse Chebyshev case, where ε_s^* corresponds to the stopband ripple factor actually selected during the design process, cf [Gazs85a], the parameter ξ_1 being fixed by (5.23).

5.2.7 Elliptic antimetric lattice-type WDFs

In case of elliptic antimetric lattice-type WDFs, the preliminary design steps including filter order selection and design margin distribution are handled according to the original formulas (31) – (33) and (48) – (65) from [Gazs85a]. The next parameters are then calculated :

$$c_{4,i} = \frac{q_4}{\cos\left[\pi \cdot (i-0.5)/N\right]} \qquad \text{for} \quad i=1,2,\ldots,N/2; \tag{5.32}$$

$$c_{j-1,i} = \frac{1}{2 \cdot q_{j-1}} \left(c_{j,i} + c_{j,i}^{-1} \right) \qquad \text{for} \quad j=4,3,2,1; \tag{5.33}$$

$$y_i = 1/c_{0,i}; \tag{5.34}$$

$$A_i = \frac{-2 \cdot w_0 \cdot q_0 \cdot \phi_p}{1+(w_0 \cdot y_i)^2} \cdot \sqrt{1-\left(q_0^2 + q_0^{-2} - y_i^2\right) \cdot y_i^2}\ ; \tag{5.35a}$$

$$B_i = \frac{w_0^2 + y_i^2}{1+(w_0 \cdot y_i)^2} \cdot (q_0 \cdot \phi_p)^2. \tag{5.35b}$$

The poles of S_{11} are obtained from (5.27), and are distributed over S_1 and S_2 applying the method described in Subsection 5.2.3. The parameter δ_s is specified by (5.31b) also in the elliptic case, ε_s^* corresponding to the stopband ripple factor selected during the design process, cf [Gazs85a]. ξ_1 is determined by (5.23).

In the bireciprocal case, the formulas (5.35a,b) are replaced by :

$$A_i = \frac{2}{1+y_i^2} \cdot \sqrt{1-\left(q_0^2 + q_0^{-2} - y_i^2\right) \cdot y_i^2}\ ; \qquad B_i = 1. \tag{5.36a,b}$$

Finally, the auxiliary parameters :

$$c'_{4,i} = \frac{q_4}{\cos(i \cdot \pi / N)}, \qquad \text{for} \quad i=0,1,\ldots,(N/2)-1; \tag{5.37}$$

$$c'_{j-1,i} = \frac{1}{2 \cdot q_{j-1}} \left(c'_{j,i} + c'^{-1}_{j,i} \right), \quad \text{for} \quad j=4,3,2,1; \tag{5.38}$$

$$y'_i = 1/c'_{0,i}; \tag{5.39}$$

are evaluated, such that the frequencies of zero passband loss :

$$f_{0,i} = (F/\pi)\cdot \arctan\left(q_0 \cdot \phi_p \cdot y_i\right), \qquad i = 1,2,...,N/2; \tag{5.40}$$

the transmission zeros :

$$f_{\infty,i} = (F/\pi)\cdot \arctan\left(q_0 \cdot \phi_p / y_i\right), \qquad i = 1,2,...,N/2; \tag{5.41}$$

the frequencies of maximum passband loss :

$$f_{\max\, p,i} = (F/\pi)\cdot \arctan\left(q_0 \cdot \phi_p \cdot y_i'\right), \qquad i = 1,2,...,N/2; \tag{5.42}$$

and the frequencies of minimum stopband attenuation :

$$f_{\min\, s,i} = (F/\pi)\cdot \arctan\left(q_0 \cdot \phi_p / y_i'\right), \qquad i = 1,2,...,N/2; \tag{5.43}$$

can be determined. Expressions (5.40) – (5.43) are useful for certain applications.

5.2.8 Critical frequencies for elliptic symmetric lattice WDFs

As a complement to [Gazs85a] for symmetric lattice WDFs, the frequencies of maximum passband loss and of minimum stopband attenuation can be achieved substituting (5.37) with :

$$c_{4,i}' = \frac{q_4}{\cos(i\cdot\pi/N)} \quad \text{for} \quad i = 0,1,...,(N-1)/2; \tag{5.44}$$

where the range of index i changes only. Equations (5.38) – (5.39), and (5.42) – (5.43) apply then likely to the antimetric case.

5.2.9 Examples

Several examples selected from [Gazs85a] but applied to antimetric filters are described below.

Example 1: Butterworth antimetric lowpass filter

Filter specifications (same as in Example 1 from [Gazs85a]) :

Passband : $f_p = 3.4\,\text{kHz}$; $a_p = 0.5\,\text{dB}$; (5.45a,b)

Stopband : $f_s = 6.0\,\text{kHz}$; $a_s = 65\,\text{dB}$; (5.45c,d)

Sampling frequency : $F = 16\,\text{kHz}$. (5.45e)

The minimum filter degree is $N_{\min} = 7.63$, so that $N = 8$ is chosen. The auxiliary design parameters k_s and k_p defined in (34a,b) from [Gazs85a] are then processed from the filter specifications and selected degree. Since both parameters are positive :

$$k_s = 0.0540 \leq \gamma \leq k_p = 0.1060; \tag{5.46}$$

a bireciprocal implementation is not feasible. Selecting $\gamma = 0.0625$ in order to assign the larger part of the design margin to the stopband, one achieves the filter parameters listed in Table 5.5, the corresponding filter response being depicted in Figure 5.3. The pole configuration obtained in the ψ-domain is shown in Figure 5.2a.

Figure 5.3a presents in particular the phase response of the allpass :

$$H'(z) = H_1(z)/H_2(z); \tag{5.47}$$

which is the z-domain counterpart of $S'(\psi)$ in (5.17a), and whose phase response $\beta_{H'}(\Omega)$ is controlling the amplitude response of H_{11} according to (5.17b) and (3.74) – (3.76).

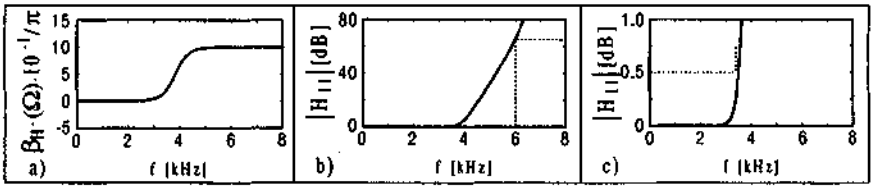

Figure 5.3: 8th-order Butterworth antimetric lowpass filter :
a) Unwrapped phase $\beta_{H'}$; b) Attenuation $|H_{11}|$;
c) Passband attenuation $|H_{11}|$.

		ν	θ_i/π, $\mathrm{Re}\{z_{\infty i\nu}\}$	$\mathrm{Im}\{z_{\infty i\nu}\}$
H_1	θ_1/π	—	−0.25977537719406	—
	$z_{\infty 1\nu}$	1	0.05231399824605	0.81933582215180
		2	0.03415591601124	0.30302258292284
		3	0.03158371655286	−0.09839409809681
		4	0.04020626591088	−0.53383889454568

Table 5.5: Parameters specifying the filter illustrated in Figure 5.3.

Example 2: Bireciprocal Butterworth antimetric lowpass filter

Applying the same specifications (5.45) as in Example 1, but selecting this time $N=10$, results in a larger design margin, and the auxiliary parameters k_s and k_p become :

$$k_s = -0.1322 \leq \gamma \leq k_p = 0.1319; \tag{5.48}$$

i.e. $k_s < 0$ and $k_p > 0$. It is thus possible to select $\gamma = 0$, leading to a bireciprocal implementation, the corresponding filter parameters being listed in Table 5.6, whereas Figure 5.4 illustrates the filter response. The ψ-domain pole configuration is shown in Figure 5.2b.

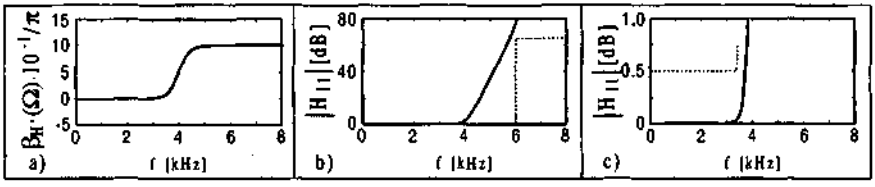

Figure 5.4: 10th-order bireciprocal Butterworth antimetric lowpass :
a) Unwrapped phase $\beta_{H'}$; b) Attenuation $|H_{11}|$;
c) Passband attenuation $|H_{11}|$.

		ν	θ_i/π, $\mathrm{Re}\{z_{\infty i\nu}\}$	$\mathrm{Im}\{z_{\infty i\nu}\}$
H_1	θ_1/π	—	−0.25	—
	$z_{\infty 1\nu}$	1	0	0.85408068546347
		2	0	0.41421356237310
		3	0	0.07870170682462
		4	0	−0.24007875908012
		5	0	−0.61280078813993

Table 5.6: Parameters specifying the filter illustrated in Figure 5.4.

Example 3: Chebyshev antimetric lowpass filter

Filter specifications (same as in Example 3 from [Gazs85a]) :

Passband : $f_p = 3\,\mathrm{kHz}$; $a_p = 1\,\mathrm{dB}$; (5.49a,b)

Stopband : $f_s = 5\,\mathrm{kHz}$; $a_s = 40\,\mathrm{dB}$; (5.49c,d)

Sampling frequency : $F = 16\,\mathrm{kHz}$. (5.49e)

The minimum filter degree is $N_{\min} = 4.13$, so that $N = 6$ is chosen. The design margin can then be established by evaluating the lowest possible passband ripple factor $\varepsilon_{p\,\min}$ defined in (39) from [Gazs85a]:

$$\varepsilon_{p\,\min} = 0.0342 \leq \varepsilon_p^* \leq \varepsilon_p = 0.5088. \tag{5.50}$$

Selecting $\varepsilon_p^* = 0.4$ so that most part of the design margin is assigned to the stopband, the actual passband attenuation becoming then $a_p^* = 0.645\,\text{dB}$ according to (5.2b), one obtains the filter parameters given in Table 5.7, the related filter response being illustrated in Figure 5.5.

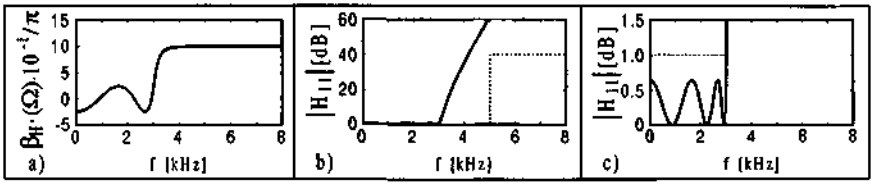

Figure 5.5: 6th-order Chebyshev antimetric lowpass filter :
a) Unwrapped phase $\beta_{H'}$; b) Attenuation $|H_{11}|$;
c) Passband attenuation $|H_{11}|$.

		ν	θ_i/π, Re$\{z_{\infty i\nu}\}$	Im$\{z_{\infty i\nu}\}$
H_1	θ_1/π	—	−0.30218075668495	—
	$z_{\infty 1\nu}$	1	0.35479284769217	0.86592715139795
		2	0.65735545876089	0.25223160020901
		3	0.48819311778971	−0.64506856518177

Table 5.7: Parameters specifying the filter illustrated in Figure 5.5.

Example 4: Elliptic antimetric lowpass filter

Filter specifications (same as Example 4 in [Gazs85a]) :

Passband : $f_p = 3.4\,\text{kHz}$; $a_p = 0.2\,\text{dB}$; (5.51a,b)

Stopband : $f_s = 4.6\,\text{kHz}$; $a_s = 65\,\text{dB}$; (5.51c,d)

Sampling frequency : $F = 16\,\text{kHz}$. (5.51e)

The minimum filter degree is $N_{\min} = 5.96$, so that $N = 8$ is chosen to provide enough design margin ($N = 6$ could fit as well, but would

require high precision filter coefficients). Referring to equation (52) in [Gazs85a], the minimum value of the stopband edge frequency is $f_{s\,\min} = 3.86\,\text{kHz}$, and the actual stopband edge frequency f_s^* should be chosen so as to fulfil :

$$f_{s\,\min} = 3.86\,\text{kHz} \le f_s^* \le f_s = 4.60\,\text{kHz}. \tag{5.52}$$

Selecting $f_s^* = 4.50\,\text{kHz}$ to allocate most of the design margin to the pass- and stopbands, the remainder part being assigned to the transition band [Gazs85a], it is possible to evaluate the lowest possible passband ripple factor $\varepsilon_{p\,\min}$ from (59) in [Gazs85a] :

$$\varepsilon_{p\,\min} = 0.0093 \le \varepsilon_p^* \le \varepsilon_p = 0.2170. \tag{5.53}$$

Selecting the actual passband ripple factor $\varepsilon_p^* = 0.18$ to assign the larger part of the design margin to the stopband, which fixes the corresponding actual passband attenuation to $a_p^* = 0.13848\,\text{dB}$ from (5.2b), and the actual stopband attenuation to $a_s^* = 90.71\,\text{dB}$, yields the filter parameters provided in Table 5.8. The corresponding filter response is illustrated in Figure 5.6, whereas the critical frequencies defined by (5.40) – (5.43) are given in Table 5.9.

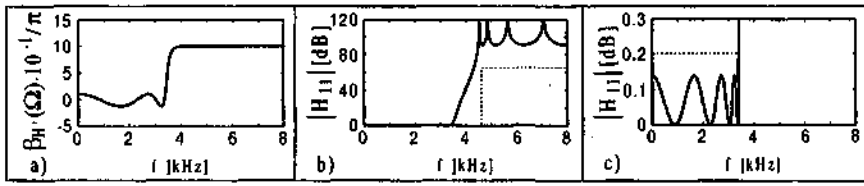

Figure 5.8: 8th-order elliptic antimetric lowpass filter :
a) Unwrapped phase $\beta_H \cdot$; b) Attenuation $|H_{11}|$;
c) Passband attenuation $|H_{11}|$.

		ν	θ_l/π, $\text{Re}\{z_{\infty l\nu}\}$	$\text{Im}\{z_{\infty l\nu}\}$
H_1	θ_1/π	—	-0.28052450312371	—
	$z_{\infty 1\nu}$	1	0.20468294350947	0.93642211238009
		2	0.41072763046873	0.60056483916294
		3	0.54194886369330	-0.23006453964813
		4	0.27404665598165	-0.81731285151753

Table 5.8: Parameters specifying the filter illustrated in Figure 5.6.

i	$f_{0,i}$ [kHz]	$f_{\infty,i}$ [kHz]	$f_{\max p,i}$ [kHz]	$f_{\min s,i}$ [kHz]
1	0.879 30	4.536 75	1.655 31	4.500 00
2	2.273 13	4.858 42	2.729 07	4.651 60
3	3.045 61	5.646 13	3.249 86	5.180 17
4	3.363 57	7.085 37	3.400 00	6.281 72

Table 5.9: Critical frequencies.

Example 5: Bireciprocal elliptic antimetric lowpass filter

The same specifications (5.51) are considered as in Example 4, selecting however N=10 instead, which is suitable for a bireciprocal realization. The actual stopband edge frequency f_s^* should then fit into the next interval :

$$f_{s\,\min} = 4.50\,\text{kHz} \le f_s^* \le f_s = 4.60\,\text{kHz}. \tag{5.54}$$

Choosing $f_s^* = 4.58\,\text{kHz}$, the range for the actual passband ripple factor is established :

$$\varepsilon_{p\,\min} = 359.7929 \cdot 10^{-6} \le \varepsilon_p^* \le \varepsilon_p = 562.3414 \cdot 10^{-6}. \tag{5.55}$$

Selecting $\varepsilon_p^* = \varepsilon_{p\,\min}$, which corresponds to the marginal passband attenuation $a_p^* = 0.6\,\mu\text{dB}$ while fixing the stopband attenuation to $a_s^* = 68.88\,\text{dB}$, leads to the filter parameters provided in Table 5.10, the corresponding filter response being illustrated in Figure 5.7. Finally, the critical frequencies of the filter are listed in Table 5.11.

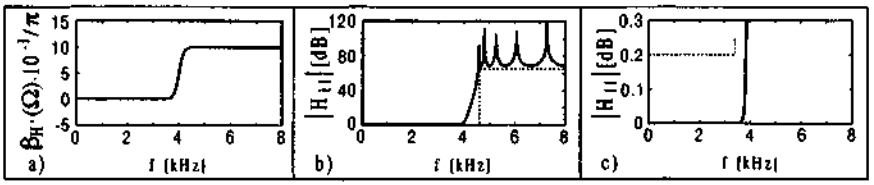

Figure 5.7: 10th-order elliptic antimetric lowpass filter :
a) Unwrapped phase β_H ; b) Attenuation $|H_{11}|$;
c) Passband attenuation $|H_{11}|$.

		ν	θ_i/π, $\mathrm{Re}\{z_{\infty i\nu}\}$	$\mathrm{Im}\{z_{\infty i\nu}\}$
H_1	θ_1/π	—	−0.25	—
	$z_{\infty 1\nu}$	1	0	0.93577542142542
		2	0	0.63197358951259
		3	0	0.14404311871961
		4	0	−0.41206829753994
		5	0	−0.80066203701216

Table 5.10: Parameters specifying the filter illustrated in Figure 5.7.

i	$f_{0,i}$ [kHz]	$f_{\infty,i}$ [kHz]	$f_{\max p,i}$ [kHz]	$f_{\min s,i}$ [kHz]
1	$F/2 - f_{\infty,5}$	4.583 69	$F/2 - f_{\min s,5}$	4.559 96
2	$F/2 - f_{\infty,4}$	4.784 31	$F/2 - f_{\min s,4}$	4.656 67
3	$F/2 - f_{\infty,3}$	5.242 83	$F/2 - f_{\min s,3}$	4.975 62
4	$F/2 - f_{\infty,2}$	6.059 67	$F/2 - f_{\min s,2}$	5.600 03
5	$F/2 - f_{\infty,1}$	7.285 06	$F/2 - f_{\min s,1}$	6.625 84

Table 5.11: Critical frequencies.

5.3 Warped bireciprocal lattice-type WDFs

When a symmetric or antimetric bireciprocal lossless two-port is undergoing a lowpass-to-lowpass frequency transformation, the complementary lowpass/highpass filter responses of the network, which are originally featuring a symmetry centered on $f_s/4$, with sampling frequency f_s, are getting *warped*. The 3 dB attenuation frequency originally located at $f_s/4$ is then shifted to a new frequency labeled $f_{3\,\mathrm{dB}}$, a parameter controlling essential properties of the achieved network. In the frame of this report, bireciprocal lattice-type WDFs obtained following this procedure will be denoted as "warped" due to the shape of their frequency response.

The motivations for using such filters are of different nature. First, regarding applications requiring signal analysis/synthesis filter pairs, including extension to filterbanks, there is sometimes a need for adjusting the width of the subbands to the handled signal and/or application requirements in a more flexible way than as offered by classical solutions. This is for instance the case for higher-quality

audio analysis/coding/recognition algorithms relying on auditory perceptual models, cf e.g. [Lain96, Härm97a, Evan98] for the context.

The second interest is related to implementation simplifications induced by the poles locus. Indeed, stable bireciprocal filters are featuring poles that are either confined to $|\psi_{\infty v}|=1$, $\mathrm{Re}\{\psi_{\infty v}\}<0$, in the ψ-domain, or that are presenting circular symmetries centered on the unit-circle along (4.24) and (4.29) in the symmetric and antimetric cases, respectively. The poles of warped bireciprocal filters are demonstrated to feature precisely the same circular symmetries, but centered on a circle with radius $|\psi_{\infty v}|<1$ for $f_{3\,\mathrm{dB}}<f_s/4$, or $|\psi_{\infty v}|>1$ for $f_{3\,\mathrm{dB}}>f_s/4$.

For N th-order *symmetric* lattice WDFs, the resulting pole configuration implies that $(N-1)/2$ WDF adaptor coefficients become identical [1] – though different from zero – and are solely controlled by $f_{3\,\mathrm{dB}}$. It is then possible to optimize the implementation of these filters by selecting $f_{3\,\mathrm{dB}}$ such that the adaptor coefficients reduce to a minimum number of shift-and-add operations, thus achieving (partly) multiplierless solutions [2].

It is noticed that warped bireciprocal lattice-type WDFs are internally operating at highest sampling frequency when used in a multirate configuration. Moreover, it is observed that the warping process is mapping bireciprocal elliptic filters onto the whole class of so-called minimum Q-factor elliptic filters [Mili99], whereas Butterworth filters are merely transformed into standard non-bireciprocal Butterworth filters presenting no additional interest to those already identified in [Gazs85a]. Only elliptic filters are thus further discussed.

Two authoring teams have studied the design of *symmetric* warped bireciprocal lattice WDFs. The first team composed of Güllüoglu and Gazsi seemingly discovered the subject in the frame of a systematic study of frequency transformations applied to symmetric lattice

---

[1] This property is also verified for warped bireciprocal symmetric lattice WDFs with non-prototype lowpass amplitude or mixed amplitude/phase responses, a fact that was to our knowledge not cited before. In this case, dedicated approximation methods shall however be elaborated.

[2] Suitable filter structures exploiting the pole configuration to optimally implement warped bireciprocal *antimetric* lattice-type WDFs were to our knowledge not yet found.

WDFs [Güll86]. The feasible design interval of $f_{3\,\mathrm{dB}}$ was identified [Güll86], pp. 32-35, in view of getting an optimal quantized value for the $(N-1)/2$ identical WDF adaptor coefficients, whereas an adaptation of the design framework [Gazs85a] was presented in [Gazs85b].

A second team represented by Milic and Lutovac recently published an extended study of the subject, following a different approach. Based on minimal Q-factor analog elliptic filters [Rabr94, Rabr93, Luto92], they first proposed realizations of odd-degreed elliptic half-band filters implemented in cascaded [Luto96], parallel [Mili96, Luto96], and bireciprocal symmetric lattice WDF forms [Luto96] [3]. A detailed sensitivity analysis [Luto98] was undertaken to achieve multiplierless filters [Luto97]. Finally, this team proposed the warped bireciprocal symmetric lattice WDF structure with fully quantized adaptor coefficients [Mili97, Mili99], whereas an economic realization for 1/3 band filters with partly quantized coefficients was formerly published in [Luto96].

As a matter of fact, referring to the class of minimal Q-factor elliptic filters, warped bireciprocal WDFs can be viewed as resulting from a generalization of bireciprocal WDFs, the latter becoming a particular but important case of the former.

The objectives of this subsection are to establish the fundamental equation characterizing warped bireciprocal lattice-type WDFs, and to present a unified design method to achieve *elliptic* prototype lowpass responses by adapting the framework developed in [Gazs85a], the symmetric case being already covered by [Gazs85b].

5.3.1 Principle

Referring to bireciprocal WDFs expressed in the ψ-domain, cf Subsection 4.5.1, the lowpass-to-lowpass transformation used to achieve warped bireciprocal WDFs merely consists in applying :

$$\phi \mapsto \phi/\phi_{3\,\mathrm{dB}}\,, \qquad \text{with} \qquad \phi_{3\,\mathrm{dB}} = \tan(\pi \cdot f_{3\,\mathrm{dB}}/f_s)\,. \tag{5.56a,b}$$

Expression (4.16a) is then becoming :

$$\varphi_{S'}(\phi/\phi_{3\,\mathrm{dB}}) - \varphi_{S'}(0) = \varphi_{S'}(\infty) - \varphi_{S'}(\phi_{3\,\mathrm{dB}}/\phi)\,; \tag{5.57a}$$

---

[3] Even-ordered elliptic half-band filters realized with second-order cells were also considered in [Mili95].

so that (4.16c) is replaced by :

$$\varphi_{S'}(\phi/\phi_{3\,\mathrm{dB}})\Big|_{\phi=\phi_{3\,\mathrm{dB}}} = 0.5\cdot[\varphi_{S'}(0)+\varphi_{S'}(\infty)]. \tag{5.57b}$$

Accordingly, (4.19) gets :

$$\left|S_{i1}(j\phi/\phi_{3\,\mathrm{dB}})\right|^2\Big|_{\phi=\phi_{3\,\mathrm{dB}}} = 1/2; \qquad \text{for } i=1,2. \tag{5.58}$$

Equation (5.56a) implies that the allpass function $S'(\psi)$ specified in (4.9) and featuring (4.10a,b) for bireciprocal WDFs is mapped onto $S'(\psi/\phi_{3\,\mathrm{dB}})$ in tbe warped bireciprocal case, yielding :

$$\text{for } q=1: \qquad S'(\psi/\phi_{3\,\mathrm{dB}}) = -S'(\phi_{3\,\mathrm{dB}}/\psi); \tag{5.59a}$$

$$\text{for } q=-1: \qquad S'(\psi/\phi_{3\,\mathrm{dB}}) = -1/S'(\phi_{3\,\mathrm{dB}}/\psi); \tag{5.59b}$$

where the parameter q distinguishes bireciprocal WDFs of the first and second kind, cf Section 4.3. The characteristic function of warped bireciprocal WDFs is then determined from (5.59a,b) :

$$C(\phi_{3\,\mathrm{dB}}/\psi) = q\cdot r/C(\psi/\phi_{3\,\mathrm{dB}}), \tag{5.60}$$

with parameter r specified in (4.5). Finally, the passband and stopband edge frequencies that are verifying :

$$\phi_{pass} = 1/\phi_{stop} \quad \Leftrightarrow \quad \phi_{pass}\cdot\phi_{stop} = 1 \tag{5.61a}$$

for bireciprocal WDFs, are mapped onto :

$$\phi_{pass}/\phi_{3\,\mathrm{dB}} = \phi_{3\,\mathrm{dB}}/\phi_{stop} \quad \Leftrightarrow \quad \phi_{pass}\cdot\phi_{stop} = \phi_{3\,\mathrm{dB}}^2 \tag{5.61b}$$

for warped bireciprocal WDFs [Gazs85b, Güll86, Mili97].

5.3.2 Design method for warped bireciprocal elliptic lattice-type WDFs

The design procedure for warped bireciprocal elliptic lattice-type WDFs and relying on the framework [Gazs85a] is described in Table 5.12. As indicated, the steps involving the filter degree selection and the establishment of the design margin shall be adapted. The notation of [Gazs85a] is adopted for the remainder of this section.

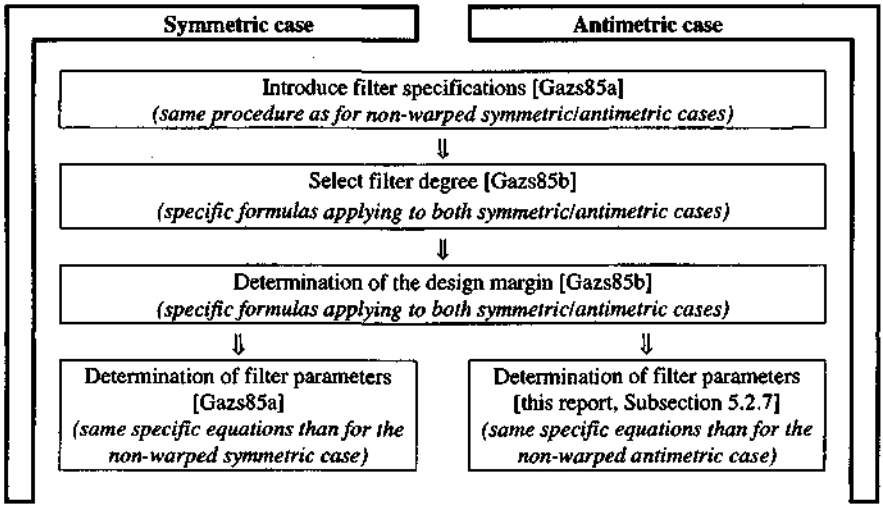

Table 5.12: Design method for warped bireciprocal lattice-type WDFs (derived from analog elliptic minimal Q-factor prototype filters).

Filter degree selection

The design process starts by labeling the specified passband and stopband ripple factors as ε'_p, ε'_s. Secondary passband and stopband ripple factors ε_p and ε_s are then derived thereof which shall satisfy $\varepsilon_p = 1/\varepsilon_s$ to achieve warped bireciprocal responses, thus setting :

$$\varepsilon_p = \min\{\varepsilon'_p, 1/\varepsilon'_s\}; \qquad \varepsilon_s = \max\{1/\varepsilon'_p, \varepsilon'_s\}; \tag{5.62a,b}$$

which is most often equivalent to :

$$\varepsilon_p = 1/\varepsilon'_s; \qquad \varepsilon_s = \varepsilon'_s. \tag{5.63a,b}$$

Assuming that (5.63a,b) apply, the minimum filter degree $N_{\min}$ specified in (5.14b) becomes [Gazs85b] :

$$N_{\min} = \frac{16 \cdot \ln(2 \cdot \varepsilon_s)}{\ln(2 \cdot k_4)}. \tag{5.64}$$

The appropriate filter degree selection is then performed as usual, choosing an odd (even) degree $N \geq N_{\min}$ for symmetric (antimetric) lattice-type WDFs.

Determination of the design margin

Following the design framework in [Gazs85a], equation (48b) in [Gazs85a] necessarily applies, fixing $r_0 = \varepsilon_s$. According to (52a) in [Gazs85a], and referring to (5.3a,b), the lower stopband edge frequency is getting :

$$\phi_{s\,\min} = \phi_p \cdot x_0^2; \tag{6.65a}$$

which corresponds to the next minimum value of $\phi_{3\,\mathrm{dB}}$ using (5.61b) :

$$\phi_{3\,\mathrm{dB}\,\min} = \sqrt{\phi_p \cdot \phi_{s\,\min}} = \phi_p \cdot x_0. \tag{5.65b}$$

Hence, instead of selecting the actual stopband edge frequency ϕ_s^* in tbe prescribed range :

$$\phi_{s\,\min} \le \phi_s^* \le \phi_s; \tag{6.66a}$$

as suggested in (53) from [Gazs85a], it is possible to choose the related actual frequency $\phi_{3\,\mathrm{dB}}^*$:

$$\phi_{3\,\mathrm{dB}\,\min} \le \phi_{3\,\mathrm{dB}}^* \le \phi_{3\,\mathrm{dB}} = \sqrt{\phi_p \cdot \phi_s}. \tag{5.66b}$$

For symmetric lattice WDFs, as will be confirmed later, $\phi_{3\,\mathrm{dB}}^*$ is directly determining tbe value of $(N-1)/2$ identical WDF adaptor coefficients γ_{2i} :

$$\gamma_{2i} = \frac{1-\phi_{3\,\mathrm{dB}}^{*2}}{1+\phi_{3\,\mathrm{dB}}^{*2}} \quad \Leftrightarrow \quad \phi_{3\,\mathrm{dB}}^* = \sqrt{\frac{1-\gamma_{2i}}{1+\gamma_{2i}}}; \quad \text{for } i = 1,2,\ldots(N-1)/2. \tag{5.67a,b}$$

In order to optimize the actual quantized value γ_{2i}^* so as to minimize the number of shift-and-adds, (6.66b) shall be replaced by:

$$\frac{1-\phi_{3\,\mathrm{dB}\,\min}^2}{1+\phi_{3\,\mathrm{dB}\,\min}^2} = \frac{1-\phi_p \cdot \phi_{s\,\min}}{1+\phi_p \cdot \phi_{s\,\min}} \ge \gamma_{2i}^* \ge \frac{1-\phi_{3\,\mathrm{dB}}^2}{1+\phi_{3\,\mathrm{dB}}^2} = \frac{1-\phi_p \cdot \phi_s}{1+\phi_p \cdot \phi_s}; \tag{6.66c}$$

where the inequality signs are reversed with respect (5.66b), since $\mathrm{d}\,\gamma_{2i}/\mathrm{d}\,\phi_{3\,\mathrm{dB}}^* < 0$ for $\phi_{3\,\mathrm{dB}}^* > 0$ according to (5.67a). Once γ_{2i}^* is fixed, $\phi_{3\,\mathrm{dB}}^*$ is retrieved from (5.67b) with $\gamma_{2i} = \gamma_{2i}^*$.

For antimetric lattice-type WDFs, no suitable implementation structure being known for the warped bireciprocal case, it suffices to select $\phi^*_{3\,\mathrm{dB}}$ out of the range (5.66b).

The design process resumes by substituting (55a) in [Gazs85a] with :

$$q_0 = \phi^*_{3\,\mathrm{dB}} / \phi_p \,. \tag{5.68}$$

Moreover, (59) – (61) in [Gazs85a] are supplanted by :

$$\varepsilon^*_p = 1/\varepsilon^*_s = 1/m_0 . \tag{5.69}$$

Finally, the parameter w_0 in (65) from [Gazs85a] is fixed to :

$$w_0 = -1 ; \tag{5.70}$$

for warped bireciprocal WDFs.

Determination of the filter parameters

As indicated in Table 5.12, the filter parameters are determined exactly in the same way than for non-warped non-bireciprocal filters, applying directly the formulas from [Gazs85a] in the symmetric case, or those provided in Subsection 5.2.7 for antimetric filters.

Still, it is worth reformulating the main expressions. Hence, equations (70a), (71a) from [Gazs85a] are becoming :

$$A_i = \frac{2 \cdot \phi^*_{3\,\mathrm{dB}}}{1 + y_i^2} \cdot \sqrt{1 - \left(q_0^2 + q_0^{-2} - y_i^2\right) \cdot y_i^2} \;\; ; \quad B_i = \phi^{*2}_{3\,\mathrm{dB}} ; \tag{5.71a,b}$$

with $i = 1,2,\ldots(N-1)/2$ for symmetric filters, and $i = 1,2,\ldots N/2$ for antimetric filters. Moreover, in the symmetric case, equations (66a), (72a), and (73a) in [Gazs85a] are superseeded by :

$$\gamma_0 = \left(1 - \phi^*_{3\,\mathrm{dB}}\right) \Big/ \left(1 + \phi^*_{3\,\mathrm{dB}}\right) . \tag{5.72}$$

$$\gamma_{2i-1} = \frac{A_i - B_i - 1}{A_i + B_i + 1} ; \quad \gamma_{2i} = \frac{1 - B_i}{1 + B_i} = \frac{1 - \phi^{*2}_{3\,\mathrm{dB}}}{1 + \phi^{*2}_{3\,\mathrm{dB}}} ; \tag{5.73a,b}$$

for $i = 1,2,\ldots(N-1)/2$, thus confirming (5.67a). It is observed from (5.72) that the WDF adaptor coefficient γ_0 is also determined by

$\phi^*_{3\,\mathrm{dB}}$. However, assuming that the latter is fixed by (5.67b), γ_0 can usually not be exactly represented in quantized form, and is then approximated. The optimal quantization of the WDF adaptor coefficients γ_{2i-1} can then be performed making a sensitivity analysis along the method described in [Mili99].

5.3.3 Examples

Two examples of warped bireciprocal elliptic WDFs of symmetric and antimetric type are described below.

Example 1: Warped bireciprocal elliptic lowpass filter of symmetric type

Filter specifications :

Passband : $f_p = 5.1\,\mathrm{kHz}$; $a_p = 0.1\,\mathrm{dB}$; (5.74a,b)

Stopband : $f_s = 6.0\,\mathrm{kHz}$; $a_s = 55\,\mathrm{dB}$; (5.74c,d)

Sampling frequency : $F = 16\,\mathrm{kHz}$. (5.74e)

Non-warped reference filter

A non-warped filter is first designed for comparison purposes. Applying the framework in [Gazs85a], the minimum filter degree is $N_{\min} = 5.67$, so that $N = 7$ is selected. The actual stopband edge frequency f_s^* shall then be chosen within the next range :

$$f_{s\,\min} = 5.59\,\mathrm{kHz} \le f_s^* \le f_s = 6.00\,\mathrm{kHz}. \tag{5.75}$$

Setting $f_s^* = 5.9\,\mathrm{kHz}$, the permissible values of the actual passband ripple factor ε_p^* are determined :

$$\varepsilon_{p\,\min} = 0.0269 \le \varepsilon_p^* \le \varepsilon_p = 0.1526. \tag{5.76}$$

Selecting $\varepsilon_p^* = 0.13$, which fixes the actual passband attenuation to $a_p^* = 0.07278\,\mathrm{dB}$, and the actual stopband attenuation to $a_s^* = 68.68\,\mathrm{dB}$, results in the filter parameters provided in Table 5.13. The corresponding filter response is illustrated in Figure 5.8. The lattice WDF adaptor coefficients are listed in Table 5.14, their indexation scheme being specified in [Gazs85a].

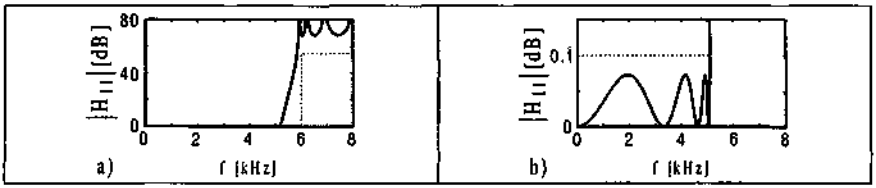

Figure 5.8: Non-warped 7th-order elliptic symmetric lowpass filter : a) Attenuation $|H_{11}|$; b) Passband attenuation $|H_{11}|$.

		ν	θ_i/π, $\mathrm{Re}\{z_{\infty i\nu}\}$	$\mathrm{Im}\{z_{\infty i\nu}\}$
H_1	θ_1/π	—	0	—
	$z_{\infty 1\nu}$	1	0.14376608575026	0
		2	−0.28900912995962	0.75409961847298
		3	$z_{\infty 13} = z^*_{\infty 12}$	
H_2	θ_2/π	—	0	—
	$z_{\infty 2\nu}$	1	−0.42794555096594	0.84665818654054
		2	−0.03515218911283	0.52470416901359
		3, 4	$z_{\infty 2\nu} = z^*_{\infty 2(5-\nu)}$	

Table 5.13: Parameters specifying the filter illustrated in Figure 5.8.

i	γ_{2i}	γ_{2i-1}
0	0.14376608575026	—
1	−0.05507373031949	−0.27655014137966
2	−0.34984921902117	−0.65219251178112
3	−0.45047671141703	−0.89996747942765

Table 5.14: WDF adaptor coefficients (indexation according to [Gazs85a]).

Warped bireciprocal filter

A warped bireciprocal filter is next designed according to the same specifications (5.74). Equation (5.64) indicates that the minimum degree is $N_{\min} = 8.30$, so that $N = 9$ is selected. The permissible range of the common WDF adaptor coefficients is established from (5.66c) :

$$\gamma_{2i\,\min} = -0.580834 \le \gamma^*_{2i} \le \gamma_{2i} = -0.548345; \qquad (5.77)$$

with $i=1,2,3,4$. Setting $\gamma_{2i}^{*}=-(2^{-1}+2^{-4})=-0.5625$ fixes the actual passband attenuation to $a_p^{*}=9\,\mu\,\mathrm{dB}$, and the actual stopband attenuation to $a_s^{*}=57.26\,\mathrm{dB}$, resulting in the parameters and the lattice WDF adaptor coefficients listed in Tables 5.15 and 5.16, respectively. The corresponding filter response is illustrated in Figure 5.9.

Hence, the implementation of the warped bireciprocal filter requires 5 multiplications, and 4 double shifts-and-adds, compared to the non-warped solution which needs 7 multiplications. The number of delays should however also be taken into account to make a fair comparison. Also, the group delay is not the same for both solutions.

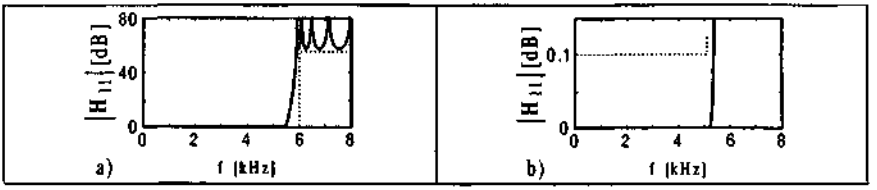

Figure 5.9: Warped 9th-order elliptic symmetric lowpass filter :
a) Attenuation $|H_{11}|$; b) Passband attenuation $|H_{11}|$.

		ν	θ_i/π, $\mathrm{Re}\{z_{\infty i\nu}\}$	$\mathrm{Im}\{z_{\infty i\nu}\}$
H_1	θ_1/π	—	0	—
	$z_{\infty 1\nu}$	1	−0.30791593829745	0
		2	−0.53362043662225	0.78266617252140
		3	−0.40520041460409	0.52585664326284
		4, 5	$z_{\infty 1\nu}=z_{\infty 1(6-\nu)}^{*}$	
H_2	θ_2/π	—	0	—
	$z_{\infty 2\nu}$	1	−0.47430537807415	0.67930370996437
		2	−0.33794464524854	0.29559157232832
		3, 4	$z_{\infty 2\nu}=z_{\infty 2(5-\nu)}^{*}$	

Table 5.15: Parameters specifying the filter illustrated in Figure 5.9.

i	γ_{2i}	γ_{2i-1}
0	– 0.30791593829745	—
1	– 0.5625	– 0.20158096088369
2	– 0.5625	– 0.44071258525899
3	– 0.5625	– 0.68641912204142
4	– 0.5625	– 0.89731710799023

Table 5.16: WDF adaptor coefficients (indexation according to [Gazs85a]).

Improved warped bireciprocal filter

The constraint imposed by (5.62) implies that the passband attenuation is most often featuring a quasi-maxflat response with a substantial margin at the edge frequency of the passband. This is the case for the warped bireciprocal filter depicted in Figure 6.9. It is then worth exploiting this margin, trying to reduce the degree of the warped bireciprocal filter, and/or the number of non-zero bits appearing in the coefficients γ_{2i} [Mili97] [4].

Hence, an attempt is made to design a new warped bireciprocal WDF specifying a lower passband edge frequency $f_p' = 4.9\,\text{kHz}$, the other specifications in (5.74) remaining unchanged. The minimum filter degree becomes $N_{\min} = 7.80$, implying that the effective filter degree is kept at $N = 9$. The range of γ_{2i}^* is then updated as follows :

$$\gamma_{2i\,\min} = -0.551963 \le \gamma_{2i}^* \le \gamma_{2i} = -0.486123; \tag{5.78}$$

with $i = 1,2,3,4$. Choosing $\gamma_{2i}^* = -2^{-1} = -0.5$ sets the actual stopband attenuation to $a_s^* = 57.03\,\text{dB}$. The resulting filter parameters and adaptor coefficients are provided in Tables 5.17 and 5.18, respectively, and the filter response is shown in Figure 5.10. It is observed that the *original* passband specifications (5.74a,b) are fulfilled.

Hence, the last warped bireciprocal filter configuration offers an improved solution, reducing the number of shifts-and-adds to 4 single shift operations. The remaining margin of the filter response can be used to quantize the coefficients γ_{2i-1}.

---

[4] Conversely, for applications that are sensitive to the group delay in the passband, the preservation of this margin is useful to maintain the peak of the group delay at sufficient distance from the passband edge frequency.

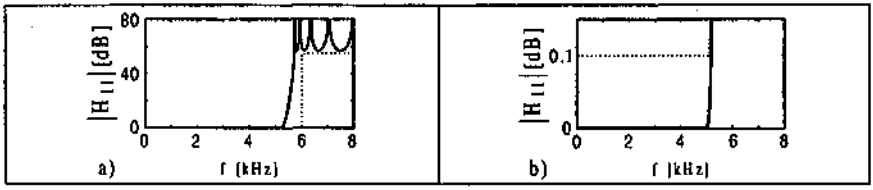

Figure 5.10: Improved warped 9th-order elliptic symmetric filter :
a) Attenuation $|H_{11}|$; b) Passband attenuation $|H_{11}|$.

		ν	θ_i/π, $\mathrm{Re}\{z_{\infty i\nu}\}$	$\mathrm{Im}\{z_{\infty i\nu}\}$
H_1	θ_1/π	—	0	—
	$z_{\infty 1\nu}$	1	−0.26794919243112	0
		2	−0.47336357041117	0.81815720485262
		3	−0.35587515914734	0.54484264489043
		4, 5	$z_{\infty 1\nu} = z^*_{\infty 1(7-\nu)}$	
H_2	θ_2/π	—	0	—
	$z_{\infty 2\nu}$	1	−0.41891328174430	0.70722329525788
		2	−0.29498107908132	0.30481220334710
		3, 4	$z_{\infty 2\nu} = z^*_{\infty 2(5-\nu)}$	

Table 5.17: Parameters specifying the filter illustrated in Figure 5.10.

i	γ_{2i}	γ_{2i-1}
0	−0.26794919243112	—
1	−0.5	−0.17992431632529
2	−0.5	−0.42350063658934
3	−0.5	−0.67565312697720
4	−0.5	−0.89345428164466

Table 5.18: WDF adaptor coefficients (indexation according to [Gazs85a]).

Example 2: Warped bireciprocal elliptic lowpass filter of antimetric type

Keeping the same specifications (5.74), a warped bireciprocal elliptic WDF of antimetric type is designed. Since $N_{\min} = 8.30$, $N = 10$ is selected, leading to the next interval for the actual frequency $f^*_{3\,\mathrm{dB}}$:

$$f_{3\,\mathrm{dB\,min}} = 5.37\,\mathrm{kHz} \le f_{3\,\mathrm{dB}}^{*} \le f_{3\,\mathrm{dB}} = 5.57\,\mathrm{kHz}; \tag{5.79}$$

defined as : $$f_{3\,\mathrm{dB}}^{*} = \frac{F}{\pi} \cdot \arctan\left(\phi_{3\,\mathrm{dB}}^{*}\right). \tag{5.80}$$

Retaining $f_{3\,\mathrm{dB}}^{*} = 5.5\,\mathrm{kHz}$, which sets the actual passband attenuation to $a_p^{*} = 2\,\mu\,\mathrm{dB}$, and the actual stopband attenuation to $a_s^{*} = 63.07\,\mathrm{dB}$, results in the filter parameters provided in Table 5.19 and the filter response illustrated in Figure 5.11.

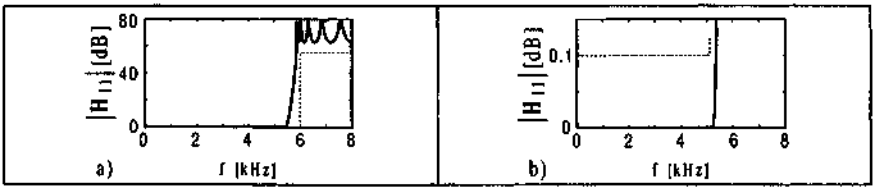

Figure 5.11: Warped 10th-order elliptic antimetric lowpass filter :
a) Attenuation $|H_{11}|$; b) Passband attenuation $|H_{11}|$.

		ν	θ_i/π, $\mathrm{Re}\{z_{\infty i\nu}\}$	$\mathrm{Im}\{z_{\infty i\nu}\}$
H_1	θ_1/π	—	−0.15634694000763	—
	$z_{\infty 1\nu}$	1	−0.53058171718081	0.79279679676948
		2	−0.41976630917910	0.57871844261077
		3	−0.30996396839362	0.14058145194416
		4	−0.35563216539478	−0.39213229283992
		5	−0.47949188787144	−0.70442368113930

Tabie 5.19: Parameters specifying tbe filter illustrated in Figure 5.11.

Lower-order warped bireciprocal filter

Observing as for the symmetric case that the design margin available at the passband edge frequency is relevant, a new warped bireciprocal filter is designed with $f_p' = 4.9\,\mathrm{kHz}$, leading to $N_{\min} = 7.80$, which allows for a degree reduction downto $N = 8$. Doing so, $f_{3\,\mathrm{dB}}^{*}$ shall be chosen according to the constraints :

$$f_{3\,\mathrm{dB\,min}} = 5.45\,\mathrm{kHz} \le f_{3\,\mathrm{dB}}^{*} \le f_{3\,\mathrm{dB}} = 5.49\,\mathrm{kHz}; \tag{5.81}$$

showing that the design margin is tight. Setting $f^*_{3\,\mathrm{dB}} = 5.48\,\mathrm{kHz}$ fixes $a^*_s = 56.22\,\mathrm{dB}$. The achieved filter parameters are given in Table 5.20, whereas the attenuation response is depicted Figure 5.12. The *original* passband specifications (5.74a,b) are noticed to be satisfied.

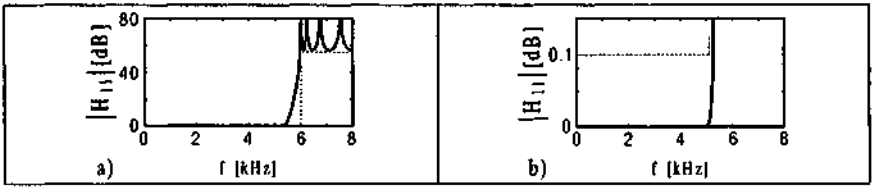

Figure 5.12: Warped 8th-order elliptic antimetric lowpass filter :
a) Attenuation $|H_{11}|$; b) Passband attenuation $|H_{11}|$.

		ν	θ_i/π, $\mathrm{Re}\{z_{\infty i\nu}\}$	$\mathrm{Im}\{z_{\infty i\nu}\}$
H_1	θ_1/π	—	−0.15773875800594	—
	$z_{\infty 1\nu}$	1	−0.51092307968437	0.77470414630975
		2	−0.36237009796235	0.43444527086002
		3	−0.30723054399275	−0.15747961945336
		4	−0.43753065976976	−0.63436526667171

Table 5.20: Parameters specifying the filter illustrated in Figure 5.12.

5.4 Conclusion

In this chapter, the design of lattice-type WDFs is handled by proposing two extensions of the framework [Gazs85a]. The first one concerns the approximation of lowpass prototype antimetric filters featuring Butterworth, Chebyshev, and elliptic responses, including the bireciprocal case, relying on an algebraic approximation method initially proposed in [Darl78] for symmetric filters.

The second extension covers the design of warped bireciprocal lattice-type WDFs suitable for multiplierless implementation in the symmetric case, both symmetric and antimetric elliptic prototype lowpass approximations being handled.

Merging the proposed approximation methods with the initial framework [Gazs85a], one achieves an enhanced design environment that

is easily usable also by non-specialists, presenting a general interest not exclusively linked to WDF filter design, and that could be interfaced with dedicated (VLSI/DSP) filter implementation tools.

Contributions

The main contributions of the chapter considered as original to the best knowledge of the author are :

- **C5–I**: Extension to the *antimetric* case of the prototype lowpass filter design framework published in [Gazs85a] by adapting the algebraic prototype filter approximation method proposed in [Darl78], both initially limited to the symmetric case. Moreover, a systematic scheme for distributing the filter poles over the lattice branches is proposed, cf Figure 5.2, that is valid for any (necessarily even) degree of the filter, the filter parameter ξ_1 defined in (5.15c) being correspondingly specified in (5.23).
- **C5–II**: Identification of the fundamental equation (5.60) characterizing symmetric/antimetric warped bireciprocal WDFs, where (5.60) can be exploited in various ways to get new filter configurations, additionally to the symmetric prototype lowpass case already published in [Gazs85b, Güll86, Mili97, Mili99]. In particular, (5.60) can serve the purpose of studying WDF implementations for multirate signal analysis / synthesis filter pairs operating at arbitrary fractional ratios of sampling rates.
- **C5–III**: Incorporation of the design of *antimetric*-type warped bireciprocal WDF filters to the framework [Gazs85a], with handling of the available design margin. It is recalled that the symmetric case was exhaustively studied in [Güll86, Mili97, Mili99], the integration of the symmetric case into the framework [Gazs85a] being carried out in [Gazs85b].
- **C5–IV**: Based on (5.60), identification of the fact that warped bireciprocal lattice-type WDFs with non-prototype lowpass amplitude or mixed amplitude/phase responses can be designed, provided that adequate approximation techniques are elaborated. As a particular case mentioned in Footnote 1 of the chapter, symmetric warped bireciprocal WDFs are then featuring $(N-1)/2$ identical WDF adaptor coefficients as in the prototype lowpass case, and are thus amenable to efficient multiplierless implementations.

- **C5–V**: Moreover, specific Hilbert Transformers are noticed to be implementable in form of transformed warped bireciprocal lattice-type WDFs, cf Chapter 6, the symmetric case potentially leading again to multiplierless structures.

Further potential research

Based on the former considerations, the next subjects are proposed for potential further research:

- Design of a *suitable antimetric lattice-type WDF structure* providing for an efficient realization of standard antimetric filters, but also of warped bireciprocal antimetric filters, rendering multiplierless implementations possible in the latter case.

  Two cases are considered : 1) complete WDF implementation of reference two-ports, with access to both input and output signal pairs; 2) implementation of scalar transfer functions only.

- Study of *non-prototype lowpass amplitude and mixed amplitude/phase approximation* for warped bireciprocal WDFs (both symmetric and antimetric cases, including also the extension to bandpass responses), with establishment of design guidelines if suitable.

- Elaboration of design rules for *warped bireciprocal Hilbert Transformers* for minimum phase and non-minimum phase cases.

- Study of *tunable warped bireciprocal WDFs*, including control of parameter variation rete to maintain (transient) signal distortions induced by the parameter variation under a certain threshold.

- Based on the expression of the characteristic function featured by warped bireciprocal WDFs, cf (5.60), study of *multirate signal analysis/synthesis filter pairs operating at fractional ratios of sampling frequencies*, distinguishing: 1) rational, and 2) irrational sampling ratios, with extension to complete WDF filterbanks.

- Others.

Chapter 6

Digital Hilbert Transformers

6.1 Introduction

Oscillatory phenomena and signals are often preferably described using their *amplitude* and *phase* (or *frequency*). However, for a real time-varying signal $y_1(t) = a(t) \cdot \cos(\phi(t))$ with amplitude $a(t)$ and phase $\phi(t)$, the notions of amplitude and phase (and thus frequency) are ambiguous, y_1 being a scalar expression of two unknowns a and ϕ, which cannot be explicitly and uniquely defined from y_1 [Vakm98, Cobe99].

To alleviate this ambiguity, Gabor introduced the concept of *Analytic Signals* and the intimately related *Hilbert Transform* [Gabo46], giving rise to large fields of activities in telecommunications, measurement and instrumentation techniques, physics, etc. [Vakm98].

Analytic signals and the Hilbert Transform were of course soon adopted for discrete time signal processing, where Discrete Hilbert Transformers (DHT) have been successfully used in a variety of application fields [Oppe89, Hahn96, Poul96], including *telecommunications* (e.g. signal modulation [Kamm92], effective sampling techniques for real bandpass signals), *instrumentation* (e.g. characterization of nonlinear processes, vibration analysis), *biomedical signal processing* (e.g. ECG, measurement of heart rate fluctuations), *speech processing* (e.g. pitch determination [Hess83], long term speech prediction for compression, detection of voicing signal components, speech/speaker

recognition), *image processing* [Hahn96], and *radar techniques* [Ronq96].

For applications requiring the detection or estimation of limited sets of frequency components, DHTs are offering efficient solutions for the *Envelope Detection* (non-instantaneous analysis), for the *Instantaneous Envelope/Magnitude Detection*, and for the *Instantaneous Phase Detection* [Boas92a, Boas92b]. When applicable, very economic and accurate solutions can be achieved with *spectral subband* decomposition methods [Ronq96] using decimated DHTs [Croc83].

Among the various structures available for the implementation of DHTs [Hahn96], this chapter is essentially considering causal structures, including linear phase Finite Impulse Response Filters (FIR) [Herr69, Oppe89], and Infinite Impulse Response Filters (IIR) derived from analog reference filters, and based either on allpass networks, or on Lattice Wave Digital Filters [Meer84, Fett86, Schü87].

The chapter is organized as follows. Section 6.2 recalls the definition and features of Analytic Signals and the Digital Hilbert Transform. A classification of DHT structures is provided in Section 6.3. Next, the properties of selected *causal* DHT structures are discussed in Section 6.4, and a detailed list of the corresponding design parameters is given in Section 6.5. The selection of DHT performance measurement criteria and their influence on the design and approximation procedure is covered in Section 6.6. The approximation of DHTs is briefly handled in Section 6.7, whereas Section 6.8 is devoted to the transformation of half-band lowpass filters into midband DHTs. Finally, the conclusions are drawn in Section 6.9.

6.2 Digital Hilbert Transform

6.2.1 Ideal Digital Hilbert Transform

By definition [Oppe89, Hahn96], a complex time-discrete signal $y(n) = y_1(n) + j \cdot y_2(n)$, composed of the real sequences $y_1(n)$ and $y_2(n)$ devoid of any DC component, is denoted *analytic* when y_2 is related to y_1 through the ideal (and non-causal) DHT $H_{21\,Ideal}$:

$$Y_2(e^{j\cdot\Omega}) = H_{21\,Ideal}(e^{j\cdot\Omega}) \cdot Y_1(e^{j\cdot\Omega}), \tag{6.1a}$$

$$Y_i(e^{j\cdot 2k\cdot\pi}) = 0, \quad i = 1,2, \quad k = 0, \pm 1, \pm 2, \ldots \tag{6.1b}$$

Limiting the discussion for the remainder of the chapter to the basic frequency range $|\Omega| < \pi$, the ideal DHT is defined as :

$$H_{21\,Ideal}(e^{j\cdot\Omega}) = -j \cdot \mathrm{sign}(\Omega) = e^{-j\cdot(\pi/2)\cdot\mathrm{sign}(\Omega)}. \tag{6.2}$$

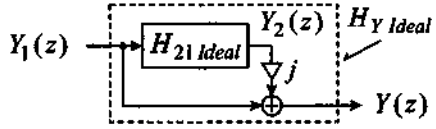

Figure 6.1: Relation between DHT and analytic signal (ideal case).

Hence, the spectrum of the analytic signal is given by (Figure 6.1) :

$$Y(e^{j\cdot\Omega}) = H_{Y\,Ideal}(e^{j\cdot\Omega}) \cdot Y_1(e^{j\cdot\Omega}), \tag{6.3}$$

$$H_{Y\,Ideal}(e^{j\cdot\Omega}) = 1 + j \cdot H_{21\,Ideal}(e^{j\cdot\Omega}), \tag{6.4a}$$

$$= 1 + \mathrm{sign}(\Omega). \tag{6.4b}$$

Under *ideal conditions*, it is therefore observed that :

(i) $H_{Y\,Ideal}$ and Y have by construction a vanishing spectrum for non-positive frequencies;

(ii) $H_{21\,Ideal}(z)$ is a real function, whereas $H_{Y\,Ideal}(z)$ is a complex one;

(iii) applying the same approximation strategy, the design of $H_{21\,Ideal}$ or $H_{Y\,Ideal}$ results in a *strictly equivalent* solution.

Furthermore, $H_{21\,Ideal}$ is a real unit-bounded function which is thus amenable to approximated realization using pseudo-passive/lossless networks [Fett86].

6.2.2 Practical Digital Hilbert Transform

In practice, instead of applying the ideal DHT, a causal and thus realizable three-terminal network is implemented, cf Figure 6.2, whose

effect is in particular to introduce a (non-necessarily constant) delay $\tau(\Omega)$ normalized to the sampling period T_s.

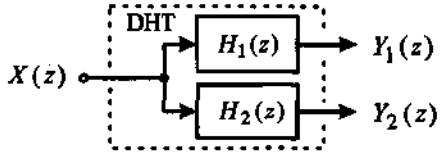

Figure 6.2: Block diagram of the DHT (real input signal).

The resulting network is specified by (cf Figure 6.3) :

$$Y_i(z) = H_i(z) \cdot X(z); \quad i = 1,2; \quad X(e^0) = 0, \tag{6.5}$$

$$Y(z) = H_Y(z) \cdot X(z), \tag{6.6}$$

$$H_Y(z) = H_1(z) + j \cdot H_2(z) = \left[1 + j \cdot H_{21}(z)\right] \cdot H_1(z), \tag{6.7}$$

$$H_{21}(e^{j\cdot\Omega}) = H_2(e^{j\cdot\Omega}) \big/ H_1(e^{j\cdot\Omega}) \cong H_{21\,Ideal}(e^{j\cdot\Omega}), \tag{6.8}$$

for $$0 < a \le |\Omega| \le b < \pi, \quad a \ll 1, \quad (\pi - b) \ll 1. \tag{6.9}$$

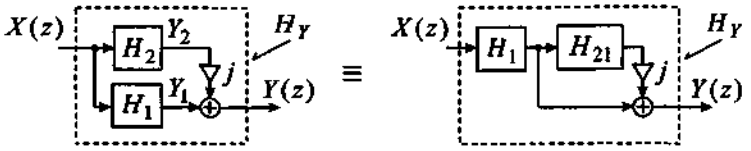

Figure 6.3: Relation between DHT and analytic signal (practical case).

Under *physical realization conditions*, it is observed that :

(i) the causal DHT is characterized by the quality of the amplitude and phase responses of H_{21}, but also by those of H_1 and H_2;

(ii) applying the same approximation strategy, the design of H_{21} or H_Y may result in *different* solutions, and the target function (H_{21} or H_Y) should be selected according to the application.

For certain applications, (quasi-) linearity of the phase responses of H_i can be of significance.

	$H_{21}(e^{j\cdot\omega\cdot T})$		$H_i(e^{j\cdot\omega\cdot T})$ for $i=1,2$		References
	Unitary Ampl. Ratio	Quadrature Phase Resp.	Unitary Ampl. Resp.	Linear Phase	
FIR : *General*					
Linear phase	AUR	Exact	Exact for H_1 Almost for H_2	Exact	[Herr69, Rabi74]
IIR : *General*					[Stef82a] *(non-causal)*
Allpass based :					
➢ Phase splitter	Exact	AQP	Exact	NLP	[Gold69, Dawe85, Rega88b]
➢ Non-causal	Exact	AQP	Exact	Exact / ALP	[Ansa87, Czar82, Stef82b]
➢ ALP including a pure delay	Exact	AQP	Exact	ALP	[Schü87, Jian91]
➢ General ALP	Exact	AQP	Exact	ALP	[Anso97a]
LWDF based :					
➢ Phase splitter	AUR	Exact	ACA	NLP	[Meer84]
➢ Non-causal	AUR	Exact	ACA	Exact / ALP	
➢ ALP including a pure delay	AUR	Exact	ACA	ALP	[Schü87, Chen92]
➢ General ALP	AUR	Exact	ACA	ALP	[Anso97a]

AUR : Almost Unitary amplitude Ratio between Y_1 and Y_2;
AQP : Almost Quadrature Phase resp. between Y_1 and Y_2;
NLP : Non-Linear Phase response between X and Y_i;
ACA : Almost Constant Amplitude resp. between X and Y_i (but not necessarily unitary).
ALP : Almost Linear Phase response between X and Y_i.

Table 6.1: Synopsis of major categories of DHT structures.

6.3 Classification of DHT structures

For $0 < \Omega < \pi$, (6.2) shows that $H_{21} \cong H_{21\,Ideal}$ can be interpreted :

(i) either as a single passband amplitude selective filter, surrounded by two *don't care* bands bounded by unity to ensure pseudo-passivity / losslessness;
(ii) or as an allpass function.

Accordingly, various structures based on Finite Impulse Response (FIR) and Infinite Impulse Response (IIR) filters are available for the implementation of DHTs [Hahn96]. Table 6.1 provides a synopsis of the major DHT network categories [Anso97b]. The different configurations are characterized by the amplitude and phase responses of H_{21}, H_1, and H_2. The selection between these solutions is made according to the application requirements, and the efficiency of each configuration (selectivity, linear phase requirement, group delay, complexity).

FIR based DHTs

In Table 6.1, all non-exact linear phase FIR DHT configurations are grouped under the generic term *General FIR*. These are including e.g. non-linear phase and quasi-linear phase implementations, or the para-unitary lattice FIR [Vaid88]. These configurations are not further discussed in this chapter.

With respect to exact linear phase FIR DHTs, it is noted that two configurations are available, namely Type III and Type IV FIR filters [Oppe89, Herr69, Rabi74], cf Table 6.2. In order to comply with the notation introduced in Subsection 6.2.2, and with later developments in Section 6.4, the FIR filters mentioned in Table 6.2 are assigned to $H_2(z)$. For $0 < \Omega < \pi$, FIR Type III and Type IV filters are featuring a bandpass- and highpass-shaped amplitude response, respectively, cf Table 6.3. FIR Type IV filters can be approximated to achieve a bandpass-shaped amplitude response as well.

Table 6.3 indicates also whether economic DHT implementations are possible or not when the frequency range (6.9) is specified symmetrically around $\Omega = \pm\pi/2$, i.e. $b = \pi - a$ (so-called *midband* DHTs). For FIR Type III filters, each second coefficient is then vanishing, i.e.

$H_2(z) = \hat{H}_2(z^2)$, resulting in a lower implementation complexity [Herr69, Rabi74], especially for multirate applications. This simplification is not possible for FIR Type IV filters.

Type IV FIR filters are not any more considered in this chapter.

Linear phase FIR	Parity of filter degree N_2	Symmetry of coefficients	Transfer function
Type III	Even N_2	Odd symmetry : $h_k = -h_{(N_2-k)}$, $k = 0,1,\ldots,N_2$	$H_2(z) = \sum_{k=0}^{N_2} h_k \cdot z^{-k}$
Type IV	Odd N_2		

Table 6.2: Type III and IV linear phase FIR filters.

	Shape of $H_{21}(e^{j\omega T})$ for $0 < \Omega < \pi$		Economic midband DHT implementation	Ref.
	Bandpass	Highpass		
FIR : Type III	Yes	No	Possible	[Oppe89]
Type IV	Possible	Yes	Not possible	"
IIR : Allpass based	—	—	Possible	
Symmetric LWDF	Yes	No	Possible	[Meer84]

Table 6.3: Frequency response for linear phase FIR and IIR allpass/LWDF based DHTs.

IIR based DHTs

Regarding IIR DHTs, two kinds of filter classes were retained for detailed discussion in this chapter, namely *allpass* and *Lattice Wave Digital Filter* (LWDF) based DHT structures, because of their known advantages (i.e. robustness with respect to finite precision effects, etc.). All remaining DR DHT implementation possibilities are referred to as *General IIR* DHTs in Table 6.1, and are not further considered.

Allpass and LWDF based DHTs can be realized either as *phase splitters*, *Almost Linear Phase* (ALP) networks including a pure delay, or so-called *General ALP* networks, cf Table 6.1. It is noted that LWDF filters used for DHTs are exclusively of *Symmetric* type [Fett86] to ensure an exact phase shift of $\pm\pi/2$ between the two

output signals of tbe filters. *Antimetric* type LWDFs would not be adequate, because their output signals are featuring a phase shift of 0 or π. As mentioned in Table 6.3, LWDF DHTs have a bandpass-shaped frequency response for $0 < \Omega < \pi$. Furthermore, it is observed that both allpass and LWDF structures are amenable to economic implementations for midband DHTs, cf Table 6.3.

Non-causal IIR DHTs were also proposed in the literature, e.g. [Czar82, Stef82a, Stef82b], cf Table 6.1. In practice, such filters are factorized into cascaded causal and anti-causal sub-filters, with intermediate time-reversal of the (segmented) sequence of the signal to be processed, similarly to the scheme described in [Powe91]. Although such filters are featuring either an exact linear or ALP phase response depending on their precise implementation [Powe91], their design requires a thorough analysis to properly select the length of the signal segments, so as to keep the resulting harmonic distortion, group delay, and processing delay at an acceptable level. These structures were not considered in this report.

6.4 Selected causal DHT structures

6.4.1 Finite Impulse Response filter based DHTs

The first configuration to be discussed consists in FIR filters with exactly linear phase response (τ = constant) between $X(z)$, and $Y_i(z)$ for $i = 1,2$. Hence, H_2 is selected as an FIR Type III filter of even degree N_2, whereas H_1 is a pure delay of degree N_1 :

$$H_{2\,FIR}(z) = \sum_{k=0}^{N_2} h_k \cdot z^{-k}, \quad H_{1\,FIR}(z) = z^{-N_1}, \qquad (6.10a,b)$$

with $N_2 = 2 \cdot N_1$, and $h_k = -h_{(N_2-k)}$ for $k = 0,1,...,N_1$, and $h_{N_1} = 0$. The corresponding block diagram is depicted in Figure 6.4 :

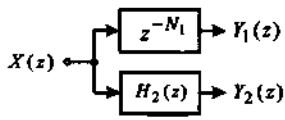

Figure 6.4: Block diagram of linear phase FIR DHTs.

After reformulation of $H_{2\,FIR}$, the expression of the DHT is derived :

$$H_{21\,FIR}(z) = \sum_{k=1}^{N_1} h_{(N_1-k)} \cdot \left[z^{k} - z^{-k} \right]. \tag{6.11}$$

The corresponding spectrum can be written in a compact form : (i) by observing that $H_{21\,FIR}$ is approximating a constant response within each frequency range specified by (6.9), i.e. there are no sign changes within the bands; and (ii) by exploiting the odd frequency response in (6.11) :

$$H_{21\,FIR}(e^{j\cdot\Omega}) = -j \cdot \mathrm{sign}(\Omega) \cdot \left| H_{21\,FIR}(e^{j\cdot\Omega}) \right|. \tag{6.12}$$

Hence, $H_{21\,FIR}$ meets the phase response of $H_{21\,Ideal}$ exactly, whereas the amplitude response is approximated. Finally, the amplitude response of $H_{Y\,FIR}$ is derived :

$$\left| H_{Y\,FIR}(e^{j\cdot\Omega}) \right| = \left| 1 + \mathrm{sign}(\Omega) \cdot \left| H_{21\,FIR}(e^{j\cdot\Omega}) \right| \right|. \tag{6.13}$$

FIR filters are usually implemented in direct form [Oppe89], in which case the signal Y_1 (cf Figure 6.4) is directly available for FIR Type III filters [1], without explicit realization of $H_{1\,FIR}$.

6.4.2 Infinite Impulse Response allpass based DHTs

Alternatively, DHTs can be implemented using IIR allpass (AP) filters $A_i(z)$ of degree N_i (cf Figure 6.5) :

$$H_{i\,AP}(z) = A_i(z), \quad i = 1,2, \tag{6.14}$$

resulting in an allpass type DHT of degree N :

$$H_{21\,AP}(z) = A_1^{-1}(z) \cdot A_2(z), \quad N = N_1 + N_2. \tag{6.15}$$

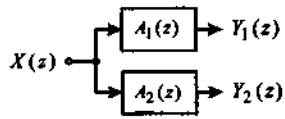

Figure 6.5: Block diagram of IIR allpass based DHTs.

[1] Y_1 is not directly available for FIR Type IV, implying possible additional costs.

The frequency responses are then given for $i=1,2$ by :

$$A_i\left(e^{j\cdot\Omega}\right)=e^{-j\cdot\beta_{Ai}(\Omega)}, \tag{6.16}$$

$$H_{21\,AP}\left(e^{j\cdot\Omega}\right)=e^{-j\cdot\beta_{21\,AP}(\Omega)},\quad \beta_{21\,AP}(\Omega)=\beta_{A2}(\Omega)-\beta_{A1}(\Omega), \tag{6.17a,b}$$

where β_{Ai} and $\beta_{21\,AP}$ are the phase responses of A_i and $H_{21\,AP}$, respectively. Comparing (6.17) to (6.2), $H_{21\,AP}$ is seen to match the amplitude response of $H_{21\,Ideal}$ exactly, whereas the phase response is approximated over the frequency range (6.9). Clearly, the specified[2] phase response over (6.9) is given by (6.18), implying in turn (6.19) :

$$\beta_{21\,APs}(\Omega)=(\pi/2)\cdot\mathrm{sign}(\Omega), \tag{6.18}$$

$$[\beta_{A2}(\Omega)-\beta_{A1}(\Omega)]\cdot\mathrm{sign}(\Omega)>0,\quad N_2\geq N_1. \tag{6.19}$$

The amplitude response of $H_{Y\,AP}$ is finally obtained :

$$\left|H_{Y\,AP}(e^{j\cdot\Omega})\right|=2\cdot\left|\cos\left(\beta_{21\,AP}/2-\pi/4\right)\right|. \tag{6.20}$$

Depending on the selected structure and phase approximation, A_1 and A_2 are either featuring a Non-Linear Phase (NLP) response (so-called *phase splitters*), or an Almost Linear Phase (ALP) response when required.

6.4.2.1 Phase splitters

Phase splitters are designed by the sole approximation of $\beta_{21\,AP}$, applying a certain optimality criterion (e.g. maximally flat, minimax), without separate consideration of β_{A1} or β_{A2} [Gold69, Schü87]. The design is performed by approximating $H_{21\,AP}$ as defined by (6.15)-(6.17) over the frequency range (6.9) using the specifications (6.18). The achieved unstable allpass $H_{21\,AP}$ is then factorized to assign the stable poles to $A_2(z)$, and the unstable ones to $A_1^{-1}(z)$.

For applications that are insensitive to the phase response of $H_{i\,AP}$, phase splitters clearly provide the most efficient solution in terms of selectivity, computational load, and realization costs [Schü87]. It is recommended to implement the allpass functions A_i according to

---

[2] Specified quantities are denoted by suffix "s".

[Fett86] to ensure best functionality even under finite arithmetic conditions.

For phase splitters, it is observed that $H_{Y\,AP}$ is a minimum phase function.

6.4.2.2 ALP structures with pure delay component

When required, allpass based DHTs can be realized with an Almost Linear Phase (ALP) response, in which case two categories of structures can be applied. The first category – discussed in this subsection – is given when one of the A_i reduces to a pure delay. This solution is simple to apply (elementary approximation problem) and often referred to, e.g. [Schü87], although it is offering a reduced number of design parameters (filter coefficients) with respect to the filter degree.

Let us concretely assume that A_2 is a pure delay, in which case the specified pbase response β_{A1s} of A_1 is derived from (6.16) and (6.18) :

$$A_2(z) = z^{-N_2}, \quad \beta_{A1s}(\Omega) = N_2 \cdot \Omega - \beta_{21\,APs}. \tag{6.21}$$

Hence, A_1 is forced to approximate a non-integer delay over the specified frequency range (6.9), ensuring jointly : (i) the realization of $H_{21\,AP}$, and (ii) a quasi-linear phase response of the overall $H_{Y\,AP}$, cf equation (6.7). A similar development applies of course when A_1 and A_2 are interchanged.

6.4.2.3 General ALP structures

The second category of allpass based ALP DHTs corresponds to the so-called *General ALP* structures, where both constituent A_i are non-trivial. This configuration provides the maximum number of free parameters for a given degree $N = N_1 + N_2$.

The specifications to fulfill are given by $\beta_{21\,APs}$ according to (6.18), together with the linear pbase condition :

$$\beta_{Ais}(\Omega) = \tau_s \cdot \Omega + \mathrm{sign}(\Omega) \cdot \mu_i, \quad i = 1,2 \tag{6.22}$$

where the specified group delay τ_s is a design parameter with limited freedom, and where the constant parameters μ_i are chosen so as to satisfy (6.18) :

$$\mu_2 - \mu_1 = \pi/2. \tag{6.23}$$

Basically, General ALP DHTs require the simultaneous approximation of two real objective functions, which can be selected as (application dependent) :

(i) $\beta_{21\,AP}$ together with one of the β_{Ai}, the other β_{Ai} being derived from there;

(ii) $\beta_{21\,AP}$ together with a linear combination of β_{Ai}.

In addition to the selection of τ_s and μ_i, the number of available filter parameters can be distributed on demand over the two objective functions, so as to find the best tradeoff between tightness of $\beta_{21\,AP}$ approximation, and almost linear phase achievement for β_{A1} and β_{A2}. General ALP DHTs are therefore very flexible and considered as the most interesting allpass based structures for ALP.

6.4.3 Lattice Wave Digital Filter based DHTs

The last DHT configurations to be discussed are implemented as IIR symmetric Lattice Wave Digital Filters, cf Chapter 3, first introduced by Nouta [Nout74], and by Fettweis and al. [Fett74a], following complementary approaches. Seemingly, their application to the design of DHTs was first discussed in [Meer84].

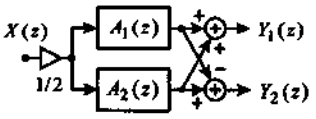

Figure 6.6: Block diagram of LWDF based DHTs.

For the sake of consistency in the chapter, LWDF DHT structures are relabeled according to Figure 6.6. They are composed of two real allpass functions A_i of degree N_i, $i=1,2$, and feature two doubly complementary transfer functions $H_{i\,LWDF}$ of degree $N = N_1 + N_2$:

$$H_{i\,LWDF}(z) = 0.5 \cdot [A_2(z) + (-1)^{(i-1)} A_1(z)]. \tag{6.24}$$

The phase responses β_{Ai} of A_i are still defined by (6.16). Introducing the quantities :

$$\beta_{\Sigma\,LWDF} = (\beta_{A2} + \beta_{A1})/2\,; \quad \beta_{\Delta\,LWDF} = (\beta_{A2} - \beta_{A1})/2, \tag{6.25}$$

the frequency and phase responses of $H_{i\,LWDF}$ are obtained :

$$H_{2\,LWDF}\left(e^{j\cdot\Omega}\right) = -j\cdot\mathrm{sign}(\Omega)\cdot e^{-j\cdot\beta_{\Sigma\,LWDF}}\cdot\left|\sin(\beta_{\Delta\,LWDF})\right|, \tag{6.26}$$

$$H_{1\,LWDF}\left(e^{j\cdot\Omega}\right) = e^{-j\cdot\beta_{\Sigma\,LWDF}}\cdot\left|\cos(\beta_{\Delta\,LWDF})\right|, \tag{6.27}$$

$$\beta_{H1\,LWDF} = \beta_{\Sigma\,LWDF}\,; \quad \beta_{H2\,LWDF} = \beta_{\Sigma\,LWDF} + \frac{\pi}{2}\cdot\mathrm{sign}(\Omega). \tag{6.28}$$

In (6.26) and (6.27), the spectrum of $H_{i\,LWDF}$ is provided in a compact form achieved by observing that no sign changes are affecting $\beta_{\Delta\,LWDF}$ within each of the frequency ranges specified by (6.9).

Hence, $H_{21\,LWDF}$ meets the phase response of $H_{21\,Ideal}$ exactly, whereas the amplitude response is approximated :

$$H_{21\,LWDF}\left(e^{j\cdot\Omega}\right) = -j\cdot\mathrm{sign}(\Omega)\cdot\left|\tan(\beta_{\Delta\,LWDF})\right|. \tag{6.29}$$

The specifications of $\beta_{\Delta\,LWDFs}$ are, (6.19) remaining valid :

$$\beta_{\Delta\,LWDFs}(\Omega) = (\pi/4)\cdot\mathrm{sign}(\Omega), \tag{6.30}$$

so that $\left|H_{i\,LWDF}\right| \equiv \sqrt{2}/2$ in the frequency range (6.9). The amplitude response of $H_{Y\,LWDF}$ is then easily derived :

$$\left|H_{Y\,LWDF}(e^{j\cdot\Omega})\right| = \sqrt{2}\cdot\left|\sin\left(\beta_{\Delta\,LWDF} + \pi/4\right)\right|. \tag{6.31}$$

Equation (6.31) sbows that :

(i) the maximum value of $\left|H_{Y\,LWDF}\right|$ is scaled by $\sqrt{2}$ versus $\left|H_{Y\,FIR}\right|$ and $\left|H_{Y\,AP}\right|$ provided in (6.13) and (6.20);

(ii) apart from this factor $\sqrt{2}$, (6.31) and (6.20) are identical for $\beta_{\Delta\,LWDF} = \beta_{21\,AP}/2$.

Considering the tight connection between allpass and LWDF based DHTs, the latter can similarly be subdivided into phase splitter structures, ALP networks containing a pure delay, and General ALP configurations. This issue will not be further developed here, except that General ALP LWDF DHTs should be approximated selecting $\beta_{\Delta\,LWDF}$ and $\beta_{\Sigma\,LWDF}$ as objective functions.

6.5 Design parameters

Table 6.4 provides the design parameters for FIR DHTs, including possible filter degrees, specified amplitude response, group delay and complexity measure.

Specified Freq. range	Degree (*Note 1*)	Specified amplitude resp. over freq. range (6.9)	Group delay	Complexity (*Note 2*)
General $(b \neq \pi - a)$	$2 \cdot m + 2$	$\left\| H_{21}\left(e^{j\omega \cdot T}\right)\right\|_s =$	$\tau_{H1} = \tau_{H2}$	$N/2$
Symmetric $(b = \pi - a)$	$4 \cdot m - 2$	$= \left\| H_2\left(e^{j\omega \cdot T}\right)\right\|_s = 1$	$= N_1$	$(N+2)/4$

Table 6.4: Design parameters for FIR Type III DHT structures;
(*Note 1*: $N = N_2 = 2 \cdot N_1$; $m = 1,2,3,\ldots$).
(*Note 2*: Indicates Nb of non-zero filter coefficients = Nb of multiplications / sampling period)

Table 6.5 proceeds similarly for allpass and LWDF based DHTs, all parameters applying jointly to both categories of structures. It is noted that different types of DHT networks with distinct behavior are identified according to the parity of $N = N_1 + N_2$, and assignment of the pure delay to A_1 or A_2 (cf Subsection 6.4.2.2). Hence, one distinguishes :

- two types of Phase Splitters PS1 and PS2 for odd and even degree N, respectively;
- three types of ALP DHTs, namely type ALP1 of odd degree N, where A_1 reduces to a pure delay; type ALP2 of odd degree N, with pure delay A_2; and type ALP3 of even degree N, with pure delay A_1;
- two types of General ALP DHTs GALP1 and GALP2 for odd and even degree N, respectively.

For General ALP DHTs, the provided phase specifications, indicated for positive frequencies, are suggested values among other possible choices, cf (6.22) and (6.23). The same applies to the group delay.

Finally, a distinction is made in Tables 6.4 and 6.5 according to the possible symmetry of the frequency range (midband DHTs).

DHT	Structure	Type	References
Allpass based	Phase Splitter	PS1	[Gold69, Ansa87]
		PS2	[Gold69]
	ALP with pure delay	ALP1	[Schü87]
		ALP2	
		ALP3	[Anso97a]
	General ALP	GALP1	[Anso97a]
		GALP2	[Anso97a]
LWDF based	Phase Splitter	PS1	[Meer84]
		PS2	
	ALP with pure delay	ALP1	[Schü87, Jian91]
		ALP2	
		ALP3	[Anso97a]
	General ALP	GALP1	[Anso97a]
		GALP2	[Anso97a]

Table 6.6: References related to Table 6.5.

6.5.1 Midband DHTs

As already mentioned in Section 6.3, an important situation occurs when the frequency range (6.9) is specified symmetrically around $\Omega = \pm\pi/2$, i.e. $b = \pi - a$. In this case, FIR DHTs can be expressed in function of z^2 (half of coefficients cancelled). For allpass and LWDF DHTs of PS1, ALP1, ALP2, and GALP1 type (Table 6.5), the same applies to the constituent A_i, $i = 1,2$, apart from a separate z^{-1} factor for N_i odd. This results in substantial savings already discussed in Chapters 2 and 4.

Midrange DHTs of type PS2 and GALP2 as specified in Table 6.5 are verifying $A_1(z) = \pm A_2(-z)$, i.e. only half of the filter coefficients are independent. However, all coefficients are usually significant (read: non-zero), and the implementation costs are thus higher for PS2 and GALP2 for $b = \pi - a$ than for PS1, ALP1, and GALP1 type DHTs.

Examples of equiripple midband DHTs designed with $|\Omega| \in [a, b] = [0.1 \cdot \pi, 0.9 \cdot \pi]$ are provided in Figures 6.7a-h for the different implementation structures, which were chosen with a similar degree so as to compare their responses.

Specified freq. range	Structure	Type	Degree N	N_1	N_2
General ($b \neq \pi - a$)	Phase Splitter	PS1	$2 \cdot m+1$	$(N-1)/2$	$(N+1)/2$
		PS2	$2 \cdot m$	$N/2$	$N/2$
	ALP with pure delay	ALP1	$2 \cdot m+1$	$(N-1)/2$ A_1 pure delay	$(N+1)/2$
		ALP2	$2 \cdot m+3$	$(N-1)/2$	$(N+1)/2$ A_2 pure delay
		ALP3	$2 \cdot m+2$	$N/2$ A_1 pure delay	$N/2$
	General ALP	GALP1	$2 \cdot m+1$	$(N-1)/2$	$(N+1)/2$
		GALP2	$2 \cdot m+2$	$N/2$	$N/2$
Symmetric ($b = \pi - a$)	Phase Splitter	PS1	$2 \cdot m+1$	$(N-1)/2$	$(N+1)/2$
		PS2	$2 \cdot m$	$N/2$	$N/2$
	ALP with pure delay	ALP1	$4 \cdot m-1$	$(N-1)/2$ A_1 pure delay	$(N+1)/2$
		ALP2	$4 \cdot m+1$	$(N-1)/2$	$(N+1)/2$ A_2 pure delay
		ALP3	$4 \cdot m$	$N/2$ A_1 pure delay	$N/2$
	General ALP	GALP1	$4 \cdot m+1$	$(N-1)/2$	$(N+1)/2$
		GALP2	$2 \cdot m+2$	$N/2$	$N/2$

Table 6.5: Design parameters for IIR allpass based and for LWDF

Specified phase responses (here for $0 < a \le \Omega \le b < \pi$)	Group delay [3]	Nb of indep. parameters	Complexity [4]
$\beta_{21s} = \pi/2$	NLP	N	N
$\beta_{21s} = \pi/2$	NLP	N	N
$\beta_{A1s} = N_1 \cdot \omega \cdot T$ $\beta_{A2s} = N_1 \cdot \omega \cdot T + \pi/2$	$\tau_{A1} = (N-1)/2$ $\tau_{A2} = (N-1)/2$	$(N+1)/2$	$(N+1)/2$
$\beta_{A1s} = N_2 \cdot \omega \cdot T - \pi/2$ $\beta_{A2s} = N_2 \cdot \omega \cdot T$	$\tau_{A1} = (N+1)/2$ $\tau_{A2} = (N+1)/2$	$(N-1)/2$	$(N-1)/2$
$\beta_{A1s} = (N/2) \cdot \omega \cdot T$ $\beta_{A2s} = (N/2) \cdot \omega \cdot T + \pi/2$	$\tau_{A1} = N/2$ $\tau_{A2} = N/2$	$N/2$	$N/2$
$\beta_{A1s} = (N/2) \cdot \omega \cdot T - \pi/4$ $\beta_{A2s} = (N/2) \cdot \omega \cdot T + \pi/4$	$\tau_{A1} = N/2$ $\tau_{A2} = N/2$	N	N
$\beta_{A1s} = (N-1) \cdot \omega \cdot T/2$ $\beta_{A2s} = \beta_{A1s} + \pi/2$	$\tau_{A1} = (N-1)/2$ $\tau_{A2} = (N-1)/2$	N	N
$\beta_{21s} = \pi/2$	NLP	$(N-1)/2$	$(N-1)/2$
$\beta_{21s} = \pi/2$	NLP	$N/2$	N [5]
$\beta_{A1s} = N_1 \cdot \omega \cdot T$ $\beta_{A2s} = N_1 \cdot \omega \cdot T + \pi/2$	$\tau_{A1} = (N-1)/2$ $\tau_{A2} = (N-1)/2$	$(N+1)/4$	$(N+1)/4$
$\beta_{A1s} = N_2 \cdot \omega \cdot T - \pi/2$ $\beta_{A2s} = N_2 \cdot \omega \cdot T$	$\tau_{A1} = (N+1)/2$ $\tau_{A2} = (N+1)/2$	$(N-1)/4$	$(N-1)/4$
$\beta_{A1s} = (N/2) \cdot \omega \cdot T$ $\beta_{A2s} = (N/2) \cdot \omega \cdot T + \pi/2$	$\tau_{A1} = N/2$ $\tau_{A2} = N/2$	$N/2$	$N/2$
$\beta_{A1s} = (N/2) \cdot \omega \cdot T - \pi/4$ $\beta_{A2s} = (N/2) \cdot \omega \cdot T + \pi/4$	$\tau_{A1} = N/2$ $\tau_{A2} = N/2$	$(N-1)/2$	$(N-1)/2$
$\beta_{A1s} = (N-1) \cdot \omega \cdot T/2$ $\beta_{A2s} = \beta_{A1s} + \pi/2$	$\tau_{A1} = (N-1)/2$ $\tau_{A2} = (N-1)/2$	$N/2$	N [5]

based DHT midband structures ($N = N_1 + N_2$; $m = 1,2,3,\ldots$).

---

3 NLP : Non Linear Phase.

4 Indicates Nb of non-zero filter coeffs. = Nb of multiplications / sampling period.

5 Coefficients of A_1 and A_2 are interrelated.

For illustration purpose, Figures 6.7b-h display each the response of AP and LWDF based DHTs composed of exactly the same constituent allpass filters A_1 and A_2.

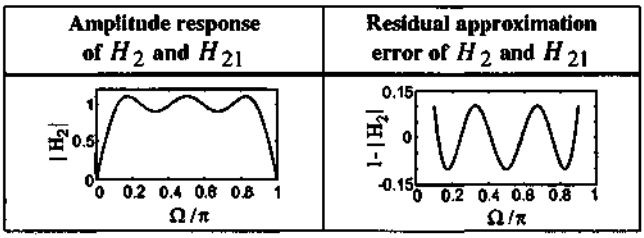

Figure 6.7a: Midband FIR Type III DHT: $N = N_2 = 10$, $N_1 = N_2/2 = 5$.

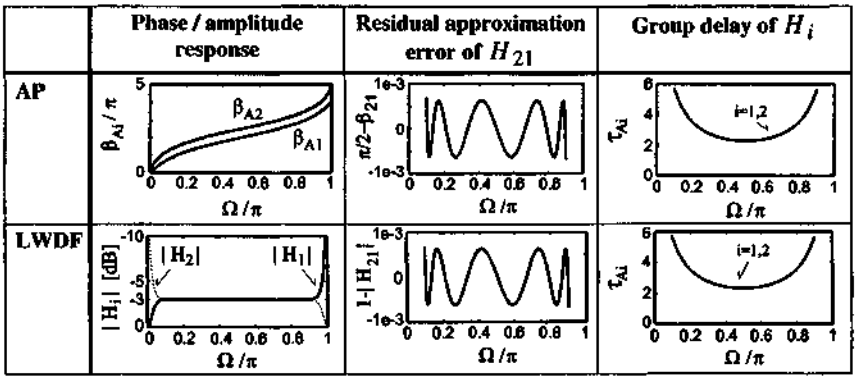

Figure 6.7b: Midband PS1 DHTs: $N_1 = 4$, $N_2 = 5$, $N = N_1 + N_2 = 9$.

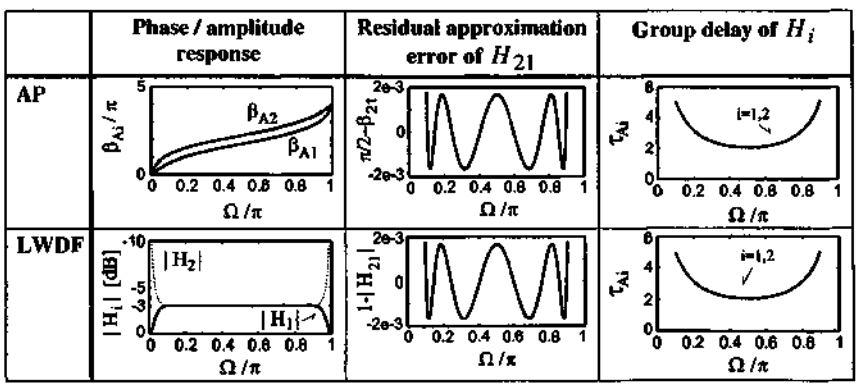

Figure 6.7c: Midband PS2 DHTs: $N_1 = N_2 = 4$, $N = N_1 + N_2 = 8$.

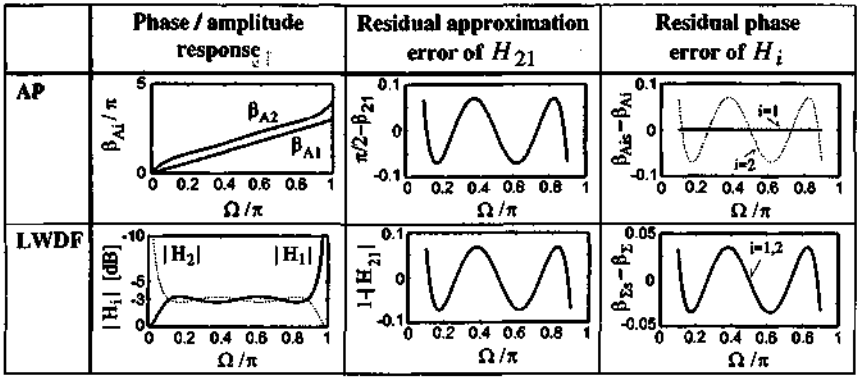

Figure 6.7d: Midband ALP1 DHTs: $N_1 = 3,\ N_2 = 4,\ N = N_1 + N_2 = 7.$

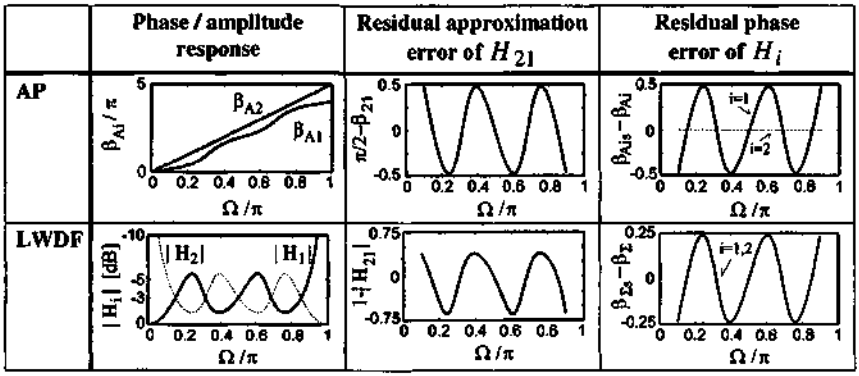

Figure 6.7e: Midband ALP2 DHTs: $N_1 = 4,\ N_2 = 5,\ N = N_1 + N_2 = 9.$

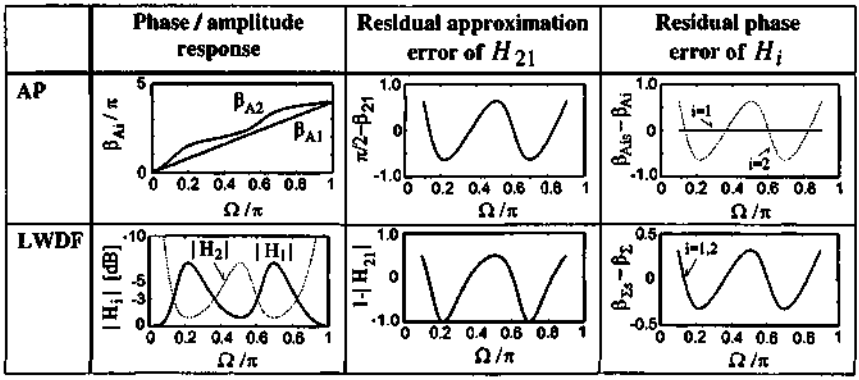

Figure 6.7f: Midband ALP3 DHTs: $N_1 = N_2 = 4,\ N = N_1 + N_2 = 8.$

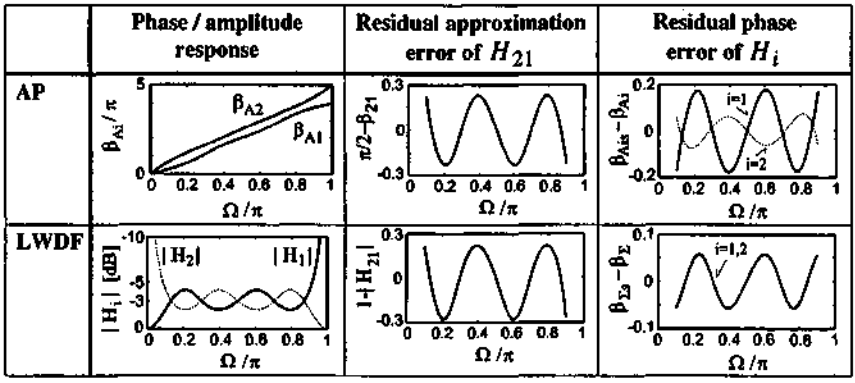

Figure 6.7g: Midband GALP1 DHTs: $N_1 = 4,\ N_2 = 5,\ N = N_1 + N_2 = 9$.

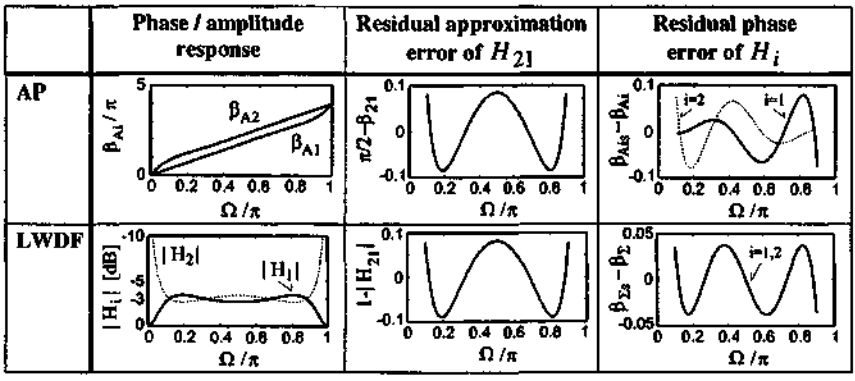

Figure 6.7h: Midband GALP2 DHTs: $N_1 = N_2 = 4,\ N = N_1 + N_2 = 8$.

PS1, PS2, ALP1, ALP2, and ALP3 allpass and LWDF based DHTs are designed by taking $\beta_{21\,AP}(\Omega) = 2 \cdot \beta_{\Delta\,LWDF}(\Omega)$ as objective function. GALP1 and GALP2 allpass and LWDF based DHTs are in turn achieved by choosing $\beta_{21\,AP}(\Omega) = 2 \cdot \beta_{\Delta\,LWDF}(\Omega)$ and $\beta_{\Sigma\,LWDF}(\Omega)$ as objective functions, with assignment of two free filter coefficients to each function.

Tables 6.7 and 6.8 (the allpass coefficients d_v are specified following (2.3)) provide the DHT parameters corresponding to Figures 6.7a-h, with the following performance measures :

$$\delta_{FIR} = \max_{\Omega} \left(1 - \left|H_{21\,FIR}\right|\right), \tag{6.32}$$

$$\delta_{AP1} = \max_{\Omega} \left| \frac{\pi}{2} - \beta_{21\,AP} \right|; \quad \delta_{AP2} = \max_{\Omega,i} \left| \beta_{Ais} - \beta_{Ai} \right|, \; i = 1,2; \tag{6.33}$$

$$\delta_{LWDF1} = \max_{\Omega} \left| 1 - \left| H_{21\,LWDF} \right| \right|; \tag{6.34}$$

$$\delta_{LWDF2} = 0.5 \cdot \left[\max_{\Omega} \left(1 - \left| H_{21\,LWDF} \right| \right) - \min_{\Omega} \left(1 - \left| H_{21\,LWDF} \right| \right) \right]; \tag{6.35}$$

$$\delta_{LWDF3} = \max_{\Omega} \left| \beta_{\Sigma\,LWDFs} - \beta_{\Sigma\,LWDF} \right|. \tag{6.36}$$

Although Figures 6.7a-h are corresponding to particular specifications (selected frequency range, $b = \pi - a$, equiripple approximation, etc.), i.e. the results should be interpreted cautiously before drawing general conclusions, certain tendencies become nevertheless apparent. Hence, the following observations are made (midband DHTs) :

- for applications that are insensitive to the pbase of H_1 and H_2 (cf Figures 6.2 and 6.3), it is confirmed that Phase Splitters PS1 and PS2 of both allpass and LWDF kind clearly provide the most efficient solution in terms of selectivity, computetional load (degree), and realization costs (PS1 offering better savings than PS2 in the midband case);
- for applications needing an ALP response, ALP1 and GALP2 allpass and LWDF structures are competitive candidates with respect to FIR Type III. It is observed that LWDF ALP1 and GALP2 perform better that FIR Type III regarding the tightness of tbe H_{21} approximation, at cost of a non-exact phase of H_1 and H_2.
- for LWDF DHTs, the tangent function in (6.29) is noticed to be asymmetric around $\pm\pi/4$. An equiripple approximation of $\beta_{\Delta\,LWDF}$ does certainly result in an equiripple response of $H_{21\,LWDF}$, but with an offset as can be seen from Figures 6.7b-h. This effect should be taken into account during the approximation process [Meer84], using for instance :
  - $H_{21\,LWDF}$ as objective function, instead of $\beta_{\Delta\,LWDF}$;

➢ or keeping $\beta_{\Delta\, LWDF}$ as objective function, but replacing the specified value (6.30) with :

$$\beta_{\Delta\, LWDFs}(\Omega) = (\pi/4 - \eta)\cdot \mathrm{sign}(\Omega), \tag{6.37}$$

so as to compensate for the offset observed in $H_{21\, LWDF}$. The parameter η is then iteratively estimated, e.g. applying the Fibonacci optimization method [Rao84].

Equation (6.35) gives an *a priori* estimation of the approximation ripple achieved for $H_{21\, LWDF}$ after compensation of the offset induced by the tangent function.

It is finally remarked that this offset vanishes for very small approximation ripples, and can be disregarded in case of very tight approximation of $H_{21\, Ideal}$.

- for GALP1 and GALP2 allpass based DHTs, it is adviced to select one of the phase responses β_{A1} or β_{A2} as objective function for the control of the ALP phase, instead of their sum.
- midband PS1, ALP1, ALP2, and GALP1 allpass and LWDF based DHTs are all featuring an *anti-symmetric* response of β_{A1} and β_{A2} about $\Omega = \pi/2$. Consequently, H_{21}, and the phase of H_i, $i = 1,2$, are all anti-symmetric, whereas the group delay of H_i is symmetric about $\Omega = \pi/2$.

DHT parameters	FIR Type III
$N = N_2$	10
$h_0 = -h_{10}$	-1.0750001710e-01
$h_1 = -h_9$	0
$h_2 = -h_8$	-1.8301341833e-01
$h_3 = -h_7$	0
$h_4 = -h_6$	-6.2638790942e-01
h_5	0
δ_{FIR}	0.10186

Table 6.7: Parameters of the midband FIR DHT displayed in Figure 6.7a.

DHT parameters		PS1	PS2	ALP1	ALP2	ALP3	GALP1	GALP2
N		9	8	9	9	8	9	8
A_1	N_1	4	4	4	4	4	4	4
	d_4	1	1	1	1	1	1	1
	d_3	0	4.978547858e-01	0	0	0	0	4.901957070e-01
	d_2	-6.251900243e-01	-6.492230201e-01	0	4.705420305e-01	0	2.332396699e-01	-1.167443854e-01
	d_1	0	-2.039314022e-01	0	0	0	0	6.803815447e-02
	d_0	4.3553039828e-02	4.703544117e-02		3.522990680e-01	0	1.534186919e-01	-3.279737231e-02
A_2	N_2	5	4	5	5	4	5	4
	d_5	1	1	1	1	1	1	1
	d_4	0	-4.978547858e-01	0	0	-9.932686674e-01	0	-4.901957070e-01
	d_3	-1.118241182e+00	-6.492230201e-01	-4.745080554e-01	0	4.873293696e-01	-2.383681038e-01	-1.167443854e-01
	d_2	0	2.039314022e-01	0	0	-5.520069174e-01	0	-6.803815447e-02
	d_1	2.3683054413e-01	4.703544117e-02	-1.178550042e-01	0	3.659004939e-01	-9.014468258e-02	-3.279737231e-02
	d_0	0			0		0	
ALP DHT	δ_{AP1}	6.2926582e-04	1.6650070e-03	6.9845941e-02	4.7738340e-01	6.4365350e-01	2.4234772e-01	8.5235835e-02
	δ_{AP2}			6.9845941e-02	4.7738340e-01	6.4365350e-01	1.7815420e-01	7.9415959e-02
LWDF DHT	δ_{LWDF1}	6.2946390e-04	1.6663909e-03	7.2403939e-02	6.4316190e-01	1.0003740e+00	2.7730890e-01	8.9086457e-02
	δ_{LWDF2}	6.2926591e-04	1.6650067e-03	6.9959743e-02	5.1728957e-01	7.5023464e-01	2.4720646e-01	8.5442536e-02
	δ_{LWDF3}			3.4922970e-02	2.3869170e-01	3.2182675e-01	5.7003858e-02	3.7512638e-02

Table 8.8: Parameters of the midband allpass and LWDF DHT structures displayed in Figures 6.7b-h.

- similar to FIR Type III configurations, midband PS2 and GALP2 allpass and LWDF based DHTs are in contrast characterized by a *symmetric* response of H_{21} about $\Omega = \pi/2$. Moreover, *LWDF* DHTs are featuring *anti-symmetric* phase responses of $H_{i\,LWDF}$, $i=1,2$, and thus a *symmetric* group delay of $H_{i\,LWDF}$ about $\Omega = \pi/2$. These structures are identified as potentially attractive for certain applications.

In summary, compared to FIR Type III configurations, PS1, PS2, ALP1 et GALP2 allpass and LWDF DHT structures are considered as useful for concrete applications. In contrast, ALP2, ALP3, and probably also GALP1 DHT structures should a priori be disregarded for practical use, in view of their weak selectivity.

In any case, complementary work consisting in a systematic design of FIR, allpass, and LWDF DHTs should be performed over the available parameter ranges, so as to identify the application fields (i.e. specification areas) where each DHT structure is more competitive. Further degrees of freedom available for GALP1 and GALP2 configurations, given by (6.22) and (6.23), should also be investigated.

6.5.2 Symmetric responses of midband PS2 and GALP2 LWDF DHTs

As already stated, the constituent allpass filters of midband PS2 and GALP2 LWDF DHTs are verifying :

$$A_1(z) = (-1)^{\xi} \cdot A_2(-z), \quad \text{with } \xi = 0,1. \tag{6.38}$$

Hence, using equations (2.6) – (2.8), the phase responses of A_1 and A_2 are shown to be related by :

$$\beta_{A1}(\Omega) = N \cdot \pi/2 - \beta_{A2}(\pi - \Omega) - \xi \cdot \pi, \tag{6.39}$$

with $N = N_1 + N_2$, and where the minus sign in front of the factor $\xi \cdot \pi$ was chosen to comply with (6.18) and (6.19). Accordingly, the following expression is derived :

$$\begin{aligned} 2 \cdot \beta_{\Delta\,LWDF}(\Omega) &= \beta_{A2}(\Omega) - \beta_{A1}(\Omega) \\ &= \beta_{A2}(\Omega) + \beta_{A2}(\pi - \Omega) - N \cdot \pi/2 + \xi \cdot \pi. \end{aligned} \tag{6.40}$$

Equation (6.40) demonstrates that $\beta_{\Delta\,LWDF}$ and thus $|H_{21\,LWDF}|$ are both featuring a symmetric response about $\Omega = \pm\pi/2$ for maximally flat or equiripple approximation, cf Figures 6.7c and 6.7h. Moreover, under the same conditions, the expression :

$$2 \cdot \beta_{\Sigma\,LWDF}(\Omega) = \beta_{A2}(\Omega) - \beta_{A2}(\pi - \Omega) + N \cdot \pi/2 - \xi \cdot \pi, \qquad (6.41)$$

shows that the phase response of $H_{i\,LWDF}$, $i = 1,2$, is anti-symmetric about $\Omega = \pm\pi/2$, resulting in a symmetric group delay of $H_{i\,LWDF}$, which is of interest for GALP2 DHT structures, cf Figure 6.7h.

PS2 and GALP2 LWDF DHTs are therefore felt as potentially attractive for applications requiring these symmetries.

6.6 Performance measurement criteria

The selection of appropriate and *uniform* performance measurement criteria is important :

(i) to provide a basis for comparison of *different* structures;

(ii) to decide upon design and approximation strategies;

(iii) to verify the fulfillment of application specifications.

In this report, we are concerned by assessing two kinds of responses : approximation of $H_{21\,Ideal}$, and linearity of the phase responses of H_i $i = 1,2$, when required. The last assessment is obvious from (6.10), (6.14), (6.16), and (6.28), and will not be further discussed.

The tightness of the approximation of $H_{21\,Ideal}$ can in turn be evaluated through two criteria [Anso97a] :

- *Direct* measurement of H_{21};
- *Indirect* measurement of H_{21}.

6.6.1 First criterion : direct measurement of H21

The direct measurement of H_{21} can be done using the next formula :

$$H_{21}\left(e^{j\cdot\Omega}\right) = \left[1 - \Delta(\Omega)\right] \cdot e^{-j\cdot\left[(\pi/2)\cdot\mathrm{sign}(\Omega) - \varepsilon(\Omega)\right]} \qquad (6.42)$$

where $\Delta(\Omega)$ is an even function accounting for the amplitude approximation error of H_{21}, whereas $\varepsilon(\Omega)$ is an odd function corresponding to the phase approximation error.

Hence, the following formulas are derived for $a \leq |\Omega| \leq b$:

FIR DHT : $\mathcal{E} \equiv 0, \quad \delta_{FIR} = \max_{\Omega} |\Delta(\Omega)|$

$$= \max_{\Omega} \left| 1 - \left| H_{21\,FIR} \right| \right| \qquad (6.43)$$

Allpass DHT : $\Delta \equiv 0, \quad \delta_{AP} = \max_{\Omega} |\mathcal{E}(\Omega)|$

$$= \max_{\Omega} \left| \beta_{21\,APs} - \beta_{21\,AP} \right| \qquad (6.44)$$

LWDF DHT : $\mathcal{E} \equiv 0, \quad \delta_{LWDF} = \max_{\Omega} |\Delta(\Omega)|$

$$= \max_{\Omega} \left| 1 - \left| H_{21\,LWDF} \right| \right| \qquad (6.45)$$

where the quantity δ is a measure of the maximum deviation of H_{21} from the specified (amplitude or phase) response.

Clearly, FIR and LWDF type DHTs are providing corresponding results (approximation of the amplitude of H_{21}) and their performance is therefore immediately comparable.

The difficulty stems from the fact that allpass based DHTs are featuring a phase approximation of H_{21}, which is not directly commensurable with an amplitude approximation. In this case, a comparison between structures has to be performed application dependently, cf [Czar82].

Finally, selecting the direct measurement of H_{21} for assessing the quality of the DHTs affects the design strategy of LWDF DHTs, in the sense that the offset observed in $H_{21\,LWDF}$ induced by the tangent function bas to be compensated, cf Subsection 6.5.1.

6.6.2 Second criterion : indirect measurement of H21

The second criterion providing this time a *uniform* performance evaluation, consists in an indirect measurement of H_{21}. This is achieved by using the definition of analytic signals, featuring by construction a vanishing spectrum for non-positive frequencies.

Hence, measuring the attenuation of H_Y achieved for $-b \leq \Omega \leq -a$, one obtains an indirect measure of the quality of the approximation of H_{21}, cf (6.4) and (6.7), which is commensurable for all DHT structures. Accordingly, equations (6.13), (6.20), and (6.31) apply

directly after prior normalization by 2, 2, and $\sqrt{2}$ for FIR, allpass, and LWDF DHTs, respectively.

For FIR DHTs, both criteria are leading to the same result, cf (6.13) and (6.43).

Allpass and LWDF based DHTs are in turn observed to be directly comparable using the second performance measurement criterion, since $H_{Y\,AP}$ and $H_{Y\,LWDF}$ are identical after normalization, according to (6.20) and (6.31). Consequently, LWDF DHTs designed using to the second criterion do not feature any offset of $H_{21\,LWDF}$.

Most important, the final choice of the measurement criterion should be dictated by the application.

6.7 Approximation of DHTs

Almost any approximation method available for FIR, allpass and LWDF *filters* can be used for the approximation of *DHTs*, where various optimality criteria (e.g. maximally flat, minimax, etc.) can be applied. However, specific approximation methods have also been developed for designing DHTs [Koll90].

For minimax/equiripple approximation of FIR DHTs, tables of filter coefficients can be found in [Herr69] (FIR Type III), and in [Rabi74] (FIR Type III + IV). On the other hand, explicit formulas to compute the coefficients of maximally flat midband FIR DHTs are provided in [LeBi96] (FIR Type III) and in [Dumi97] (FIR Type III + IV). A complementary approach was recently developed by Hermanowicz at TU Gdansk / Poland [Dabr97] for the design of FIR DHTs with reduction of the Gibbs phenomenon.

For allpass based DHTs, explicit formulas can be found in [Stef82b] for the design of minimax phase splitters (type PS2), whereas a table of strongly quantized allpass coefficients (Canonic Signed Digit fixed point representation) is given in [Dawe85], also for minimax-like approximation.

Finally, it should be mentioned that Digital Hilbert Transformers can be systematically derived from half-band lowpass filters using transformation methods recalled below.

6.8 Transformation of half-band lowpass filters into midband DHTs

It is known that applying an elementary frequency shift, a real half-band lowpass filter can be transformed into a complex bandpass filter with passband centered around $\Omega = \pi/2$, from which a real midband Digital Hilbert Transformer can be derived [Crys68]. The filter degree remains unchanged.

More precisely, let us consider a half-band lowpass filter $H_{LP}(z)$ featuring a maximum attenuation a_p in the passband $|\Omega| \le \Omega_p$, and a minimum attenuation a_s in the stopband $\Omega_s \le |\Omega| \le \pi$, with $\Omega_s = \pi - \Omega_p$. Applying the transformation :

$$H_{BP}(z) = H_{LP}(-j \cdot z). \tag{6.46}$$

the zeros and poles of the half-band lowpass filter H_{LP} are merely rotated counterclockwise by 90 degrees. As a result, the passband of H_{LP} is shifted onto the frequency range $a \le \Omega \le b$, with $a = \pi/2 - \Omega_p$, and $b = \pi/2 + \Omega_p$, whereas the stopband of H_{LP} is mapped onto $-b \le \Omega \le -a$.

Clearly, the real half-band lowpass filter H_{LP} is transformed into a complex bandpass filter H_{BP}, whose passband is symmetrically centered around $\Omega = \pi/2$, i.e. $b = (\pi - a)$, and with a stopband symmetrically centered around $\Omega = -\pi/2$, cf Figure 6.8.

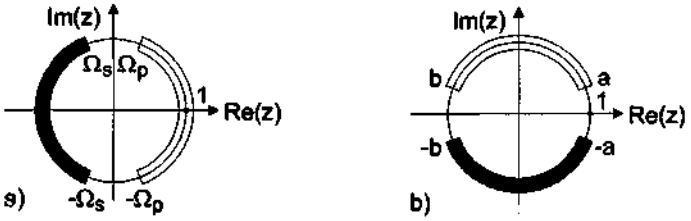

Figure 8.8: Mapping of the passband and stopband ranges : a) Original real half-band lowpass filter; b) Derived complex bandpass with symmetric passband and stopband.

The amplitude response of H_{LP} is preserved by H_{BP}, apart from the frequency shift of $\Omega = \pi/2$. Moreover, if H_{LP} is a minimum phase function, H_{BP} will be as well [Henk97b].

The function H_{BP} in (6.46) precisely corresponds to the transfer function H_Y described in (6.7), except for a possible scale factor γ :

$$H_Y(z) = \gamma \cdot H_{BP}(z) = \gamma \cdot H_{LP}(-j \cdot z). \tag{6.47}$$

The real DHT H_{21} is then derived from $H_Y = H_1 + j \cdot H_2$ by straightforward identification of H_1 and H_2, and final evaluation of $H_{21} = H_2 / H_1$.

Finally, standard frequency transformation methods can be applied to the achieved midband DHT H_{21} to obtain an asymmetric frequency response, i.e. $b \neq (\pi - a)$. This can be done using allpass-type transformations for IIR DHT networks [Cons70], or mappings similar to [Oppe76, Croc76] for FIR DHTs.

6.6.1 Transformation of half-band lowpass FIR filters

This transformation is known from [Jack75]. An N th-order FIR Type I linear phase half-band lowpass filter, where N is an even degree, is given by [Oppe89]:

$$H_{LP}(z) = z^{-N_1} \cdot \left[h_{N_1} + \sum_{\nu=1}^{m} h_{(N_1-2\nu+1)} \cdot \left(z^{2\nu-1} + z^{-(2\nu-1)} \right) \right] \tag{6.48}$$

with :

$$N = 4 \cdot m - 2, \quad m = 1,2,3,\ldots; \quad N_1 = N/2, \quad \text{and} \quad h_{N_1} = 1. \tag{6.49}$$

All odd indexed coefficients of the filter – except the central one h_{N_1} – are zero valued. H_{BP} is then readily derived :

$$H_{BP}(z) = j^{N_1} \cdot z^{-N_1} \cdot \left[1 + j \cdot \sum_{\nu=1}^{m} (-1)^{\nu} \cdot h_{(N_1-2\nu+1)} \cdot \left(z^{2\nu-1} - z^{-(2\nu-1)} \right) \right]. \tag{6.50}$$

Defining the scaling factor as $\gamma = j^{-N_1}$, H_Y becomes :

$$H_Y(z) = H_1(z) + j \cdot H_2(z) = \gamma \cdot H_{BP}(z) \tag{6.51}$$

from which H_1 and H_2 are easily achieved :

$$H_1(z) = z^{-N_1}, \tag{6.52a}$$

$$H_2(z) = z^{-N_1} \cdot \sum_{\nu=1}^{m} (-1)^{\nu} \cdot h_{(N_1-2\nu+1)} \cdot \left(z^{2\nu-1} - z^{-(2\nu-1)} \right). \quad (6.52b)$$

Equations (6.52a,b) are complying with (6.10) and (6.11). This result confirms that a half-band FIR Type I lowpass filter is mapped onto a midrange FIR Type III DHT of same degree.

6.8.2 Transformation of half-band lowpass LWDFs of symmetric type

The transformation of minimum phase half-band lowpass IIR filters (general structure) into allpass based Phase Splitters was mentioned in [Gold69]. This concerned IIR filters of odd / even degree, resulting in PS1 and PS2 type allpass DHTs.

The application of this transformation to map *odd* degreed half-band (or bireciprocal) lowpass LWDF filters into allpass DHTs was discussed in [Dawe85, Ansa87, Rega88b], the LWDF configurations being of *symmetric* type, cf Chapter 3. References [Dawe85, Ansa87] concentrated on the derivation of PS1 allpass based DHT structures. In contrast, the mapping rules provided in [Rega88b] were stated in a general way for an odd-degree, and can thus also be applied to achieve ALP1, ALP2, and GALP1 allpass based DHT networks, although this feature was not explicitly mentioned by the authors.

The transformation method is recalled below for filter networks of degree $N = 4 \cdot m + 1$, $m = 1,2,3,\ldots$. The resulting allpass DHT structures are thus of PS1, ALP2, and GALP1 type, cf Table 6.5. Only half of the PS1 configurations are handled with these filter degrees.

From (4.22) and (6.24), a half-band lowpass LWDF of symmetric type is specified by :

$$H_{LP}(z) = 0.5 \cdot [\, A_1(z) + A_2(z) \,]; \quad N = N_1 + N_2 = 4 \cdot m + 1; \quad (6.53)$$

with $$A_1(z) = \hat{A}_1(z^2), \qquad N_1 = 2 \cdot m; \quad (6.64a)$$

and $$A_2(z) = z^{-1} \cdot \hat{A}_2(z^2), \qquad N_2 = 2 \cdot m + 1. \quad (6.54b)$$

H_{LP} can thus be reformulated as :

$$H_{LP}(z) = 0.5 \cdot [\, \hat{A}_1(z^2) + z^{-1} \cdot \hat{A}_2(z^2) \,], \quad (6.55)$$

and the corresponding complex bandpass becomes :

$$H_{BP}(z) = H_{LP}(-j \cdot z) = 0.5 \cdot [\hat{A}_1(-z^2) + j \cdot z^{-1} \cdot \hat{A}_2(-z^2)]. \quad (6.56)$$

Selecting $\gamma = 2$ in (6.47), H_1 and H_2 are found to be :

$$H_1(z) = \hat{A}_1(-z^2), \quad H_2(z) = z^{-1} \cdot \hat{A}_2(-z^2). \quad (6.57)$$

The result corroborates (6.14), demonstrating that MP1 (odd degreed Minimum Phase), ALP2, and GALP1 half-band lowpass LWDFs of symmetric type (degree $N = 4 \cdot m + 1$) can be mapped onto PS1, ALP2, and GALP1 midband allpass based DHTs (same degree).

Clearly, the development above proceeds similarly to map MP1 and ALP1 half-band lowpass LWDFs (this time of degree $N = 4 \cdot m - 1$) onto PS1 and ALP1 midband allpass based DHTs, which concludes the demonstration for all considered allpass DHT configurations.

It is further recalled that minimum phase half-band lowpass LWDFs are featuring purely imaginary poles [Poly72, Benn88, Vaid93], cf Figure 6.9a. Consequently, the derived complex minimum phase bandpass filter H_{BP} is exclusively composed of real poles, cf Figure 6.9b.

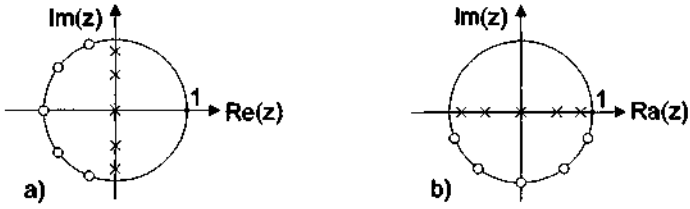

Figure 6.9: Pole and zero configurations :
a) for an odd degreed minimum phase half-band lowpass LWDF;
b) for the derived minimum phase complex bandpass.

Optionally, the achieved midband allpass based DHTs can be mapped onto LWDF DHTs replacing the network of Figure 6.5 by the one of Figure 6.6. Depending on the application, the resulting filter coefficients should however be reoptimized due to the asymmetric response of the tangent function in (6.29).

6.8.3 Transformation of half-band lowpass LWDFs of antimetric type

In this subsection, it is shown that even degreed half-band lowpass LWDF filters of *antimetric* type can be transformed into midband allpass DHTs of same degree, and conversely.

Real antimetric type lowpass LWDFs (even degree N) are realized with a single *complex* allpass of degree $N/2$, cf Subsection 3.4.17 [Meer83, Vaid87a]. After transformation, the resulting allpass based DHTs are real, and composed of two *real* allpasses. The resulting allpass DHTs are of PS2 and GALP2 type of degree $N = 2 \cdot m$ and $N = 2 \cdot m + 2$, respectively, with $m = 1,2,3,\ldots$, cf Table 6.5.

The transfer function of antimetric type LWDFs is, cf (3.104a) :

$$H_{LP}(z) = 0.5 \cdot \left[A(z) + \overline{A(z)} \right]. \tag{6.58}$$

In the *half-band* (bireciprocal) case, $A(z)$ of degree N_A is specified by (2.98a) with $N_0 = 0$, and exclusion of real pole configurations :

$$A(z) = \lambda \cdot j^{N/2} \cdot \prod_{\mu=1}^{n_1} \left(\frac{1 + \alpha_\mu \cdot \hat{z}}{\hat{z} + \alpha_\mu} \right) \cdot \prod_{\nu=1}^{n_2} \left(\frac{1 + d_\nu \cdot \hat{z} + e_\nu \cdot \hat{z}^2}{\hat{z}^2 + d_\nu \cdot \hat{z} + e_\nu} \right) \tag{6.59a}$$

with $\hat{z} = j \cdot z; \quad \lambda = \pm e^{\pm j\pi/4}, \quad N_A = n_1 + 2 \cdot n_2 = N/2.$ (6.59b)

The transformed functions $A(-j \cdot z)$ and $\overline{A(-j \cdot z)}$ are then evaluated :

$$A(-j \cdot z) = \lambda \cdot j^{N/2} \cdot A_1(z), \tag{6.60a}$$

$$\overline{A(-j \cdot z)} = \lambda^* \cdot j^{N/2} \cdot (-1)^{n_1} \cdot A_1(-z); \tag{6.60b}$$

$$A_1(z) = \prod_{\mu=1}^{n_1} \left(\frac{1 + \alpha_\mu \cdot z}{z + \alpha_\mu} \right) \cdot \prod_{\nu=1}^{n_2} \left(\frac{1 + d_\nu \cdot z + e_\nu \cdot z^2}{z^2 + d_\nu \cdot z + e_\nu} \right) \tag{6.60c}$$

so as to achieve the symmetric bandpass (6.46) :

$$\begin{aligned} H_{BP}(z) = H_{LP}(-j \cdot z) &= 0.5 \cdot \left[A(-j \cdot z) + \overline{A(-j \cdot z)} \right] \\ &= 0.5 \cdot \lambda \cdot j^{N/2} \cdot \left[A_1(z) + \lambda^{-2} \cdot (-1)^{n_1} \cdot A_1(-z) \right]. \end{aligned} \tag{6.61}$$

Hence, selecting :

$$\gamma = 2 \cdot \lambda^{-1} \cdot j^{-N/2}, \tag{6.62}$$

and observing that $\lambda^{-2} \cdot (-1)^{n_1} = \pm j$, one obtains from (6.47) :

$$H_Y(z) = \gamma \cdot H_{BP}(z) = [\, A_1(z) \pm j \cdot A_1(-z) \,]. \qquad (6.63)$$

Finally, the constituent functions H_1 and H_2 of the derived midband allpass DHT are found to be :

$$H_1(z) = A_1(z), \quad H_2(z) = \pm A_1(-z). \qquad (6.64a,b)$$

It is thus demonstrated that even degreed half-band lowpass LWDF filters of antimetric type can be transformed into midband allpass DHTs of same degree, and conversely. More specifically, minimum phase and GALP2 half-band lowpass LWDFs of antimetric type are mapped onto midband PS2 and GALP2 allpass DHTs. The corresponding network degrees are $N = 2 \cdot m$ and $N = 2 \cdot m + 2$, respectively, with $m = 1,2,3,\ldots$.

Similarly to symmetric LWDFs, minimum phase half-band lowpass LWDFs of antimetric type are characterized by purely imaginary poles [Meer83]. As a consequence, the derived bandpass H_{BP}, as well as the constituent allpass functions H_1 and H_2 of the resulting PS2 DHT, are all purely real.

Again, the allpass based DHTs obtained after transformation can be further converted into LWDF DHTs, substituting the network of Figure 6.5 by the one provided in Figure 6.6. Depending on the targeted application, the filter coefficients of the so achieved LWDF DHTs should possibly be reoptimized due to the tangent function in (6.29).

It is worth noticing here that the original lowpass LWDF of *antimetric* type is then mapped onto a *symmetric* type LWDF implementing the DHT, which is an interesting result.

6.8.4 Synopsis

A synopsis on the transformation from half-band lowpass filters to corresponding midband DHT networks, and vice-versa, is given in Table 6.9.

Transformation							Filter degree ([6])	Refs. on transformation
Lowpass half-band filters				Midband DHTs				
Filter type	Structure	Type		Filter type	Structure	Type		
FIR [Oppe89]	Linear phase	Type I	⇔	**FIR** [Oppe89]	Linear phase	Type III	Even N_2	[Jack75]
Symmetric LWDF	Min. phase	MP1	⇔	**Allpass** based	Phase Splitter	PS1	Odd N	[Dawe85, Ansa87, Rega88b] *[Gold69]* ([7])
	ALP with pure delay	ALP1	⇔		ALP with pure delay	ALP1	Odd N	
		ALP2	⇔			ALP2	Odd N	
						ALP3	Even N	
	General ALP	GALP1	⇔		General ALP	GALP1	Odd N	
Antimetric LWDF	Min. phase	MP2	⇔		Phase Splitter	PS2	Even N	[Anso97b] *[Gold69]* ([7])
	General ALP	GALP2	⇔		General ALP	GALP2	Even N	[Anso97b]
Symmetric LWDF	Min. phase	MP1	⇔	**Symmetric LWDF** based	Phase Splitter	PS1	Odd N	
	ALP with pure delay	ALP1	⇔		ALP with pure delay	ALP1	Odd N	
		ALP2	⇔			ALP2	Odd N	
						ALP3	Even N	
	General ALP	GALP1	⇔		General ALP	GALP1	Odd N	
Antimetric LWDF	Min. phase	MP2	⇔		Phase Splitter	PS2	Even N	[Anso97b]
	General ALP	GALP2	⇔		General ALP	GALP2	Even N	[Anso97b]

Table 6.9 : Transformation from lowpass half-band filters into midband DHTs.

[6] Filter degree remains unchanged by the transformation process; $N = N_1 + N_2$.

[7] The transformation mentioned in [Gold69] does not refer to LWDF networks.

6.9 Conclusion

This chapter was devoted to studying Digital Hilbert Transformers along topics that will be summarized in the list of contributions.

There is one issue that is important to notice. When the frequency response $H_Y(z)$ of DHTs – cf (6.7) and Figure 6.3 – is featuring a stopband that is not covering the entire frequency range $-\pi \le \Omega \le 0$, as it is the case for the DHT configurations discussed in this chapter, one has to take care that the input signal $X(z)$ is devoid of any spectral energy at frequencies that are not filtered out by $H_Y(z)$. Otherwise, the DHT is leaking, since its output signal $Y(z)$ possesses spectral contents at non-positive frequencies, condition (6.1b) being in particular violated, and the analyticity of the signal $Y(z)$ is then consequently affected.

In case the input signal $X(z)$ is not naturally complying with all operational conditions, two solutions are possible. The first one consists in preconditioning $X(z)$ with a real filter preceding the DHT and rejecting the injuring spectral contents (e.g. notch filter centered at $\Omega = 0$, and at $\Omega = \pm\pi$ according to the DHT used).

The second possibility consists in designing a complex DHT with $H_Y(z)$ featuring a stopband extending to $-\pi \le \Omega \le 0$ as proposed in [Reil94] for FIR implementations. For allpass-based and lattice WDF-based DHT structures we propose the next alternatives :

i) Design a slightly warped bireciprocal lattice-type WDF lowpass filter with $f_{3\,\mathrm{dB}} < f_s/4$, cf Section 5.3, followed by the transformation (6.46);

ii) Apply a transformation from half-band lowpass filter to a midband DHT, followed by a complex first-order allpass-based frequency transformation;

iii) Directly design a complex DHT embedding all functionalities.

Contributions

To the best knowledge of the author, the next contributions of the chapter are considered as original :

- **C6–I**: Systematic study of causal Digital Hilbert Transformers, related properties, frequency responses, and implementation structures, results of particular interest being :
  - **C6–I/1**: Classification of major categories of DHT structures as discussed in Section 6.3, where the amplitude and phase responses of $H_{21}(z)$, but also those of the constitutive filters $H_i(z)$, $i=1,2$, are distinguished, providing a synopsis in Table 6.1.
  - **C6–I/2**: Determination of design parameters for general and symmetric FIR DHTs, as well as for general and midband allpass-based and lattice WDF-based DHT structures, as indicated in Tables 6.4 and 6.5, thoroughly comparing their features, and illustrating all cases with examples in the series of Figures 6.7.
  - **C6–I/3**: Following Subsection 6.5.2, identification of an IIR network featuring an Almost Linear Phase response together with symmetric group delay and symmetric approximation of the Hilbert response around a quarter of the sampling frequency (actually the GALP2 lattice WDF DHT structure).
  - **C6–I/4**: Comparison of two DHT performance measurement criteria relying on different sets of error measures (cf Section 6.6), the selection between them being done according to the application.
- **C6–II**: Review of a known transformation method to convert low-pass/highpass half-band filter pairs into midband DHTs (Section 6.8), providing a synoptic view in Table 6.9. Moreover, even-degreed half-band lattice WDFs of *antimetric* type were observed to be transformed into *symmetric* lattice WDF DHTs, a feature that was not cited before. Also, prior examples involving even-degreed symmetric lattice WDF DHTs were not found in the literature.

Further potential research

Potential further research is proposed for the subjects listed below :

- Systematic design of FIR, allpass, and LWDF DHTs over the available parameter ranges, in order to identify specification areas and related application fields each of the DHT structures is best suiting to.
- In the scope of analytic signal filtering problems, study of the joint approximation of the DHT and succeeding real filter, including analysis of the improvements.
- As an extension of the covered subject, study of differential DHTs and differentiation operators, establishing a list of implementation structures and comparing their performance, considering in particular WDF-based solutions.
- Others.

Chapter 7

Eigenfilter Approximation of Allpass Filters and Lattice-Type WDFs

7.1 Introduction

The eigenfilter approach was introduced by Vaidyanathan and Nguyen [Vaid87b] as an alternative weighted least-squares discrete-time filter approximation method. In this design method, the objective function is expressed in a quadratic form, and the filter coefficients are obtained as an eigenvector of a particular real, symmetric and positive-definite matrix Q.

Compared to certain other approximation techniques, the eigenfilter approach features a simple and flexible formulation, supporting frequency-domain, time-domain, or mixed time/frequency-domain specifications [Vaid87b, Pei94a]. In addition, it can be adapted to various filter classes/structures, and does not request an initial guess of the solution.

The eigenfilter technique was first applied to linear-phase FIR filters [Vaid87b], with a later generalization for arbitrary amplitude / phase response FIR filters [Nguy93]. Further applications concern the design of mono- and two-dimensional IIR filters [Pei94a, Chen96]. More recently, the method was specialized for real [Nguy94] or complex [Pei94b] allpass filters, where the allpass functions can be applied

either to phase-equalization problems, or to designing IIR lattice filters composed of elementary allpass networks [Nguy94, Pei94b, Fett74a, Fett81a, Vaid87a].

This chapter addresses the design of complex and real allpass eigenfilters, including the design of Lattice-type Wave Digital Filters, the major contribution concerning the derivation of the general form of the eigenfilter matrix Q. The internal structure of this matrix is revealed, leading to a substantial improvement of the computational implementation of the eigenfilter approximation technique. The basic results were formerly published in [Anso95].

The remainder of the chapter is organized as follows. Section 7.2 provides the matrix formulation of the allpass design problem. In Section 7.3, the connection between the weighted least squares and the eigenfilter approximation methods are recalled, including definition of the eigenfilter matrix Q, and discussion of related properties. The internal structure of the Q matrix is then identified in Section 7.4, from which a complexity measure of the eigenfilter design method is established. The corresponding design algorithm is then presented in Section 7.5, and illustrated by two examples provided in Section 7.6, before drawing the conclusions in Section 7.7.

7.2 Matrix formulation of the allpass design problem

The transfer function (2.3a,b) of an Nth-order complex allpass is recalled [1] :

$$A(z)=\frac{z^N\cdot\tilde{D}(z)}{D(z)}=\frac{z^N\cdot\sum_{\nu=0}^{N}d_\nu^*\cdot z^{-\nu}}{\sum_{\nu=0}^{N}d_\nu\cdot z^{\nu}},\quad\text{with } d_N\neq 0 \qquad (7.1a,b)$$

The pbase response $\beta_A(\Omega)$ of the allpass is then specified by :

$$\beta_A(\Omega)=-\mathrm{Arg}\left\{\ A\left(e^{j\cdot\Omega}\right)\right\}=-[N\Omega+2\beta_D(\Omega)], \qquad (7.2)$$

[1] The definition of $A(z)$ and the sign of the phase response $\beta_A(\Omega)$ are differing from those used in [Anso95].

$$\beta_D(\Omega) = -\arctan\left(\frac{\sum_{\nu=0}^{N} d_{R\nu}\cdot\sin(\nu\Omega) + d_{I\nu}\cdot\cos(\nu\Omega)}{\sum_{\nu=0}^{N} d_{R\nu}\cdot\cos(\nu\Omega) - d_{I\nu}\cdot\sin(\nu\Omega)}\right), \tag{7.3}$$

with coefficients :

$$d_\nu = d_{R\nu} + j\cdot d_{I\nu}. \tag{7.4}$$

Referring to Table 2.1, it is observed that the allpass defined in (7.1) – (7.4) counts (2·N+2) real parameters $d_{R\nu}$ and $d_{I\nu}$, for $\nu = 0,\ldots,N$, i.e. one more than the canonic number of free parameters of an N-th order complex allpass. This redundancy will be later alleviated by introducing a constraint into the approximation process.

7.2.1 Ideal filter response

Ideally, the allpass is assumed to match the specified phase response $\beta_{As}(\Omega)$ *exactly*. In this case, one achieves from (7.2) – (7.3) [2] :

$$\beta_{Ds}(\Omega) = -0.5\cdot[N\Omega + \beta_{As}(\Omega)], \tag{7.5}$$

$$\tan(\beta_{Ds}(\Omega)) = \frac{\sin(\beta_{Ds}(\Omega))}{\cos(\beta_{Ds}(\Omega))} = \frac{-\sum_{\nu=0}^{N} d_{R\nu}\cdot\sin(\nu\Omega) + d_{I\nu}\cdot\cos(\nu\Omega)}{\sum_{\nu=0}^{N} d_{R\nu}\cdot\cos(\nu\Omega) - d_{I\nu}\cdot\sin(\nu\Omega)}. \tag{7.6}$$

After cross-multiplication and further trigonometric simplifications, the last expression can be rewritten as :

$$\sum_{\nu=0}^{N} d_{R\nu}\cdot\sin(\beta_{Ds}+\nu\Omega) + \sum_{\nu=0}^{N} d_{I\nu}\cdot\cos(\beta_{Ds}+\nu\Omega) = 0, \tag{7.7}$$

where the equivalence between (7.6) and (7.7) is discussed e.g. in [Lang93], pp. 23-25. Introducing the vector notation :

$$\begin{cases} d = [\,d_{R0} \;\; d_{R1} \;\; \ldots \;\; d_{RN} \mid d_{I0} \;\; d_{I1} \;\; \ldots \;\; d_{IN}\,]^T \\ C(\Omega) = [\,c_{R0} \;\; c_{R1} \;\; \ldots \;\; c_{RN} \mid c_{I0} \;\; c_{I1} \;\; \ldots \;\; c_{IN}\,]^T \end{cases} \tag{7.8}$$

$$\begin{cases} c_{R\nu} = \sin(\beta_{Ds}+\nu\Omega) \\ c_{I\nu} = \cos(\beta_{Ds}+\nu\Omega) \end{cases}, \quad \text{with } \nu = 0,1,\ldots,N; \tag{7.9}$$

---

[2] Specified quantities are denoted by suffix "s".

$[.]^T$ denoting transposition, leads to the equivalent inner product form [Pei94b] :

$$d^T \cdot C(\Omega) = 0. \tag{7.10}$$

Clearly, for real allpass filters $d_{I\nu} = 0$, $\forall \nu$, and the $c_{I\nu}$ terms are simply dropped.

7.2.2 Actual filter response

In practice, the actual pbase response will hardly match the desired response identically, and the left hand-sided term in (7.10) will be affected by the error function [Pei94b] :

$$e(\Omega) = d^T \cdot C(\Omega). \tag{7.11}$$

Comparing (7.11), (7.7), and (7.5), it is recognised that the error function $e(\Omega)$ is non-linearly related to the phase response error.

7.3 WLS approximation of complex allpass eigenfilters

The Weighted Least-Squares (WLS) approximation of the complex allpass $A(z)$ corresponds to the following unconstrained optimization problem :

$$\text{minimize} \qquad E_{WLS} = \int_{\Gamma} W(\Omega) \cdot e(\Omega)^2 \cdot d\Omega \tag{7.12}$$

where Γ denotes the frequency region of interest, and $W(\Omega)$ is a non-negative weighting function. Using (7.11), E_{WLS} can be restated :

$$\begin{aligned} E_{WLS} &= \int_{\Gamma} W(\Omega) \cdot \left[d^T \cdot C \right]^2 \cdot d\Omega \\ &= d^T \cdot \left[\int_{\Gamma} W(\Omega) \cdot C \cdot C^T \cdot d\Omega \right] \cdot d = d^T \cdot Q \cdot d \end{aligned} \tag{7.13}$$

with the specific Q matrix :

$$Q = \int_{\Gamma} W(\Omega) \cdot C \cdot C^T \cdot d\Omega. \tag{7.14}$$

One deduces from the WLS formulation that Q is a real, symmetric, and definite-positive matrix [Vaid87b]. As such, all eigenvalues of Q are real and strictly positive [Cull72]. Introducing the constraint $d^T \cdot d = 1$, so as to reduce the parameters to the canonical number of free parameters, and to avoid any trivial solution [Vaid87b], (7.12) can be replaced by the constrained optimization problem :

$$\begin{cases} \text{minimize} & E_{WLS} = \int_{\Gamma} W(\Omega) \cdot e(\Omega)^2 \cdot d\Omega \\ \text{subject to} & d^T \cdot d = 1 \end{cases} \tag{7.15}$$

which is equivalent to the next formulation using the Lagrange multiplier optimization method [Rao84] :

$$\begin{cases} (Q - \lambda \cdot I) \cdot d = 0 \\ d^T \cdot d = 1, \end{cases} \tag{7.16}$$

where I denotes the N x N unit-matrix, and 0 the N x 1 zero column-vector. Hence, the solution vector d to the WLS approximation problem is simply an eigenvector of Q. According to Rayleigh's principle, this eigenvector corresponds to the minimum eigenvalue of Q [Vaid87b, Pei94a, Nguy93, Nguy94, Pei94b] and can easily be processed using the iterative power method [Vaid87b, Golu89].

It should be noticed that there are no direct means to enforce the stability of the designed allpass filters. Instead, the stability is *indirectly* controlled by the specified phase response $\beta_{As}(\Omega)$. Stability should thus be checked after design.

7.4 Internal structure of the eigenfilter matrix

The eigenfilter matrix Q is featuring several symmetries which are best identified rewriting $C(\Omega)$ as :

$$C(\Omega) = \left[\frac{C_R(\Omega)}{C_I(\Omega)}\right]; \quad \begin{cases} C_R(\Omega) = [c_{R0} \quad c_{R1} \quad \cdots \quad c_{RN}]^T \\ C_I(\Omega) = [c_{I0} \quad c_{I1} \quad \cdots \quad c_{IN}]^T \end{cases} \tag{7.17}$$

from which one derives :

$$C \cdot C^T = \begin{bmatrix} C_R \\ \hline C_I \end{bmatrix} \cdot \left[\, C_R^T \mid C_I^T \, \right] = \left[\begin{array}{c|c} C_R \cdot C_R^T & C_R \cdot C_I^T \\ \hline C_I \cdot C_R^T & C_I \cdot C_I^T \end{array} \right]. \tag{7.18}$$

Inserting the last expression into (7.14) lets the internal structure of the Q matrix become apparent :

$$Q = \int_\Gamma W(\Omega) \cdot \left[\begin{array}{c|c} C_R \cdot C_R^T & C_R \cdot C_I^T \\ \hline C_I \cdot C_R^T & C_I \cdot C_I^T \end{array} \right] \cdot d\Omega = \left[\begin{array}{c|c} Q_{RR} & Q_{RI} \\ \hline Q_{IR} & Q_{II} \end{array} \right], \tag{7.19}$$

with, cf (7.18) : $$Q_{IR} = Q_{RI}^T . \tag{7.20}$$

Each of the sub-matrices Q_{RR}, Q_{RI}, Q_{IR}, and Q_{II} can in turn be decomposed into Toeplitz- and Hankel-form matrices, leading to a highly regular problem formulation. For that purpose, let us consider an entry of Q_{RR} :

$$Q_{RR}(\mu,\nu) = \int_\Gamma W(\Omega) \cdot c_{R\mu} \cdot c_{R\nu} \cdot d\Omega \tag{7.21}$$

with $\mu,\nu = 0,1,...,N$, and :

$$\begin{aligned} c_{R\mu} \cdot c_{R\nu} &= \sin(\beta_{Ds} + \mu\Omega) \cdot \sin(\beta_{Ds} + \nu\Omega) \\ &= 0.5 \cdot \{ \cos[(\mu-\nu)\cdot\Omega] - \cos[2\beta_{Ds} + (\mu+\nu)\cdot\Omega] \} \end{aligned} \tag{7.22}$$

Introducing matrices P_1 and P_2 with elements :

$$P_1(\mu,\nu) = (\mu-\nu)\cdot\Omega ; \quad P_2(\mu,\nu) = 2\beta_{Ds} + (\mu+\nu)\cdot\Omega , \tag{7.23}$$

it is possible to rewrite (7.21) in matrix form :

$$Q_{RR} = 0.5 \cdot \int_\Gamma W(\Omega) \cdot [\cos(P_1) - \cos(P_2)] \cdot d\Omega . \tag{7.24}$$

Equations (7.23) show that P_1 is a skew-symmetric Toeplitz matrix, whereas P_2 corresponds to a Hankel matrix, as can be readily verified for $N = 3$:

$$P_1 = \begin{pmatrix} 0 & -1 & -2 & -3 \\ 1 & 0 & -1 & -2 \\ 2 & 1 & 0 & -1 \\ 3 & 2 & 1 & 0 \end{pmatrix} \cdot \Omega ; \quad P_2 = 2\beta_{Ds} + \begin{pmatrix} 0 & 1 & 2 & 3 \\ 1 & 2 & 3 & 4 \\ 2 & 3 & 4 & 5 \\ 3 & 4 & 5 & 6 \end{pmatrix} \cdot \Omega . \tag{7.25}$$

Considering the configuration of matrices P_1 and P_2 together with the even symmetry $\cos(\pm x) = \cos(x)$, it is observed that Q_{RR} can be decomposed into two constituent matrices Q_{C1} and Q_{C2} according to (7.26) and (7.27), where Q_{C1} is shown to feature a Toeplitz symmetry, whereas Q_{C2} is characterized by a Hankel form symmetry.

$$\begin{cases} Q_{RR} = Q_{C1} - Q_{C2} \\ Q_{II} = Q_{C1} + Q_{C2} \end{cases} ; \quad \begin{cases} Q_{RI} = Q_{S1} + Q_{S2} \\ Q_{IR} = -Q_{S1} + Q_{S2} \end{cases} \tag{7.26}$$

Hence, Q_{C1} and Q_{C2} are composed of only $(N+1)$ and $(2N+1)$ different entries, respectively. The remaining entries of Q_{C1} and Q_{C2} are then structurally determined.

Proceeding similarly for Q_{II}, Q_{RI}, and Q_{IR}, the remaining expressions in (7.26) and (7.27) are achieved. It is observed that Q_{II} is determined by the same constituent matrices Q_{C1} and Q_{C2} than Q_{RR}.

$$\begin{cases} Q_{C1} = 0.5 \cdot \int_{\Gamma} W(\Omega) \cdot \cos(P_1) \cdot d\Omega ; & [Symmetric\ Toeplitz] \\ Q_{C2} = 0.5 \cdot \int_{\Gamma} W(\Omega) \cdot \cos(P_2) \cdot d\Omega ; & [Hankel] \\ Q_{S1} = 0.5 \cdot \int_{\Gamma} W(\Omega) \cdot \sin(P_1) \cdot d\Omega ; & [Skew-symmetric\ Toeplitz] \\ Q_{S2} = 0.5 \cdot \int_{\Gamma} W(\Omega) \cdot \sin(P_2) \cdot d\Omega ; & [Hankel]. \end{cases} \tag{7.27}$$

Q_{RI} and Q_{IR} require the computation of Q_{S1} and Q_{S2}, which are counting N and $(2N+1)$ different entries, respectively. The entries of the main diagonal of Q_{S1} are identical to zero and should not be explicitly calculated. Moreover, only one of the matrices Q_{RI} and Q_{IR} has to be processed, since they are interrelated by (7.20).

Finally, the evaluation of the Q matrix of an N-th order complex allpass filter requires the computation of $(6N+3)$ different entries in (7.27). For real allpass filters, this figure reduces to $(3N+2)$ entries, since only Q_{RR} has to be processed [3]. Further simplifications may occur in case of filter configuration symmetries, e.g. for the design of half-band filters.

---

[3] The provided complexity figures were updated with respect to [Anso95].

7.5 Design algorithm

The straight implementation of the eigenfilter design method results in the following algorithm :

Procedure *{Elementary design algorithm for complex allpass eigenfiler}*

Begin

Step 1: *{ Initialization }*
Read allpass degree N, the specified frequency region of interest Γ, the specified phase response β_{As}, and the non-negative weighting function $W(\Omega)$.

Step 2: *{ Execution of elementary eigenfilter design procedure }*
Compute the eigenfilter Q matrix according to (7.26) and (7.27), and get the allpass filter coefficients.

Step 3: *{ Final verification }*
Verify achieved phase response and approximation error; Check the filter stability explicitly.

End.

The computation of the integrals occurring in (7.27) can be neatly implemented using Simpson's formula [Spie68, Abra70], which assumes an odd number of equally spaced samples for each integration interval.

Two strategies can be followed for the practical computation of the integrals in (7.27). The first one consists in performing the integration over the *whole* frequency domain, resulting in a single integration interval, with a typical number of samples situated between 201 and 501 according to the required frequency resolution. Frequency ranges that are not significant to the filter approximation (don't care bands) are then discriminated assigning a zero value to the weighting function $W(\Omega)$ at the corresponding frequencies. Conversely, strictly positive values are assigned to $W(\Omega)$ for all significant frequency ranges, where it is noticed that the distribution of the approximation error can be steared by adjusting the value of $W(\Omega)$.

A second strategy for computing the integrals in (7.27) consists in performing integrations over separate intervals, where the frequency

resolution (i.e. number of samples) is selected for each interval according to the expected filter selectivity, and to the requested control of the approximation error.

Clearly, the relation between the specified phase response β_{As}, the weighting function, and the resulting phase approximation error, is not easily predictable, so that it is barely possible to determine beforehand the appropriate weighting function so as to achieve a certain distribution (read: control) of the phase approximation error.

It is therefore necessary to embed the eigenfilter approximation method into an iterative optimization scheme, where the weighting function is updated according to the actual phase approximation error, as it is presented below for a quasi-equiripple design.

Procedure { Design algorithm for quasi-equiripple allpass eigenfiler }

Begin

Step 1: *{ Initialization }*
Read allpass degree N, the specified frequency region of interest Γ, the specified phase response β_{As}, and the nonnegative weighting function $W(\Omega)$.

Step 2: *{ Iterated execution of elementary eigenfilter design proc. }*

While quasi-equiripple phase response is not met :

Compute the eigenfilter Q matrix according to (7.26) and (7.27), and get the allpass filter coefficients.

Determine the envelope of the phase approximation error as given in [Nguy94].

Update the weighting function accordingly.

EndWhile;

Step 3: *{ Final verification }*
Verify achieved phase response and approximation error;
Check the stability explicitly.

End.

The weighting function can be appropriately updated using the envelope (i.e. the curve connecting local maxima) of the phase approxima-

tion error, as described in [Nguy94]. The approximation process is then terminated after convergence, which may be detected using different criteria, for instance by measuring the *variation* of the achieved allpass coefficients. In this case, when the variation of the allpass coefficients obtained after two consecutive iterations is getting below a threshold, the approximation process is terminated. Detailed implementation informations can be found, e.g. in [Nguy94].

7.6 Examples

7.6.1 Example of phase equalization

The first application example concerns the phase equalization of a complex filter $H(z)$ featuring an amplitude selectivity as shown in Figure 7.1, and affected by a noticeable phase distortion in the passband. $H(z)$ corresponds to a frequency-shifted sixth-order Chebyshev filter with passband $\Omega \in [-0.07 \cdot \pi,\ 0.37 \cdot \pi]$, and a passband amplitude ripple of 1 dB.

Hence, a complex allpass filter $A(z)$ is designed in cascade with $H(z)$ to achieve the following responses :

$$G(z) = H(z) \cdot A(z)\ ; \quad \beta_G(\Omega) = \beta_H(\Omega) + \beta_A(\Omega) \tag{7.28}$$

where the overall phase response is assumed to be almost linear in the passband :

$$\beta_G(\Omega) \approx \tau_0 \cdot \Omega + \Theta_0 . \tag{7.29}$$

The target group delay τ_0 and phase shift Θ_0 are not known beforehand but can be iteratively estimated, where τ_0 should be kept as low as possible, while ensuring the stability of the allpass filter. One technique to achieve this objective consists in applying (multivariate) Fibonacci sequences [Rao84] to τ_0 and Θ_0 in order to approach the optimal value in a predefined number of steps. For each selected value of these parameters, one performs the eigenfilter design algorithm to approximate the allpass filter.

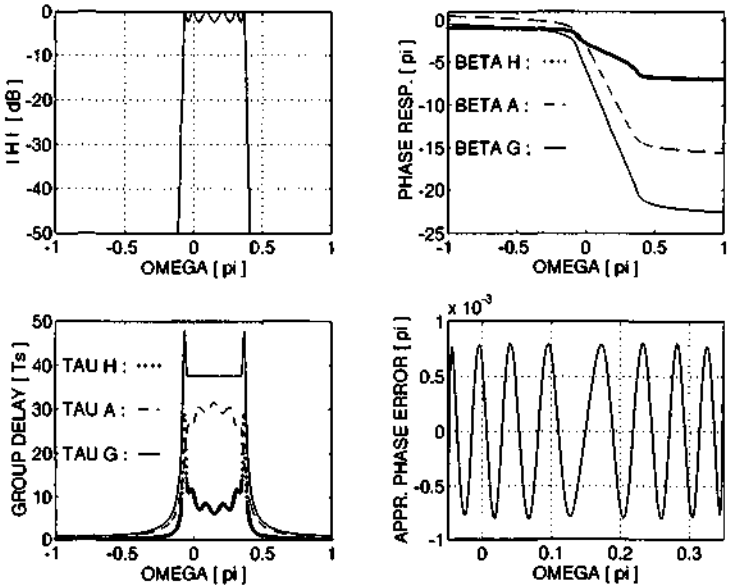

Figure 7.1: Example of quasi-equiripple phase equalization:
a) Upper left: Amplitude resp. of complex filter to be compensated;
b) Upper right: Phase responses [4];
c) Lower left: Corresponding group delay;
d) Lower right: Phase approximation error.

7.6.2 Example of lattice WDF design

The second example concerns the design of a real Almost Linear Phase (ALP) bandpass lattice WDF of symmetric type:

$$H(z) = 0.5 \cdot [\, A_1(z) - A_2(z) \,], \quad N = N_1 + N_2 \tag{7.30}$$

and

$$A_1(z) = z^{-N_1}. \tag{7.31}$$

Clearly, the allpass $A_2(z)$ is requested to approximate the specified phase response $\beta_{A2s}(z) = N_1 \cdot \Omega$ within the first stopband, $\beta_{A2s}(z) = N_1 \cdot \Omega + \pi$ in the passband, and $\beta_{A2s}(z) = N_1 \cdot \Omega + 2\pi$ in the upper

[4] The phase responses are represented in Figures 7.1 and 7.2 with reverse sign compared to the definition in (2.6).

stopband, from which it is understood that $N_2 = N_1 + 2$ is verified to achieve best selectivity.

For the considered example, the filter orders $N_1 = 28$, $N_2 = 30$, i.e. $N = 58$, were selected. The passband is defined for $\Omega \in [0.2\pi,\ 0.4\pi]$, and the stopbands for $\Omega \in [0,\ 0.15\pi] \cup [0.45\pi,\ \pi]$.

The resulting amplitude response of $H(z)$, and phase response of $A(z)$ defined as :

$$A(z) = A_2(z) \ / \ A_1(z) \tag{7.32}$$

are shown in Figure 7.2. As expected, $\beta_A(\Omega)$ features a staircase-shaped response with phase steps of π, as required by the specifications for discrimination between passband and stopbands.

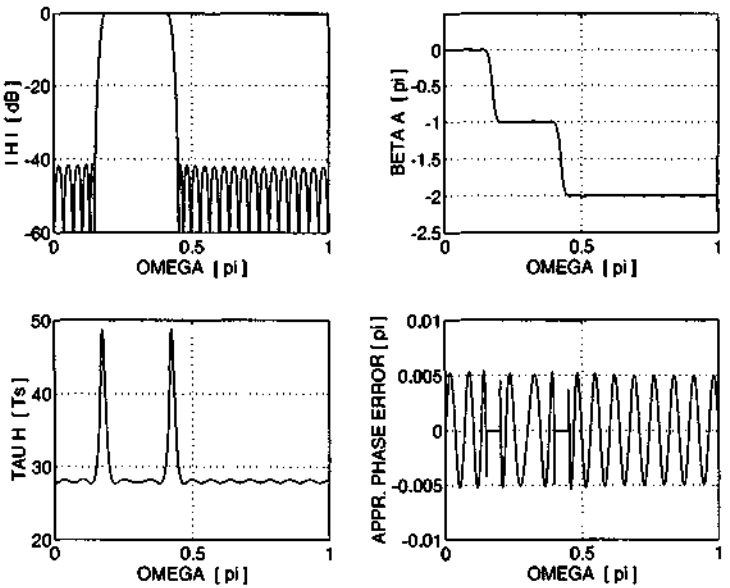

Figure 7.2: Example of real ALP bandpass LWDF filter design:
a) Uper left: Amplitude response of achieved ALP bandpass;
b) Upper right: Phase response [4] of allpass A;
c) Lower left: Corresponding group delay;
d) Lower right: Phase approximation error.

7.7 Conclusion

This chapter was devoted to analyzing basic properties featured by eigenfilter approximation methods adapted to the design of allpass functions and lattice-type WDFs following [Nguy94, Pei94b].

As a particular case of weighted least-squares approximation techniques, the eigenfilter approach relies on a real, symmetric, and definite-positive matrix $\boldsymbol{Q}$ whose internal structure is revealed in the chapter, so that the precise number of independent entries of $\boldsymbol{Q}$ is identified. Moreover, the coefficients of the approximated allpass are merely provided by the eigenvector of $\boldsymbol{Q}$ corresponding to the minimum eigenvalue of $\boldsymbol{Q}$.

The eigenfilter approach offers the advantage that the approximation problem formulation is simple, and supports frequency-based, time-based, and mixed frequency/time-domain specifications.

Conversely, as a particular weighted least-squares technique, the eigenfilter approach is only controlling the general *shape* of the approximated response, without guaranteed precise fulfillment of important features such as stability, and prescribed transmission zeros and/or minimum loss passband frequencies for lattice-type WDFs.

After publication of [Anso95], the attention of the author was drawn to the fact that eigenfilter approaches – due to their essentially matrix oriented processing – require substantially more computational operations than certain other methods [Henk95]. This is particularly the case compared to interpolation techniques relying on compact recurrence formulae, either for allpass and IIR filters [Henk81a, Henk80a, Föld91], or FIR filters [Leeb89], which in addition offer a precise control of stability (IIR case) and prescribed operational points. Regarding mixed time-frequency approximation problems, the author was informed about a technique supporting the transposition of mixed time-frequency specifications into the sole frequency domain [Henk95, Henk80b].

From the practical point of view, the allpass eigenfilter approximation method proved to be reliable for phase equalization problems and Almost Linear Phase filter design. However, the design of

(minimum-phase) amplitude-approximated lattice-type WDF filters showed to be sensitive to convergence problems, leading to periodic variations of the filter coefficient configurations during the iterative approximation process. Further efforts should thus be deserved to this issue to achieve robust and general purpose eigenfilter methods.

Still, it is believed that the eigenfilter technique, viewed as a general purpose optimization tool, does provide an interesting framework for quick design of (suboptimal) filters, requiring a moderate development effort only, and limited circuit theory background knowledge.

Contributions

The contribution of the chapter considered as original to the best knowledge of the author is :

- **C7-1**: Identification and formulation of the internal symmetries characterizing the eigenfilter matrix Q for complex and real allpass functions, leading to computational load reductions during the execution of allpass eigenfilter-based approximations.

Further potential research

The next subjects are proposed for potential further research:

- The prioritary topic needing further research concerns *robustness improvement* of the eigenfilter approximation technique applied to allpass functions and lattice-type WDFs, enhancing in particular the stability and convergence of the approximation algorithm for enlarged classes of filter responses.
- A secondary subject is given by the reformulation of the eigenfilter matrix Q in Section 7.4 for allpass filters featuring specific symmetries, including allpass networks with purely even phase response, half-band symmetric allpass functions, etc..
- Others.

Chapter 8

Conclusion

8.1 Summary and contributions

This work aimed at studying (complex and real) allpass networks and Wave Digital Filters, emphasizing lattice-type structures for the latter, in view of designing robust filters fulfilling general purpose or specific requirements in numerous signal processing application fields, including telecommunications, consumer electronics, multimedia, telesurveillance, bio-medical applications, instrumentation, microsystems design, and many further domains of interest.

The objectives were threefold, namely i) studying the fundamentals of allpass networks and WDFs, as covered in Chapters 2 and 3; ii) studying particular filter subclasses, i.e. (multirate) half-band WDFs and Digital Hilbert Transforms, as treated in Chapters 4 and 6; and iii) discussing selected filter approximation methods handled in Chapters 5 and 7.

Whenever possible, the subjects were processed methodologically, performing classifications when appropriate, so as to establish clear links – or to emphasize differences – between topics already known from publications, and to identify other topics that were not yet covered in the literature (cf e.g. Table 3.5). Additionally, the methodological approach helps in generalizing results to potentially identify new fundamental properties, from which various specific filter configurations can be generated (cf e.g. equation (5.60), leading to contributions C5–IV and C5–V).

Many properties were achieved by *analyzing* different kinds of *elementary filter response symmetries*, as it was for instance the case in Chapter 2 when decomposing complex allpass functions according to their even/odd phase response constituents. These response symmetries can most often be directly linked to specific filter configurations, or to particular sets of filter coefficients, as illustrated in Chapter 2 by the example of half-band symmetric allpass functions, or in Chapters 4 and 5 by (warped) bireciprocal WDFs, etc..

Clearly, this link between filter response symmetries and filter configurations/coefficients can be exploited in filter *design* procedures, especially by adapting (infinite or finite precision) filter approximation methods, so as to generate filter configurations that are *structurally* (and thus exactly) featuring the desired response symmetries, even when the filter coefficients are coarsely approximated, e.g. in view of minimizing the computational load, and/or the implementation costs, and/or the power consumption.

Further detailed discussions and conclusions on the work done are provided at the end of each chapter.

Contributions

A set of 20 claimed original contributions was established along the report, certain of these claims being further subdivided into partial claims. These contributions are fully described in the conclusions of the corresponding chapters, including the Appendix.

8.2 Perspectives

Many aspects related to the studied domain remain open to further research of either theoretical or practical nature, specific subjects of research being listed at the end of the chapters.

Important extension possibilities are given by the study of: i) non-reciprocal and general reciprocal WDFs; ii) multirate signal analysis/synthesis filter pairs and filterbanks operating at fractional ratios of sampling frequencies; iii) dedicated approximation methods for allpass filters and WDFs, including for non-prototype amplitude and mixed amplitude/phase responses, and valid for both infinite and finite precision filter coefficients; iv) application examples; v) others.

Appendix

Terminology and Mathematical Background

A.1 Introduction

This appendix provides the elementary terminology, definitions, and mathematical background referred to in the report.

The chapter is structured as follows. Section A.2 is first recalling various properties of real and complex functions. Section A.3 is next specifying the frequency domains considered in the report. Sections A.4 and A.5 are then defining the frequency responses in the so-called ψ-domain and z-domain, respectively. The bilinear transform of rational and polynomial functions are discussed in Sections A.6 and A.7, followed by the definition of several fundamental properties verified by single filter functions, or by sets of filter functions, which are described in Section A.8. Short conclusions are finally drawn in Section A.9.

A.2 Real and complex functions

The mathematical quantities (constants, variables, and functions) discussed in the report all belong to the *natural integer*, *signed integer*, *real*, and *complex* number systems ($\mathbb{N}$, $\mathbb{Z}$, $\mathbb{R}$, $\mathbb{C}$).

To improve readability, scalar quantities are represented with plain-text symbols, e.g. Function(x), whereas vectors and matrices are denoted by bold-faced symbols, e.g. **FunctionMatrix**(x).

A.2.1 Real functions

A function $f(\psi)$ is defined as a *real function* when it is real-valued for a real argument ψ, i.e. $f(\psi) \in \mathbb{R}$ for $\psi \in \mathbb{R}$.

A.2.2 Complex functions

A function $f(\psi)$ is specified as a *complex function* when it is complex-valued even if the argument ψ is restricted to the real domain. The following decomposition can be applied :

$$f(\psi) = f_{Ra}(\psi) + j \cdot f_{Ia}(\psi), \quad \text{with} \quad j = \sqrt{-1} \tag{A.1}$$

$$\psi = \xi + j \cdot \phi, \quad \text{with} \quad \xi, \phi \in \mathbb{R} \tag{A.2}$$

where $f_{Ra}(\psi)$ and $f_{Ia}(\psi)$ are real functions. f_{Ra} and f_{Ia} are specified as the *real analytic* and *imaginary analytic* parts of $f(\psi)$.

A.2.3 Analytic functions

Let $f(\psi)$ be a complex function in some region $\Re$ of the ψ-plane, and let the derivative of $f(\psi)$ be defined as :

$$\dot{f}(\psi) = \lim_{\Delta\psi \to 0} \frac{f(\psi + \Delta\psi) - f(\psi)}{\Delta\psi},$$

provided that the limit exists independent of the manner in which $\Delta\psi \to 0$. If the derivative $\dot{f}(\psi)$ exists at all points ψ of the region $\Re$, then $f(\psi)$ is said to be *analytic* [1] in $\Re$ and is referred to as an *analytic function in* $\Re$. Reformulating $f(\psi)$ as :

$$f(\psi) = f'_{Ra}(\xi, \phi) + j \cdot f'_{Ia}(\xi, \phi),$$

a necessary condition for $f(\psi)$ to be analytic in $\Re$ is that f'_{Ra} and f'_{Ia} satisfy the *Cauchy-Riemann equations* in $\Re$:

$$\frac{\partial f'_{Ra}(\xi,\phi)}{\partial \xi} = \frac{\partial f'_{Ia}(\xi,\phi)}{\partial \phi}, \quad \frac{\partial f'_{Ra}(\xi,\phi)}{\partial \phi} = \frac{-\partial f'_{Ia}(\xi,\phi)}{\partial \xi}.$$

---

[1] The terms *regular* and *holomorphic* are used as synonyms for analytic.

The Cauchy-Riemann equations become in addition a sufficient condition for $f(\psi)$ to be analytic in $\Re$ in case the former partial derivatives are continuous in $\Re$ [Spie74, Lavr77].

A point ψ_0 at which $f(\psi)$ fails to be analytic is called a *singular point* or a *singularity* of $f(\psi)$. There are different kinds of singularities, including *isolated singularities, poles, branch points, removable singularities, essential singularities,* and *singularities at infinity,* which can be classified using the Laurent series of $f(\psi)$ [Spie74].

A.2.4 Even and odd functions

It is recalled that a real or complex function $f(\psi)$ satisfying $f(\psi)=f(-\psi)$ is said to by *even,* whereas it is *odd* for $f(\psi)=-f(-\psi)$. Any function, either real or complex, can be decomposed into its even and odd constituents denoted f_E and f_O, respectively :

$$f(\psi)=f_E(\psi)+f_O(\psi)\ , \tag{A.3}$$

$$f_E(\psi)=\frac{1}{2}\cdot\left[f(\psi)+f(-\psi)\right],\quad f_O(\psi)=\frac{1}{2}\cdot\left[f(\psi)-f(-\psi)\right]. \tag{A.4a,b}$$

Derivative of even and odd functions

The (total) first derivative of any real or analytic complex function $f(\psi)$, evaluated at any non-singular point of the ψ-plane [Youn73], is denoted :

$$\dot{f}(\psi)=\mathrm{d}\,f(\psi)\ /\ \mathrm{d}\psi\ . \tag{A.5}$$

Whenever they exist, higher-order derivatives are achieved by iterated application of (A.5). By vertue of (A.4), the first derivative of f_E and f_O evaluated at non-singular points is :

$$\dot{f}_E(\psi)=\frac{1}{2}\cdot\left[\dot{f}(\psi)-\dot{f}(-\psi)\right],\quad \dot{f}_O(\psi)=\frac{1}{2}\cdot\left[\dot{f}(\psi)+\dot{f}(-\psi)\right]. \tag{A.6a,b}$$

Hence, the first derivative of an even (odd) function is odd (even). The rule for higher-order derivatives is then obtained by induction, cf Table A.1.

		$\frac{d f(\psi)}{d\psi}$	$\frac{d^{2m} f(\psi)}{d\psi^{2m}}$	$\frac{d^{(2m+1)} f(\psi)}{d\psi^{(2m+1)}}$
$f(\psi)$	Even	Odd	Even	Odd
	Odd	Even	Odd	Even

Table A.1: First-order and higher-order derivatives of even / odd functions $(m = 1,2,...)$.

A.2.5 Complex conjugation

The *complex conjugate* of a variable ψ is denoted by ψ^*, and the complex conjugate of a function $f(\psi)$ by $f^*(\psi)$:

$$f^*(\psi) = [\, f(\psi) \,]^*. \tag{A.7}$$

A.2.6 Biconjugation

The *biconjugate* of a complex function $f(\psi)$ is defined as :

$$\overline{f(\psi)} = f^*(\psi^*). \tag{A.8}$$

The biconjugate has been introduced to precisely determine the real and imaginary analytic parts of a function [Meer83] :

$$\begin{aligned} \mathrm{Ra}\{f(\psi)\} &= f_{Ra}(\psi) = \frac{1}{2} \cdot \left[f(\psi) + \overline{f(\psi)} \right] \\ \mathrm{Ia}\{f(\psi)\} &= f_{Ia}(\psi) = \frac{1}{2j} \cdot \left[f(\psi) - \overline{f(\psi)} \right]. \end{aligned} \tag{A.9a,b}$$

It is noticed that :

$$\mathrm{Ra}\{\overline{f(\psi)}\} = \mathrm{Ra}\{f(\psi)\}, \qquad \mathrm{Ia}\{\overline{f(\psi)}\} = -\mathrm{Ia}\{f(\psi)\}. \tag{A.10}$$

A.2.7 Paraconjugation

The *paraconjugate* of a complex function $f(\psi)$ is given by :

$$f_*(\psi) = f^*(-\psi^*) = \overline{f(-\psi)}. \tag{A.11}$$

Para-even and para-odd functions

A function satisfying $f(\psi) = f_*(\psi)$ is said to be *para-even*, whereas it is called *para-odd* for $f(\psi) = -f_*(\psi)$. Any complex function can be

decomposed into its para-even and para-odd constituents denoted $f_e(\psi)$ and $f_o(\psi)$, respectively :

$$f(\psi) = f_e(\psi) + f_o(\psi). \tag{A.12}$$

$$f_e(\psi) = \frac{1}{2}\cdot\left[\, f(\psi) + f_*(\psi) \,\right], \quad f_o(\psi) = \frac{1}{2}\cdot\left[\, f(\psi) - f_*(\psi) \,\right]. \tag{A.13a,b}$$

Hence :

$$f = f_e \iff f_o = 0; \qquad f = f_o \iff f_e = 0. \tag{A.14a,b}$$

For *real* functions, the paraconjugate becomes $f_*(\psi) = f(-\psi)$, and the para-even/odd constituents simply reduce to the even/odd parts of $f(\psi)$, respectively.

Product and quotient of para-even and para-odd functions

In view of the former definitions, it is observed that the product of two para-even or two para-odd functions is para-even; conversely, the product of a para-even with a para-odd function is para-odd :

$$f_e(\psi)\cdot g_e(\psi) = [\, f_e(\psi)\cdot g_e(\psi)\,]_* \quad \Rightarrow \quad \text{para-even;} \tag{A.15a}$$

$$f_o(\psi)\cdot g_o(\psi) = [\, f_o(\psi)\cdot g_o(\psi)\,]_* \quad \Rightarrow \quad \text{para-even;} \tag{A.15b}$$

$$f_e(\psi)\cdot g_o(\psi) = -[\, f_e(\psi)\cdot g_o(\psi)\,]_* \quad \Rightarrow \quad \text{para-odd.} \tag{A.15c}$$

Same features are obviously verified for the quotient of para-even/odd functions.

Transformation of para-even/odd functions into para-odd/even ones

As a particular case of (A.15b,c), selecting $g_o = \pm j$, it is noticed that a para-even (para-odd) function f becomes para-odd (para-even) :

$$[\, \pm j\cdot f_e(\psi)\,] = -[\, \pm j\cdot f_e(\psi)\,]_* \quad \Rightarrow \quad \text{para-odd.} \tag{A.16a}$$

$$[\, \pm j\cdot f_o(\psi)\,] = +[\, \pm j\cdot f_o(\psi)\,]_* \quad \Rightarrow \quad \text{para-even.} \tag{A.16b}$$

Para-even and para-odd functions evaluated along the imaginary axis

According to (A.11), the paraconjugate of *any* function $f(\psi)$ evaluated along the purely imaginary axis $\psi = j\cdot\phi$, $\phi \in \mathbb{R}$, is equal to its complex conjugate :

$$f_*(j\cdot\phi) = f^*(j\cdot\phi). \tag{A.17}$$

It follows from (A.13), (A.14) and (A.17) that a para-even (para-odd) function evaluated along $\psi = j\cdot\phi$ is a purely real-valued (imaginary-valued) function :

$$f = f_e \quad \Rightarrow \quad f_o(j\cdot\phi) = j\cdot \mathrm{Im}\{ f(j\cdot\phi)\} = 0, \tag{A.18a}$$

$$f = f_o \quad \Rightarrow \quad f_e(j\cdot\phi) = \mathrm{Re}\{ f(j\cdot\phi)\} = 0. \tag{A.18b}$$

Accordingly, the argument of *any* complex function $f = f_e + f_o$ processed along the imaginary axis $\psi = j\cdot\phi$ is achieved using :

$$\mathrm{Arg}\{ f(j\cdot\phi)\} = \arctan(-j\cdot f_o(j\cdot\phi)/f_e(j\cdot\phi)) . \tag{A.19}$$

Real and imaginary analytic parts of para-even/odd functions

The following equations are verified by definition, applying (A.11) :

$$f_e(\psi) = f_{e*}(\psi) = \overline{f_e(-\psi)}, \quad f_o(\psi) = -f_{o*}(\psi) = -\overline{f_o(-\psi)} . \tag{A.20a,b}$$

Introducing (A.20a,b) into (A.9a,b), it is demonstrated that the real analytic and imaginary analytic parts of a para-even (para-odd) function are even (odd) and odd (even), respectively :

$$\mathrm{Ra}\{f_e(\psi)\} = \frac{1}{2}\cdot[f_e(\psi) + f_e(-\psi)] = G_E(\psi) \quad \Rightarrow \quad \text{Even;} \tag{A.21a}$$

$$\mathrm{Ia}\{f_e(\psi)\} = \frac{1}{2j}\cdot[f_e(\psi) - f_e(-\psi)] = G_O(\psi) \quad \Rightarrow \quad \text{Odd;} \tag{A.21b}$$

$$\mathrm{Ra}\{f_o(\psi)\} = \frac{1}{2}\cdot[f_o(\psi) - f_o(-\psi)] = H_O(\psi) \quad \Rightarrow \quad \text{Odd;} \tag{A.21c}$$

$$\mathrm{Ia}\{f_o(\psi)\} = \frac{1}{2j}\cdot[f_o(\psi) + f_o(-\psi)] = H_E(\psi) \quad \Rightarrow \quad \text{Even.} \tag{A.21d}$$

Accordingly, any para-even and para-odd complex function can be reformulated as follows, using the real functions G_E, G_O, H_E, and H_O defined in (A.21) :

$$f_e(\psi) = G_E(\psi) + j \cdot G_O(\psi), \quad f_o(\psi) = H_O(\psi) + j \cdot H_E(\psi). \qquad \text{(A.22a,b)}$$

Derivative of para-even and para-odd functions

Taking into account Table A.1, the form of the first (total) derivative of analytic para-even and para-odd functions, evaluated at non-singular points, is directly achieved from (A.22), resulting in Table A.2. The form of higher-order (total) derivatives is merely deduced by induction, and omitted for conciseness.

		$\mathrm{Ra}\{\dot{f}(\psi)\}$	$\mathrm{Ia}\{\dot{f}(\psi)\}$	$\dot{f}(\psi)$
$f(\psi)$	Para-even	Odd	Even	Para-odd
	Para-odd	Even	Odd	Para-even

Table A.2: First-order derivative of para-even and para-odd functions.

Polynomial functions

For polynomial functions, the paraconjugate has the following form :

$$f(\psi) = \sum_{\nu=0}^{N} a_\nu \cdot \psi^\nu \quad \Rightarrow \quad f_*(\psi) = \sum_{\nu=0}^{N} a_\nu^* \cdot (-\psi)^\nu, \qquad \text{(A.23)}$$

or
$$f(\psi) = a_N \cdot \prod_{\nu=1}^{N} (\psi - \psi_{0\nu})$$
$$\Rightarrow \quad f_*(\psi) = (-1)^N \cdot a_N^* \cdot \prod_{\nu=1}^{N} (\psi + \psi_{0\nu}^*), \qquad \text{(A.24)}$$

from which it is observed that the zeros $\psi_{0\nu}$ of $f(\psi)$ are mapped onto $(-\psi_{0\nu}^*)$ for $f_*(\psi)$.

Para-even and para-odd polynomials

Clearly, for para-even/odd polynomials, i.e. $f(\psi) = \pm f_*(\psi)$, the set of zeros of $f(\psi)$ and $f_*(\psi)$ become identical, i.e. $\{\psi_{0\nu}\} \equiv \{-\psi^*{}_{0\nu}\}$. The zeros are thus occurring as follows for $\psi = \xi + j \cdot \phi$:

$\xi_0 \neq 0 \quad \Rightarrow$ paired zeros $(\psi_{0\nu}, -\psi_{0\nu}^*)$, incl. multiplicity; (A.25a)

$\xi_0 = 0 \quad \Rightarrow$ single or multiple zeros on axis $\mathrm{Re}\{\psi\} = 0$. (A.25b)

Using (A.23), one obtains a set of conditions to be verified by the coefficients of para-even/odd polynomials (cf Table A.3) :

			Cooditions to be fulfilled	
			For ν even :	For ν odd :
$f(\psi)$ para-even	$\Rightarrow$	$f_o(\psi)=0$	$\mathrm{Im}\{a_\nu\}=0$	$\mathrm{Re}\{a_\nu\}=0$
$f(\psi)$ para-odd	$\Rightarrow$	$f_e(\psi)=0$	$\mathrm{Re}\{a_\nu\}=0$	$\mathrm{Im}\{a_\nu\}=0$

Table A.3: Coefficients of para-even/odd polynomials .

Tbe most general form of para-even/odd polynomials of degree N is thus given by :

$$f_e(\psi) = F_1(\psi^2) + j\cdot\psi\cdot F_2(\psi^2) \qquad \text{(A.26a)}$$

$$f_o(\psi) = \psi\cdot F_3(\psi^2) + j\cdot F_4(\psi^2) \qquad \text{(A.26b)}$$

where $F_i(\psi)$ are real polynomials of degree N_i, $i=1,2,3,4$, with :

$$N = 2\cdot(N_1+N_2)+1; \qquad N = 2\cdot(N_3+N_4)+1. \qquad \text{(A.27a,b)}$$

It is noted that (A.26a,b) complies with (A.22a,b).

Mapping of para-even/odd polynomials into real polynomials

Performing the substitution $\psi \to (\pm j\cdot\psi)$ in (A.26a), it is deduced that a *para-even* polynomial f_e can be mapped into a *real* polynomial, the real (imaginary) analytic part of f_e being transformed into the even (odd) part of the resulting polynomial, cf (A.28a). Applying the same procedure to the para-odd polynomial f_o in (A.26b), and multiplying by j, one obtains (A.28b) [2] :

$$f_e(\pm j\cdot\psi) = F_1(-\psi^2) \mp \psi\cdot F_2(-\psi^2) \qquad \text{(A.28a)}$$

$$j\cdot f_o(\pm j\cdot\psi) = \mp\psi\cdot F_3(-\psi^2) - F_4(-\psi^2)\,. \qquad \text{(A.28b)}$$

Conversely, any *real* polynomial F composed of its even and odd constituents :

$$F(\psi) = F_1(-\psi^2) + \psi\cdot F_2(-\psi^2) \qquad \text{(A.29)}$$

---

[2] These mappings are useful to simplify the implementation of certain types of allpass functions, cf Section 2.6, including so-called bireciprocal filters based thereof, cf Chapter 4.

can be mapped onto the *para-even* polynomial f_e given in (A.26a) using the substitution $\psi \rightarrow (j \cdot \psi)$. A para-odd polynomial can further be achieved multiplying the result by $(\pm j)$, cf (A.16a).

Argument of para-even/odd polynomials along the imaginary axis

According to (A.18), the argument of para-even/odd polynomials evaluated along $\psi = j \cdot \phi$ is shown to be *constant* :

$$\mathrm{Arg}\{ f_e(j \cdot \phi) \} = \quad k \cdot \pi, \qquad k \in \mathbb{Z}, \qquad \text{(A.30a)}$$

$$\mathrm{Arg}\{ f_o(j \cdot \phi) \} = \pi/2 + k \cdot \pi, \qquad \text{(A.30b)}$$

except for possible steps of value $l \cdot \pi$, $l \in \mathbb{Z}$, encountered along $\psi = j \cdot \phi$ when ϕ equals the imaginary part of the zeros of f_e and f_o, respectively.

Rational functions

Clearly, the case of rational functions is handled by applying to the numerator and denominator the properties derived for polynomials.

In particular, it is easily demonstrated that equations (A.26a,b), and thus (A.28a,b), are also fulfilled for complex para-even/odd rational functions, $F_i(\psi)$ corresponding now to real rational functions, with $i = 1,2,3,4$. Tbe demonstration is omitted for conciseness.

Transcendental functions

The paraconjugate of the exponential function is merely achieved using Taylor's series expansion [Abra70] :

$$[\exp(f(\psi))]_* = \exp(f_*(\psi)). \qquad \text{(A.31)}$$

The paraconjugates of the hyperbolic functions are then obtained :

$$[\cosh(f(\psi))]_* = \cosh(f_*(\psi)); \quad [\sinh(f(\psi))]_* = \sinh(f_*(\psi)); \quad \text{(A.32a,b)}$$

$$[\tanh(f(\psi))]_* = \tanh(f_*(\psi)); \quad [\coth(f(\psi))]_* = \coth(f_*(\psi)). \quad \text{(A.33a,b)}$$

A.2.8 Reciprocation

The *reciprocal* of any real or complex polynomial $f(\psi)$ of degree N is specified by :

$$\check{f}(\psi) = \psi^N \cdot f(1/\psi) \tag{A.34}$$

where f and $\check{f}$ are assumed to be devoid of any zero located at the origin, so that they are uniquely interrelated, and of same degree.

Circularly symmetric and circularly anti-symmetric polynomials

A real or complex polynomial fulfilling $f(\psi) = \check{f}(\psi)$ is said to be *circularly symmetric* (CS), whereas it is called *circularly anti-symmetric* (CA) [3] for $f(\psi) = -\check{f}(\psi)$. Any polynomial can be decomposed into its CS and CA parts denoted $f_{cs}(\psi)$ and $f_{ca}(\psi)$, respectively :

$$f(\psi) = f_{cs}(\psi) + f_{ca}(\psi), \tag{A.35}$$

$$f_{cs}(\psi) = \frac{1}{2} \cdot \left[f(\psi) + \check{f}(\psi) \right], \quad f_{ca}(\psi) = \frac{1}{2} \cdot \left[f(\psi) - \check{f}(\psi) \right]. \tag{A.36a,b}$$

Location of zeros

Rewriting the formula (A.34) in an explicit form :

$$f(\psi) = \sum_{\nu=0}^{N} a_\nu \cdot \psi^\nu \quad \Rightarrow \quad \check{f}(\psi) = \sum_{\nu=0}^{N} a_\nu \cdot \psi^{(N-\nu)}, \tag{A.37}$$

$$\begin{aligned} \text{or} \quad & f(\psi) = a_N \cdot \prod_{\nu=1}^{N} (\psi - \psi_{0\nu}) \\ \Rightarrow \quad & \check{f}(\psi) = a_N \cdot \prod_{\mu=1}^{N} (-\psi_{0\mu}) \cdot \prod_{\nu=1}^{N} (\psi - 1/\psi_{0\nu}), \end{aligned} \tag{A.38}$$

the zeros $\psi_{0\nu}$ of f are clearly mapped onto $1/\psi_{0\nu}$ for $\check{f}$. Furthermore, for CS and CA polynomials, the set of zeros of f and $\check{f}$ become identical, i.e. $\{\psi_{0\nu}\} \equiv \{1/\psi_{0\nu}\}$. The zeros are thus occurring as follows, including any multiplicity in each case :

$$\psi_{0\nu} = \pm 1 \quad \Rightarrow \text{ self-reciprocal zero;} \tag{A.39a}$$

---

[3] Circularly (anti-) symmetric polynomials are also termed (anti-) mirror-image polynomials. Moreover, circularly anti-symmetric polynomials are sometimes also called anti-circularly symmetric [Bose85].

$\psi_{0\nu} \in \mathbb{R}, \psi_{0\nu} \neq \pm 1 \quad \Rightarrow$ pair of reciprocal zeros $(\psi_{0\nu}, 1/\psi_{0\nu})$; (A.39b)

$\psi_{0\nu} \in \mathbb{C}, |\psi_{0\nu}| = 1 \quad \Rightarrow$ complex conjugate zeros $(\psi_{0\nu}, \psi_{0\nu}^*)$ (A.39c)

$\psi_{0\nu} \in \mathbb{C}, |\psi_{0\nu}| \neq 1 \quad \Rightarrow$ pair of reciprocal zeros $(\psi_{0\nu}, 1/\psi_{0\nu})$; (A.39d)

In case $f_{cs}(\psi)$ and/or $f_{ca}(\psi)$ become real, (A.39d) is replaced by :

$\psi_{0\nu} \in \mathbb{C}, |\psi_{0\nu}| \neq 1 \quad \Rightarrow$ quadruplets $(\psi_{0\nu}, \psi_{0\nu}^*, 1/\psi_{0\nu}, 1/\psi_{0\nu}^*)$. (A.39e)

Introducing (A.39a-e) into (A.38) and (A.37), the next properties are obtained, N_1 indicating the number of zeros at $\psi_{0\nu} = 1$ [Bose85] :

	Conditions to be fulfilled		
	Parity of N_1	Coefficients	
		$\nu = 1,2,...,N$	For N even
$f(\psi)$ CS $\Rightarrow$ $f_{ca}(\psi) = 0$	N_1 even	$a_\nu = a_{N-\nu}$	———
$f(\psi)$ CA $\Rightarrow$ $f_{cs}(\psi) = 0$	N_1 odd	$a_\nu = -a_{N-\nu}$	$a_{N/2} = 0$

Table A.4: Basic properties of real and complex CS and CA polynomials.

A.2.9 Para-reciprocation

The *para-reciprocal* [Dels78] of a complex function $f(\psi)$ is defined by [4]:

$$\tilde{f}(\psi) = f^*(1/\psi^*) = \overline{f(1/\psi)}. \tag{A.40}$$

Para-reciprocal polynomials

The notation (A.40) is maintained for polynomials in order to comply with usual literature, e.g. [Vaid87a, Vaid93]. One should then take care of the difference between (A.40) and (A.34).

Para-circularly symmetric and anti-symmetric polynomials

A complex polynomial of degree N satisfying $f(\psi) = \psi^N \cdot \tilde{f}(\psi)$ is said to be *para-circularly symmetric* (PCS), while it is termed *para-circu-*

[4] The $f(\psi) \Rightarrow \tilde{f}(\psi)$ mapping is also referred to as the *tilde-operator*, or the *tilde notation*, e.g. [Vaid87a], or [Vaid93] p. 28.

larly anti-symmetric (PCA) for $f(\psi)=-\psi^N\cdot\tilde{f}(\psi)$. Any complex polynomial can be split into its PCS and PCA constituents :

$$f(\psi)=f_{pcs}(\psi)+f_{pca}(\psi). \tag{A.41}$$

$$f_{pcs}(\psi)=\frac{f(\psi)+\psi^N\cdot\tilde{f}(\psi)}{2}\,,\quad f_{pca}(\psi)=\frac{f(\psi)-\psi^N\cdot\tilde{f}(\psi)}{2}\,. \tag{A.42a,b}$$

Location of zeros

One derives from (A.40) :

$$f(\psi)=\sum_{\nu=0}^{N}a_\nu\cdot\psi^\nu \quad\Rightarrow\quad \psi^N\cdot\tilde{f}(\psi)=\sum_{\nu=0}^{N}a_\nu^*\cdot\psi^{(N-\nu)}, \tag{A.43}$$

$$\begin{aligned}&\text{or}\quad f(\psi)=a_N\cdot\prod_{\nu=1}^{N}(\psi-\psi_{0\nu})\\ &\Rightarrow\quad \psi^N\cdot\tilde{f}(\psi)=a_N^*\cdot\prod_{\mu=1}^{N}(-\psi_{0\mu}^*)\cdot\prod_{\nu=1}^{N}(\psi-1/\psi_{0\nu}^*)\,,\end{aligned} \tag{A.44}$$

and the zeros $\psi_{0\nu}$ of f are clearly mapped onto $1/\psi_{0\nu}^*$ for $\psi^N\cdot\tilde{f}(\psi)$. Furthermore, for PCS and PCA polynomials, the set of zeros of f and $\psi^N\cdot\tilde{f}(\psi)$ are just the same, i.e. $\{\psi_{0\nu}\}=\{1/\psi_{0\nu}^*\}$. The zeros are thus appearing as follows, including any multiplicity in each case :

$\psi_{0\nu}=\pm1 \quad\Rightarrow$ self-reciprocal zero; (A.45a)

$\psi_{0\nu}\in\mathbb{R},\ \psi_{0\nu}\neq\pm1 \quad\Rightarrow$ pair of reciprocal zeros $(\psi_{0\nu},1/\psi_{0\nu})$; (A.45b)

$\psi_{0\nu}\in C,\ |\psi_{0\nu}|=1 \quad\Rightarrow$ self-para-reciprocal zero; (A.45c)

$\psi_{0\nu}\in C,\ |\psi_{0\nu}|\neq1 \quad\Rightarrow$ pair of " " " " $(\psi_{0\nu},1/\psi_{0\nu}^*)$. (A.45d)

The features listed in Table A.5 are then obtained, N_1 designating again the number of zeros at $\psi_{0\nu}=1$:

	Conditions to be fulfilled		
	Parity of N_1	Coefficients	
		$\nu=1,2,\ldots,N$	For N even
$f(\psi)$ PCS $\Rightarrow$ $f_{pca}(\psi)=0$	N_1 even	$a_\nu = a_{N-\nu}^*$	$\mathrm{Im}\{a_{N/2}\}=0$
$f(\psi)$ PCA $\Rightarrow$ $f_{pcs}(\psi)=0$	N_1 odd	$a_\nu=-a_{N-\nu}^*$	$\mathrm{Re}\{a_{N/2}\}=0$

Table A.5: Basic properties of complex PCS and PCA polynomials.

A.3 Frequency domains

Adopting the approach followed in the field of Wave Digital Filters [Fett86, Bahe84], three complementary frequency domains are considered in the report :

- the *p-domain* (p-plane), where p is the actual complex frequency;
- the ψ-*domain* (ψ-plane), ψ corresponding to Richards' variable used for the design of commensurate distributed reference filters;
- the z-*domain* (z-plane), where z is the common complex frequency variable applied for digital signal processing.

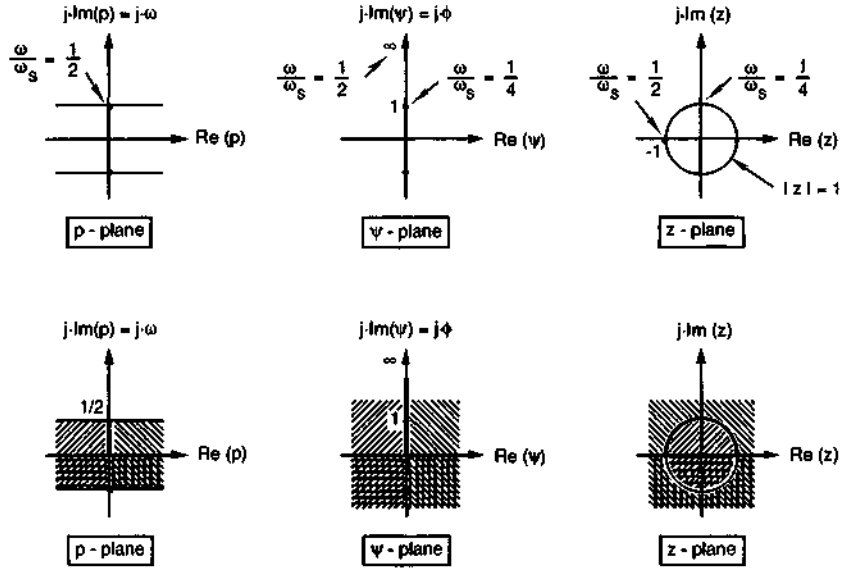

Figure A.1: Mapping between the considered complex frequency domains.

Formally, the variables are defined as follows [Fett86] :

$$\psi = (z-1)/(z+1)\ ; \qquad \psi = \tanh(p \cdot T_s/2)\ ; \qquad \text{(A.46a,b)}$$

$$z = (1+\psi)/(1-\psi)\ ; \qquad z = \exp(p \cdot T_s)\ ; \qquad \text{(A.47a,b)}$$

$$p = \frac{2}{T_s} \cdot \operatorname{arctanh}(\psi)\ ; \qquad p = \frac{1}{T_s} \cdot \operatorname{Ln}(z)\ ; \qquad \text{(A.48a,b)}$$

$$T_S = 1/f_S \; ; \qquad \omega_S = 2\pi \cdot f_S \; . \tag{A.49a,b}$$

where T_S and f_S correspond to the sampling period and sampling frequency, respectively. As can be seen, the ψ and z variables are interrelated by the (forward) bilinear transform T_B [Jury73] :

$$H(z) = T_B\{S(\psi)\} = S(\psi) \Big|_{\psi = (z-1)/(z+1)} \tag{A.50}$$

and the inverse bilinear transform T_{IB} :

$$S(\psi) = T_{IB}\{H(z)\} = H(z) \Big|_{z = (1+\psi)/(1-\psi).} \tag{A.51}$$

It is noticed that T_B is normalized, according to what is practiced in the WDF field [Fett86]. Both variables ψ and z are thus normalized and dimensionless. This is in contrast to another used definition $T'_B = (2/T_S) \cdot T_B$, cf [Jack89, Oppe89, Anto93].

The relationship between real frequencies ω in the p-plane and real frequencies ϕ in the ψ-plane is given by :

$$\phi = \tan(\omega \cdot T_S/2) \; ; \qquad p = j \cdot \omega \; ; \qquad \psi = j \cdot \phi . \tag{A.52a,b,c}$$

In particular, real frequencies ω lying in the Nyquist range $(0 \le \omega \le \pi \cdot f_S)$ are exactly mapped in a one-to-one correspondence onto the range $(0 \le \phi \le \infty)$, see Figure A.1. Furthermore, stable filters in one domain are mapped onto stable filters in the other domains :

$$\begin{aligned} \mathrm{Re}(\psi) > 0 \;\; &\Leftrightarrow \;\; \mathrm{Re}(p) > 0 \;\; \Leftrightarrow \;\; |z| > 1 \\ \mathrm{Re}(\psi) = 0 \;\; &\Leftrightarrow \;\; \mathrm{Re}(p) = 0 \;\; \Leftrightarrow \;\; |z| = 1 \\ \mathrm{Re}(\psi) < 0 \;\; &\Leftrightarrow \;\; \mathrm{Re}(p) < 0 \;\; \Leftrightarrow \;\; |z| < 1. \end{aligned} \tag{A.53}$$

It follows from (A.52a) that the bilinear transform introduces a non-linear distortion of the real frequency values when passing from the ψ-domain to the z-domain and vice-versa. This distortion – denoted as the *frequency warping effect* – is irrelevant in the design process of linear time-invariant digital filters, since it can be precompensated by adjusting the filter specifications.

Finally, the *normalized frequency* Ω is introduced, with a principal value limited to $0 \le \Omega \le \pi$ for real filters, and to $-\pi \le \Omega \le \pi$ for complex filters :

$$\Omega = \omega \cdot T_s \,. \tag{A.54}$$

A.3.1 Correspondences induced by the bilinear transform

The next relations can be established from (A.46a) and (A.47a) :

ψ-domain		z-domain
$S(\psi) \mapsto S(-\psi)$	$\Leftrightarrow$	$H(z) \mapsto H(1/z)$
$S(\psi) \mapsto S(1/\psi)$	$\Leftrightarrow$	$H(z) \mapsto H(-z)$

Table A.6: Correspondences induced by the bilinear transform.

A.4 Frequency responses in the ψ-domain

In the report, the filter design is considered in botb ψ and z-domains. This section is devoted to defining the frequency responses in the ψ-domain, first in their analytic form.

A.4.1 Complex amplitude and phase responses

The transfer function $S(\psi)$ of a filter is specified by :

$$S(\psi) = \exp\left(-\left[X(\psi) + \Phi(\psi)\right]\right), \quad \text{with } X = X_e,\ \Phi = \Phi_o, \tag{A.55}$$

where $X(\psi)$ and $\Phi(\psi)$ are the *complex attenuation* and *complex phase* of $S(\psi)$, respectively. By definition, $X(\psi)$ is para-even, whereas $\Phi(\psi)$ is para-odd. Hence, according to (A.18), X and Φ are shown to be purely real and imaginary valnad for real frequencies $\psi = j \cdot \phi$, $\phi \in \mathbb{R}$, which agrees with standard notations :

$$X(j \cdot \phi) = \chi(\phi),\ \Phi(j \cdot \phi) = j \cdot \varphi(\phi), \text{ with } \chi(\phi), \varphi(\phi), \phi \in \mathbb{R}. \tag{A.56a,b}$$

It follows from (A.55) that $X(\psi)$ and $\Phi(\psi)$ are expressed as :

$$X(\psi) = -\frac{1}{2} \cdot \ln\left[S(\psi) \cdot S_*(\psi) \right], \quad \Phi(\psi) = -\frac{1}{2} \cdot \ln\left[\frac{S(\psi)}{S_*(\psi)} \right]. \quad \text{(A.57a,b)}$$

A.4.2 Complex group delay

The *complex group delay* $T(\psi)$ of $S(\psi)$ is defined by :

$$T(\psi) = \frac{\mathrm{d}}{\mathrm{d}\psi} \Phi(\psi). \quad \text{(A.58)}$$

Assuming that S is a rational function, i.e. $S(\psi) = N(\psi)/D(\psi)$, the complex group delay can be rewritten using (A.57b) :

$$\mathrm{T}(\psi) = \frac{-1}{2} \cdot \left[\left(\frac{\dot{N}(\psi)}{N(\psi)} - \frac{\dot{N}_*(\psi)}{N_*(\psi)} \right) - \left(\frac{\dot{D}(\psi)}{D(\psi)} - \frac{\dot{D}_*(\psi)}{D_*(\psi)} \right) \right]. \quad \text{(A.59)}$$

To evaluate the right hand-sided part of (A.59), let us consider the polynomial $N(\psi)$ and its derivative $n(\psi)$, which, according to Table A.2, are related as given below :

$$n = n_e + n_o = \dot{N}, \quad \text{with } n_e = \dot{N}_o, \; n_o = \dot{N}_e. \quad \text{(A.60)}$$

Hence, the next result is obtained :

$$\dot{N}/N - \dot{N}_*/N_* = 2 \cdot (N_e \cdot n_e - N_o \cdot n_o) / (N_e^2 - N_o^2). \quad \text{(A.61)}$$

Consequently, it is demonstrated that expression (A.61), and by extension also the group delay $T(\psi)$ in (A.59), are :

i) rational functions;

ii) para-even, and thus of form (A.26a), $F_i(\psi)$ in (A.26a) corresponding to real rational functions with $i = 1,2$;

iii) real-valued for real frequencies $\psi = j \cdot \phi$, $\phi \in \mathbb{R}$, according to (A.18), i.e. $T(j \cdot \phi) = \tau(\phi)$.

A.4.3 Responses for real frequencies

For $\psi = j \cdot \phi$, the attenuation and phase responses take the form :

$$\chi(\phi) = X(j \cdot \phi) = -\mathrm{Re}\{ \ln(S(j \cdot \phi)) \}$$
$$= -\frac{1}{2} \cdot \ln\left| S(j \cdot \phi) \cdot S_*(j \cdot \phi) \right| = -\ln\left| S(j \cdot \phi) \right|, \quad \text{(A.62)}$$

$$\varphi(\phi) = -j \cdot \Phi(j \cdot \phi) = -\mathrm{Im}\{\ln(S(j \cdot \phi))\}$$
$$= \frac{j}{2} \cdot \ln\left[S(j \cdot \phi)/S_*(j \cdot \phi)\right] = -\mathrm{Arg}\{S(j \cdot \phi)\}, \qquad \text{(A.63)}$$

where tbe attenuation measured in decibel is defined by :

$$a(\phi) = -20 \cdot \log_{10}\left|S(j \cdot \phi)\right| = (20/\ln 10) \cdot \chi(\phi) \qquad \text{[dB]}. \qquad \text{(A.64)}$$

The group delay is then given by :

$$\tau(\phi) = T(j \cdot \phi) = \frac{\mathrm{d}}{\mathrm{d}\phi}\, \varphi(\phi). \qquad \text{(A.65)}$$

A.5 Frequency responses in the z-domain

In this section, the frequency responses are given in the z-domain. The notation is slightly changed with respect to the ψ-domain.

A.5.1 Amplitude and phase responses

In the z-domain, the frequency response of any complex or real discrete-time function $H(z)$ is evaluated on the unit-circle $|z|=1$:

$$H\left(e^{j\Omega}\right) = H(z)\Big|_{z=e^{j\Omega}} = \left|H\left(e^{j\Omega}\right)\right| \cdot e^{-j\beta_H(\Omega)} \qquad \text{(A.66)}$$

where $|H(e^{j\Omega})|$ is the *amplitude response* and $\beta_H(\Omega)$ the *phase response* of $H(z)$. Alternatively to $|H(e^{j\Omega})|$, the *attenuation* response $a_H(\Omega)$ is defined :

$$a_H(\Omega) = -20 \cdot \log_{10}\left|H\left(e^{j\Omega}\right)\right| \qquad \text{[dB]}. \qquad \text{(A.67)}$$

A.5.2 Unwrapped phase response

Since the phase response

$$\beta_H(\Omega) = -\mathrm{Arg}\left\{H\left(e^{j\Omega}\right)\right\} \qquad \text{(A.68)}$$

is a multi-valued function, it is not uniquely related to the corresponding filter function. In practice, only the *Principal Value* $\beta_{H\,PV}(\Omega)$ of $\beta_H(\Omega)$ is usually considered [5] :

$$-\pi \le \beta_{H\,PV}(\Omega) \le \pi \;;\quad \beta_H(\Omega) = \beta_{H\,PV}(\Omega) + 2\pi \cdot k_H(\Omega) \qquad \text{(A.69)}$$

where $\beta_{H\,PV}(\Omega)$ and the true phase response $\beta_H(\Omega)$ are related by the frequency dependent integer factor $k_H(\Omega)$. If necessary, $\beta_H(\Omega)$ can be reconstructed from $\beta_{H\,PV}(\Omega)$ using various *phase unwrapping* techniques to determine the factor $k_H(\Omega)$:

- from $\beta_{H\,PV}(\Omega)$ alone in the simplest case (critical approach, especially when the poles or zeros of $H(z)$ become clustered);
- from $\beta_{H\,PV}(\Omega)$ together with its derivative (more reliable methods) [AlNa89, Kraj92, Trib77];
- other approach [Henk96], derived from [Henk84], page 77 bis.

Recently, phase unwrapping methods were also proposed for complex signals and multidimensional signals, e.g. [Yama98, Yama95].

In this report, unwrapped phase responses are evaluated with respect to the reference point :

$$\beta_H(\Omega = 0) = \beta_{H\,PV}(\Omega = 0), \quad \text{with [5]} \quad -\pi \le \beta_H(\Omega = 0) \le \pi, \qquad \text{(A.70)}$$

involving by definition $k_H(\Omega = 0) = 0$.

A.5.3 Group delay

The phase characteristic of a filter can also be represented by the *group delay*, normalized to the sampling period T_s :

$$\tau_H(\Omega) = \frac{d\beta_H(\Omega)}{d\Omega} \quad [T_s]. \qquad \text{(A.71)}$$

---

[5] Usually, the Principal Value is formally specified either over the range $-\pi < \beta_{H\,PV}(\Omega) \le \pi$, or over the range $-\pi \le \beta_{H\,PV}(\Omega) < \pi$, avoiding a simultaneous inclusion of both limits at $\pm\pi$, thus providing for a unique definition of $k(\Omega)$ in (A.69). In practice, the selection between both definitions depends on the used computer and/or software. In this report, the range of $\beta_{H\,PV}$ was extended to $-\pi \le \beta_{H\,PV}(\Omega) \le \pi$ to cover both cases, assuming that $k(\Omega)$ is properly and uniquely processed by the underlying computer/software.

A.6 Bilinear transform of rational functions

The bilinear transform of stable and irreducible rational functions is obtained by a mere application of the forward bilinear transform T_B defined in (A.50).

It is observed that singular points at $\psi = 1$ are mapped onto $z = \infty$ through T_B. However, assuming the rational function $S(\psi)$ in (A.50) stable, these singular points at $\psi = 1$ may only occur in the nmmerator of $S(\psi)$. $S(\psi)$ is then specified as follows, s_0 corresponding to a complex constant :

$$S(\psi) = s_0 \cdot \frac{(\psi - 1)^{M_1} \cdot \prod_{\mu=1}^{M_2} (\psi - \psi_{0\mu})}{\prod_{\nu=1}^{N} (\psi - \psi_{\infty\nu})}, \qquad \text{(A.72)}$$

with $M = M_1 + M_2$, $0 \le M \le N$, $N \ge 1$,

and $\psi_{0\mu} \neq 1$, for $\mu = 1, 2, ..., M_2$.

Applying the bilinear transform, one achieves :

$$H(z) = T_B\{S(\psi)\} = h_0 \cdot (z+1)^{(N-M)} \cdot \frac{\prod_{\mu=1}^{M_2} (z - z_{0\mu})}{\prod_{\nu=1}^{N} (z - z_{\infty\nu})}, \qquad \text{(A.73a)}$$

$$\text{with} \quad h_0 = s_0 \cdot \frac{(-2)^{M_1} \cdot \prod_{\mu=1}^{M_2} (1 - \psi_{0\mu})}{\prod_{\nu=1}^{N} (1 - \psi_{\infty\nu})}, \qquad \text{(A.73b)}$$

$$\text{and} \quad z_{0\mu} = \frac{1+\psi_{0\mu}}{1-\psi_{0\mu}}, \quad z_{\infty\nu} = \frac{1+\psi_{\infty\nu}}{1-\psi_{\infty\nu}}. \qquad \text{(A.73c)}$$

It is noticed that $H(z)$ possesses $(N - M)$ zeros at $z = -1$. Furthermore, indicating the degree of a polynomial by $\deg(\cdot)$, and denoting the numerator and denominator of $H(z)$ by num_H and den_H, respectively, it is remarked that :

$$M_1 = 0 \quad \Rightarrow \quad \deg(num_H) = \deg(den_H) = N; \qquad \text{(A.74a)}$$

$$M_1 > 0 \quad \Rightarrow \quad \begin{cases} \deg(num_H) = N - M_1, \\ \deg(den_H) = N. \end{cases} \qquad \text{(A.74b)}$$

As a consequence, $\deg(num_H) \leq \deg(den_H)$, so that causality is guaranteed for $H(z)$ in addition to stability when applying T_B to a stable and causal $S(\psi)$. The situations presented in Table A.7 are then distinguished.

	Forward bilinear transform T_B → / ← Inverse bilinear transform T_{IB}				
	$S(\psi)$			$H(z)$	
Case	Type	Parameters		Type	Parameters
1	All-pole	$M_1 = M_2 = M = 0$	$\Leftrightarrow$	——	$\deg(num_H) = N$ $\deg(den_H) = N$ $\exists N$ zeros at $z = -1$
2	——	$M_2 = 0,\ M = M_1 = N$ $\exists N$ zeros at $\psi = 1$	$\Leftrightarrow$	All-pole	$\deg(num_H) = 0$ $\deg(den_H) = N$
3	——	$M_1 = 0$ $M = M_2$ $\exists N$ poles at $\psi = -1$	$\Leftrightarrow$	Causal FIR	$\deg(num_H) = N$ $\deg(den_H) = N$ $\exists N$ poles at $z = 0$
4	Allpass	$M = N$ $\lvert s_0 \rvert = 1$ $\exists M_1$ poles at $\psi = -1$ $\psi_{0\nu} = -\psi^*_{\infty\nu}$ $\nu = 1,\ldots,M_2$.	$\Leftrightarrow$	Allpass	$\deg(num_H) = N - M_1$ $\deg(den_H) = N$ $\exists M_1$ poles at $z = 0$ $z_{0\nu} = 1/z^*_{\infty\nu}$ $\nu = 1,\ldots,M_2$.

Table A.7: Correspondence between different types of rational filter functions.

A.6.1 Bilinear transform of allpass functions

According to the fourth entry in Table A.7, an allpass function is expressed in the ψ-domain by :

$$S(\psi) = s_0 \cdot \left(\frac{\psi - 1}{\psi + 1}\right)^{M_1} \cdot \prod_{\nu=1}^{M_2} \left(\frac{\psi + \psi^*_{\infty\nu}}{\psi - \psi_{\infty\nu}}\right), \tag{A.75}$$

with $1 \leq M = M_1 + M_2 = N$,

$\psi_{\infty\nu} \neq -1$, for $\nu = 1,2,\ldots,M_2$; and $\lvert s_0 \rvert = 1$.

And the corresponding allpass function in the z-domain is :

$$H(z) = \mathrm{T_B}\{S(\psi)\} = h_0 \cdot z^{-M_1} \cdot \prod_{\nu=1}^{M_2} \left(\frac{z - 1/z^*_{\infty\nu}}{z - z_{\infty\nu}} \right), \qquad \text{(A.76a)}$$

$$\text{with} \quad h_0 = s_0 \cdot (-1)^{M_1} \cdot \prod_{\nu=1}^{M_2} \left(\frac{1 + \psi^*_{\infty\nu}}{1 - \psi_{\infty\nu}} \right), \qquad \text{(A.76b)}$$

$$\text{and} \quad \psi_{\infty\nu} \neq -1, \quad z_{\infty\nu} \neq 0, \quad \text{for } \nu = 1,2,...,M_2 .$$

The next relation is moreover established from (A.76b) :

$$|s_0| = 1 \quad \Rightarrow \quad |h_0| = \prod_{\nu=1}^{M_2} |z_{\infty\nu}| . \qquad \text{(A.76c)}$$

Alternative expressions often used for $S(\psi)$ and $H(z)$ are :

$$S(\psi) = \sigma \cdot \frac{g_*(\psi)}{g(\psi)} = \sigma \cdot \prod_{\nu=1}^{N} \left(\frac{\psi + \psi^*_{\infty\nu}}{\psi - \psi_{\infty\nu}} \right), \quad \forall\ \psi_{\infty\nu},\ \nu = 1,2,...,N ; \qquad \text{(A.77a)}$$

$$\text{with} \quad \sigma = s_0 \cdot (-1)^N ; \qquad \text{(A.77b)}$$

where $g(\psi)$ is a monic [6] polynomial, that is strictly Hurwitz for a strictly stable $S(\psi)$, and :

$$H(z) = \lambda \cdot \prod_{\nu=1}^{N} \left(\frac{1 - z^*_{\infty\nu} \cdot z}{z - z_{\infty\nu}} \right), \quad \forall\ z_{\infty\nu}, \quad \nu = 1,2,...,N ; \qquad \text{(A.78a)}$$

where the constant λ only depends on the poles $z_{\infty\nu}$ distinct from the origin :

$$\lambda = h_0 \cdot \prod_{\nu=1}^{M_2} \left(\frac{-1}{z^*_{\infty\nu}} \right) = \sigma \cdot \prod_{\nu=1}^{M_2} \left(\frac{1 - \psi^*_{\infty\nu}}{1 - \psi_{\infty\nu}} \right), \qquad \text{(A.78b)}$$

$$\text{with} \quad \psi_{\infty\nu} \neq -1, \quad z_{\infty\nu} \neq 0, \quad \nu = 1,2,...,M_2 .$$

It is deduced from (A.77b) and (A.78b) that :

$$|s_0| = 1 \quad \Rightarrow \quad |\sigma| = 1 \quad \Rightarrow \quad |\lambda| = 1. \qquad \text{(A.78c)}$$

---

[6] A polynomial is *monic* when its leading coefficient, associated to the highest power of the independent variable, is equal to +1 [Bele68, p. 406].

A.7 Bilinear transform of polynomial functions

It is useful to consider polynomial functions separately to observe how the symmetries (i.e. eveness, oddness, etc.) are transferred from one domain to the other. However, it is necessary to replace the forward and inverse bilinear transforms defined in (A.50) and (A.51), respectively, by the modified forward and inverse bilinear transforms T_{BP} and T_{IBP} specified below :

$$F(z) = T_{BP}\{f(\psi)\} = (z+1)^N \cdot f(\psi) \Big|_{\psi=(z-1)/(z+1)} \tag{A.79}$$

$$f(\psi) = T_{IBP}\{F(z)\} = (1-\psi)^N \cdot F(z) \Big|_{z=(1+\psi)/(1-\psi)} \tag{A.80}$$

so that a polynomial $f(\psi)$ of degree N in the ψ-domain is mapped onto a proper polynomial $F(z)$ in the z-domain, and vice-versa. The following correspondence table is then established :

Modified forward bilinear transform T_{BP} →				
Original polynomial in ψ-domain			**Target polynomial in z-domain**	
Polynomial type	Expression		Expression	Polynomial type
Even	$f(\psi) = f(-\psi)$	$\Rightarrow$	$F(z) = \tilde{F}(z)$	CS
Odd	$f(\psi) = -f(-\psi)$	$\Rightarrow$	$F(z) = -\tilde{F}(z)$	CA
Para-even	$f(\psi) = f_*(\psi)$	$\Rightarrow$	$F(z) = z^N \cdot \tilde{F}(z)$	PCS
Para-odd	$f(\psi) = -f_*(\psi)$	$\Rightarrow$	$F(z) = -z^N \cdot \tilde{F}(z)$	PCA
CS	$f(\psi) = \tilde{f}(\psi)$	$\Rightarrow$	$F(z) = (-1)^N F(-z)$	Even / Odd
CA	$f(\psi) = -\tilde{f}(\psi)$	$\Rightarrow$	$F(z) = -(-1)^N F(-z)$	Odd / Even
PCS	$f(\psi) = \psi^N \cdot \tilde{f}(\psi)$	$\Rightarrow$	$F(z) = (-1)^N F_*(z)$	Para-even/odd
PCA	$f(\psi) = -\psi^N \cdot \tilde{f}(\psi)$	$\Rightarrow$	$F(z) = -(-1)^N F_*(z)$	Para-odd/even

Table A.8: Correspondence between different types of polynomial functions.

It is remarked that Table A.8 holds for polynomials $f(\psi)$ possessing zeros located at $\psi = 1$, cf the discussion made in Section A.6, in which case $f(\psi)$ and $F(z)$ are not of same degree.

It is further noticed that proper CS, CA, PCS, and PCA polynomials in the ψ-domain (z-domain) should be devoid of any zero located at $\psi = 0$ ($z = 0$). The corresponding even, odd, para-even, and para-odd polynomials in tbe z-domain (ψ-domain) will then be devoid of any zero situated at $z = 1$ ($\psi = -1$).

A.8 Properties of single filter functions and sets of filter functions

The next definitions are given in the z-domain, but they apply as well in the ψ-domain using appropriate adjustments determined by the bilinear transform T_B.

A.8.1 Minimum, non-minimum, and maximum phase functions

It is recalled that the transmission zeros of a rational function – either complex or real – merely correspond to the zeros of its numerator polynomial. This definition applies to (causal and stable) Infinite Impulse Response (IIR) filters, and to (causal) Finite Impulse Response (FIR) filters.

Still by definition, a complex or real function is termed *minimum phase* when its transmission zeros are all confined to the closed unit-circle in the z-plane, i.e. $|z_{0\nu}| \leq 1$, $\forall \nu \in N$. Similarly, a function is denoted as *non-minimum phase* when at least one of its transmission zeros is located outside the closed unit-circle. Finally, a function features a *maximum phase* response when all its transmission zeros are situated outside the closed unit-circle. As an example, non-pathological allpass functions are of maximum phase type.

A.8.2 Power complementarity

A set of N discrete-time functions $[H_1(z), \ldots, H_N(z)]$ is said to be *power-complementary* if the next property is verified [Fett86,Vaid90]:

$$\sum_{k=1}^{N} \tilde{H}_k(z) \cdot H_k(z) = c, \quad c > 0, \quad \text{for all } z. \tag{A.81}$$

The power complementarity condition of a system expresses that the global energy or steady-state power of its signals is preserved. In particular, the global energy (steady-state power) of the input signals is then equal to the global energy (steady-state power) of the output signals. For a (pseudo-) lossless system, $c = 1$ [Fett86, Vaid90].

A.8.3 Allpass complementarity

Similarly, a set of discrete-time functions $[H_1(z), ..., H_N(z)]$ is said to be *allpass-complementary* wben the next equation is fulfilled [Fett86, Vaid90] :

$$\sum_{k=1}^{N} H_k(z) = A(z) \ , \quad A(z) \text{ being an allpass function.} \tag{A.82}$$

This property indicates that a signal filtered by a set of allpass complementary functions can be reconstructed exactly, except for a possible phase distortion.

A.8.4 Double complementarity

A set of discrete-time functions is called *doubly complementary* when both power and allpass complementarity conditions are met [Fett86, Vaid90]. The double complementarity condition plays a major role in signal analysis and signal synthesis algorithms (branching filters, filter banks, polyphase filters, etc.).

A.8.5 Magnitude complementarity

A set of N discrete-time functions $[H_1(z), ..., H_N(z)]$ is said to be *magnitude-complementary* if they are featuring the next property :

$$\sum_{k=1}^{N} |H_k(z)| = c, \quad c > 0, \quad \text{for } z = e^{j\cdot\Omega} \tag{A.83}$$

For (pseudo-) lossless systems, $c = 1$.

A.8.6 Double magnltude complementarity

Finally, a set of discrete-time functions is called *doubly magnitude complementary* when both magnitude and allpass complementarity

conditions are fulfilled [7]. The double magnitude complementarity condition is useful for the design of signal analysis and synthesis algorithms requiring a certain insensitivity to phase mismatch between the constituent signals. Applications have been referred to in the field of high quality loudspeaker crossovers.

A.9 Conclusion

In this appendix, a certain number of elementary concepts and definitions were recalled as a general background for the report, emphasizing issues related to complex polynomials and rational functions.

Contributions

Although important parts of the developments, identified properties, and proofs were elaborated by the author himself for the sake of this report, no claim of originality is expressed for any specific topic presented in this appendix, the subject being certainly trivial for mathematicians, or specialists in circuit theory or automatic control.

CA–I: Still, the author feels that the systematic organization of the appendix and the overall compiled information offer a certain level of originality for the circuits and systems engineering community.

[7] No particular name designating this feature could be found in the literature; hence, the term "doubly magnitude complementar(it)y" introduced here is probably not known / understood outside of the report.

References

Acronyms used

AC	IEEE Transactions on Automatic Control.
AEÜ	International Journal of Electronics and Communications (*Archiv für Elekronik und Übertragungstechnik*).
ASSP	IEEE Transsctions Acoustics, Speech, and Signal Processing.
CAS	IEEE Transactions on Circuits and Systems.
CAS–I	IEEE Transactions on Circuits and Systems–I: Fundamental Theory and Applications.
CAS–II	IEEE Transactions on Circuits and Systems–II: Analog and Digital Signal Processing.
CT	IEEE Transactions on Circuit Theory.
CTA	International Journal on Circuit Theory and Applications.
ECCTD	European Conference on Circuit Theory and Design.
EL	Electronics Letters.
EUSIPCO	European Signal Processing Conference.
ICASSP	IEEE International Conference on Acoustics, Speech, and Signal Processing.
ISCAS	IEEE International Symposium on Circuits and Systems.
SCS	International Symposium on Signals, Circuits, and Systems.
SP	IEEE Transactions on Signal Processing.
SPNH	Signal Processing, North-Holland.

Chapter 1

[Fett71] A. Fettweis, "Digital Filter Structures Related to Classical Filter Networks", *AEÜ*, Vol. 25, Feb. 1971, pp. 79-89.

[Fett86] A. Fettweis, "Wave Digital Filters : Theory and Practice", *Proc. of IEEE*, Vol. 74, No. 2, pp. 270-327, Feb. 1986; Correction to "Wave Digital Filters : Theory and Practice", *Proc. of IEEE*, Vol. 75, No. 5, May 1987, p. 729.

[Gazs85a] L. Gazsi, "Explicit Formulas for Lattice Wave Digital Filters", *CAS*, Vol. 32, No. 1, Jan. 1985, pp. 68-88.

Chapter 2

[Abra70] M. Abramowitz, I. A. Stegun (Eds.), *Handbook of Mathematical Functions with Formulas, Graphs, and Mathematical Tables*, Dover Publication, NY, USA, 9th corrected Ed., 1970 (original Ed. 1964).

[Anso99] M. Ansorge, F. Pellandini, "Relationship between phase response symmetries and stability of complex allpass functions", *Proc. of SCS'99*, Iasi, Romania, July 6-7, 1999, pp. 33-36.

[Anso00] M. Ansorge, "Generalized allpass transformations", unpublished document, University of Neuchâtel, Switzerland, 2000.

[Baue95] P. Bauer, *Stability Tests for Polynomials*, Chapter 44 in [Chen95a], pp. 1247-1267.

[Bele68] V. Belevitch, *Classical Network Theory*, Holden-Day, San Francisco, CA, USA, 1968.

[Bish96] R. H. Bishop, R. C. Dorf, C. E. Rohrs, M. Mansour, and R.T. Stefani, *Stability Tests*, Chapter 9 in [Levi96], pp. 131-156.

[Bose85] N. K. Bose, *Digital Filters: Theory and Applications*, North-Holland, Elsevier Publ. Co., Amsterdam, NL, 1985.

[Bose94] N. K. Bose, "Argument Conditions for Hurwitz and Schur Polynomials from Network Theory", *AC*, Vol. 39, No. 2, Feb. 1994, pp. 345-344.

[Chen95a] W.-K. Chen, Ed., *The Circuits and Filters Handbook*, CRC Press and IEEE Press, Boca Raton, Florida, USA, 1995.

[Cons70] A. G. Constandinides, "Spectral transformations for digital filters", *Proc. of IEE*, Vol. 117, No. 8, Aug. 1970, pp. 1585-1590.

[Decz72] A. G. Deczky, "Synthesis of Recursive Digital Filters Using the Minimum-p Error Criterion", *IEEE Trans. on Audio and Electroacoustics*, Vol. AU-20, No. 4, Oct. 1972, pp. 257-263.

[Decz73] A. G. Deczky, *Computer-Aided Synthesis of Digital Filters in the Frequency Domain*, Sc. D. Thesis, Swiss Federal Institute of Technology, Zürich, Switzerland, 1973.

[Decz74] A. G. Deczky, "Equiripple and Minimax (Chebyshev) Approximations for Recursive Digital Filters", *ASSP*, Vol. 22, No. 2, April 1974, pp. 98-111.

[Dedi95] H. Dedieu, P. Rada, "A Simple and Efficient Algorithm for Group Delay Equalization" *Proc. of ECCTD'95*, Istanbul, Turkey, Aug. 27-31, pp. 917-920.

[Dels84] P. Delsarte, Y. V. Genin, Y. G. Kamp, "Application of the Index Theory of the Pseudo-lossless Functions to the Bistritz Stability Test", *Philips J. Res.*, Vol. 39, 1984, pp. 226-241.

[Dels85] P. Delsarte, Y. V. Genin, Y. G. Kamp, "Pseudo-Lossless Functions with Application to the Problem of Locating the Zeros of a Polynomial", *CAS*, Vol. 32, No. 4, April 1985, pp. 373-381.

[Fett72b] A. Fettweis, "Pseudopassivity, Sensitivity, and Stability of Wave Digital Filters", *CT*, Vol. 19, No. 6, Nov. 1972, pp. 668-673.

[Fett85] A. Fettweis, J. A. Nossek, K. Meerkötter, "Reconstruction of Signals after Filtering and Sampling Rate Reduction", *ASSP*, Vol. 33, No. 4, Aug. 1985, pp. 893-902.

[Fett86] **Already referred to in Chapter 1.**

[Föld91] J. Földvári-Orosz, T. Henk, E. Simonyi, "Simultaneous Amplitude and Phase Approximation for Lumped and Sempled Filters", *CTA*, Vol. 19, Jan.-Feb. 1991, pp. 77-100. See also [Henk93].

[Gazs85a] **Already referred to in Chapter 1.**

[Güll86] S. N. Güllüoglu, *Diskrete Optimierung von Wellendigitalfiltern, insbesondere von Brücken-Wellendigitalfiltern mit Zweitoradaptatoren*, PhD Thesis, Report, TU-Bochum, 1986.

[Henk81a] T. Henk, "The Generation of Arbitrary-Phase Polynomials by Recurrence Formulae", *CTA*, Vol. 9, 1981, pp. 461-478.

[Henk81b] T. Henk, "New Criteria for the Hurwitz Test of Polynomials", *Proc. of ECCTD'81*, The Hague, NL, Aug. 1981, pp. 449-452.

[Henk93] T. Henk, M. Abo-Zahhad, "Comments on 'Simultaneous amplitude and phase approximation for lumped and sampled filters", *CTA*, Vol. 21, 1993, pp. 559-561. See also [Föld91].

[Iwak91] H. Iwakura, "New Frequency Transformations for Complex Digital Filters", *EL*, Vol. 27, No. 22, 24th Oct. 1991, pp. 2083-2085.

[Keel96] L. H. Keel, S. P. Bhattacharyya, "Phase properties of Hurwitz Polynomials", *AC*, Vol. 41, No. 5, May 1996, pp. 733-734.

[Khal98] H. K. Khalil, A. R. Teel, L. Praly, E. Sontag, *Stability*, Chapter 56 in [Levi96], pp. 889-908.

[Laak96] T. I. Laakso, V. Välimäki, M. Karjalainen, U. K. Laine, "Splitting the Unit Delay: Tools for Fractional Delay Filter Design", *IEEE Mag. Signal Proc.*, Vol. 13, No. 1, Jan. 1996, pp. 30-60.

[Lang92] M. Lang, "Optimal Weighted Phase Equalization According to the L_∞-Norm", *SPNH*, Vol. 27, April 1992, pp. 87-98.

[Lang93] M. Lang, *Ein Beitrag zur Phasenapproximation mit Allpässen*, PhD Thesis, Erlangen, Germany, 1993.

[Leeb92] F. Leeb, *Entwurf von Filtern, insbesondere von Wellendigitalfiltern, mit vorgeschriebenm Dämpfungs- und Phasenverhalten"*, PhD Thesis, Bochum, Germany, 1992. Edited by VDI-Verlag, Düsseldorf, Germany, Series 10, No. 210, 1992.

[Levi96] W. S. Levine, Editor, *The Control Handbook*, CRC Press and IEEE Press, Boca Raton, Florida, USA, 1996.

[Lopa96] K. A. Loparo, X. Feng, *Stability of Stochastic Systems*, Chapter 64 in [Levi96], pp. 1105-1126.

[Meer83] K. Meerkötter, "Antimetric Wave Digital Filters Derived from Complex Reference Circuits", *Proc. of ECCTD'83*, Stuttgart, FRG, Sept 6-8, 1983, pp. 217-220.

[Noss83] J. A. Nossek, H.-D. Schwartz, "Wave Digital Lattice Filters with Applications in Communication Systems", *Proc. of ISCAS'83*, Newport Beach, CA, USA, May 1983, pp. 845-848.

[Renf87a] M. Renfors, T. Saramäki, "Recursive Nth-Band Digital Filters – Part I: Design and Properties", *CAS*, Vol. 34, No. 1, Jan. 1987, pp. 24-39.

[Renf87b] M. Renfors, T. Saramäki, "Recursive Nth-Band Digital Filters – Part II: Design of Multistage Decimators and Interpolators", *CAS*, Vol. 34, No. 1, Jan. 1987, pp. 40-51.

[Schü84] H. W. Schüssler, *Digitale Signalverarbeitung I: Analyse diskreter Signale und Systeme*, Springer-Verlag, Berlin, FRG, 1994.

[Tarr95] I. F. Tarrad, T. Henk, "Design of Bireciprocal Wave Digital Filters with Prescribed Amplitude Characteristics by Phase Approximation", *AEÜ*, Vol. 49, No. 4, 1995, pp. 215-221.

[Vaid87a] P. P. Vaidyanathan, P. A. Regalia, S. K. Mitra, "Design of Doubly-Complementary IIR Digital Filters Using a Single Complex Allpass Filter, With Multirate Applications", *CAS*, Vol. 34, No. 4, April 1987, pp. 378-389.

[Vaid87c] P. P. Vaidyanathan, S. K. Mitra, "A Unified Structural Interpretation of Some Well-Known Stability Test Procedures for Linear Systems", *Proc. of IEEE*, Vol. 75, No. 4, April 1987, pp. 478-497.

[Vaid93] P. P. Vaidyanathan, *Multirate systems and filter banks*, Prentice Hall, Englewood Cliffs, N.J., USA, 1993.

[Youn73] D. M. Young, R. T. Gregory, *A Survey of Numerical Mathematics*, Volume 1, Dover Publ. Inc., New York, USA, 1973, pp. A.3-A.15.

Chapter 3

[Acha90] J. I. Acha, F. Torres, "Realization of Complex Digital Filters Based on the LBC Two-Pair Extraction Procedure", *CTA*, Vol. 18, 1990, pp. 563-575.

[Anso00] **Already referred to in Chapter 2.**

[Anto93] A. Antoniou, *Digital Filters: Analysis, Design, and Applications*, 2nd Edition, McGrsw Hill, New York, USA, 1993.

[Bahe84] H. Baher, *Synthesis of Electrical Networks*, John Wiley & Sons, Chichester, UK, 1984.

[Bahr98] A. A. Bahrath, "Scale steersbility of a class of complex digital filters", *EL*, Vol. 34, No. 11, May 28th, 1998, pp. 1087-1088.

[Bele68] **Already referred to in Chapter 2.**

[Blin76] H. J. Blinchikoff, A. I. Zversv, *Filtering in the Time and Frequency Domains*, John Wiley & Sons, New York, USA, 1976.

[Blej90] M. Bleja, M. Domanski, "Subband Coding of Monochrome Images Using Nonseparable Recursive Filters", *Proc. of EUSIPCO'90*, Barcelona, Spain, Sept. 1990, pp. 841-844.

[Boit90] R. Boite, H. Leich, *Les filtres numériques : analyse et synthèse des filtres unidimensionnels*, Masson, 3rd Ed. Paris, F, 1990.

[Boyd82] S. Boyd, L. O. Chua, "On the Passivity Criterion for LTI *N*-Ports", *CTA*, Vol. 10, 1982, pp. 323-333.

[Brut75] L. T. Bruton, "Low-Sensitivity Digital Ladder Filters", *CAS*, Vol. 22, No. 3, March 1975, pp. 168-176.

[Butt88] H.-J. Butterweck, J. Ritzerfeld, M. Werter, *Finite Wordlength Effects in Digital Filters: A Review*, Report EUT ISSN 0167-9708;88-E-205, Eindhoven University of Technology, Eindhoven, The Netherlands, Oct. 1988.

[Butt89] H.-J. Butterweck, J. Ritzerfeld, and M. Werter, "Finite Wordlength Effects in Digital Filters", *AEÜ*, Vol. 43, No. 2, 1989, pp. 76-89.

[Carl62] H. J. Carlin, D. C. Youla, "The (non)realizability of the complex ideal transformer", *CT*, Vol. 9, p.412, 1962.

[Carl83] H. J. Carlin, B. S. Yarman, "The Double Matching Problem: Analytic and Real Frequency Solutions", *CAS*, Vol. 30, No. 1, Jan. 1983, pp. 15-28.

[Chen95a] **Already referred to in Chapter 2.**

[Chen95b] W.-K. Chen, *Design of Broadband Matching Networks*, Chapter 74 in [Chen95a], pp. 2304-2334.

[Cort92] F. Corthay, *Oversampled Digital Leapfrog Filters*, Ph. D. Thesis, IMT, University of Neuchâtel, Switzerland, May 1992.

[Croc75] R. E. Crochiere, A. V: Oppenheim, "Analysis of Linear Digital Networks", *Proc. of IEEE*, Vol. 63, No. 4, April 1975, pp. 581-595.

[Dabr86] A. Dabrowski, "Suppression of Parasitic Oscillations in Communication Systems with Wave Digital Filters", *Archiwum Elektrotechniki, Polska Akademia Nauk, Komitet Elektrotechniki, Komitet Elektroniki i Telekomunikacji*, Wareaw, Poland, Vol. XXXV, No. 3/4, 1986, pp. 941-955.

[Dabr87a] A. Dabrowski, A. Fettweis, "Generalized Approach to Sampling Rate Alteration in Wave Digital Filters", *CAS*, Vol. 34, No. 6, June 1987, pp. 678-686.

[Dabr87b] A. Dabrowski, "Modulation and Wave Digital Filtering with Recovery of Reflected Pseudopower", *Proc. 1987 Int'l. Conf. on Digital Signal Processing*, Florenre, Italy, Sept. 1987 *(no page numbering)*.

[Darl39] S. Darlington, "Synthesis of reactance 4-poles which produce prescribed insertion loss characteristics", *J. of Mathematics and Physics*, Vol. 18, No. 1, March 1939, pp. 257-353.

[Dedi94] H. Dedieu, C. Dehollain, J. Neirynck, G. Rhodes, "New Broadband-Matching Circuit", *CTA*, Vol. 22, 1994, pp. 61-69.

[Depr80] E. Deprettere, P. Dewilde, "Orthogonal Cascade Realization of Real Multiport Digital Filters", *CTA*, Vol. 8, 1980, pp. 245-272.

[Deso75] C. A. Desoer, "On the Relation between Pseudo-Passivity and Hyperstability", *CAS*, Vol. 22, No. 11, Nov. 1975, pp. 897-898.

[Doma84] M. Domanski, "Structural Pseudolosslessness and Structural Pseudopassivity of 1-D and 2-D Digital Filters", *Proc. of ICASSP'84*, San Diego, California, USA, 1984, pp. 20.8.1-20.8.4.

[Doma91] M. Domanski, "Efficient Wave Filter Banks for Subband Coding of Images", *AEÜ*, Vol. 45, No. 3, 1991, pp. 160-167.

[Ebbi90] H.-D. Ebbinghaus, H. Hermes, F. Hirzebruch, M. Koecher, K. Mainzer, J. Neukirch, A. Prestel, and R. Remmert, *Numbers*, Springer Verlag, New York, 1990.

[Feis65] K. H. Feistel, R. Unbehauen, "Tiefpässe mit Tschebyscheff-Charakter der Betriebsdämpfung im Sperrbereich und maximal geebneter Laufzeit", *Frequenz*, Bd. 19, Nr. 8, 1965, pp. 262-282.

[Fett69] A. Fettweis, "Cascade synthesis of lossless two-ports by transfer matrix factorization", published in *Proc. 1969 NATO Advanced Study Institute on Network Theory*, R. Boite (Ed.), Gordon and Breach, N. Y., USA, 1972, pp. 43-103.

[Fett71] **Already referred to in Chapter 1.**

[Fett72a] A. Fettweis, "On the Connection Between Multiplier Word Length Limitation and Roundoff Noise in Digital Filters", *CT*, Vol. 19, No. 5, Sept. 1972, pp. 486-491.

[Fett72b] **Already referred to in Chapter 2.**

[Fett73] A. Fettweis, "Roundoff Noise and Attenuation in Digital Filters and Fixed-Point Arithmetic", *CT*, Vol. 20, March 1973, pp. 174-175.

[Fett74a] A. Fettweis, H. Levin, A. Sedlmeyer, "Wave Digital Lattice Filters", *CTA*, Vol. 2, June 1974, pp. 203-211.

[Fett74b] A. Fettweis, "On Sensitivity and Roundoff Noise in Wave Digital Filters", *ASSP*, Vol. 22, No. 5, Oct. 1974, pp. 383-384.

[Fett75] A. Fettweis, K. Meerkötter, "Suppression of Parasitic Oscillations in Wave Digital Filters", *CAS*, Vol. 22, No. 3, March 1975, pp. 239-246.

[Fett81a] A. Fettweis, "Principles of Complex Wave Digital Filters", *CTA*, Vol. 9, April 1981, pp. 119-134.

[Fett81b] A. Fettweis, "Scattering Properties of Real and Complex Lossless 2-ports", *Proc. of IEE*, Vol. 128, 1981, Part G, pp. 147-148.

[Fett82] A. Fettweis, J. A. Nossek, "Sampling Rate Increase and Decrease in Wave Digital Filters", *CAS*, Vol. 29, No. 12, Dec. 1982, pp. 797-806.

[Fett84a] A. Fettweis, "Digitel Circuits and Systems", *CAS*, Vol. 31, No. 1, Jan. 1984, pp. 31-48.

[Fett84b] A. Fettweis, "Some properties of Scattering Hurwitz Polynomials", *AEÜ*, Vol. 38, No. 3, 1984, pp. 171-176.

[Fett86] **Already referred to in Chapter 1.**

[Fett87] A. Fettweis, "Multi-Dimensional Digital Filters with Closed Loss Behaviour Designed by Complex Network Theory Approximation", *CAS*, Vol. 34, No. 4, April 1987, pp. 338-344.

[Fett88] A. Fettweis, "Passivity and Losslessness in Digital Filters", *AEÜ*, Vol. 42, No. 1, Jan./Feb. 1988, pp. 1-8.

[Fett89] A. Fettweis, "New Results in Wave Digital Filtering", *Proc. URSI Int'l. Symp. on Signals, Systems, and Electronics*, ISSSE'89, Erlangen, Germany, Sept. 1989, pp. 17-23.

[Fett90] A. Fettweis, "Design of Orthogonal and Related Digital Filters by Network-Theory Approach", *AEÜ*, Vol. 44, No. 2, March/April 1990, pp. 65-74.

[Fett92a] A. Fettweis, G. Hemetsberger, *Grundlagen der Theorie elektrischer Schaltungen*, Universitätsverlag Dr. Brockmeyer, Bochum, FRG, 1992.

[Fett92b] A. Fettweis, "Discrete Modelling of Lossless Fluid Dynamic Systems", *AEÜ*, Vol.46, No. 4, 1992, pp. 209-218.

[Fett92c] A. Fettweis, "Discrete Passive Modelling of Physical Systems Described by PDEs", *Proc. of EUSIPCO'92*, Brussels, Belgium, Aug. 1992, pp. 55-62.

[Fett94] A. Fettweis, "Multidimensional Wave-Digitel Principles: From Filtering to Numerical Integration", *Proc. of ICASSP'94*, Adeleide, South Australia, April 1994, pp. VI-173 – VI-181.

[Föld91] **Already referred to in Chapter 2.**

[Frai69] L. Fraiture, J. J. Neirynck, "Theory of Unit-Elements Filters", *Revue H. F.*, Vol. 7, 1969, pp. 325-340.

[Fuku96] M. Fukumoto, K. Ueda, S.-I. Takahashi, "Realization of Four Real Coefficient Transfer Functions by One Hypercomplex Transfer Function", *Proc. of ECCTD'95*, Istanbul, Turkey, Aug. 1995, pp. 975-978.

[Gazs86a] L. Gazsi, "Quasi-bireciprocal and Multirate Wave Digital Filters", *Frequenz*, Vol. 40, No. 11/12, 1986, pp. 289-296.

[Göck90] H. G. Göckler, "The Wave Digital Parallel Form for Arbitrary Transfer Charscteristics", *Proc. of EUSIPCO'90*, Barcelona, Spain, Sept. 1990, pp. 545-548.

[Gray79] A. H. Gray, "Passive Cascaded Lattice Digital Filters", *Proc. of ICASSP'79*, Washington DC, USA, April 1979, pp. 359-362.

[Gu94] Q. Gu, M. N. S. Swamy, "On the Design of a Broad Class of 2-D Recursive Digital Filters with Fan, Diamond and Elliptically-Symmetric Responses", *CAS–II*, Vol. 41, No. 9, Sept. 1994, pp. 603-614.

[Hahn86] H. Hahn, J. Büddefeld, B. J. Hosticka, U. Kleine, "CORDIC Realization of Power-Wave Digital Filters", *Proc. of ECCTD'85*, Prague, Czechoslovakia, Sept. 1985, pp. 607-510.

[Härm97b] A. Härmä, U. K. Laine, M. Karjalainen, "An Experimental Audio Codec Based on Warped Linear Prediction of Complex Valued Signals", *Proc. of ICASSP'97*, Munich, D, April 21-24, 1997, Vol. 1, pp. 323-327.

[Härm98] A. Härmä, U. K. Laine, M. Karjalainen, "Backward Adaptive Warped Lattice for Wideband Stereo Coding", *Proc. of EUSIPCO'98*, Island of Rhodes, Greece, Sept. 8-11, 1998, pp. 729-732.

[Hasl81a] M. Hasler, J. Neirynck, *Filtres Electriques*, Traite d'Electricité, Vol. 19, Editions Georgi, Saint-Saphorin, CH, 1981.

[Hasl81b] M. Hasler, "Lossless 2-ports Between Non-Reactive Terminations", *CTA*, Vol. 9, 1981, pp. 89-101.

[Henk81a] **Already referred to in Chapter 2.**

[Henk96] T. Henk, TU Budapest, Hungary; Private Communication, June-July 1996.

[Henk97a] T. Henk, TU Budapest, Hungary; Private Communication, January-February 1997.

[Host85] B. Hosticka, J. Büddefeld, U. Kleine, "Power-Wave Digital Filters Using CORDIC Adaptors", *AEÜ*, Vol. 39, 1985, pp. 242-244.

[ICAS94] "Multidimensional Wave Digital Filters", Special Session, *Proc. of ICASSP'94*, Adelaide, South Australia, April 1994, pp. VI-1 – VI-28.

[IEEE82] *IEEE Trans. on Communications*, Special Issue on Transmultiplexers, Vol. 30, No. 7, Part. 1, July 1982.

[Janc93] G.-R. Janczyk, *Mehrdimensionale Interpolation unter Verwendung von Wellendigitalfiltern*, PhD Report, Fortschr.-Ber. VDI Reihe 10, Nr. 262, VDI Verlag, Düsseldorf, Germany, 1993.

[Jarm91] M. R. Jarmasz, G. O. Martens, "A Simplified Synthesis of Lossless Cascade Analog and Digital Two-Port Networks", *CAS*, Vol. 31, No. 12, Dec. 1991, pp. 1501-1516.

[Jarm94] M. R. Jarmasz, V. Cheng, G. O. Martens, "Synthesis of Pipelinable Complex Wave Digital Filters", *CAS–II*, Vol. 41, No. 2, Feb. 1994, pp. 105-116.

[Kama97] M. Kamata, S.-I. Takahashi, "Orthogonal Filter with Hypercomplex Coefficients, Including Cases of Complex and Real Ones", *Proc. of ECCTD'97*, Budapest, Hungary, Aug./Sept. 1997, pp. 594-598.

[Kant89] I. L. Kantor, A. S. Solodovnikov, *Hypercomplex Numbers; an elementary introduction to algebras*, Springer-Verlag, New-York, USA, 1989.

[Kubi85a] G. Kubin, "Wave Digital Filters : Voltage, Current, or Power Waves ?", *Proc. of ICASSP'85*, Tampa, FL, USA, March 1985, Vol. 1, pp. 69-72.

[Kubi85b] G. Kubin, "On the stability of wave digital filters with time-varying coefficients", *Proc. of ECCTD'85*, Prague, Czechoslovakia, Sept. 1985, pp. 499-502.

[Lang93] **Already referred to in Chapter 2.**

[Laws90] S. Lawson, A. Mirzai, *Wave Digital Filters*, Ellis Horwood Ltd, Chichester, UK, 1990.

[Lind96] L. F. Lind, "Complex coefficient data transmission filters", *EL*, Vol. 32, No. 6, March 14th, 1996, pp. 516-517.

[Meer79] K. Meerkötter, *Beiträge zur Theorie der Wellendigitalfilter*, PhD Report, Technical University of Bochum, Bochum, Germany, 1979.

[Meer80a] K. Meerkötter, "Incremental Pseudopassivity of Wave Digital Filters", *Proc. of EUSIPCO'80*, Lausanne, Switzerland, Sept. 1980, pp. 27-32.

[Meer80b] K. Meerkötter, "Complex Passive Networks and Wave Digital Filters", *Proc. of ECCTD'80*, Warsaw, Poland, Sept. 1980, pp. 24-35.

[Meer83] **Already referred to in Chapter 2.**

[Naga90a] N. Nagai, Ed., *Linear circuits, systems and signal processing; advanced theory and applications*, Dekker, New York, USA, 1990.

[Naga90b] N. Nagai, *Complex Transmission-Line Circuit and Complex Wave Digital Filter*, Chapter 12 in [Naga90a], pp. 343-388.

[Nits93] G. Nitsche, *Numerische Lösung partieller Differentialgleichungen mit Hilfe von Wellendigitalfiltern*, PhD Report, Technical University of Bochum, Bochum, Germany, 1993.

[Noss83] **Already referred to in Chapter 2.**

[Nout74] R. Nouta, "The Jaumann structure in Wave Digital Filters", *CTA*, Vol. 2, June 1974, pp. 163-174.

[Nout75] R. Nouta, "Wave-Digital Cascade Synthesis", *CTA*, Vol. 3, 1975, pp. 231-247.

[Nowr90] B. Nowrouzian, N. Bartley, L. T. Bruton, "Design and DSP-Chip Implementation of a Novel Bilinear-LDI Digital Jaumann Filter", *CAS*, Vol. 37, No. 6, June 1990, pp. 695-706.

[Nowr93] B. Nowrouzian, "New Approach to the Exact Design of LDI Digital Allpass Networks Having a Follow-The-Leader Configuration", *EL*, Vol. 29, No. 17, 19th Aug. 1993, pp. 1554-1556.

[Orch66] H. J. Orchard, "Inductorless filters", *EL*, Vol. 2, June 1966, pp. 224-225.

[Padm91] M. Padmanabhan, K. Martin, "Resonator-Based Filter-Banks for Frequency-Domain Applications", *CAS*, Vol. 38, No. 10, Oct. 1991, pp. 1145-1159.

[Padm96] M. Padmanabhan, K. Martin, G. Péceli, *Feedback-Based Orthogonal Digital Filters – Theory, Applications, and Implementation*, Kluwer Acad. Publ., Boston, MA, USA, 1996.

[Paul86] R. Pauli, R. Saal, "Mathematische und physikalische Bedeutung komplexer Bezugsgrössen in der Netzwerktheorie", *AEÜ*, Vol. 40, No. 6, 1986, pp. 335-341.

[Paul89] R. Pauli, "Darlington's Theorem and Complex Normalization", *CTA*, Vol. 17, 1989, pp. 429-446.

[Péce88] G. Péceli, "Sensitivity of Resonator-Based Digital Filters", *CAS*, Vol. 35, No. 9, Oct. 1988, pp. 1195-1197.

[Péce89] G. Péceli, "Resonator-Based Digital Filters", *CAS*, Vol. 36, No. 1, Jan. 1989, pp. 156-159.

[Pras87] K. S. Prasad, C. Eswaran, V. G. K. Murti, "On the Stopband Sensitivity of Digital Filters", *CAS*, Vol. 34, No. 6, May 1987, pp. 682-584.

[Ragh91] D. Raghuramireddy, R. Unbehauen, "New structures for complex digital filters", *SPNH*, Vol. 25, 1991, pp. 23-34.

[Rao87] C. V. K. P. Rao, P. Dewilde, "On Lossless Transfer Functions and Orthogonal Realizations", *CAS*, Vol. 34, No. 6, June 1987, pp. 677-678.

[Rega87] P. A. Regalia, S. K. Mitra, "A Class of Magnitude Complementary Loudspeaker Crossovers", *ASSP*, Vol. 35, No. 11, Nov. 1987, pp. 1509-1516.

[Rega88a] P. A. Regalia, S. K. Mitra, "Phase Sensitivity Properties of Cascaded Digital Lattice Allpass Filters", *SPNH*, Vol. 15, 1988, pp. 1-21.

[Rega88b] P. A. Regalia, S. K. Mitra, P. P. Vaidyanathan, "The Digital All-Pass Filter: A Versatile Signal Processing Building Block", *Proc. of IEEE*, Vol. 76, No. 1, Jan. 1988, pp. 19-37.

[Seal79] R. Saal, *Handbook of Filter Design*, Backnang, FRG, AEG-Telefunken, 1979.

[Sars87] T. Saramäki, T.-H. Yu, S. K. Mitra, "Very Low Sensitivity Realization of IIR Digital Filters Using a Cascade of Complex All-Pass Structures", *CAS*, Vol. 34, No. 8, Aug. 1987, pp. 876-886.

[Scar94] G. B. Scarth, G. O. Martens, "Synthesis of Complex Lossless Two-Ports", *CTA*, Vol. 22, 1994, pp. 121-143.

[Sche98] T. Schetelig, R. Rabenstein, "Simulation of Three-Dimensional Sound Propagation with Multidimensional Wave Digital Filters", *Proc. of ICASSP'98*, Seattle, USA, May 1998.

[Schü89] H.-D. Schütte, "On adaptors for complex Wave Digital Filters", *Proc. of ISCAS'89*, Portland, Oregon, USA, May 1989, pp. 1644-1647.

[Schü90] H.-D. Schütte, J. Wenzel, Hypercomplex Numbers in Digital Signal Processing", *Proc. of ISCAS'90*, New Orleans, LA, USA, May 1990, pp. 1557-1560.

[Schü91] H.-D. Schütte, *Digitalfilter zur Verarbeitung komplexer und hyperkomplexer Signale*, Ph. D. Thesis, University of Paderborn, Germany, 1991.

[Schü94] **Already referred to in Chapter 2.**

[Sedr78] A. S. Sedra, P. O. Brackett, *Filter Theory and Design: Active and Passive*, Matrix Publishers, Inc., Beaverton, Oregon, USA, 1978.

[Sjös93] U. Sjöström, *On the Design and VLSI Implementation of Digital Signal Processing Algorithms: an Approach Using Wave Digital State Space Filters and Distributed Arithmetic*, Ph. D. Thesis, University of Neuchâtel, Switzerland, Feb. 1993.

[Suzu90] M. Suzuki, N. Nagai, *Wave Digital Filter Synthesized with the Darlington Procedure of Classical Circuit Theory*, Chapter No. 11 in [Naga90a], pp. 311-342.

[Suzu91] M. Suzuki, N. Nagai, N. Miki, "Wave Digital Filters and Orthogonal Filters Based on Extracting Two-Wire Lines", *CAS*, Vol. 38, No. 5, May 1991, pp. 534-539.

[Szen77] G. Szentirmai, "FILSYN – A General Purpose Filter Synthesis Program", *Proc. of IEEE*, Vol. 65, No. 10, Oct. 1977, pp. 1443-1458.

[Take80] T. Takebe, K. Nishikawa, M. Yamamoto, "Complex Coefficient Digital All-Pass Networks and their Applications to Variable Delay Equalizer Design", *Proc. of ISCAS'80*, Houston, TX, USA, April 28-30, 1980, pp. 605-608.

[Tan88] S. Tan, J. Vandewalle, "Fundamental Factorization Theorems for Rational Matrices over Complex or Real Fields", *Proc. of ISCAS'88*, Helsinki, Finland, June 1988, pp. 1183-1186.

[Tan92] A. C. Tan, "An Adaptive Least-Mean Square Wave Digital Filter", *Proc. of ISCAS'92*, San Diego, CA, USA, May 1992, pp. 2180-2183.

[Tan94] A. C. Tan, "Adaptive Wave Digital Fan Filters", *Proc. of ICASSP'94*, Adelaide, South Australia, April 1994, pp. VI-25 – VI-28.

[Tant95] S. Tantaratana, *Design of IIR Filters*, Section 83.2 in [Chen95a], pp. 2611-2634.

[Tarr95] **Already referred to in Chapter 2.**

[Turn86] L. E. Turner, B. K. Ramesh, "Low Sensitivity Digital LDI Ladder Filters with Elliptic Magnitude Response", *CAS*, Vol. 33, No. 7, July 1986, pp. 697-706.

[Ullr76] U. Ullrich, *Effektives Verfahren zur Ermittlung des Signalrausch-verhältnisses von Digitalfiltern unterschiedlicher Struktur*, PhD Report, Technical University of Bochum, Bochum, Germany, 1976.

[Unbe89] R. Unbehauen, G. Zimmer, "Non-reciprocal network synthesis using the generalized Richards transformation", *CTA*, Vol. 17, No. 2, 1989, pp. 125-140.

[Vaid84] P. P. Vaidyanathan, S. K. Mitra, "Low Passband Sensitivity Digital Filters: A generalized Viewpoint and Synthesis Procedures", *Proc. of IEEE*, Vol. 72, No. 4, 1984, pp. 404-423.

[Vaid85a] P. P. Vaidyanathan, S. K. Mitra, "Passivity Propecties of Low-Sensitivity Digital Filter Structures", *CAS*, Vol. 32, No. 3, March 1985, pp. 217-224.

[Vaid85b] P. P. Vaidyanathan, "A Unified Approach to Orthogonal Digital Filters and Wave Digital Filters, Based on LBR Two-Pair Extraction", *CAS*, Vol. 32, No. 7, July 1985, pp. 673-686.

[Vaid87a] **Already referred to in Chapter 2.**

[Vaid88] P. P. Vaidyanathan, P.-Q. Hoang, "Lattica Structures for Optimal Design and Robust Implementation of Two-Channel Perfect-Reconstruction QMF Banks", *ASSP*, Vol. 36, No. 1, Jan. 1988, pp. 81-94.

[Wanh81] L. Wanhammar, *An Approach to LSI Implementation of Wave Digital Filters*, Linköping Studies in Science and Technology, Diss. No. 62, Linköping University, Sweden, April 1981.

[Wanh99] L. Wanhammar, *DSP Integrated Circuits*, Academic Press, 1999

[Yarm88] B. S. Yarman, A. Fettweis, "Computer Aided Double Matching vai Parametric Representation of Brune Functions", *Proc. of ISCAS'88*, Helsinki, Finland, June 1988, pp. 2769-2772.

[Yang81] S. M. Yang, "On the Sensitivity of a Class of Wave Digital Filters", *CAS*, Vol. 28, No. 12, Dec. 1981, pp. 1158-1164.

[Youl64] D. C: Youla, "A New Theory of Broad-band Matching", *CT*, Vol. 11, March 1964, pp. 30-50.

[Youl71] D. C. Youla, "A Tutorial Exposition of some Key Network-Theoretic Ideas Underlying Classical Insertion-Loss Filter Design", *Proc. of IEEE*, Vol. 59, No. 5, May 1971, pp. 760-799.

[Zaln89] A. Zalnieriunas, "A New Wave Digital FIR Filter Structure", *AEÜ*, Vol. 43, No. 2, 1989, pp. 117-120.

[Zaln90] A. Zalnierunsa, "Adaptive Notch Digital Filters", *Proc. of ISCAS'90*, New Orleans, LA, USA, May 1990, pp. 3158-3161.

[Zhan88] S. Zhang, *Wellendigitalfilter mit Leistungswellen*, Ph. D. Thesis, University of Bochum, FRG, 1988.

[Zou89] M. Zou, X. Liu, "Design and implementation of circularly and spherically symmetric multidimensional digital filters", *SPNH*, Vol. 17, 1989, pp. 51-67.

[Zver67] A. I. Zverev, *Handbook of Filter Synthesis*, John Wiley and Sons Inc., New York, USA, 1967.

Chapter 4

[Croc83] R. E. Crochiere, L. R. Rabiner, *Multirate digital signal processing*, Prentice-Hall, Englewood Cliffs, NJ, USA, 1983.

[Dijk88] E. Dijkstre, L. Cardoletti, O. Nys, C. Piguet, M. Degrauwe, "Wave Digital Decimation Filtere in Oversampled A/D Convertere", *Proc. of ISCAS'88*, Helsinki, Finland, June 1988, pp. 2327-2330.

[Fett85] **Already referred to in Chapter 2.**

[Fett86] **Already referred to in Chapter 1.**

[Gala84] C. R. Galand, H. J. Nusabaum, "New Quadrature Mirror Filtar Structures", *ASSP*, Vol. 32, No. 3, June 1984, pp. 522-531.

[Gazs85a] **Already referred to in Chapter 1.**

[Laak96] **Already referred to in Chapter 2.**

[Meer83] **Already referred to in Chapter 2.**

[Noss83] **Already referred to in Chapter 2.**

[Nuss83] H. J. Nussbaum, "Complex Quadreture Mirror Filters", *Proc. of ICASSP'83*, Boston, MA, USA, April 14-16, 1983, pp. 221-223.

[Rega88b] **Already referred to in Chapter 3.**

[Sauv90] U. Sauvagerd, *Bitratenreduktion hochwertiger Musiksignale unter Verwendung von Wellendigitalfiltern*, PhD Thesis, Fortschr.-Ber. VDI Reihe 10, Nr. 117, VDI Verlag, Düsseldorf, Germany, 1990.

[Vaid87a] **Already referred to in Chapter 2.**

[Vaid87d] P. P. Vaidyanathan, "Quadrature Mirror Filter Banks, M-Band Extensions and Perfect-Reconstruction Techniques", *IEEE Mag. On Acoustics, Speech, and Signal Proc.*, July, 1987, pp. 4-20.

[Vaid88] **Already referred to in Chapter 3.**

[Vaid90] P. P. Vaidyanathan, "Multirate Digital Filters, Filter Banks, Polyphase Networks, and Applications: A Tutorial", *Proc. of IEEE*, Vol. 78, No. 1, Jan. 1990, pp. 56-93; Correction to " Multirate Digital Filters, Filter Banks, Polyphase Networks, and Applications: A Tutorial", *Proc. of IEEE*, Vol. 79, No. 2, Feb. 1991, p. 242.

[Vaid93] **Already referred to in Chapter 2.**

[Wong97] P. W. Wong, "Rate Distortion Efficiency of Subband Coding with Crossband Prediction", *IEEE Trans. on Information Theory*, Vol. 43, No. 1, Jan. 1997, pp. 352-356.

Chapter 5

[Darl70] S. Darlington, "Analytic Approximations to Approximations in the Chebyshev Sense", *Bell Syst. Tech. J.*, Vol. 49, No. 1, Jan. 1970, pp. 1-32.

[Darl78] S. Darlington, "Simple Algorithms for Elliptic Filters and Generalizations Thereof", *CAS*, Vol. 25, No. 12, Dec. 1978, pp. 975-980.

[Evan98] G. Evangelista, S. Cavaliere, "Discrete Frequency Warped Wavelets: Theory and Applications", *SP*, Vol. 46, No. 4, April 1998, pp. 874-885.

[Fron00] http://www.frontierd.com/dspstation.htm

[Gazs85a] **Already referred to in Chapter 1.**

[Gazs85b] L. Gazsi, S. N. Güllüoglu, "Brsnching Wave Digital Lattice Filter Design with (N+1)/2 True Multipliers", *Proc. of ECCTD'85*, Prague, Czech Rep., Sept. 1985, Vol. 2, pp. 511-514.

[Gazs86b] L. Gazsi, *Falcon Reference Manual*, Ruhr University Bochum, Germany, 1986.

[Güll86] **Already referred to in Chapter 2.**

[Härm97a] A. Härmä, U. K. Laine, M. Karjalainen, "WLPAC – A Perceptual Audio Codec in a Nutshell", *102nd Convention of Audio Engineering Society, Preprint 4420*, Munich, Germany, March 1997 (33 pages).

[Lain96] U. K. Laine, M. Huotilainen, "A Study on Auditory Resolution Using Bark-Famlet Clicks", *Proc. of ICASSP'96*, Atlants, Georgia, USA, May 1996, pp. 989-992.

[Luto92] M. D. Lutovac, D. M. Rabrenovic, "A Simplified Design of Some Cauer Filters without Jacobian Elliptic Functions", *CAS–II*, Vol. CAS-39, No. 9, Sept. 1992, pp. 666-671.

[Luto93] M. D. Lutovac, D. M. Rabrenovic, "Algebraic Design of Some Lower-Order Elliptic Filters", *EL*, Vol. 29, No. 2, 21st Jan. 1993, pp. 192-193.

[Luto96] M. Lutovac, L. Milic, "Elliptic Half-Band IIR Filters", *Facta Universitatis* (Nis), Series: Electronics and Energetics, Vol. 9, No. 1, 1998, pp. 43-59.

[Luto97] M. D. Lutovac, L. D. Milic, "Design of Computationally Efficient Elliptic IIR Filters with a Reduced Number of Shift-and-Add Operstions in Multipliers", *SP*, Vol. 45, No. 10, Oct. 1997, pp. 2422-2430.

[Luto98] M. D. Lutovac, L. D. Milic, "Design of Multiplierless Elliptic IIR Halfband Filters and Hilbert Transformers", *Proc. of EUSIPCO'98*, Island of Rhodes, Greece, Sept. 8-11, 1998, pp. 291-294.

[Mili95] L. Milic, M. Lutovac, D. Rabrenovic, "Facilities in Design and Implementation of Digital Butterworth and Elliptic Filters", *Proc. of ECCTD'95*, Istanbul, Turkey, Aug. 27-31, 1995, pp. 549-552.

[Mili96] L. D. Milic, M. D. Lutovac, "Reducing the Number of Multipliers in the Parallel Realization of Half-Band Elliptic IIR Filters", *SP*, Vol. 44, No. 10, Oct. 1998, pp. 2619-2623.

[Mili97] L. D. Milic, M. D. Lutovac, "Low-Complexity Lattice Wave Digital Filters", *Proc. of ECCTD'97*, Budapest, Hungary, Sept. 1997, pp. 1141-1144.

[Mili99] L. D. Milic, M. D. Lutovac, "Design of Multiplierless Elliptic IIR Filters with a Small Quantization Error", *SP*, Vol. 47, No. 2, Feb. 1999, pp. 469-479.

[Rabr93] D. M. Rabrenovic, M. D. Lutovac, "Minimum Stopband Attenuation of Cauer Filters without Elliptic Functions and Integrals", *CAS–I*, Vol. 40, No. 9, Sept. 1993, pp. 618-621.

[Rabr94] D. Rebrenovic, M. Lutovac, "Elliptic filters with minimal Q-factors", *EL*, Vol. 30, No. 3, 3rd Feb. 1994, pp 206-207.

Chapter 6

[Ansa87] R. Ansari, "IIR Discrete-Time Hilbert Transformers", *ASSP*, Vol. 35, No. 8, Aug. 1987, pp. 1116-1119.

[Anso97a] M. Ansorge, T. Henk, F. Pellandini, G. Gordos, "Design Parameters for Digital Hilbert Transformers", *Proc. Annual Polish-Czech-Hungarian Workshop on Circuit Theory, Signal Proce. and Applications*, PCH'97, Budapest, Hungary, Sept. 3rd-7th, 1997, pp. 5-10.

[Anso97b] M. Ansorge F. Pellandini, "Classification of Digital Hilbert Transformers", *Proc. of SCS'97*, Iasi, Romania, Oct. 2-3 1997, pp. 251-254.

[Benn88] B. J. Bennett, "A New Filter Synthesis Technique - The Hourglass", *CAS*, Vol. 35, No. 12, Dec. 1988, pp. 1489-1477.

[Boas92a] B. Boashash, "Estimating and Interpreting the Instantaneous Frequency of a Signal – Part 1: Fundamentals", *Proc. of IEEE*, Vol. 80, No. 4, April 1992, pp. 520-538.

[Boas92b] B. Boashash, "Estimating and Interpreting the Instantaneous Frequency of a Signal – Part 2: Algorithms and Applications", *Proc. of IEEE*, Vol. 80, No. 4, April 1992, pp. 540-568.

[Chen92] H. Cheng, *Rekonstruktion digitaler Signale in speziellen Mehrratensystemen unter verwendung von angenähert linearphasigen Welendigitalfiltern*, PhD Report, Fortschr.-Ber. VDI Reihe 21, Nr. 112, VDI Verlag, Düsseldorf, Germany, 1992.

[Cohe99] L. Cohen, P. Loughlin, D. Vakman, "On an ambiguity in the definition of the amplitude and phase of a signal", *SPNH*, Vol. 79, Dec. 1999, pp. 301-307.

[Cons70] **Already referred to in Chapter 2.**

[Croc76] R. E. Crochiere, L. R. Rabiner, "On the Properties of Frequency Transformations for Variable Cutoff Linear Phase Digital Filters", *CAS*, Vol. 23, No. 11, Nov. 1976, pp. 684-688.

[Croc83] **Already referred to in Chapter 4.**

[Crys68] T. H. Crystal, L. Ehrman, "The design and applications of digital filters with complex coefficients", *IEEE Trans. on Audio and Electroacoustics*, Vol. AU-16, No. 3, Sept. 1968, pp. 315-320.

[Czar82] R. Czarnach, H. W. Schüssler, G. Röhrlein, "Linear phase recursive digital filters for special applications", *Proc. of ICASSP'82*, 1982, pp. 1825-1828.

[Dabr97] A. Dabrowski, TU Poznan, Poland; Private Communication, Sept. 1997.

[Dawe85] H. Dawei, "Novel Realization of Hilbert Transformer Using Complex Wave Digital Filters", *Proc. of ECCTD'85*, Pragne, Czechoslovakia, Sept. 1985, pp. 492-495.

[Dumi97] N. Dumitriu, L. Stanciu, A. Mateescu, "Compact Formulas for Design of Maximally Flat Digital Hilbert Transformers", *Proc. of SCS'97*, Iasi, Romania, Oct. 2-3 1997, pp. 255-258.

[Fett74a] **Already referred to in Chapter 3.**

[Fett86] **Already referred to in Chapter 1.**

[Gabo46] D. Gabor, "Theory of Communications", *IEE J. Comm. Eng.*, Vol. 93, 1946, pp. 429-457.

[Gold69] B. Gold, C. M. Rader, *Digital Processing of Signals*, McGraw-Hill, N. Y., USA, 1969, pp. 90-92.

[Hahn96] S. L. Hahn, Hilbert Transforms in Signal Processing, *Artech House*, Norwood, MA, USA, 1998.

[Henk97b] T. Henk, TU Budapest, Hungary; Private Communication, Sept. 1997.

[Herr69] O. Herrmann, "Transversalfilter zur Hilbert-Transformation", *AEÜ*, Vol. 23, No. 2, Dec. 1969, pp. 581-587.

[Hess83] W. Hess, *Pitch determination of speech signals*, Springer Verlag, 1983.

[Jack75] L. B. Jackson, "On the relationship between digital Hilbert Transformers and certain low-pass filters", *ASSP*, Vol. 23, No. 8, Aug. 1975, pp. 381-383.

[Jian91] X.-R. Jiang, H. Cheng, "An Approach to the Deesign of IIR Hilbert Transfomers", *Proc. of China 1991 Int'l. Conf. on Circuits and Systems*, Shenzhen, China, June 1991, pp. 613-616.

[Kamm92] K. D. Kammeyer, *Nachrichtenübertragung*, Informationstechnik, B. G. Teubner Verlag, Stuttgart, Deutschland, 1992.

[Koll90] I. Kollar, R. Pintelon, J. Schoukens, "Optimal FIR and IIR Hilbert Transformer Design via LS and Minimax Fitting", *Proc. of IEEE Instrumentation and Measurement Technology Conf.*, San Jose, California, USA, Feb. 11-13, 1990, pp. 240-243.

[LeBi96] J. Le Bihan, "Coefficients of FIR Digitsl Differentiators and Hilbert Transformers for Midband Frequencies" *CAS-II*, Vol. 43, No. 3, March 1996, pp. 272-274.

[Meer83] **Already referred to in Chapter 2.**

[Meer84] K. Meerkötter, M. Romeike, "Wave Digital Hilbert-Transformers", *Proc. ISCAS'84*, Montreal, Canada, Vol. 1, May 1984, pp. 258-260.

[Nout74] **Already referred to in Chapter 3.**

[Oppe76] A. V. Oppenheim, W. F. G. Mecklenbräuker, R. M. Mersereau, "Variable Cutoff Linear Phase Digital Filters", *CAS*, Vol. 23, No. 4, April 1976, pp. 199-203.

[Oppe89] A. V. Oppenheim, R. W. Schafer, Discrete-Time *Signal Processing*, Prentice-Hall, Englewood Cliffs, NJ, USA, 1989.

[Poly72] G. Polya, G. Szegö, *Problems and Theorems in Analysis*, Vol. 1, Springer Verlag, New York, USA, 1972, p. 108, p. 302.

[Poul96] A. D. Poularikas (Ed.), *The Transforms and Applications Handbook*, CRC Press and IEEE Press, Boca Raton, FL, USA, 1996.

[Powe91] S. R. Powell, P. M. Chau, "A Technique for Realizing Linear Phase IIR Filters", *SP*, Vol. 39, No. 11, Nov. 1991, pp. 2425-2435.

[Rabi74] L. R. Rabiner, R. W. Schafer, "On the behaviour of minimax FIR digital Hilbert Transformers", *The Bell Syst. Tech. Journal*, Vol. 53, No. 2, Feb. 1974, pp. 363-390.

[Rao84] S. S. Rao, *Optimization theory and applications*, 2nd Ed., Wiley Eastern Ltd, New Delhi, India, 1984.

[Rega88b] **Already referred to in Chapter 3.**

[Reil94] A. Reilly, G. Frazer, B. Boashash, "Analytic Signal Generation – Tips and Traps", *SP*, Vol. 42, No. 11, Nov. 1994, pp. 3241-3245.

[Rouq96] S. Rouquette, Y. Berthoumieu, M. Najim, "Subband decomposition based on the Hilbert Transform applied to radar imaging", *Proc. of EUSIPCO'96*, Trieste, Italy, Sept. 1996, Vol. I, pp. 714-717.

[Schü87] H. W. Schüssler, J. Weith, "On the design of recursive Hilbert Transformers", *Proc. of ISCAS'87*, Dallas, TX, USA, 1987, pp. 876-879.

[Stef82a] P. Steffen, "Closed Form Design of Recursive Digital Hilbert Transformers: Exact Phase and Chebyshev Behaviour of the Magnitude", *AEÜ*, Vol. 36, No. 7/8, 1982, pp. 304-310.

[Stef82b] P. Steffen, "A New Approach to the Design of Discrete Hilbert Transformers with Exact Magnitude and Chebyshev Behaviour of the Phase", *AEÜ*, Vol. 36, No. 11/13, 1982, pp. 443-446.

[Vaid87a] **Already referred to in Chapter 2.**

[Vaid88] **Already referred to in Chapter 3.**

[Vaid93] **Already referred to in Chapter 2.**

[Vakm98] D. Vakman, *Signals, Oscillations, and Waves : A Modern Approach*, Artech House, Boston, USA, 1998.

Chapter 7

[Abra70] **Already referred to in Chapter 2.**

[Anso95] M. Ansorge, F. Pellandini, "Approximation of All-Pass Filters using the Eigenfilter Approach", *Proc of ECCTD'95*, Istenbul, Turkey, Aug. 27-31, 1995, pp. 967-970.

[Chen96] H. Chen, G. E. Ford, "A Unified Eigenfilter Approach to the Design of Two-Dimensional Zero-Phase FIR Filters with the McClellan Transform", *CAS-II*, Vol. 43, No. 8, Aug. 1996, pp. 622-626.

[Cull72] C. G. Cullen, *Matrices and Linear Transformations*, 2nd Ed., Dover Publ., NY, USA, 1972.

[Fett74a] **Already referred to in Chapter 3.**

[Fett81a] **Already referred to in Chapter 3.**

[Föld91] **Already referred to in Chapter 2.**

[Golu89] G. H. Golub, C. F. Van Loan, *Matrix Computations*, 2nd Ed., The Johns Hopkins University Press, Baltimore, USA, 1989.

[Henk80a] T. Henk, "General Algorithm for Phase-Interpolation", *Proc of ECCTD'80*, Warsaw, Poland, Sept. 2-5, 1980, pp. 271-276.

[Henk80b] T. Henk, "Modelling Considerations and Mean Square Error Analysis for PSK Data Transmission", *CTA*, Vol. 8, 1980, pp. 343-353.

[Henk81a] **Already referred to in Chapter 2.**

[Henk95] T. Henk, TU Budapest, Hungary; Private Communication, October 1995.

[Lang93] **Already referred to in Chapter 2.**

[Leeb89] F. Leeb, T. Henk, "Simultaneous Amplitude and Phase Approximation for FIR Filters", *CTA*, Vol. 17, 1989, pp. 363-374.

[Nguy93] T. Q. Nguyen, "The Design of Arbitrary FIR Digitel Filters Using the Eigenfilter Method", *SP*, Vol. 41, No. 3, March 1993, pp. 1128-1139.

[Nguy94] T. Q. Nguyen, T. I. Laakso, R. D. Koilpillai, "Eigenfilter Approach for the Design of Allpass Filters Approximating a Given Phase Response", *SP*, Vol. 42, No. 9, Sept. 1994, pp. 2257-2263.

[Pei94a] S.-C. Pei, J.-J. Shyu, "Design of 1-D and 2-D IIR Eigenfilters", *SP*, Vol. 42, No. 4, April 1994, pp. 962-966.

[Pei94b] S.-C. Pei, J.-J. Shyu, "Design of IIR multiband filters using IIR allpass filters", *SPNH*, Vol. 37, 1994, pp. 87-94.

[Rao84] **Already referred to in Chapter 6.**

[Spie68] M. R. Spiegel, *Mathematic Handbook of Formulas and Tables*, Schaum's Outline Series in Mathematics, McGraw Hill, NY, USA, 1968.

[Vaid87a] **Already referred to in Chapter 2.**

[Vaid87b] P. P. Vaidyanathan, T. Q. Nguyen, "Eigenfilters: A New Approach to Least-Squares FIR Filter Design and Applications Including Nyquist Filters", *CAS*, Vol. 34, No. 1, Jan. 1987, pp. 11-23.

Appendix

[Abra70] **Already referred to in Chapter 2.**

[AlNa89] H. Al-Nashi, "Phase Unwrapping of Digital Signals", *ASSP*, Vol. 37, No. 11, Nov. 1989, pp. 1693-1720.

[Anto93] **Already referred to in Chapter 3.**

[Bahe84] **Already referred to in Chapter 3.**

[Bele68] **Already referred to in Chapter 2.**

[Bose86] **Already referred to in Chapter 2.**

[Dels78] P. Delsarte, Y. Genin, Y. Kamp, "A Simple Approach to Spectral Factorization", *CAS*, Vol. 25, No. 11, Nov. 1978, pp. 943-946.

[Fett86] **Already referred to in Chapter 1.**

[Henk84] T. Henk, *Filter Approximation by Interpolation*, Candidate Thesis, Budapest, 1984 (in Hungarian).

[Henk96] **Already referred to in Chapter 3.**

[Jack89] L. B. Jackson, *Digital Filters and Signal Processing*, 2nd Ed., Kluwer Academic Publ., Boston, MA, USA, 1989.

[Jury73] E. I. Jury, *Theory and Application of the z-Transform Method*, John Wiley, New-York, USA, 1973.

[Kraj92] E. Krajnik, "A Simple and Reliable Phase Unwrapping Algorithm", *Proc. of EUSIPCO'92*, Brussels, Belgium, Aug. 1992, pp. 917-919.

[Lavr77] M. Lavrentiev, B. Chabat, *Méthodes de la théorie des fonctions d'une variable complexe*, Ed. Mir, Moscou, Russie, 1977.

[Meer83] **Already referred to in Chapter 2.**

[Oppe89] **Already referred to in Chapter 8.**

[Spie74] M. R. Spiegel, *Complex Variables, with an Introduction to Conformal Mapping and its Applications*, Schaum's Outline Series in Mathematics, McGraw Hill, NY, USA, 1974.

[Trib77] J. M. Tribolet, "A new phase unwrapping algorithm", *ASSP*, Vol. 25, No. 2, April 1977, pp. 170-177.

[Vaid87a] **Already referred to in Chapter 2.**

[Vaid90] **Already referred to in Chapter 4.**

[Vaid93] **Already referred to in Chapter 2.**

[Yama95] I. Yamada, K. Kurosawa, H. Hasegawa, K. Sakaniwa, "A Multidimensional Phase Unwrapping Algorithm and Zero Distribution of Complex Polynomials", *Proc. of ECCTD'95*, Istanbul, Turkey, Aug-Sept. 1995, pp. 491-494.

[Yama98] I. Yamada, K. Kurosawa, H. Hasegawa, K. Sakaniwa, "Algebraic Multidimensional Phase Unwrapping and Zero Distribution of Complex Polynomials", *SP*, Vol. 46, No. 6, June 1998, pp. 1639-1664.

[Youn73] **Already referred to in Chapter 2.**

Subject-related publications involving the author

M. Ansorge, F. Pellandini, "Relationship between phase response symmetries and stability of complex allpass functions", *Proc. of Int'l Symposium on Signals, Circuits, and Systems, SCS'99*, Iasi, Romania, July 6-7, 1999, pp. 33-36.

M. Ansorge, T. Henk, F. Pellandini, and G. Gordos, "Design Parameters for Digital Hilbert Transformers". *Proc. of Annual Polish-Czech-Hungarian Workshop on Circuit Theory, Signal Processing and Applications, PCH'97*, Budapest, Hungary, Sept. 3rd-7th, 1997, pp. 5-10.

M. Ansorge, F. Pellandini, "Classification of Digital Hilbert Transformers", *Proc. of Int'l. Symposium on Signals, Circuits, and Systems, SCS'97*, Iasi, Romania, Oct. 2-3 1997, pp. 251-254.

M. Ansorge, T. Henk, "Hilbert Transformers for Speech Processing", *Proc. of Int'l. Workshop on High Speed Networking '97*, HSN'97, Balatonfüred, Hungary, May 22-24, Vol. 2, pp. 43-47.

M. Ansorge, F. Pellandini, "Approximation of All-Pass Filters using the Eigenfilter Approach", *Proc of European Conf. on Circuit Design and Theory, ECCTD'95*, Istanbul, Turkey, Aug. 27-31, 1995, pp. 967-970.

M. Ansorge, F. Pellandini, "Characterization of Almost Linear-Phase IIR Half-Band Filters based on Allpass Networks", *Proc. of Int'l. Conf. on Signal Processing, Applications and Technology, ICSPAT'95*, Boston, MA, USA, Oct. 1995, pp. 571-577.

M. Ansorge, F. Pellandini : "Explicit Description of Lattice State-Space Wave Digital Filters", *Proc. of European Signal Proc. Conf., EUSIPCO'92*, Brussels, Belgium, Aug. 1992, pp. 997-1000.

M. Ansorge, U. Sjöström, I. Defilippis, P. Balsiger, F. Pellandini: "On the Automated Symbolic Design of Wave Digital Filters", *Proc. of Int'l. Conf. on Acoustics, Speech, and Signal Proc., ICASSP'91*, Toronto, Canada, May 1991, pp. 1561-1564.

M. Ansorge, U. Sjöström, I. Defilippis, F. Pellandini : "Symbolic Design of Ladder Wave Digital Filters", *Proc. of GRETSI-91*, Juan-Les-Pins, France, Sept. 1991, pp. 949-952.

U. Sjöström, I. Defilippis, M. Ansorge, F. Pellandini, "A Methodology for ASIC Implementation of Digital Filters", *Proc. of GRETSI-89*, Juan-Les-Pins, France, June 1989, pp. 797-800.

U. Sjöström, I. Defilippis, M. Ansorge, F. Pellandini, "CAD Environment for Digital Filter Design and Implementation", *Proc. of URSI Int'l. Symposium on Signals, Systems and Electronics, ISSSE'89*, Erlangen, FRG, Sept. 1989, pp. 601-604.

Acknowledgements

The realization of this dissertation was only possible thanks to the generous support received from many persons who are all kindly acknowledged.

First, I wish to express my respectful and deep gratitude to Professor Fausto Pellandini, Head of the Electronics and Signal Processing Laboratory at IMT Uni-Neuchâtel, for receiving me in his team, and for kindly accepting to supervise this dissertation. Indeed, working in Prof. Pellandini's Laboratory is an extremely enriching experience, and I would like here to thank him for the remarkable working conditions he cares to establish for the whole Laboratory at scientific, technical, and human levels.

Also, I am very indepted to the members of the Jury Committee, Prof. Arvind Shah, Director of IMT Uni-Neuchâtel, Prof. Murat Kunt, Head of the Signal Processing Laboratory at EPF-Lausanne, Prof. Adam Dabrowski, Head of the Electronic Circuits and Signal Processing Division at the Poznan University of Technology, Poland, and Prof. Tamás Henk, Head of the High Speed Networks Laboratory at the Budapest University of Technology and Economics, Hungary, for accepting to join the Committee and to evaluate the dissertation at a period where they were already heavily involved in numerous duties. Their appreciated remarks and observations helped very much consolidating the work done.

My particular thanks go to Prof. Tamás Henk for the fruitful cooperation established in the field of filter design, for the enriching stay I was offered to experience in his Laboratory in Budapest during the

spring of 1997, for the deep scientific knowledge he was so kind to share, and for the numerous discussions held since then.

My cordial thanks are addressed to all my present and past colleagues from the Electronics and Signal Processing Laboratory, including our System Manager Mr. Heinz Burri and our Secretary Mrs. Catherine Lehnherr, and especially my own team members, for the very friendly whilst efficient working atmosphere that could develop over the years. My colleague Dr. Ulf Sjöström, presently with Ericsson Radio Systems, Sweden, deserves here special thanks since he was the kind person introducing me into the domain of Wave Digital Filters design through his very communicative interest in the field !

Finally, hut most important, I express my sincere gratefulness to my family, in particular to my parents for their support and for awakening my interest for technical matters, and to my family-in-law for their very appreciated encouragements. My personal thanks are going to my dear wife and our sons for withstanding this period, while generously sustaining me during the preparation of this thesis, that 1 am dedicating to them.

Michael Ansorge
IMT Uni-Neuchâtel